UNIVERSITY OF CALIFORNIA
RIVERSIDE

Probing Multiphase Atmospheric Chemistry Using Advanced Mass Spectrometry

A Dissertation submitted in partial satisfaction
of the requirements for the degree of

Doctor of Philosophy

in

Chemistry

by

Wen Zhang

September 2024

Dissertation Committee:
Dr. Haofei Zhang, Chairperson
Dr. Linlin Zhao
Dr. Jingsong Zhang

The Dissertation of Wen Zhang is approved:

Committee Chairperson

University of California, Riverside

ACKNOWLEDGEMENTS

The five-year Ph.D. journeys at University of California, Riverside has been one of the most valuable fortunes in my life. There were big challenges for me to study far from home, adapt to a new environment and live alone during pandemic. I struggled but I survived. I have gained endless courage from these experiences to try anything I could think of and to overcome any hardship I might face in my career. I believe that I am ready to start new adventures. This is inseparable from the help and support of my family and friends.

I would like to express the deepest appreciation to my doctoral advisor Haofei Zhang for his dedicated guidance and unwavering support throughout my years here. You have high standards and supreme passion in research, and I would have not learned how to productively write, publish, and present my work without your timely and insightful feedback on the scientifical observations. You are kind and tolerant on the individual personalities of your students, so that I could have not insisted on chemistry as a researcher and scientist with love without your understanding and encouragement at difficult times. I feel so grateful and lucky that you are my Ph.D. research mentor who guided me to the correct way.

To the faculty at UCR, especially my other committee members, Dr. Linlin Zhao and Dr. Jingsong Zhang, I would like to thank you for your kind words and various supports to my seminar presentations and Ph.D. defense, and I also appreciate Dr. Linlin Zhao's and Dr. Ying-Hsuan Lin's help on the recommendation letters for me searching for a post-

doctoral position. Your kindness and experience as who have been deeply involved in academia are invaluable to me.

To all my friends in the lab who have worked side by side with me, I would like to express my gratitude for the days we have studied and played together. Dr. Tiffany Zhao, though at times we had conflicts on different lifestyles, how you deal with difficulties in research motivated me to make process and flourish successfully. Dr. Raphael Mayorga, my contemporaneous lab mate whom I had the most conversations every day, it has been a privilege to teach you and learn from you about the lab and the world. Dr. Chuanyang Shen, who provided creative and supportive suggestions to my publications, I would like to thank you for your friendship and the daily chats. Andy, it has been an amazing ability to share your contagious joy and compassion with others, and it's so generous to drive the lab group to beautiful beaches and good restaurants without any grievances. Sean, it has been a pleasure to work with you and talk with you, because you are always so considerate to help others at any time. Moreover, I would like to extend my sincere thanks to UCR graduates and undergraduates I met as a teaching assistant. Many thanks to the help and support to my teaching work, especially being grateful to receive Thank You cards and snacks from my cute undergraduate students.

To my friends Sandy and Elizabeth, it has been truly cherished to go traveling and hang out with you. None of my happiness would have been wonderful without your company. To my boyfriend Yuanding, I know it's very tough to keep a long-distance relationship, especially after we have been together for almost 10 years. Thank you for

your tolerance and perseverance over the years, and I wish we could reunite as soon as we get whatever we want for our careers.

To my family and family friends, I really appreciated that you respected every decision I made in my life. You might not understand it at times, but you believe in me and are willing to listen to me. I would not be here without your dedication to my education and care. It's your love and trust that let me stay calm when I encounter a challenge and let me chase my dreams with passion and persistence. I know you love me and I know I love you too.

The last thank you is given to you, each one reading here. Your involvement and support during my graduate school are critical to lead me to this point. I appreciate every interaction you have with me which helps build me and shape me.

I hope everyone is enjoying their lives, just like what I am doing right now.

ABSTRACT OF THE DISSERTATION

Probing Multiphase Atmospheric Chemistry Using Advanced Mass Spectrometry

by

Wen Zhang

Doctor of Philosophy, Graduate Program in Chemistry
University of California, Riverside, September 2024
Dr. Haofei Zhang, Chairperson

The Earth's atmosphere is composed of an enormous variety of chemical species associated with trace gases and aerosol particles whose composition and chemistry have critical impacts on the Earth's climate, air quality, and human health. Reactive volatile organic compounds (VOCs) and organic aerosols (OAs) in the atmosphere can be oxidized by oxidants in the atmosphere through a number of pathways, generating critical intermediate products such as the peroxy radicals ($RO_2^{\bullet}$), as well as the subsequent closed-shell oxygenated species which are a highly variable class of organic mixtures with diverse functional groups, such as ketone, alcohol, carboxylic acid, hydroperoxide, etc. Due to the significance to atmospheric environment, it is imperative to elucidate $RO_2^{\bullet}$-centered chemistry and understand chemical compositions of the resultant OAs on the molecular and even isomeric level. Mass spectrometry analysis as a powerful and popular analytical technique has been widely developed and applied in atmospheric chemistry for decades. In

combination with a comprehensive set of mass spectrometry instrumentation and kinetic simulations, this dissertation aims to help better understand OA formation and evolution and provide new insights in the realistic understanding of atmospheric components.

Chapter 1 introduces and reviews recently developed mass spectrometry techniques that allow for effective detection, identification, and quantification of a broad range of organic and inorganic chemical species with high sensitivity and resolution. Chapter 2, 3, 4 focus on probing $RO_2^{\bullet}$-centered bimolecular reactions in the gas phase and the particle phase that have been understudied in previous research. In Chapter 2, we demonstrate interferences caused by secondary ion chemistry in iodide-adduct chemical ionization mass spectrometry (I^--CIMS) which has been a popular analytical technique to measure a wide range of oxygenated VOC (OVOCs) due to its low selectivity. Moreover, we apply the secondary ion chemistry to inform OVOCs' functionalities and hence formation mechanisms. Chapter 3 illustrates that condensed-phase bimolecular autoxidation largely accelerates OA aging under atmospheric oxidant concentrations and impacts aerosol compositions, reversing a conventional view that multiphase (i.e., heterogeneous) oxidative aging is a slow process. Chapter 4 expands the heterogeneous study to the organic hydroperoxide formation from $RO_2^{\bullet}$ + $HO_2^{\bullet}$ reactions at aerosol particle interface via hydrogen-deuterium exchange mass spectrometry.

This dissertation provides novel advancements in mass spectrometry applications and a better understanding of the atmospheric chemical mechanisms. It may help interpret existing datasets, develop effective experimental approach to simulate atmospheric OA processes, and improve models to accurately predict OA transformation in the atmosphere

TABLE OF CONTENTS

LIST OF FIGURES

LIST OF TABLES

COPYRIGHT ACKNOWLEDGEMENTS

The text of this dissertation, in part or in full, is a reprint of the materials as they appear in the following publications:

Chapter 1: Zhang, W.; Xu, L.; Zhang, H. Recent advances in mass spectrometry techniques for atmospheric chemistry research, *Mass Spectrom. Rev.*, **2023**, *43* (5), 1091-1134.

Chapter 2: Zhang, W.; Zhang, H. Secondary ion chemistry mediated by ozone and acidic organic molecules in iodide-adduct chemical ionization mass spectrometry, *Anal. Chem.*, **2021**, *93* (24), 8595-8602.

Chapter 3: Zhang, W.; Zhao, Z.; Shen, C.; Zhang, H. Unexpectedly efficient aging of organic aerosols mediated by autoxidation, *Environ. Sci. Technol.*, **2023**, *57* (17), 6965-6974.

Chapter 4: Zhang, W.; Issa, K.; Tang, T.; Zhang, H. Role of hydroperoxyl radical in heterogeneous oxidation of oxygenated organic aerosols, *Environ. Sci. Technol.*, **2024**, *58* (10), 4727-4736.

Chapter 1 Introduction and Background

1.1 Introduction

The Earth's atmosphere is composed of an enormous variety of chemical species associated with trace gases and aerosol particles whose composition and chemistry have critical impacts on the Earth's climate, air quality, and human health. Mass spectrometry analysis as a powerful and popular analytical technique has been widely developed and applied in atmospheric chemistry for decades. Mass spectrometry allows for effective detection, identification, and quantification of a broad range of organic and inorganic chemical species with high sensitivity and resolution. This chapter aims to introduce and summarize recently developed mass spectrometry techniques, methods, and applications in atmospheric chemistry research in the past several years. Specifically, new developments of ion-molecule reactors, various soft ionization methods, and unique coupling with separation techniques are highlighted. The new mass spectrometry applications in laboratory studies and field measurements focus on improving the detection limits for traditional and emerging volatile organic compounds, characterizing multiphase highly oxygenated molecules, and monitoring particle bulk and surface compositions.

1.2 Principles and Developments of Mass Spectrometry

The chemical characterization of atmospheric gaseous and aerosol constituents has been a well-known challenge due to their extreme complexity caused by the enormous number and distinct properties of inorganic and organic species emitted and formed in the atmosphere. Both biogenic and anthropogenic sources as well as their chemical

transformations contribute to the atmospheric complexity, with the chemical and physical properties affecting the Earth's climate, outdoor and indoor air quality, and human health.[1-5] Volatile organic compounds (VOCs) are an important class of atmospheric compounds that could undergo photooxidation in the presence of various atmospheric oxidants, leading to the formation of gas-phase oxidation products with a highly variable and complex functionality and volatility.[6-9] VOCs also play a central role as precursors in the formation of secondary organic aerosols (SOA), while primary organic aerosols (POA) which are directly emitted into the air make up the other source of atmospheric OAs.[9-12] Thus, characterization of the molecular compositions of both the gas- and particle-phase organic species in the atmosphere is of vital importance to understanding the atmospheric chemical kinetics and reaction mechanism for environment assessment and planning.

With the interest of identifying and quantifying organic molecules in the atmosphere, the application of mass spectrometry-based techniques has been popular for many decades. Mass spectrometry techniques accomplish the separation and detection of analyte molecules through three processes of sample introduction, ionization, and mass-to-charge ratio examination, while the advanced innovation in any operation results in the instrument's versatile and comprehensive applications.[13] Thus, mass spectrometry can provide qualitative and quantitative analysis for a broad range of chemical species with high sensitivity and short response time.[14, 15] It is widely applied in the identification of unknown chemicals, determination of the elements' isotopic composition in a molecule, and classification of compound structures via fragmentation detection. In order to elucidate the structures of unknown chemicals, gas chromatography (GC) and liquid

chromatography (LC) coupled to mass spectrometers (i.e., GC-MS and LC-MS) emerged as the initial applications of mass spectrometry-based instruments to identify substances in atmospheric gaseous and aerosol mixtures through offline analysis.[16, 17] In these early studies, GC-MS has been widely used to separate and identify hydrocarbon mixtures as well as functionalized organics by employing derivatization techniques,[18-23] while LC-MS became a powerful technique to analyze relatively polar and high molecular-weight aerosol species.[24-26] With regards to aerosol compositional analysis, progress was made in the early 21st century to allow real-time characterization of atmospheric aerosols by the field-deployable aerosol mass spectrometer (AMS).[27-29] The AMS employs particle size selection and thermal desorption followed by electrode impact (EI) ionization, allowing for quantitively real-time measurements for the element composition, particle mass and size distributions of atmospheric aerosols.[30-32] However, the EI ionization used in AMS is a hard ionization where electrons are accelerated to 70 eV to bombard samples, leading to a high degree of sample fragmentation and thence complicated mass spectra with limited molecular information.[27-29] Despite the lack of molecular information, the high time-resolution, near-complete mass coverage, and the potential to infer bulk aerosol characteristic metrics make AMS a popular device in both laboratory studies[33-38] and ambient aerosol research.[27, 32, 39-44]

The continued pursuit of real-time and molecular-level characterization of atmospheric constituents led to the development of mass spectrometry instruments based on soft ionization techniques. Chemical ionization mass spectrometry (CIMS) is based on ion-molecule reactions to selectively ionize compounds of interest in the ion-molecule

reactor (IMR).[45] As one of the most widely used soft ionization and real-time analysis tool in atmospheric chemistry, CIMS was largely built upon the early development decades ago.[45, 46] In its early versions, the majority of CIMS applications aimed to monitor inorganic compounds,[45] except for proton transfer reaction mass spectrometers (PTR-MS), which is a CIMS that uses H_3O^+ as the reagent ion to measure chemically reduced organic compounds with proton affinity higher than water.[47, 48] In the early 2010s, the advancement of CIMS with higher sensitivity, better mass resolution, and more versatile reagent ions expanded the measurement capability to a wide range of oxygenated organic species.[49-52] In particular, these new developments allowed for a much-improved characterization of moderately to highly oxidized organic species in the atmosphere. While CIMS detects gaseous species, coupling it to aerosol inlets allows for aerosol composition measurements.[53-55] To measure aerosol constituents, another widely used soft ionization technique is electrospray ionization mass spectrometry (ESI-MS). ESI-MS was usually applied in offline analysis either by itself [56-62] or by coupling with LC.[63-69] In these studies, the aerosol samples were first collected on membrane filters, followed by solvent extraction procedures and LC-MS analysis. The sample collection, storage, and extraction may lead to undesired artifact reactions.[70-72] To overcome such artifacts, a few methods such as the nanospray desorption electrospray ionization (nano-DESI) and the paper spray (PS) ionization have been explored by directly ionizing molecules from the filter or substrate samples without solvent extraction.[13, 73-75] However, they still require samples to be collected, which loses the time resolution to monitor aerosol formation and evolution. Improvements have been made in the early 2010s to apply soft ambient ionization mass

spectrometry in real-time aerosol analysis. Notable examples include the extractive electrospray ionization (EESI),[76, 77] ambient electrospray ionization (AESI),[78] and direct analysis in real time (DART).[79-81] These studies provide valuable insights and guidance for later developments of soft ambient ionization mass spectrometry for aerosol research.

There have been many previous reviews of mass spectrometry methods applied to studying atmospheric chemistry.[82-88] But it is a rapidly growing field where many new analytical techniques, novel designs, and extended applications based on soft ionization mass spectrometry have been published in the recent several years. This chapter builds on the previous work and summarizes the new mass spectrometry methods and developments in atmospheric chemistry research. We introduce the main principles and workflows of individual mass spectrometry instruments that favor a wider range of measurements for gas-phase compounds and aerosol particles, helping understand the environmental implication of atmospheric chemistry. We further present applications of these techniques in laboratory studies, as well as outdoor and indoor field measurements on a few important research topics. Finally, we discuss several current issues and future developing directions in this field.

1.3 Soft Ionization Mass Spectrometry Techniques and Methods

Currently, mass spectrometry characterization of gaseous and aerosol species using soft ionization techniques is a rapidly developing field in atmospheric chemistry for understanding chemical composition. In this section, we introduce several analytical techniques to highlight the improved capabilities for qualitative and quantitative

measurements of atmospheric species in the last several years. The major applications and contributions to the atmospheric field of these newly designed mass spectrometry techniques are discussed in the next section.

1.3.1 Chemical ionization mass spectrometry: new IMR designs and ionization chemistries

As described above, the development of CIMS has emerged for decades, providing sensitive and rapid measurements for a wide range of atmospheric trace gases. One of the early CIMS techniques applied in the atmospheric chemistry was PTR-MS, which uses H_3O^+ as the reagent ion to ionize analyte molecules through proton transfer reactions.[47, 89-92] CIMS with other reagent ions has also been developed. In particular, numerous studies have reported CIMS measurements using various reagent ions, such as CF_3O^-, $CH_3C(O)O^-$, I^-, SF_6^-, Br^-, NO_3^-, NH_4^+, $C_2H_5OH^+$, NO^+, etc. to selectively ionize specific molecules through different ion chemistries.[49-51, 87, 93-100] In many of these development, CIMS with a time-of-flight (TOF) mass analyzer (TOF-CIMS) has been a powerful tool to quantitatively characterize inorganic and organic molecules as low as a few pptv with mass resolving power ($m/\Delta m$) up to 12000.[49, 101] **Figure 1.1** illustrates the basic configuration of a TOF-CIMS instrument. Ionization occurs in an IMR, where the configuration, residence time, pressure, electric field, and flow rate are optimized for the specific ion chemistry. In this section, we summarize new developments in recent years on IMR hardware designs, ion chemistries to enhance CIMS sensitivities and broaden measurable chemical ranges, and additional capabilities.

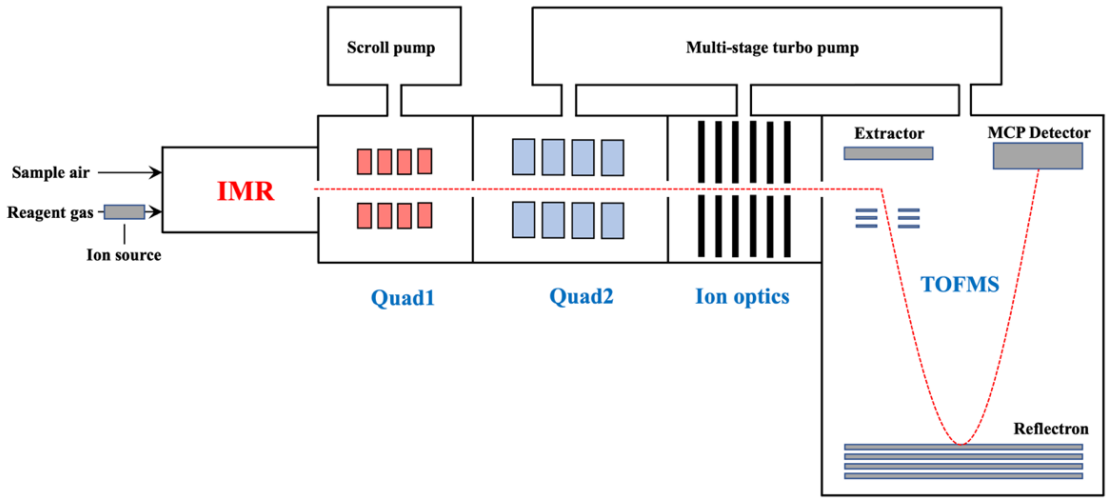

Figure 1.1 An illustrative diagram of the CIMS configuration.

1.3.1.1 New IMR designs

Vocus. Vocus is a newly developed chemical ionization source consisting of a discharge reagent-ion source and focusing ion-molecule reactor (FIMR),[102] with the configuration shown in **Figure 1.2A**. The reagent ions are produced at the central axis by a low-pressure discharge ion source comprised of two conical surfaces between which a plasma is generated. The produced ions enter through a ring offset from the central axis to ionize the air samples in the FIMR. The FIMR includes a quadrupole mounted outside of a glass tube with a resistive coating to build an inside axial electric field of a radio frequency (RF) quadrupole, focusing ions into a narrow beam on the central axis to enhance the sensitivity. Comparing with a traditional PTR-TOF, a Vocus-equipped PTR-TOF is ~ 19 times more sensitive for many VOCs (**Figure 1.3A**). According to ambient measurement comparison between a Vocus-equipped PTR-TOF and a traditional PTR-TOF, Vocus also showed much higher detection precision due to the improved sensitivity

and mass spectral resolution, which are paramount among other gas-phase measurement techniques.[15, 97, 103-105] It is also worth mentioning that Vocus exhibits an almost independent sensitivity on the relative humidity of the sample air owing to the high water vapor mixing ratio in the FIMR, in contrast to conventional PTR-MS instruments (**Figure 1.3B**). The response times of Vocus-equipped PTR-TOF are about an order of magnitude shorter than a traditional PTR-TOF.[102]

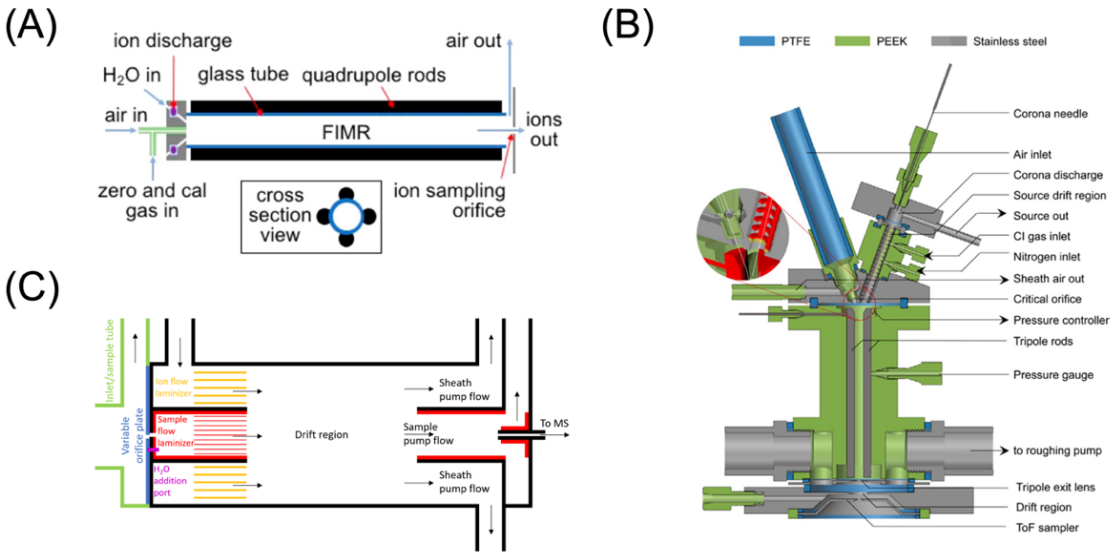

Figure 1.2 (A) Design of the Vocus consisting of a discharge reagent-ion source and a focusing ion−molecule reactor (FIMR). Reproduced with permission Krechmer et al. 2018. Copyright 2018 American Chemical Society. (B) Schematic representation of the PTR3 front part. Reproduced with permission Breitenlechner et al. 2017. Copyright 2017 American Chemical Society. (C) Schematic of the new coaxial, low-pressure IMR design to reduce wall interaction. Black lines represent stainless steel surfaces, green and blue lines represent PTFE Teflon, and red/yellow lines represent FEP or PFA Teflon. Reproduced with permission Palm et al., 2019. Copyright 2019 Palm et al.

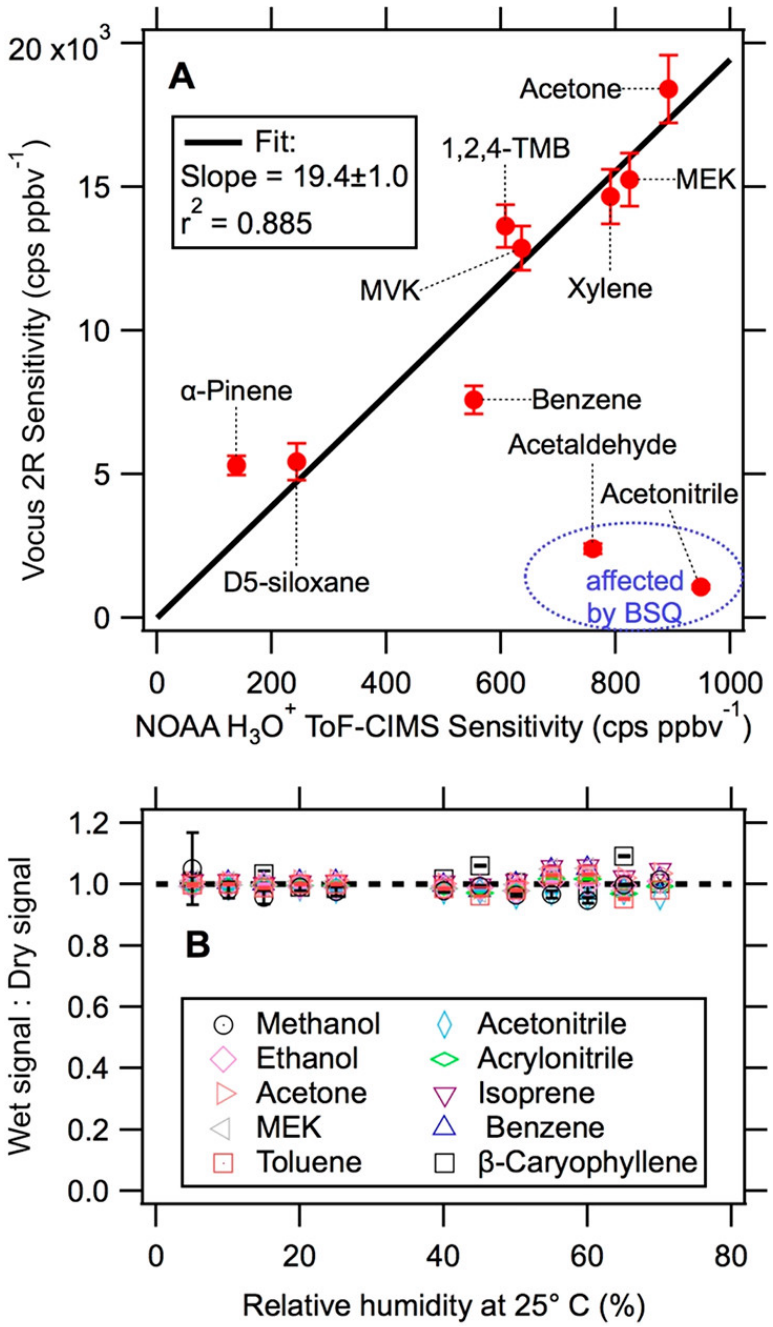

Figure 1.3 (A) Comparison of sensitivities between the Vocus PTR-TOF and NOAA PTR-TOF. Vocus sensitivities were determined during the ACTRIS-PICAB field campaign and represent an average over 24 h (12 separate calibrations). Error bars represent the 1σ standard deviation. (B) Humidity dependence of the Vocus PTR-TOF product ion signals. Reproduced with permission Krechmer et al. 2018. Copyright 2018 American Chemical Society.

PTR3. PTR3 is developed based on a standard PTR-TOF equipped with a new center-sampling inlet and an innovative IMR design.[106] A corona discharge ion source is operated in PTR3 followed by a source drift area (**Figure 1.2B**). The drift area is split into two regions, where chemical ionization gas and humidified nitrogen gas carrier are separately inserted and transported to a tripole IMR chamber. The design of splitting flow decreases the byproducts by preventing the formation of interfering primary ions and radicals. The tripole supplied with a RF voltage decouples the directions of sample gas flow (axial) and high-energy collisions (radial). As a result, the reaction time, pressure, and reduced electric field strength of PTR3 are independent of each other, leading to the possible improvement of operational parameters. Another improvement is the inlet design which minimizes wall loss by controlling symmetrical exhaustion of the sheath gas around the core flow. The new designs of PTR3 extend the reaction time thirty times longer and the pressure forty times higher compared to the standard PTR-TOF. After the pressure drops in the drift region, the gas flow is guided to a long TOF (LTOF) mass analyzer, further improving the resolving power for better separation of isobaric ions.[107] Calibration tests of different compound classes showed a result of up to 18,000 counts per second (cps)/ppbv at a mass resolving power of >8,000 m/Δm (fwhm), which exhibits a much better performance than the standard PTR-TOF.[108, 109] Further, Piel et al. introduced an extended volatility range inlet coupled with PTR3 to improve its time response by inhibiting the surface interactions of low volatility analytes within the gas inlet and the tripole IMR chamber.[110] Despite the promising features of PTR3, Holzinger et al. suggested

that it tends to form larger water clusters and deprotonation species by comparing the performances of different PTR instruments in field work.[111]

IMR design to reduce wall interactions. Reducing the interactions between relatively low-volatility analytes and IMR inner walls helps avoid sample loss and reduce response delay in CIMS measurements due to temporary adsorption of the analytes on inlet surfaces. In the study by Palm et al., a new coaxial, low pressure IMR (**Figure 1.2C**) was designed to minimize wall loss meanwhile improving sensitivity of CIMS.[112] The new design includes: (1) removing as many wall surfaces as possible and having any necessary wall surfaces be constructed from materials such as perfluoroalkoxy (PFA) Teflon, which have been reported to have minimized interactions with analytes;[113-115] (2) making the distance between analyte and surfaces as large as possible by controlling the analyte flow into a coaxial sheath, similar to previous IMR designs for the NO_3^- reagent ion;[116, 117] (3) exhausting the desorbed compounds from wall surfaces by pumping a sheath flow radially outside of a sample flow; and (4) maintaining IMR pressure constant within the range of 200 to 760 Torr even on an aircraft platform through the design of a variable orifice on the upstream side of the IMR.[118] The demonstration used I^- as the reagent ion but may be applicable to other reagent ions. As shown in Palm et al., I^- is introduced at the front of the drift region in the IMR and it ionizes analytes in the center of the drift region, such that less than 4 % of the analytes have interactions with wall surface according to diffusion calculations. As a result, the delay time of CIMS coupling with this IMR design is 3 to 10 times lower than previous CIMS versions, as illustrated in **Figure 1.4**.

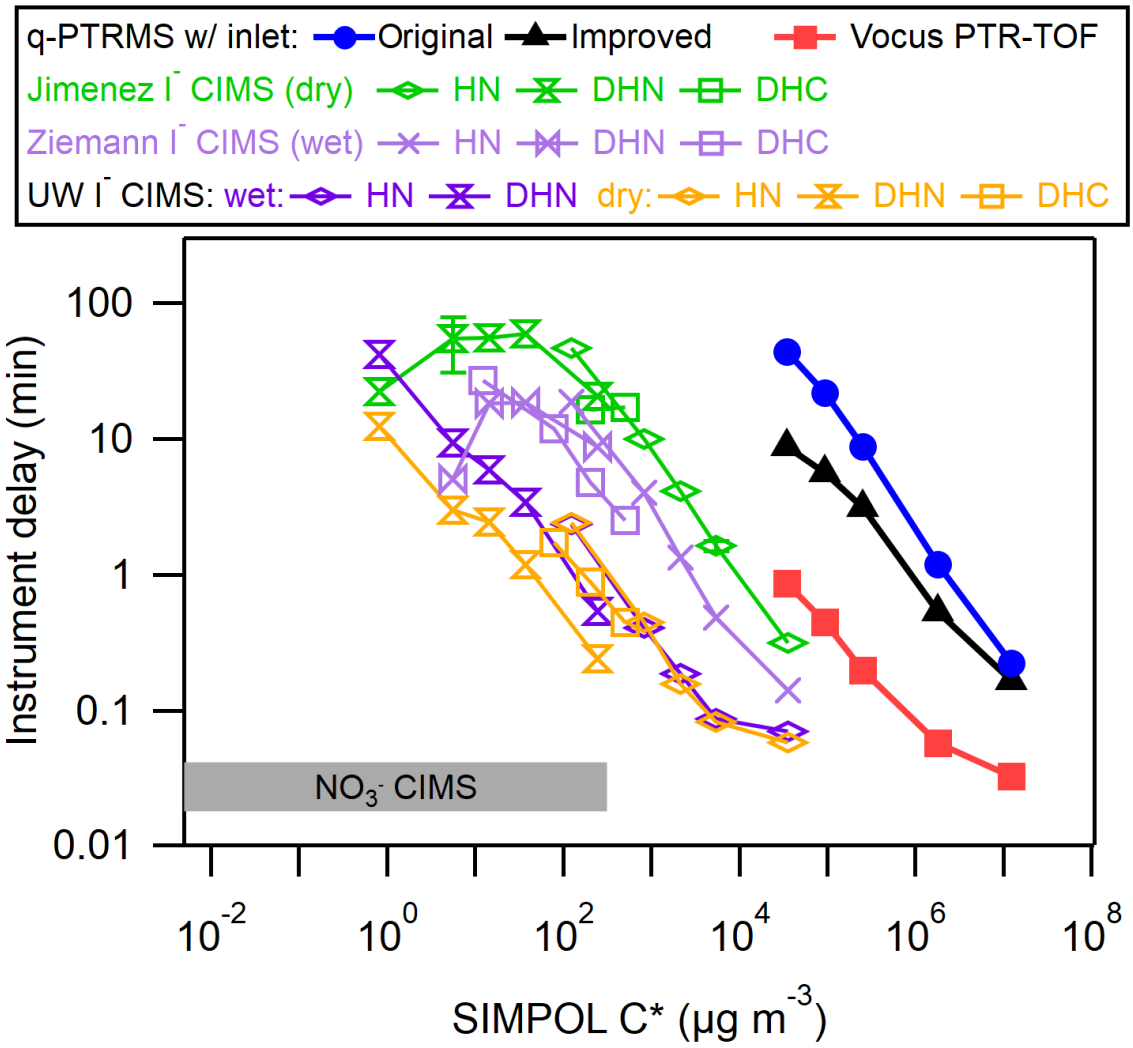

Figure 1.4 Delay times for a variety of organic molecules as a function of saturation vapor concentrations (C*, μg m^{-3}), compared with previous IMR designs including a quadrupole PTR-MS, Vocus PTR-TOF, and several I⁻CIMS instruments with different IMRs. The delay time in a NO_3^-CIMS is also shown for comparison. Reproduced with permission Palm et al., 2019. Copyright 2019 Palm et al.

1.3.1.2 Ionization chemistries in CIMS

CIMS has been widely used in *in-situ* measurements of a variety of atmospheric trace gases and aerosol species due to its excellent selectivity and sensitivity. The most common reagent ions used with CIMS include H_3O^+, NO^+, $C_6H_6^+$, $C_2H_5OH^+$, NH_4^+, and protonated amines in the positive ion mode, and I^-, $CH_3C(O)O^-$, CF_3O^-, SF_6^-, Br^-, and NO_3^- in the negative ion mode. It is essential to choose an appropriate reagent ion for CIMS to selectively and effectively ionize one or several targeted classes of compounds from a complex system. A comparison of the types of ion chemistry and targeted species by different reagent ions is listed in **Table 1.1**. Here, we focus on describing new ion chemistries studied in recent years which allow for broader applications of CIMS in identification and quantification of molecules relevant to atmospheric chemistry.

For all types of ion chemistry, the reagent ions are created from reagent gases by a radioactive ion source (e.g., ^{210}Po and 10 MBq Am), discharge,[102, 106] X-Rays,[49, 139, 140] or a vacuum ultraviolet (VUV) ion source.[132, 141] The reagent ions react with analytes in the IMR. The IMR operation conditions and configurations are designed for specific reagent ions and analyte molecules. The IMR can be held at atmospheric pressure or a reduced pressure. For instance, protonated amine and NO_3^- ion chemistries were often carried out under atmospheric pressure while most other ion chemistries require varied levels of low-pressure (2 – 200 mbar). The IMR also has a variety of designs. For example, the standard IMR used for I^-, $CH_3C(O)O^-$, SF_6^-, Br^-, etc. introduces the reagent ions perpendicularly with the mass spectrometer inlet nozzle and orthogonally to the sample flow with a mixing time ~ 100 – 200 ms.[49] The CF_3O^--CIMS IMR was designed in a transverse fashion with

Table 1.1 Summary of common CIMS reagent ions and the corresponding ion chemistries and detectable compounds.

Reagent Ion	Source Gas	Ion Source	IMR/mbar/ms	Primary Ion Chemistry	Detected Compounds	References
H_3O^+	Water vapor	Hollow cathode discharge	Ring-stack drift tube /~2/~0.1	$H_3O^+ + M \rightarrow [M+H]^+ + H_2O$	Compounds with proton affinity larger than water (e.g., majority of VOCs)	119, 120
		Glow discharge	Focusing IMR /~1/~0.1			102
		Corona discharge	Tripole/80/3			106
NO^+	Ultra-high-purity air	Hollow cathode discharge	Ring-stack drift tube /~2/0.1-0.2	$NO^+ + M \rightarrow M^+ + NO$ $\rightarrow [M-H]^+ + HNO$ $\rightarrow [M+NO]^+$	Compounds with low ionization energy or hydride transfer reaction enthalpy, otherwise favoring adduct formation (e.g., carbonyl species, small branched alkenes, some alkanes)	121, 122
$(C_6H_6)_2^+$	Benzene	^{210}Po	Canonical IMR/70/100	$(C_6H_6)_2^+ + M \rightarrow M^+ + 2{\bullet}C_6H_6$ $\rightarrow [M+(C_6H_6)_2]^+$ $\rightarrow [M+C_6H_6]^+ + C_6H_6$	Compounds with ionization energy lower than benzene, and with $C_6H_6^+$ affinity larger than benzene (e.g., dimethyl sulfide, isoprene, terpenes)	123, 124

$(C_2H_5OH)_nH^+$	Ethanol	^{241}Am	Transverse IMR/1000/~7	$(C_2H_5OH)_nH^+ + M \rightarrow [M+(C_2H_5OH)_{n-1}H]^+ + C_2H_5OH \rightarrow [M+H]^+ + nC_2H_5OH$	Compounds with proton affinity larger than ethanol (e.g., dimethyl sulfoxide, ammonia and amines)	125
		^{210}Po	Canonical IMR /20-200/~0.1			98, 126
NH_4^+	N_2/H_2O mixture	hollow cathode discharge	Ring-stack drift tube/2.3/~0.5	$NH_4^+ + M \rightarrow [M+NH_4]^+ \rightarrow [M+H]^+ + NH_3$	Compounds with proton affinities higher than ammonia; compounds with high binding enthalpies to NH_4^+ (e.g., some VOCs, OVOCs, HOMs, amines, and $RO_2^\bullet$)	127
	NH_3		Ring-stack drift tube/~2/~0.1			128
$NH_4^+ \bullet H_2O$	NH_3/H_2O mixture	Glow discharge	Focusing IMR /~3/0.2	$NH_4^+ \bullet H_2O + M \rightarrow [M+NH_4]^+ + H_2O$	Compounds with NH_4^+ affinity larger than H_2O (e.g., monoterpenes, majority of OVOCs)	129, 130
		Corona discharge	Tripole/50-70/3			97
$C_3H_7NH_3^+$	n-propylamine	^{241}Am	Flow tube IMR/1000/200-300	$C_3H_7NH_3^+ + M \rightarrow [M+C_3H_7NH_3]^+$	HOMs, Criegee Intermediate, $RO_2^\bullet$	131
I^-	CH_3I	^{210}Po	Canonical IMR/90/~120	$I^- + M \rightarrow [M+I]^-$	Compounds with high binding enthalpies to I^- (e.g., HONO,	52
		VUV	Flow tube IMR /20-50/10-20			132

		VUV	FIMR/9/30		N_2O_5, OVOCs, HOMs, $RO_2^•$)	133
Br^-	CF_3Br	^{210}Po	Canonical IMR/100/70	$Br^- + M \rightarrow [M+Br]^-$	Compounds with high binding enthalpies to Br^- (e.g., OVOCs, HOMs, $HO_2^•$, $RO_2^•$, halogen species, and sulfuric acid)	94
	CH_2Br_2	X-ray	MION/1000/30			134
$CH_3C(O)O^-$	Acetic anhydride	^{210}Po	Flow tube IMR/43/~80	$CH_3C(O)O^- + M \rightarrow [M+CH_3C(O)O]^- \rightarrow [M-H]^- + CH_3C(O)OH$	Compounds with gas-phase acidity larger than acetic acid (e.g., majority of organic acids, HOMs, and $RO_2^•$)	135
			Canonical IMR/20-100/100			49
NO_3^-	HNO_3	^{241}Am	Flow tube IMR/1000/200	$NO_3^-•(HNO_3)_n + M \rightarrow [M+NO_3]^- + (HNO_3)_n \rightarrow [M-H+HNO_3]^- + (HNO_3)_n$	Compounds with gas-phase acidity larger than HNO_3 or high binding enthalpies to NO_3^- (e.g., sulfuric acid, nitroaromatics, HOMs, and $RO_2^•$)	116, 136
CF_3O^-	CF_3OOCF_3	^{210}Po	Transverse IMR/35/~1	$CF_3O^- + M \rightarrow [M+CF_3O]^- \rightarrow [M-H+HF]^- + CF_2O$	Compounds with large gas-phase acidity or high binding enthalpies to CF_3O^- (e.g., organic acids,	137, 138

					hydroperoxides, and nitrates, H_2O_2, HNO_3, HONO, HCN, SO_2)	
SF_6^-	SF_6	^{210}Po	Flow tube IMR/~13/5-10	$SF_6^- + M \rightarrow [M\text{-}H+HF]^- + SF_5 \rightarrow [M\text{-}H]^- + HF + SF_5$	Inorganic compounds and organic acids	[96]

Note: [1]As analogous to proton affinity, we define NH_4^+ affinity and $C_6H_6^+$ affinity as the negative of the enthalpy change in the reaction between analyte and NH_4^+ or $C_6H_6^+$, respectively.

the reagent ions accelerated toward the inlet orifice by the electric field and the sample flow in a perpendicular direction, at a much shorter mixing time ~1 ms.[142] The shorter reagent ion-molecule mixing time results in the reaction in the kinetic limited regime. Another important factor of IMR design is to minimize the analyte-wall interaction. For example, for the IMR in NO_3^--CIMS targeting at low vapor pressure analytes, the reagent ions in a sheath flow are guided and accelerated via an electric field to meet the samples in parallel to minimize the wall interaction.[139] After the IMR, the ionized samples are transmitted through the ion optics. In the example shown in **Figure 1.1**, the charged ions enter a small segmented quadrupole with tunable frequency and amplitude to be effectively guided, focused and cooled, followed by a second big segmented quadrupole stage housed at nearly vacuum condition.[143] Weakly bounded ion-molecule clusters could experience collisional dissociation caused by the voltage difference between the two quadrupole regions.[45, 49, 93, 144] Finally, the primary beam travels through a series of DC optics to be further focused and accelerated before entering the mass analyzer.

With the above-described generic CIMS configuration, many ion chemistries can be employed (**Table 1.1**). The hydronium ions (H_3O^+) can ionize molecules with proton affinity higher than water, yielding protonated ion clusters via proton-transfer reactions in the drift tube. The reagent ion NO^+ is able to ionize VOCs through three different ionization mechanisms, charge transfer, hydride abstraction and cluster formation, dependent on the reaction enthalpy of compound molecules.[122] The proton- or hydride-transfer reactions are more favorable with a more negative proton or hydride transfer reaction enthalpy, otherwise the formation of $[VOC+NO]^+$ adducts occurs. Benzene cluster cations have been

used to detect dimethyl sulfide and terpenes by forming adducts.[123, 124] The $[C_2H_5OH+H]^+$ clustering process is typically applied to detect dimethyl sulfoxide, a series of nonmethane hydrocarbons, and amines.[98, 99, 145] The NH_4^+ ionization can detect a wide range of organic and inorganic species, including ketones, alcohols, peroxy radicals ($RO_2^\bullet$) and amines.[97, 127, 128, 146-148] The protonated amine ion chemistry (e.g., *n*- or *tert*-butylamine or diethylamine) has been more specifically used to measure highly oxygenated molecules (HOMs) and $RO_2^\bullet$.[131, 149, 150] Among the negative reagent ions, I^- and Br^- have been widely used to measure atmospheric relevant inorganic and organic species, including halogen-containing species, moderately OVOCs, HOMs, and $RO_2^\bullet$.[52, 94, 100, 134, 151] $CH_3C(O)O^-$ can ionize inorganic and organic acids that are more acidic than acetic acid as well as HOMs.[49, 148, 152] NO_3^- is also a well-known reagent ion to measure HOMs by forming adducts,[50, 153-155] but may have distinct sensitivities for different HOMs in comparison to $CH_3C(O)O^-$.[152] CF_3O^- has been used to detect OVOCs, organic hydroperoxides and nitrates through ion-molecule clustering or fluoride transfer reactions.[142, 156, 157] SF_6^- ionizes some inorganic compounds and organic acids through proton or fluoride transfer reactions.[96, 158, 159] As described here, the same class of organic compounds can be detected by several different ion chemistries. **Figure 1.5** shows a comparison between several popular ion chemistries in the detection suitability of α-pinene oxidation products with varied molecular composition.[15] Depending on the volatility, stability, and degree of oxygenation, the detection suitability for different ion chemistries also varies.

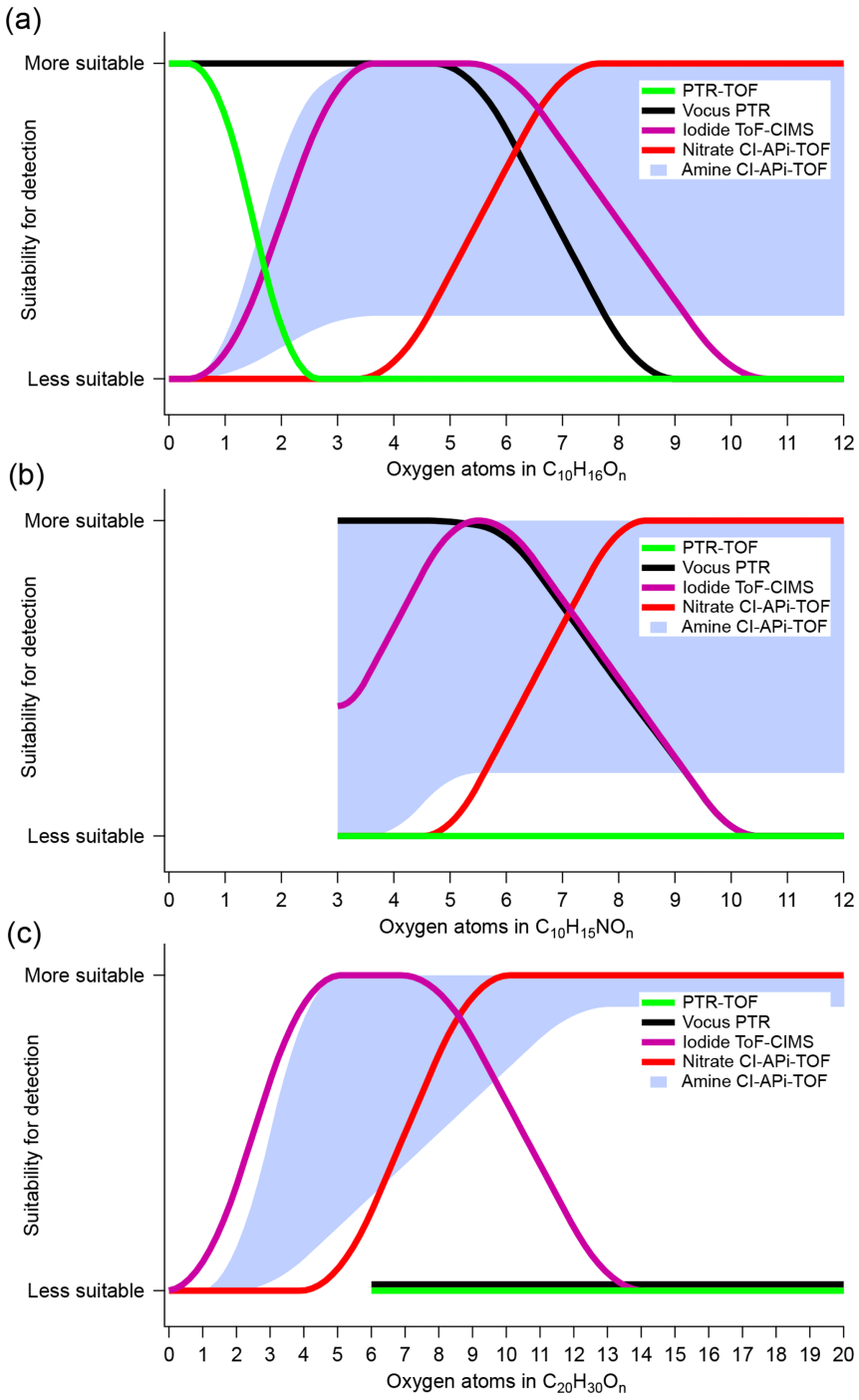

Figure 1.5 Estimated detection suitability of the different CIMS techniques for α-pinene and its oxidation products, plotted as a function of the number of oxygen atoms. Each panel symbolizes a compound group: (A) monomers, (B) organic nitrate monomers, and (C) dimers. Reproduced with permission Riva et al., 2019. Copyright 2019 Riva et al.

1.3.1.3 Extended capabilities of CIMS

Switchable reagent ion CIMS. For both laboratory research and field studies, the selective nature of CIMS may inhibit comprehensive measurements of a wide range of chemicals of interest. To overcome this limitation, a few studies have developed a switchable reagent ion (SRI, also known as selective reagent ion) approach to allow two or more reagent ion chemistries alternate during CIMS measurements. For example, the SRI-PTR-MS (or SRI-PTR-TOF) that enables switching between H_3O^+, NO^+, and O_2^+ has been used to more comprehensively characterize VOCs for years.[160-162] In addition, Brophy and Farmer developed an SRI-CIMS to switch between I^- and $CH_3C(O)O^-$ reagent ions to measure compounds across a large mass range and focus on specific species.[163] Based on the development of PTR3, more recently, Zaytsev et al. introduced a PTR3-based SRI-CIMS that can switch between H_3O^+ and NH_4^+ reagent ion chemistries within two minutes.[105, 164] Rissanen et al. developed a Multi-scheme chemical ionization inlet (MION) for fast switching between Br^- and NO_3^-, allowing multiple consecutive chemical ionization in fast repetition at atmospheric pressure.[134] The ion chemistry scheme can be changed within a second timescale by simply switching low-voltage settings, and the ion-molecule reaction time is adjustable by changing the length between two ion sources. Breitenlechner et al. recently coupled a VUV ion source to a commercial Vocus PTR-TOF in which the discharge ion source is replaced with two VUV lamps.[141] Different from the glow discharge ion source, the VUV ion source can efficiently generate both positive and negative reagent ions, allowing for the switchable polarities to access different ion chemistries such as the original H_3O^+-PTR-MS and the widely used I^--CIMS. Meanwhile,

the VUV ion source not only reduces ion fragmentation, but also inhibits the sputtering processes of fast ions which contributes to longer lifetime of the ion source region.

Thermal desorption based CIMS for aerosol analysis. Although CIMS was originally designed for real-time analysis of atmospheric trace gases, its coupling with thermal desorption-based inlets allows for measurements of chemical composition in the particle phase. One commonly used aerosol inlet in the past few years is the Filter Inlet for Gases and Aerosols (FIGAERO), which simultaneously sample gas species and collects aerosol particles on a Teflon filter followed by temperature-ramped thermal desorption to vaporize particle-phase chemicals into the gas phase.[53] The relatively short sampling time (hourly) due to its high sensitivity allowed the usage of FIGAERO-CIMS in the laboratory settings and real atmosphere.[165-167] Without filter collection, real-time particle-phase composition analysis can be achieved by direct thermal desorption, though the detection limit is degraded than the filter-based method.[168] Two common examples of such inlets are described below. The first one is the "chemical analysis of aerosol online" (CHARON) inlet system for online chemical characterization of semi-volatile submicron particle.[55] The CHARON particle inlet consists of a gas phase denuder which removes gas-phase organic compounds, an aerodynamic lens which concentrates aerosols in the subsampling flow with the combination of an inertial sampler, and a thermal desorption unit which operates at a reduced pressure of ~ 10 mbar and a constant heating temperature in the range of 50 − 250 °C for particle volatilization prior to the chemical analysis by PTR-MS.[55, 110, 169] The CHARON-PTR-MS has been successfully used for detection of organic compounds and ammonium constituents in aerosol particles.[55, 110, 170] The second example is the Vocus inlet

for aerosols (VIA), recently introduced by Häkkinen et al. for measurements of particle-phase HOMs by coupling to NO_3^-CIMS.[171, 172] Similar to the CHARON inlet, the VIA first passes aerosols samples through an activated charcoal gas denuder to remove gas-phase constituents.[172] Then the remaining aerosol species are evaporated at a chosen temperature between 25 and 300 °C by a Sulfinert-coated stainless-steel thermal desorption tube under ambient pressure.[171, 173] A dilution flow of clean air is introduced to cool down the samples before they enter the IMR.

CIMS with Orbitrap as the mass analyzer. Chemical ionization coupled to an Orbitrap mass spectrometry (CIMS-Orbitrap) has become a new technique among high-resolution CIMS instruments in atmospheric chemistry.[174, 175] Orbitrap is an ion trap mass analyzer essentially consisting of three electrodes.[176, 177] Two outer barrel-like electrodes face each other and are electrically isolated, held together with a coaxial inner spindle-like central electrode. A strictly linear electric field is generated when the voltage is applied to the outer and the central electrodes, while ions are trapped to the central electrode by the radial electric component. Ions cycle around the inner electrode by balancing the electrostatic attraction and the centrifugal force of tangential movements. Meanwhile, the axial electric component forces ions moving back and forth along the axis. As a result, the trajectories of ions inside the trap are nearly circular spiral. Ions with different mass-to-charge ratios move with the same axial frequency but different rotational frequencies, thus ions of interest with a specific mass-to-charge ratio could be selected and guiled to the analyzer. Compared to TOF-CIMS, CI-Orbitrap has much higher mass resolving power ($m/\Delta m$ of 140,000), and has been proved to be able to measure VOCs and $RO_2^\bullet$ at

atmospherically relevant concentrations.[140] Direct mass spectra comparisons of CI-Orbitrap with typical TOF-CIMS are shown in **Figure 1.6**, demonstrating the superior peak identification and formula assignment using CI-Orbitrap. A recent study showed improved sensitivity in measuring the OVOC with low concentrations down to 5×10^4 molecules cm^{-3} as well as the number of detected compounds above the 50% sensitivity threshold by optimizing different governing parameters of the chemical ionization Orbitrap Fourier transform mass spectrometry.[178] Moreover, its ability to use tandem mass spectrometry analysis allows for structural analysis of target molecules, leading to its potential applications in detecting trace-level components of atmospheric complex chemical mixtures.

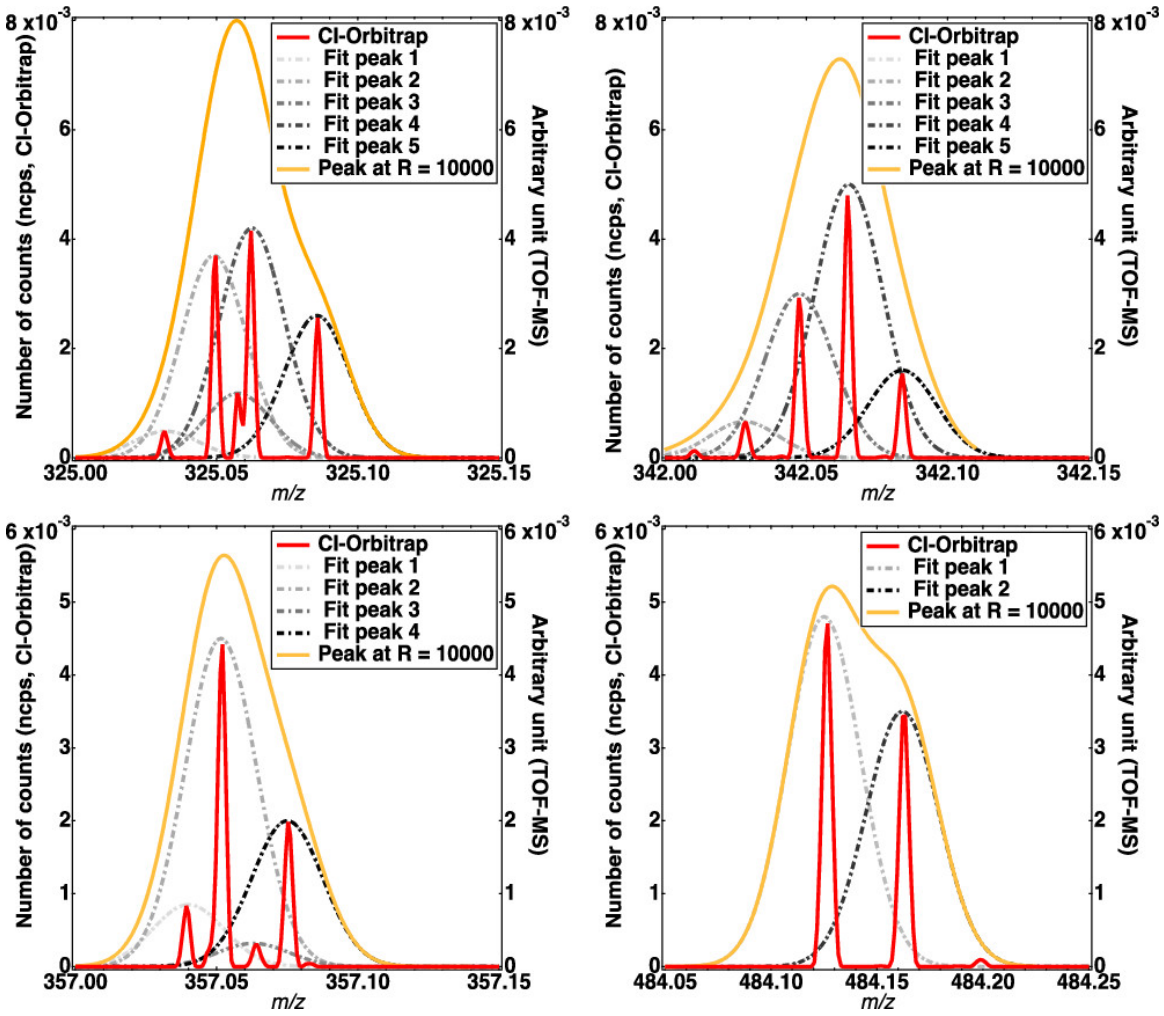

Figure 1.6 Mass spectra (red) of different HOM, at m/z 325, 342, 357, and 484, measured by a NO3-CI-Orbitrap during limonene ozonolysis. The orange trace represents the spectrum that would be observed using an instrument with mass resolving power of 10000. Dashed lines stand for the fits of individual ions. The TOF-MS signals represent synthetic data using arbitrary units and do not aim at matching the surface area measured using the CI-Orbitrap. Reproduced with permission Riva et al. 2019. Copyright 2019 American Chemical Society.

1.3.2 Ambient Ionization Techniques Designed for Aerosol Analysis

Ambient ionization usually refers to ionization methods in which molecules are ionized in their native environment, typically for condensed-phase samples in air. In the past, many ambient ionization mass spectrometry techniques were employed based on physical-chemical processes such as laser ablation, thermal desorption and vibrational excitation, enabling analysis of environmental samples.[179] In atmospheric chemistry, especially for aerosol research, ambient ionization mass spectrometry techniques are used to ionize molecules in aerosols directly in the air, allowing for nearly real-time sampling and the subsequent analysis for aerosol molecular chemical composition without sample collection, preparation or extraction.[44, 179] Recently, real-time and direct aerosol mass spectrometry analysis with soft ambient ionization has made large progress, such as extractive electrospray ionization (EESI) and direct analysis in real time (DART). The key advances of these soft ambient ionization mass spectrometry techniques are summarized in this section.

1.3.2.1 Electrospray ionization (ESI)-based techniques

EESI-MS. ESI is a well-known technique that uses electrospray to ionize polar molecules under high voltage and transfer the ions from solution phase into the gas phase as the sprayed microdroplets evaporate. As described in the Introduction, the early applications of ESI-MS in aerosol research were mostly through direct infusion of liquid samples after aerosol collection and extraction.[69, 180] The EESI technique combines ESI with online aerosol measurement as the simplified configuration shows in **Figure 1.7A**.[76,

[77, 181-183] Gas-scrubbed aerosol samples can be directly introduced into the EESI inlet, where the sample flow collides with a charged and stable solvent electrospray plume to be extracted into the bulk electrospray, which is generated by the potential difference between an ESI probe and the mass spectrometer inlet (**Figure 1.7A**). The electrospray solution is usually doped with a strong ionic compound such as sodium iodide to promote ionization by providing stronger adducts and reference signals for mass calibration.[184, 185] The angle and the distance between aerosol sample flow, the ESI probe, and the mass spectrometer inlet could be optimized for best ion signals. The aerosol molecules are ionized and ejected into the gas phase by the rapid evaporation of electrospray solvent through the Coulomb explosion mechanism.[186] Then aerosol samples enter a heated ion capillary to ensure the evaporation of electrospray droplets during the ~1 ms capillary transit before mass spectrometry analysis. Finally, the generated molecular ions are detected by a mass analyzer to obtain real-time aerosol composition measurements at a near-molecular level.[187] The reported detection limit using recently developed sensitive EESI-MS is typically on the order of 1 to 10 ng m^{-3} in 5 s.[182, 183]

EESI-MS provides a controlled ionization scheme to avoid the reliance of the conventional methods on thermal desorption, fragmentation causing by hard ionization or separated collection-extraction-analysis stages.[188-190] Although EESI-MS showed significantly different sensitivity towards different organic compounds by up to a factor of 30, the ion signals of a respective compound exhibit a linear response to compound mass over several orders of magnitude, highlighting the potential benefits of EESI to quantify atmospheric aerosols.[182, 183] According to ambient measurements, potential factors

affecting the instrument response, including the soluble inorganic matric, varied water vapor and largely varied particle sizes, only slightly disturb the aerosol detection and analysis.[169, 182, 183] With the increasing needs of using soft ambient ionization mass spectrometry methods to perform real-time measurements and quantitive characterization of aerosol compositions at the molecular level, EESI-MS is expected to provide comprehensive analysis of atmospheric aerosol species.[191, 192] For example, EESI-MS is promising as an alternative of the offline LC-ESI-MS to measure key atmospheric SOA tracers such as organosulfates in real time.[193] EESI-MS also exhibits a quantitative capability to monitor the dynamic concentrations of individual compounds in mixed organic-inorganic particles during the formation and aging of SOA, meanwhile proving a near molecular-level measurement with high resolution.[183] Furthermore, EESI could combine high time resolution, high resolving power, and detailed structural analysis to provide in-depth understanding of atmospheric chemistry. For instance, Lee et al. have developed an EESI inlet coupled to an Orbitrap to acquire molecular composition of the aerosol components at atmospherically relevant concentrations with ultrahigh mass accuracy and resolution, meanwhile shown the instrument's ability to perform online tandem mass spectrometry analysis.[187]

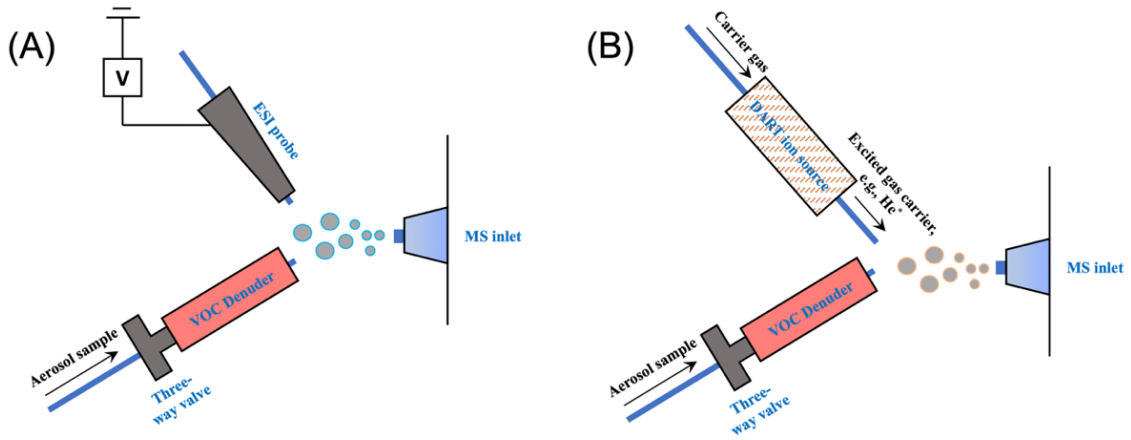

Figure 1.7 Schematics of (A) EESI and (B) DART ion sources interfacing with mass spectrometry.

ESCI-MS. Zhao et al. recently presented a new *in-situ* electrospray chemical ionization mass spectrometry (ESCI-MS) technique by coupling an ESI source to a time of flight mass spectrometer (TOF-MS), for the detection of atmospheric inorganic and organic species in the gas phase.[184] The electrospray is achieved by generating spray droplets via a high voltage power supply. The salt solutions dissolved in methanol are emitted through a fused silica spray needle housed in a cylindrical evaporation tube and are carried out by a flow of ultra-high-purity N_2 gas to the IMR, followed by a stainless-steel capillary tube which act as atmospheric pressure interface between the IMR and the mass spectrometer. Any unevaporated droplets are moved out of the effective ionization region by reagent ion source flow, excluding the interference of secondary or extractive ESI. Thus, the sample molecule reacts with the reagent ion to form an ion-molecule adduct via ligand switching reactions under atmospheric pressure in the IMR. This ESCI technique provides an extended option for both ESI-MS and CIMS applications in measurements of a broad range

of atmospheric compounds. Using I^- as the ESCI reagent ion under atmospheric pressure ionization showed high sensitivity for $RO_2^\bullet$, allowing for probing specific $RO_2^\bullet$ chemistry.[194]

PS-MS. The PS ionization mass spectrometry (PS-MS) is a variant of ESI-MS, allowing for direct and indirect detection of dissolved compounds on aerosol filter samples under ambient temperature and pressure.[73] It has been regarded as a promising offline technique to provide quick and effective filter sample analysis with quantitative capabilities in ambient measurements.[195] The paper substrate is soaked or continuously saturated with apposite solvent matrix to generate an electrospray plume from the paper tip under a certain high voltage.[73, 196] The typical PS-MS analysis requires no sample preparation, where samples are directly deposited onto the substrate and analyzed by a mass spectrometer.[195] Recently, PS-MS has also been used in single droplet analysis, where the filter chromatography papers are cut into triangular piece and then attached to a high voltage power supply.[197, 198] Microdroplets are allowed to fall on the paper. During the formation and transportation process of the spray plume, the analytes in the microdroplets are ionized and transmitted towards the mass spectrometer inlet. Because deposition location of analyte droplets on the paper substrate impacts the instrument performance, the spray tip angle and substrate geometry are adjusted to obtain the reproducibility and time scale.[197-199]

1.3.2.2 other ambient ionization techniques

DART-MS. Among the non-ESI-based ambient ionization mass spectrometry for real-time aerosol characterization, direct analysis in real time (DART) is a plasma-based technique that excites ambient molecules into ions through corona discharge of a carrier gas, such as helium, argon or nitrogen.[179, 200] Among them, helium is one of the most frequently adopted carrier gas because its electronically excited 2^3S state has 19.8eV of energy capable of ionizing atmospheric molecules.[201] The excited gas carrier containing metastable atoms flow out of the source to thermally volatilize and ionize analyte molecules which are directly introduced into the ionization region between the DART ion source and the mass spectrometer inlet (**Figure 1.7B**).[79, 179] The heated gas can improve the instrument sensitivity by increasing the surface desorption of analyte samples.[202] The metastable carrier gas atoms can react with atmospheric water and oxygen molecules to produce a secondary ionizing species such as protonated water clusters (H_3O^+) and molecular oxygen ions (O_2^+) which could ionize sample molecules to form $[M+H]^+$ in the positive mode, and superoxide anions (O_2^-) which incite analytes to $[M-H]^-$ and M^- ions in the negative ion mode through ion-molecule reactions.[79, 203, 204] Analytes with low ionization energy could be ionized directly during the process.[205] In recent years, DART-MS has been commonly used to measure aerosol components in multiphase chemistry, such as studying the uptake of gaseous hypochlorous acids,[206] $OH^•$,[205, 207, 208] and O_3,[204, 209, 210] on aerosol particles, contributing to the understand of the reaction kinetics and chemical mechanisms of OA aging.

AeroFAPA-MS. The aerosol flowing ambient-pressure afterglow (AeroFAPA) is another plasma-based soft ambient ionization mass spectrometry used in atmospheric research for real-time characterizing the molecular composition of complex aerosol matrices.[44, 211-213] This source is based on a helium glow discharge plasma to excite and ionize helium species as the primary reagent ions.[44] The helium discharge gas can directly desorb and ionize a large range of OA compounds at atmospheric pressure within its high-energy metastable state for mass spectrometry detection in the afterglow region. The particle-phase analytes need to have a certain volatility to be ionized during the temperature-driven desorption process. Besides, the usage of helium source allows for longer lifetime of the ion source electrodes due to its low sputtering activity. Similar to the DART source, the AeroFAPA technique utilizes ambient O_2 and H_2O to produce O_2^- ions through the interaction of thermal electrons and subsequently ionize aerosol molecules to form negatively charged analyte ions.[214] In addition to O_2^- ions, the signals of other reagent ions, like O^-, OH^-, HO_2^-, O_3^-, NO_2^-, and NO_3^- ions are observed in the negative mode.[211, 215] On the other hand, in the positive-mode measurements, the presence of O_2^+, N_2^+, NO^+, O_2^+, NO_2^+ as well as protonated water clusters has been reported, and these reagent ions are produced via the charge-transfer reactions between the AeroFAPA source with N_2 and H_2O molecules in the air.[215]

Ambient ionization mass spectrometry ***without external energy.*** A few ambient ionization mass spectrometry methods were recently employed to study OA composition that do not require external energy such as high voltage or heating. Sonic-spray ionization (SSI) is one of these methods.[216-218] In SSI, the mechanical action of sheath gas flow

approaches sonic velocities and generates excess charges on aerosol particles and droplets, leading to gas-phase ions. In a recent study by Wingen and Finlayson-Pitts, this method was applied to solid particles with core-shell morphologies.[218] SSI turned out to be surface-sensitive and was used to probe the surface composition of laboratory OAs. Similar to SSI, droplet-assisted ionization (DAI) as an inlet ionization technique has been recently developed for online aerosol characterization, with the advantage of no need for sample preparation or high voltage utilization.[219] The inlet interface consists of a temperature-controlled stainless-steel capillary tube. The analyte-doped droplets within water matrix are charged when they pass through the capillary from atmospheric pressure into a vacuum, and then gas-phase molecular ions are produced after these droplets undergo aerodynamic and/or thermal breakup due to pressure and temperature gradients.[219-222] DAI-MS has been applied in characterization of airborne nanoparticles[222] and the molecular components of α-pinene SOA including HOM monomers and dimers with oxygen atom number as high as 14.[219] Another soft ambient ionization mass spectrometry method without coupling to an external ionization source named inlet or vacuum ionization has been developed to study aerosol surface composition.[223] In a recent work reported by Qin et al., a triple quadrupole mass spectrometer is used to monitor aerosol interfacial molecular composition without an ion source.[224] Instead, the sublimation of solid core materials (e.g., glutaric acid) in the particles leads to the ejection of molecular ions of the surface compounds. By comparing the mass spectral intensities of core and surface materials under different coating thicknesses, the proposed ionization scheme was verified. These surface-sensitive

approaches were also found to have minimal decomposition of the analyte, providing new paths for understanding the surface composition of atmospheric aerosols.

1.3.3 Novel coupling of separation techniques and mass spectrometry

Despite that the greatly improved mass spectrometry techniques for atmospheric chemistry in the past few years have enabled lower detection limits, higher mass and time resolutions, and more comprehensiveness, structure identification and isomer separation are still challenging for mass spectrometry by itself. Tandem mass spectrometry is useful to study chemical structures for targeted analysis, but to resolve the structural/isomeric information of complex and unknown atmospheric species in a non-targeted fashion, mass spectrometry needs to be coupled with separation techniques. Column-polarity based methods (e.g., GC and LC) are well-established separation techniques to characterize atmospheric species on the isomer-resolved level. In addition, ion mobility spectrometry (IMS) separation coupling to mass spectrometry has been recently shown as a promising approach in aerosol research. In this section, we review new advances on GC, LC, and IMS coupled to mass spectrometry.

1.3.3.1 GC-CIMS

GC can separate and quantitatively characterize chemical components in complex mixtures with structural information. However, previous GC analysis usually requires sample collection and preconditioning steps, and the separation effectiveness for certain chemical classes largely relies upon the column selection.[225] The traditional GC-MS uses

either the hard EI ionization, or the relatively softer chemical ionization with reagents such as methane.[18, 226, 227] In the past several years, the development of CIMS with a variety of ionization methods led to the emergence of coupling GC and CIMS in new fashions, to provide near real-time isomer identification and quantification.

In the recently developed real-time GC-CIMS by the Wennberg group at Caltech which focused on polar oxygenated VOCs,[228-233] the sampling gases are firstly collected on the head of an RTX 1701 GC column cooled to a desired temperature using an isopropanol bath or liquid CO_2. Then analytes elute in an order depending on their polarity and are separated by the retention time. The GC eluates are diluted by carrier N_2 gas and transmitted to the IMR region of CIMS that uses CF_3O^- as the reagent ion (see 1.3.1.2). The GC-CF_3O^--CIMS can determine important atmospheric isomeric components, such as isoprene epoxydiols (IEPOX)[228] and organonitrates.[229, 230, 233-235]

Recently, Bi et al. coupled a thermal desorption aerosol gas chromatograph (TAG) to CIMS to expand GC-CIMS capability to also measure particle-phase compounds.[236] The TAG is a custom-built instrument including a sampling cell, an automatic liquid injection system and pre-separation process of a polar GC column.[237-239] In TAG-CIMS, aerosol samples are collected by the sampling cell while chemical standards are injected into the cell automatically by a liquid injection program. These compounds are thermally desorbed in helium to the column head and are separated by passing through the GC column. Moreover, the analytes may be derivatized to improve transmission efficiency and stability for the analysis of oxygenated organic compounds.[240] By coupling a TAG to a CIMS, the mass resolution of individual molecules is enhanced at the cost of extended analysis time.

Bi et al. further developed a multi-reagent ionization mode for TAG-CIMS in which I^- and zero air are both used as reagent gases.[236] This mode could determine additional chemical species by the high abundance of non-adduct ions without losing the original advantage to use I^- clusters to identify oxygenated compounds.

1.3.3.2 New methods based on LC-MS

Similar to GC-MS, LC-MS is another well-established analytical chemistry technique to combine the separation of dissolved aerosol mixtures by liquid chromatography (LC) and the mass analysis capabilities of molecularly resolved information provided by mass spectrometry. A LC-MS system equipped with an ESI and/or an atmospheric pressure chemical ionization (APCI) source is extensively used for molecular-level characterization and analysis of polar or water-soluble organic molecules commonly found in complex samples of atmospheric aerosol.[65, 66, 241-246]

Iodometry-assisted LC-MS. Organic peroxides have been shown to account for a major fraction of SOA.[247-252] In traditional studies, quantification of organic peroxides was achieved by using spectroscopic techniques coupled with iodometry. However, this method only determines total organic peroxide molar mass. Molecular characterization cannot be achieved using this approach, hindering the understanding of the organic peroxide composition. Recently, Zhao et al. combined the iodometry with LC-ESI-MS and showed that by comparing the peaks in the LC-ESI-MS with and without the iodometry treatment, specific organic peroxide species in SOA can be identified with molecular and sometimes structural information.[253, 254] In this approach, the collected SOA samples on filters are first

extracted using traditional methods.[66, 69] The extract solutions are subsequently divided into two aliquots of which one is treated with iodometry and the other without, and the concentration of a peroxide compound is achieved by comparing the signals of ions with the same retention time according to the base peak intensity chromatograms. The iodometry-assisted LC-ESI-MS were furthered used for isomer-level identification and characterization of organic peroxides from monoterpene SOA,[255-257] as well as for kinetics and chemical aging of isomer-resolved peroxide hydrolysis in aqueous-phase.[258]

LC-MS with HILIC column. Another recent development of LC techniques is to use a hydrophilic interaction liquid chromatography (HILIC) to study polar hydrophilic species in aerosol chemistry. Traditionally, reverse-phase liquid chromatography (RPLC) has been a popular method to detect polar and water-soluble components. However, RPLC measurements are extremely limited by its performance in short retention times, ion suppression effects or poor peak shapes. It has been proved that HILIC could effectively separate water-soluble organosulfates, showing its potential to identify and quantify isoprene SOA constituents.[259-261] In the study by Cui et al., an ultra-performance liquid chromatography (UPLC) with a HILIC column is interfaced to ESI-MS to measure water-soluble IEPOX-derived SOA isomers in the negative mode.[262] The UPLC parameters, such as buffers, pH values, and column temperatures, can be optimized to increase the sensitivity. The mobile phases are composed of eluents containing ammonium acetate and water, sometimes ACN, of which the eluent pH is adjusted to 9.0 with NH_4OH buffer. The column is held at a constant heated temperature (~ 35 °C). The relatively low temperature used in the HILIC method reduces the decomposition of organosulfates and other IEPOX-derived

components, improving its ability to distinguish water-soluble isomers and evaluate SOA yields in isoprene-rich regions.

1.3.3.3 IMS-MS

IMS as a powerful analytical technique has gained attention and prominence for separating structural isomers that have different molecular shapes over the last 20 years.[263, 264] But only very recently, this technique started to be applied in the field of atmospheric chemistry to separate and detect both gas- and particle-phase atmospheric constituents on the isomeric level.[265-270] In the drift-tube based IMS, ionized molecules can be separated based on their ion mobilities which arises from their collisional cross sections (CCS) and ion-molecule interactions in an inert carrier buffer gas (e.g., He or N_2). An ionization source (usually ESI and APCI) can generate charged analytes of interest under controlled pressure and temperature, and the ions are then separated in the IMS drift tube.[267-269, 271-275] The IMS drift tube is followed by a pressure reduction interface, after which ions are transmitted into the mass analyzer.[264]

The recently developed IMS-MS by Tofwerk Inc. and Aerodyne Research Inc. uses the TOF mass analyzer, similar to their TOF-CIMS configuration (see Chapter 1.3.1). Between the IMS and the TOF, the potential differences between the two quadrupoles are used for collision induced dissociation (CID) analysis where molecular ions are fragmented and weakly bound ion clusters are dissociated.[276] The resultant fragmentation mass spectrum is similar to traditional tandem mass spectrometry measurements but providing additional information of relationships between precursor ions and fragment ions as well

as spectra over the entire mass-to-charge range.[265] IMS-MS measurements are not constrained by solvent or stationary-phase like traditional LC or GC, but still allow for the ability to distinguish organic species with different structures. The drift times are instrumental-dependent value which are transferable under the same buffer gas and temperature conditions, so that the measured CCS therefore are comparable to provide structural information.[265]

Another recent application of IMS-MS was used in the real-time analysis of aerosol particles in prebiotic chemistry with a vacuum-assisted plasma ionization (VaPI) source to ionize organic molecules.[277] The VaPI ion source utilizes a glow discharge at near atmospheric pressure to generate heated plasma gases. The aerosols sampled by a sampling tee collide with the plasma gas to be chemically ionized through proton transfer reactions. Then ions of interest are transferred from the sampling tee to an IMS-MS instrument for real-time analysis. Besides, the signals of oligomer clusters formed from ion-molecule reactions are observed in real time, indicating the high reactivity of the VaPI source to provide new insights into the prebiotic aerosol chemistry.

1.4 Applications of the New Mass Spectrometry Techniques in Atmospheric Chemistry Research

The advances in mass spectrometry techniques described above are crucial for understanding the molecular and even isomeric compositions of complex atmospheric components in both the gas and particle phases and help elucidate the processes that lead to the formation and evolution of atmospheric organic species.[7, 153, 278] In the forthcoming

section, we summarize the recent applications of these techniques to highlight the key progress in the characterization and identification of a broad range of organic species in atmospheric chemistry.

1.4.1 Detection of atmospheric VOCs from traditional and emerging sources

VOCs are ubiquitous in the Earth's atmosphere. Speciation and quantification of VOCs are thus critical for understanding their emission sources, oxidation chemistry, and impacts on air quality and climate. PTR-MS is a key technique to quantitatively and sensitively measure a large variety of VOCs in real-time. The design and performance of PTR-MS have been extensively reviewed in previous publications.[47, 279] The sensitivities to different VOCs increase linearly as a function of the proton-transfer reaction rate, illustrating the quantitative ability of PTR-MS to atmospheric gas tracers.[102, 280] Yet, some VOCs under ambient conditions may have very low concentrations (e.g., pptv or even sub-pptv levels), for which detection and quantification are still challenging. In this section, we will mainly focus on specific applications of the new versions of PTR-MS, namely Vocus and PTR3, in laboratory investigation and field work of atmospheric organic vapors and show their comparison with conventional PTR-MS.

With the greatly improved sensitivity and resolving power, the Vocus PTR-TOF allows for better quantification for VOCs with high molecular weight (e.g., *m/Q* 150–300 Th) than traditional PTR-TOF (**Figure 1.4**).[15] It has been recently used to characterize and quantify VOCs and their oxidation products in both laboratory studies and field measurements.[102-105, 164, 281, 282] For example, in the first study of VOCs in forested regions

using Vocus PTR-TOF, abundant terpene-derived VOCs consisting of comprehensive elemental composition classes with CH, CHO, CHN, CHS, CHON, CHOS were reported, while oxygenated products with carbon numbers of 5–10, 15, and 20 are dominant among the hydrocarbon categories.[283] The low-volatility diterpenes was observed in real time in ambient air for first time using Vocus PTR-TOF at 2 ppt level. Vocus PTR-TOF can also efficiently detect the less oxidized organic nitrates and other nitrogen-containing organic compounds,[284] such as the product of alkyl nitrite photolysis (Nihill et al., 2021) and the organic nitrates from aromatic VOCs oxidation under varied NO_x conditions (Mehra et al., 2020). Besides the detection of atmospheric VOCs from traditional biogenic and anthropogenic sources, Vocus PTR-TOF has also shown promising capability to study VOCs from emerging sources such as the volatile chemical products (VCP) and wildfires.[285-287] In addition, Vocus PTR-TOF has allowed for the quantitative source attribution of indoor VOC emissions.[288, 289] For instance, it is applied in the detection and quantification of numerous products from human skin ozonolysis,[290] the quantitative analysis of metabolic exhaled breath,[291] the dark production of potentially toxic cyanogen chloride during blench cleaning process,[292] and the examination of VOCs and crystal monomers released from liquid crystal display screens.[289]

Very similar to Vocus PTR-TOF, PTR3 is well suited to detect atmospheric VOCs due to its high sensitivity to atmospheric trace gases, resulting in one of its widest usages to monitor the gas-phase reactant precursors in the new particle formation (NPF) studies. For example, PTR3 has been used in NPF studies through monitoring the gas-phase reactant concentrations of isoprene,[293, 294] monoterpenes[107, 294-297] and other VOCs[105, 107,

[298, 299]. In α-pinene ozonolysis experiments conducted in the CLOUD chamber, PTR3 shows good agreement of oxidation products with a NO_3^--TOF-CIMS.[106, 139] In this study, over 1000 formulas were obtained by PTR3, showing a detection range for broader volatility compound species with much higher sensitivity to α-pinene and monomeric and dimeric oxidation products (**Figure 1.8**).[106] Further, as mentioned above, Zaytsev et al. developed a novel instrumentation based on PTR3 with switching regent ions of H_3O^+ and NH_4^+ for qualitative and quantitative measurements of VOCs with a large range of volatilities.[97] This technique was used to detect and quantify both ring-retaining products and ring-scission products derived from a series of toluene and 1,2,4-trimethylbenzene photooxidation, while the H_3O^+ mode is more sensitive to less oxidized molecules but NH_4^+ to larger and more functionalized compounds.[164]

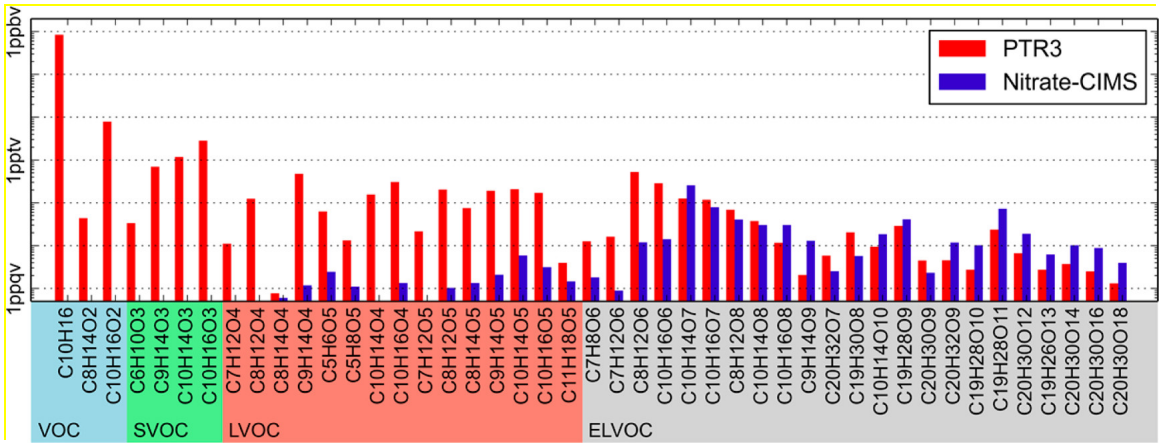

Figure 1.8 PTR3 (red) and NO_3^--TOF-CIMS (blue) results from an ozonolysis experiment of 1 ppb α-pinene and 40 ppb ozone at the CLOUD chamber at 5 °C and a relative humidity of 38%. Exact masses were used to assign sum formulas that are organized as a function of saturation vapor pressure ranging by volatilities. Reproduced with permission Breitenlechner et al. 2017. Copyright 2017 American Chemical Society.

1.4.2 Highly Oxidized Molecules (HOMs)

The HOMs are a class of organic compounds containing six or more oxygen atoms with high O/C ratios, usually formed via autoxidation chemistry involving $RO_2^{\bullet}$ in the atmosphere.[139, 153, 300] They consist of a wide range of chemical functional groups (e.g. −OH, =O, and −OOH) and may be key components of atmospheric SOA after partitioning to the particle phase due to their extremely low volatility.[152, 301, 302] In this section we will review recent studies that applied the above-described mass spectrometry techniques to characterize and quantify HOMs.

Because HOMs are formed from $RO_2^{\bullet}$ autoxidation, it is thus important to detect not only the closed-shell HOMs themselves, but also the HOMs-$RO_2^{\bullet}$. This was shown to be feasible by using CIMS with NO_3^-, $CH_3C(O)O^-$, I^-, Br^-, NH_4^+, and pronated amines as the reagent ions (see **Table 1.1**).[131, 148, 149, 151, 153, 164, 298, 303] Among these methods, NO_3^--CIMS has the highest selectivity to HOMs with high number of oxygens and was the first technique developed for HOMs detection.[152, 153, 302, 304] It observed HOMs formation from oxidation of monoterpenes,[50, 134, 153, 302] isoprene,[117, 302] aromatic VOCs,[151, 305, 306] and other VOCs[134, 304, 307]. Initial studies using NO_3^--CIMS, concluded that HOMs are formed at higher yields in monoterpene ozonolysis, but not in $^{\bullet}$OH oxidation.[153] However, later studies by Berndt et al. found that $^{\bullet}$OH oxidation of monoterpenes also produces high yields of HOMs, which can be more sensitively detected by $CH_3C(O)O^-$—CIMS.[152] This results also suggest that CIMS with different ionization methods may lead to distinct sensitivities for different HOMs molecules. In addition, Br^- and I^- are the other two reagent ions to couple with CIMS and measure HOMs.[151, 166, 194, 267, 298] They are less selective than

NO_3^- and $CH_3C(O)O^-$. Further, NH_4^+-CIMS is the least selective method among the mentioned ion chemistries which measures a wide range of species from hydrocarbons to HOMs.[148] Consistently, the new NH_4^+ PTR3 has been shown to be more sensitive to HOMs with low volatility in the atmosphere than a typical PTR-TOF.[106] Lastly, protonated amines as the reagent ions have been used to measure HOM dimer formation from $RO_2^\bullet$ cross reactions in the oxidation of α-pinene[150] and 1,3,5-trimethylbenzene[131].

In addition to CIMS, Zhao et al. applied different reagent ions (e.g., I^-, NO_3^-, $C_2H_3O^-$, Li^+, Na^+, K^+, and NH_4^+) to the ESCI-MS, and compared the obtained gas-phase chemical composition including HOMs from α-pinene ozonolysis with typical CIMS.[184] They concluded that ESCI-MS with I^- as reagent ions have high sensitivity, comparable to the I^--CIMS. It was also found that monomeric products ($n_C \leq 10$) are evident in all ion modes, but most dimeric products are only observed in the Na^+ ion mode. Besides, the reagent ion Na^+ is more sensitive to less oxidized species ($n_O \leq 3$) than I^- or NO_3^-, consistent with the observations in previous studies.[52, 308, 309] CIMS with both I^- and NO_3^- could detect HOMs with similar oxygen contents, while the different signal intensities might be caused by the identities and locations of the functional groups.[52, 152] In a later study, Zhao et al. used I^--ESCI-MS coupled with a LTOF device to detect HOMs derived from α-pinene ozonolysis, including 150 gaseous dimers identified as $C_{16–20}H_{24–34}O_{4–13}$ which contribute to 5–60% of SOA mass yields.[310]

Besides the measurements of gaseous HOMs using CIMS with the above-mentioned reagent ions, CIMS can be coupled with a FIGAERO to detect the condensed HOMs in the particle phase.[165, 166, 311, 312] For example, Mohr et al. reported an ambient

observation in Finland that a large variety of dimers with $C_{16–20}H_yO_{6–9}$ were formed from monoterpene oxidation in both the gas and particle phases by employing $CH_3C(O)O^-$ and I^- as the reagent ions in FIGAERO-CIMS.[166] In this study, the total dimer concentrations were quantified in the two phases on the same order of magnitude and estimated a dimer contribution of 5% to the early stage of particle growth, highlighting the importance of HOMs condensation for aerosol growth. In addition to the FIGAERO-CIMS measurements, ESI-based techniques have also been used to monitor HOMs in the particle phase, both in real time and offline. Specifically, EESI-MS has been used to characterize HOMs in SOA from α-pinene ozonolysis as well as the real-time degradation of individual monomer and dimer HOMs species to investigate the effect of HOMs on the SOA evolution (**Figure 1.9**).[185] Through the online EESI-MS characterization of SOA composition, this study further proposed that particle-phase reactions such as the decomposition of reactive oxygen species and the evaporation of volatile carboxylic acid play an important role in the SOA aging.[313] Lee et al. used EESI-MS to measure the monomer and dimer HOM distributions in α-pinene SOA, which showed good agreement with other particle-phase HOMs measurements using offline techniques.[139, 187, 219] Furthermore, in a Zurich field deployment of EESI-MS, a similar result of dominant factors and mechanisms in the oxidation of monoterpenes has been reported to be consistent with NO_3^--CIMS measurements of gas-phase HOM formation in a Finland forest.[314, 315] Finally, organic nitrate HOMs were observed in the $NO_3^\bullet$-derived α-pinene SOA using both FIGAERO-CIMS and EESI-MS, suggesting their large contribution to SOA aging.[316, 317]

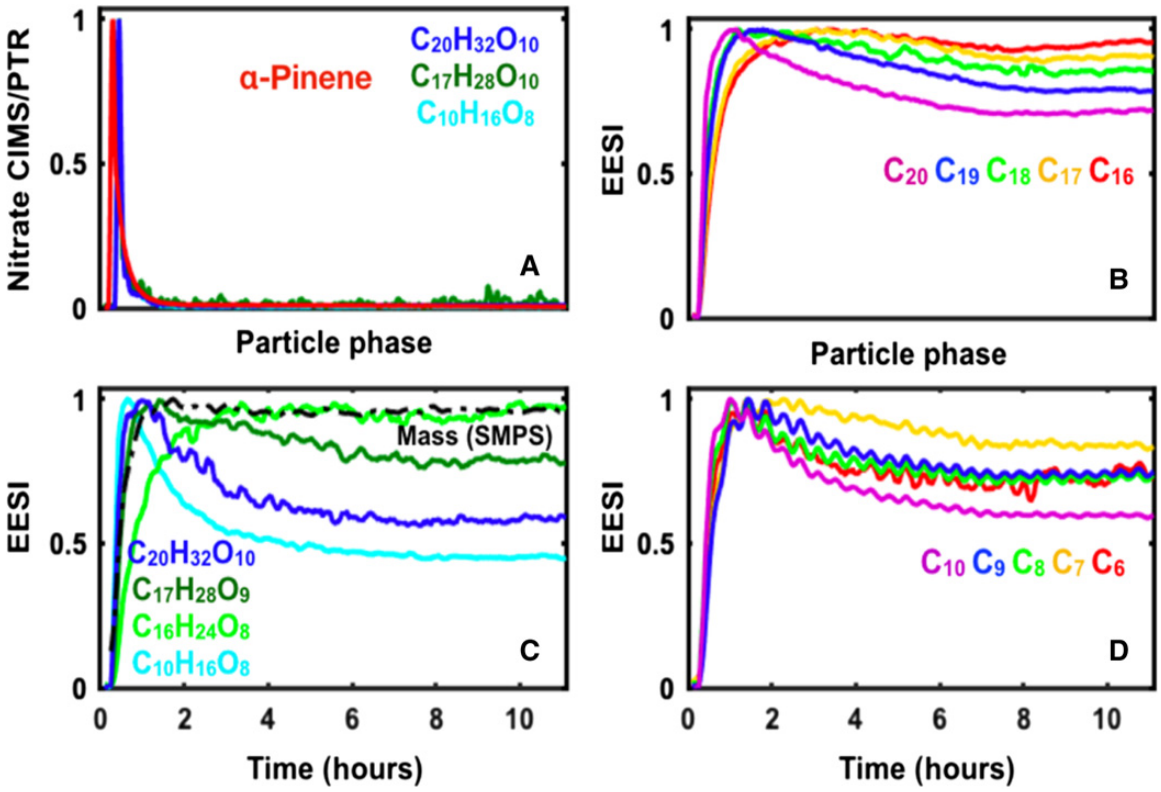

Figure 1.9 Time evolution of particle and gas-phase composition for α-pinene ozonolysis. (A) α-Pinene injection into the chamber (~ 35 ppbv) measured by PTR-TOF and gas-phase evolution of its oxidation products measured by NO_3^--TOF-CIMS. (B) Time evolution of particle phase dimers, grouped by their carbon number. (C) Time evolution of three dimers and one monomer measured in the particle phase showing very distinct behavior despite similar saturation vapor concentration. (D) Time evolution of particle phase monomers, grouped by their carbon number. All signals are normalized to the maximum EESI-MS signal recorded for the respective ion during the displayed period. Reproduced with permission Pospisilova et al., 2020. Copyright 2020 Pospisilova et al.

Other than the CIMS and EESI applications, recent developments in the combination of separation methods with mass spectrometry have also enabled new findings on HOM formation and composition. Krechmer et al. employed IMS-MS with the NO_3^- chemical ionization source for online measurements of gas-phase HOMs derived from α-pinene and limonene oxidation, meanwhile the number of isomers for each HOM formula is obtained by drift times.[265] Zhang et al. present the characterization of α-pinene derived HOMs in the form of $C_{8–10}H_{12–18}O_{4–9}$ monomers and $C_{16–20}H_{24–36}O_{8–14}$ dimers using IMS-MS with ESI.[318] In this work, through the application of CID to fragment dimer ions after mobility separation, the fragmented monomer ions with the same drift time can be determined; hence, IMS-MS enables the investigation of HOM dimer structures (**Figure 1.10**). Zhao et al. coupled IMS-MS with I^--CIMS analysis to separate and identify isomeric HOMs from α-pinene ozonolysis, and proposed an autoxidation rate of 20-fold faster of ring-opened $C_{10}H_{15}O_4$ $RO_2^\bullet$ than the ring-retained ones which are produced simultaneously in α-pinene ozonolysis.[267] Integrating IMS-MS and I^--CIMS measurements, Mayorga et al. observed a series of HOMs characterized as organic nitrates and nitrooxy $RO_2^\bullet$ derived from the oxidation of limonene, meanwhile emphasized a significant contribution of nitrooxy $RO_2^\bullet$ autoxidation and sequential $NO_3^\bullet$ oxidation to HOM yields.[319] Moreover, the iodometry-assisted LC-ESI-MS method was used to study the fate of peroxide monomers ($C_{8–10}H_{12–18}O_{5–8}$) and dimers ($C_{15–20}H_{22–34}O_{5–14}$) in SOA samples derived from α-pinene oxidation, demonstrating the potential of iodometry-assisted LC-ESI-MS to separate and identify HOMs that contain peroxide functional groups on the isomeric level (**Figure 1.11**).[255]

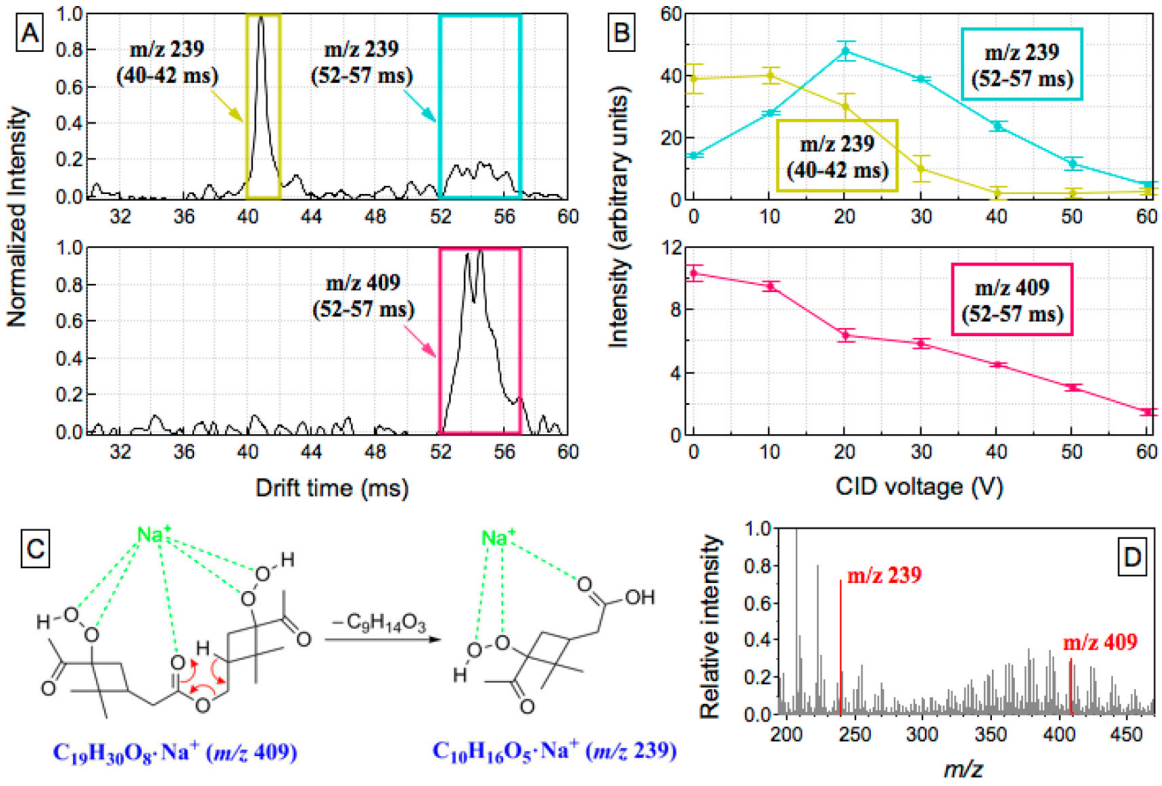

Figure 1.10 (A) Ion mobility spectra for one pair of precursor-fragment ion adducts as a representative example of the dimers from α-pinene ozonolysis. The ion adduct at m/Q 239 Th with a drift time of 40 – 42 ms is assigned to a monomer product ($C_{10}H_{16}O_5$) and the ion adduct at m/Q 409 Th with a drift time of 52 – 57 ms is assigned to a dimer product ($C_{19}H_{30}O_8$). The ion adduct at m/Q 239 Th with a drift time of 52 – 57 ms is assigned to the fragment ion from CID of its precursor ion at m/Q 409 Th. (B) Intensity profiles of these three ion adducts as a function of the collision energy, as characterized by the CID voltage. (C) Proposed McLafferty rearrangement for the CID of the $C_{19}H_{30}O_8Na^+$ dimer to the $C_{10}H_{16}O_5Na^+$ monomer. (D) Positive IMS-MS mass spectrum of SOA from α-pinene ozonolysis. Reproduced with permission Zhang et al. 2017. Copyright 2017 American Chemical Society.

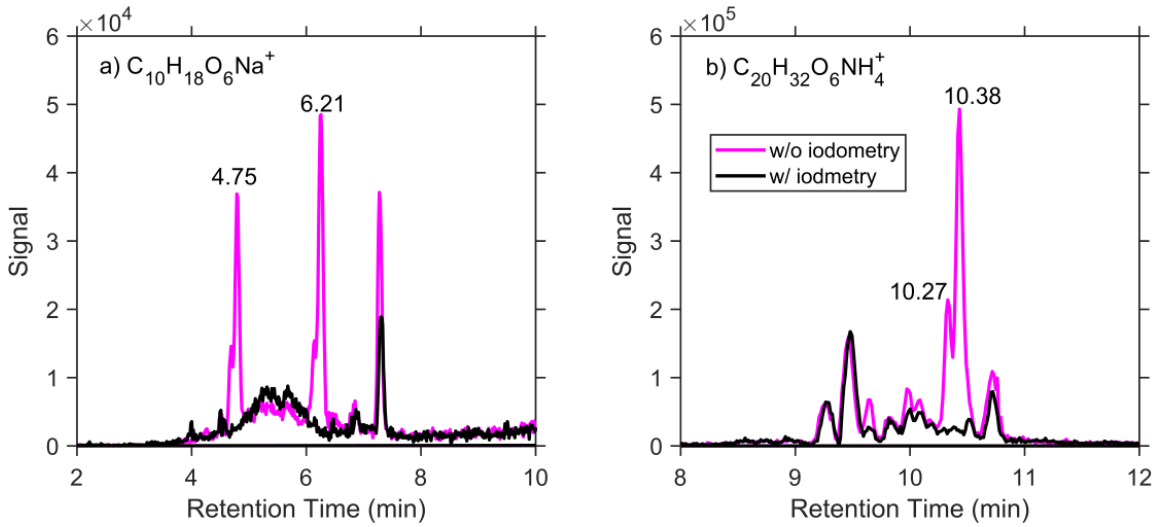

Figure 1.11 Extracted LC-ESI-MS ion chromatograms of (A) $C_{10}H_{18}O_6Na^+$ and (B) $C_{20}H_{32}O_6NH_4^+$ measured for SOA samples treated with (black) and without (magenta) iodometry. The isomer peaks of $C_{10}H_{18}O_6Na^+$ at 4.75 and 6.21 min and $C_{20}H_{32}O_6NH_4^+$ at 10.27 and 10.38 min are assigned to organic peroxides. Reproduced with permission Yao et al. 2022. Copyright 2022 American Chemical Society.

1.4.3 Real-time OA Bulk and Surface Molecular Composition

Real-time measurements of OA molecular composition have long been desired. Although thermal desorption methods coupled with CIMS have made this possible,[53, 320, 321] heating-induced artifacts have been a concern to interfere accurate interpretation of OA molecular composition. In contrast, the recently developed EESI-MS overcomes the issue and is able to perform online OA molecular composition without extensive heating.[40, 169, 182] Despite the ongoing debate of the ionization mechanism by EESI, it is often considered to measure the compositions of the aerosol bulk.[169] In recent EESI-MS studies, the spray solution is usually a mixture of water and methanol/acetonitrile, doped with ~100 ppm of a strong ionic compound like sodium iodide, such that analytes are detected as $[M + Na]^+$ adducts in positive mode and as $[M - H]^-$ ions in the negative mode.[169, 182, 187] EESI-MS quantification can be accomplished by performing mass calibrations of atomized aerosol particles, where ion abundance displays a linear response to mass due to the lack of matrix interference.[183, 189, 314] EESI-MS has been successfully deployed for ground-based ambient sampling, aircraft tests, and laboratory experiments, demonstrating its versatile applications and reliable performance in various environmental conditions.[169, 182, 313, 322-324] In an example of EESI-MS performance shown in **Figure 1.12**, the time series of levoglucosan and nitrocatechol measured by EESI-MS in wildfire smoke aerosols exhibited excellent agreements with other bulk aerosol measurements and gas-phase tracers.[169]

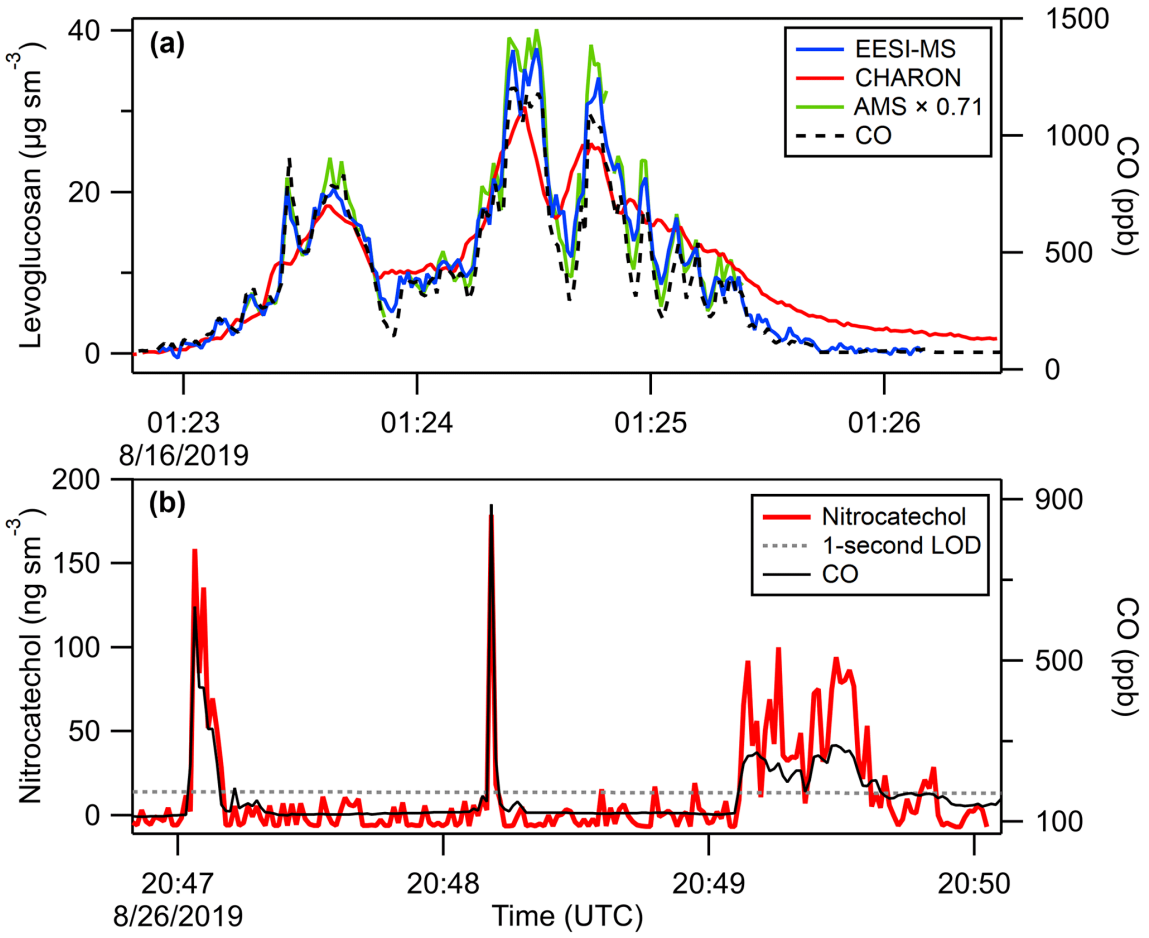

Figure 1.12 Examples of (A) levoglucosan and (B) nitrocatechol time series measured by EESI-MS from wildfire smoke aerosol, including comparison to CHARON PTR-MS and AMS (scaled by a factor of 0.71 to show temporal agreement). Carbon monoxide measurements are included to show the boundaries and structure of the smoke plumes. Reproduced with permission Pagonis et al., 2021. Copyright 2021 Pagonis et al.

Qi et al. and Stefenelli et al. presented some of the first ambient measurements using EESI-MS to characterize OA molecular composition in Zurich, a Switzerland urban site.[40, 314] In these studies, the real-time analysis for atmospheric aerosols on a near-molecular level was provided to determine the emissions sources and investigate physicochemical processes. Coupling the EESI-MS measurements with positive matrix factorization (PMF) analysis, these studies determined biogenic emissions as major and secondary sources contributing to OA mass during summer and winter, respectively. Furthermore, through combining with co-located measurements, various EESI-MS studies of the ground and aircraft aerosol samples provided valuable insights into the OA bulk properties and molecular composition, suggesting that the unban OA were mostly derived from oxidation of terpenes and aromatic hydrocarbons,[43, 325] biomass burning,[40, 169, 326, 327] cigarette smoke,[40, 326] and cooking emissions.[323] EESI-MS has also been applied in *in-situ* analysis of metals in aerosols. A wide range of ion adducts formed by the reactions between disodium ethylenediamine tetraacetic acid (EDTA) dihydrate and water-soluble metal compounds and trace elements were detected using the negative ion mode.[328] Moreover, EESI-MS was used in the indoor air studies for quantitative OA composition measurements. Brown et al. have detected over 200 unique indoor OA molecular species using EESI-MS, including fatty acids, carbohydrates, phthalates and low-volatility siloxanes, which are strongly consistent with the results from FIGAERO-CIMS and other techniques.[189]

In laboratory studies, researchers have used EESI-MS to measure the molecular composition and time series of oxidation products in α-pinene derived SOA in both positive and negative ion modes.[183, 185] Liu et al. have utilized EESI to measure the particle-phase

products formed from •OH heterogeneous oxidation of organophosphate flame retardants and liquid crystal monomers in real-time, to study their toxicological mechanism on photooxidation.[329, 330] Besides, EESI-MS was often combined with gas-phase analytical approaches to characterize the formation and evolution of SOA in laboratory research. Lamkaddam et al. demonstrated that over half of isoprene oxidation products partitioned into the cloud droplets and were further oxidized, leading to the formation of in-cloud aqueous SOA, by determining the particle bulk molecular composition using EESI-MS and the gaseous composition using PTR-TOF and NO_3^--CIMS.[331] Because of the capability to detect aerosols with a large range of particle sizes, EESI-MS has also been used to study the molecular composition of ultrafine particles as small as 20 nm from naphthalene or β-caryophyllene oxidation.[190]

In contrast to that EESI-MS is used in both ambient aerosol composition studies and laboratory SOA composition, the other ambient ionization mass spectrometry such as DART-MS has been more often used to measure laboratory aerosol composition in multiphase chemistry, such as the heterogeneous oxidation of model OA systems, including multifunctional carboxylic acids,[81, 207, 332-335] alkenes,[204, 206, 336] organosulfates[205, 208, 337, 338]. In most of these studies, the comprehensive molecular characterization of the oxidation products by DART-MS allowed for elucidation of the OA heterogeneous oxidation mechanisms. In addition, the quantitative nature of DART-MS measurements also make it possible to use the kinetic results to help understand the effects of aerosol phase state,[81] aerosol viscosity,[207] and organic-inorganic mixing[335].

In addition to the aerosol bulk composition, it is often important to also understand the surface composition of aerosol particles, especially when it is different than that of the aerosol bulk. The surface chemistry provides unique insights in aerosol formation and evolution, helping better understanding their impacts on air quality, human health, and atmospheric climate. In fact, the above-described DART-MS was first reported to be a surface-sensitive technique, when not assisted by sample vaporization.[79, 200, 207] For example, Zhao et al. studied the multiphase reactions between submicron diacid particles and gas-phase amines, proposing that DART-MS probes ~ 30 nm the surface layer of the particles.[184] Using this technique, the surface composition of SOA from α-cedrene oxidation were characterized (**Figure 1.13**).[184] Besides DART-MS, the ambient sonic spray ionization mass spectrometry and the inlet ionization mass spectrometry are also powerful approaches to uniquely identify the surface molecular components of OA in the atmosphere. Wingen and Finlayson-Pitts and Qin et al. has utilized these techniques to study the surface compositions of organic particles using model OA and SOA systems, providing new insights into aerosol surface composition, chemistry, and gas-particle interactions.[218, 224]

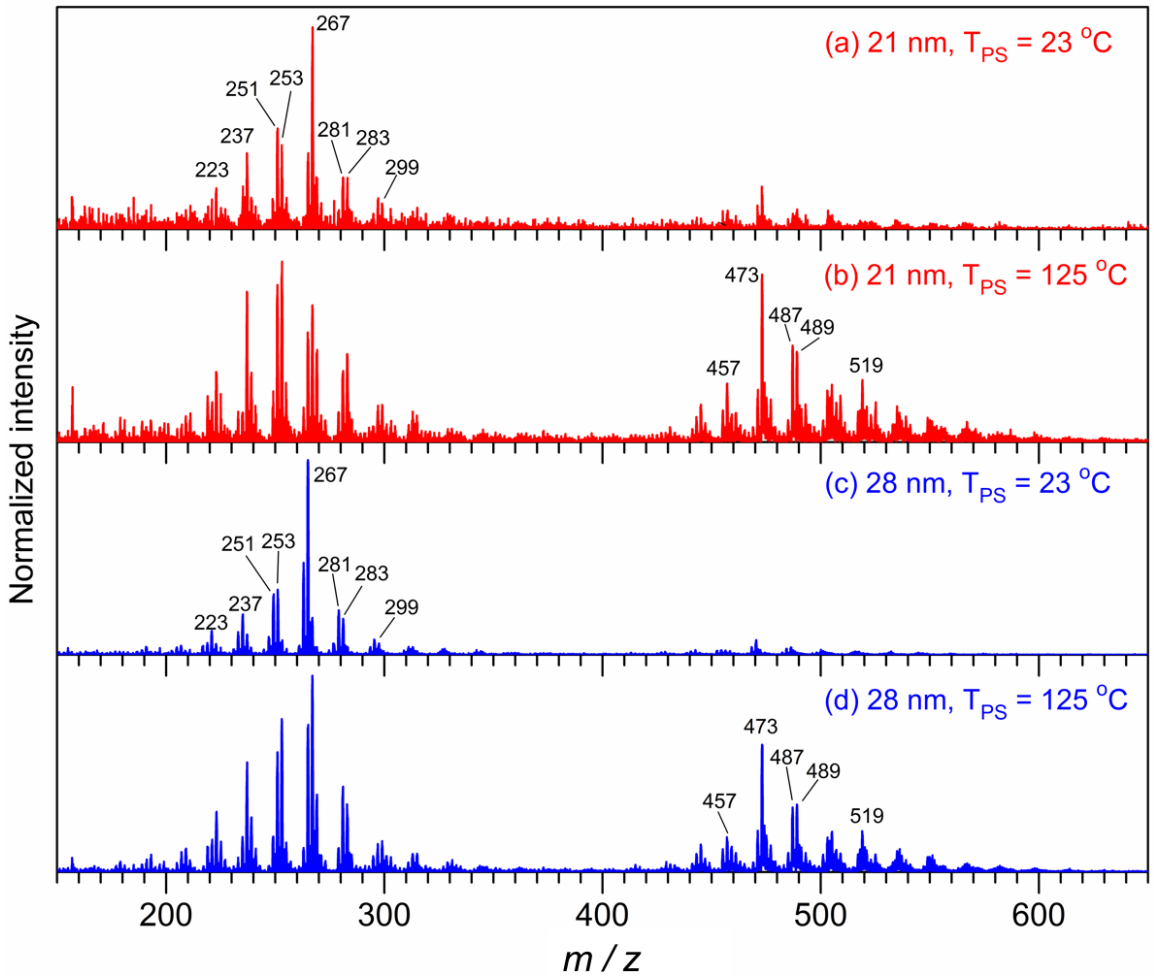

Figure 1.13 DART-MS mass spectra of polydisperse α-cedrene SOA particles with surface weighted geometric mean diameters of 21 nm (A–B) and 28 nm (C–D) at particle stream temperatures (T_{PS}) of 23 and 125 °C. Reproduced with permission Zhao et al., 2017. Copyright 2017 Zhao et al.

1.4.4 Isomer-level Identification and Quantification

Atmospheric organic constituents are largely comprised of structural isomers, from VOCs to low-volatility species in aerosols.[339] Thus, resolving the atmospheric organic mixtures on the isomeric level is crucial for understanding reaction kinetics, chemical mechanisms, and environmental impacts. The GC pre-separation process prior to mass spectrometry analysis has the ability to offer unique retention time for isomers, leading to the potential of GC-CIMS in detecting isomeric distributions derived from the oxidation of diverse atmospheric species. GC-CIMS using CF_3O^- as the reagent ion has been largely used in these applications to unravel the reaction kinetics, oxidation products, and reaction mechanisms. For example, Teng et al. resolved the gas-phase isomeric hydroxy nitrates that are formed via reactions of NO + $RO_2^\bullet$ derived from OH-initiated oxidation of isoprene to quantify the $RO_2^\bullet$ isomerization rates and the reversible conversion between alkyl radical and $RO_2^\bullet$ (**Figure 1.14**).[232] Vasquez et al. used the same technique and showed that different isoprene-derived hydroxy nitrate isomers have distinct hydrolysis rates and hence different effects on NO_x recycling.[340] Kurtén et al. suggested that nitrate radical oxidation of α-pinene favors the formation of volatile pinonaldehyde via bond scissions of nitrooxy alkoxy radicals over low-volatility organonitrate by experimentally quantifying the isomeric hydroperoxyl nitrates using GC-CF_3O^--CIMS and computationally calculating the barriers and rate constants of the different bond scission pathways.[235] In addition to biogenic VOC oxidation processes, the isomer-resolved identification and quantification of dominated phenol and hydroxy nitrates from the oxidation of bicyclic $RO_2^\bullet$ radicals in the presence of NO have implied the new benzene oxidation mechanism under atmospheric

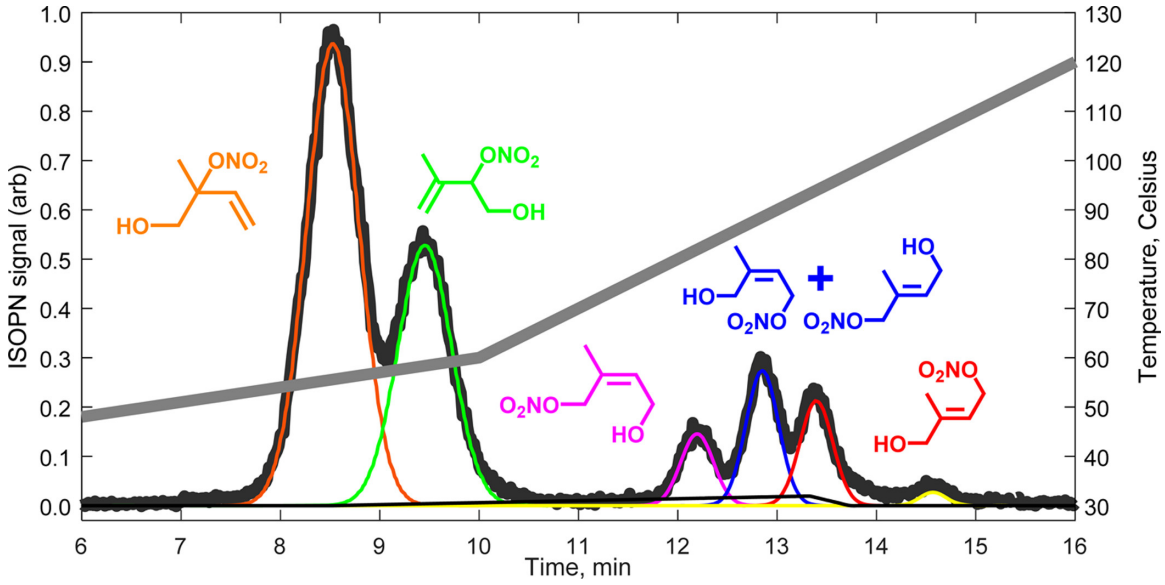

Figure 1.14 The distribution of isoprene hydroxynitrate isomers from isoprene photooxidation measured by the Caltech GC-CIMS. These isomers are separated using GC and detected as a cluster ion with CF_3O^- observed at m/Q 232 Th. The grey line shows the GC oven temperature as a function of time. Reproduced with permission Teng et al. 2017. Copyright 2017 American Chemical Society.

conditions.[230] Other regent ions such as NO^+ and its hydrated ion $NO \cdot H_2O^+$ were developed in the positive mode of GC-CIMS to characterize less oxygenated compounds, such as, non-methane organic gaseous isomers from biomass burning via GC-NO^+-CIMS,[108] and benzene and its oxidation product glyoxal via GC-$NO \cdot H_2O^+$-CIMS[230].

Iodometry-assisted LC-ESI-MS has been a helpful method to separate and distinguish organic peroxide isomers. As has been mentioned earlier, isomer-resolved characterization of peroxide monomers and dimers produced from α-pinene ozonolysis was achieved by this technique.[255] In this work, a total of 75 organic peroxides were observed in α-pinene-derived SOA via iodometry-assisted LC-ESI-MS in both the positive and negative ion modes. Meanwhile, the varied abundance of most organic peroxides during the evaporation process suggested the significance to develop a comprehensive technique in aerosol chemistry to identify molecular structure of peroxide isomers and other atmospheric species. In the study by Zhao et al., α-acyloxyalkyl hydroperoxides as organic peroxides formed via stabilized Criegee intermediates from α-pinene ozonolysis reacting with carboxylic acids were identified using iodometry-assisted LC-ESI-MS.[253] They determined the total organic peroxide content in α-pinene SOA and reported a lower total mass yield than previous work using the spectroscopic method, which could be explained by the rapid decomposition or inefficient ionization in LC-ESI-MS for certain peroxides.[247-249, 251, 341, 342] This group further utilized the technique to characterize isomer-resolved molecular composition of α-pinene and isoprene oxidation, including identifying isomer-resolved dimer esters derived from acyl $RO_2^{\bullet}$ during α-pinene ozonolysis,[257]

measuring C_5–C_{20} isomeric species during the oxidation of isoprene and monoterpene mixtures,[256] and investigating the hydrolysis stability of individual peroxide compounds[258].

The IMS-MS could separate isomeric compounds based on ion mobilities by providing a unique drift time of each isomer at the same mass-to-charge ratio, indicating its ability to resolve structural isomers which are otherwise challenging to be distinguished in typical mass spectrometry measurements. In the study carried out by Krechmer et al., three isomers of hydroxy sulfate ester derived from the reactive uptake of IEPOX onto wet acidic sulfate aerosols were characterized over distinct drift times by IMS-MS.[265] Further studies have used this capability to demonstrate OA compositional evolution during aging[343] and heating[168] on the isomeric level. In addition, by comparing with the ion mobilities of authentic standards, oxidation products during heterogeneous $^{\bullet}$OH oxidation of model OA compounds can be structurally verified, hence providing important insights into the multiphase oxidation mechanisms (**Figure 1.15**).[268] Lastly, the IMS-MS was used to distinguish actual dimers with covalent bonds from artifact clusters resulted from ESI by monitoring the dimer ion fragmentation with increased collision-induced dissociation voltage.[271] This led to the first report of dimer formation during heterogeneous $^{\bullet}$OH oxidation of OA. Most of these above-mentioned IMS-MS applications were possible owing to the additional mobility separation. Otherwise, the formula-level measurements and potential matrix effects in typical ESI-MS would make the findings challenging to explain.

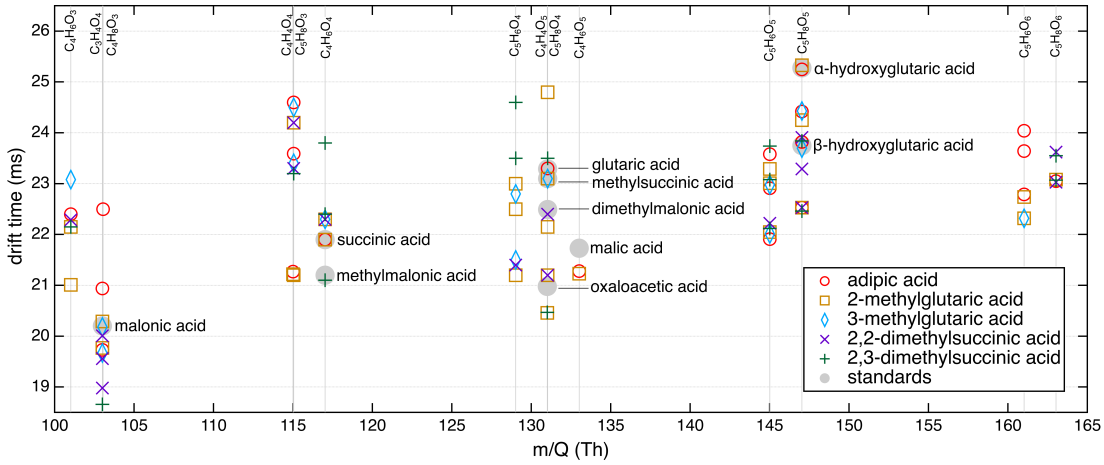

Figure 1.15 IMS-MS drift time – m/Q diagram of major fragmentation products in the heterogeneous oxidation of five studied OA systems (see legend). The drift times of relevant available chemical standards are labeled, helping identifying oxidation products. Reproduced with permission Zhao et al. 2020. Copyright 2020 American Chemical Society.

1.5 Current Issues

In Chapter 1.5, we summarize new developments of mass spectrometry techniques in the field of atmospheric chemistry and their applications to identify and quantify a broad range of atmospheric chemicals in both the gas and particle phases. Although these new developments have made unprecedented advancements in understanding atmospheric composition and processes, a few unsolved issues still remain.

1.5.1 Instrument artifacts

Despite versatile CIMS development with new IMR designs and various reagent ions, a remaining issue is the measurement artifacts. The artifacts may arise from a number of physical and chemical processes. First, the interactions between relatively low-volatile analytes and instrument inner walls, such as absorption or desorption processes, have been suggested to contribute to negative or positive artifacts in measured chemical concentrations.[112, 344] Second, chemical reactions may occur in the sample inlets. For example, artifacts were found by different air sampling configurations due to the reactions between air samples and overloading filters.[108, 115] Third, secondary chemistry between components in the IMR during chemical ionization may cause interference to chemical composition analysis. Dörich et al. reported the biased detection of HNO_3 as NO_3^- in the presence of peroxyacetic nitric anhydride (PAN), peroxyacetic acid and O_3 using I^--CIMS.[345] Zhang et al. further proposed the interactions between a strong oxygen donor such as O_3 or peracids and acidic organics such as carboxylic acids or organic hydroperoxides in the IMR region of I^--CIMS, causing the formation of monomer and

dimer iodide adducts to interfere the measurement of molecular compositions.[346] In addition, Bernhammer et al. reported secondary reactions between organic precursors in the PTR3 reaction chamber that interference the measurements of isoprene-derived HOMs and might cause an overestimation of both the nucleation rate and the growth rate.[347] Last but not least, fragmentation of chemicals or ions may occur for certain ionization chemistries. For instance, Li et al. showed that the commonly observed peroxide dimers using many CIMS techniques were found to have small signals in Vocus PTR-TOF, because the protonation in PTR leads to fragmentation of such compounds.[348] However, as we described earlier, many of the same dimers were successfully measured by PTR3 (**Figure 1.8**), despite its similar ionization technique with Vocus PTR-TOF.[106] The contrasting results may suggest that the dimer fragmentation in Vocus PTR-TOF could be caused by other reasons rather than protonation. Further investigation is warranted.

In addition to the artifacts for gas-phase CIMS measurements, a common problem in characterizing particle-phase compounds using vaporization-based methods is thermal decomposition.[165, 349-351] More importantly, thermal decomposition was found to occur even at moderately heated temperatures for multifunctional compounds.[168] For the ESI-based techniques that apply minimal heating, artifact may also exist. In particular, ESI has been known to generate microdroplets with charges at the surface, where chemistry could occur at much faster rates than in the bulk.[352-355] It is thus unclear whether some of the products observed via ESI-MS could be formed during ESI, rather than in the intrinsic aerosol processing. Another uncertainty is whether the entire microdroplet or aerosol sample is probed by ESI and EESI. Some previous studies have reported that ESI-MS only

sample the outermost surface layers of the microdroplet.[356] We suggest these questions to be carefully investigated in future research to better understand the measurements of atmospheric aerosol molecular composition.

1.5.2 Bias caused by selectivity of ionization methods

Lastly, it is important to point out that selectivity of ionization methods can often cause bias for molecular analysis. As described earlier, the HOM formation yield from α-pinene + OH may have very different results by using NO_3^--CIMS vs. $CH_3C(O)O^-$-CIMS.[153, 357] In another example, it was reported that very different light-absorbing chromophores in biomass burning OAs were determined using ESI vs. atmospheric pressure photoionization.[358] These results suggest that multiple complementary ionization methods need to be applied to the same sample or same reaction system for more comprehensive characterization.

1.6 Aims and Scope of Dissertation

The aims of this dissertation are to (1) address and improve the applications of mass spectrometry technique in atmospheric chemistry; (2) examine gas-phase and particle-phase chemical composition of OA systems through experiments and kinetic simulations. We focus on the role of $RO_2^{\bullet}$ dynamics in the aerosol oxidation and expand the investigation on $RO_2^{\bullet}$-centered chemistry from the molecular level to isomer level coupled with improved mass spectrometry technique. By carrying out laboratory experiments under various chemical conditions and timescales to mimic atmospheric process, we intend to fill the critical knowledge gap between laboratory measurements and ambient observations. The overall scope of this dissertation is for furthering development of mass spectrometry techniques and expand current understanding in chemical dynamics and molecular composition of aerosol chemistry.

Chapter 2 studies the gas-phase oxidation chemistry of VOCs in real time using I^--CIMS technique. We report the occurrence of the secondary ion chemistry from interactions between a strong oxygen donor (such as O_3 and peracids) and acidic OVOCs (such as carboxylic acids and organic hydroperoxides) in the IMR region of I^--CIMS. Such interactions can lead to acidic organic molecules (HA or HB) clustering with $[IO]^-$ (e.g., $[HA+IO]^-$) and dimer adducts ($[A+B+I]^-$), in addition to the well-known iodide clusters ($[HA+I]^-$). This ion chemistry was probed using common chemical standards as well as the gas-phase oxidation products of a-pinene and isoprene in a flowtube reactor. The results show that the secondary ion chemistry can lead to misinterpretations of molecular compositions and distributions of the gas-phase products and an overestimation of the

elemental O/C ratio overall. Nevertheless, the varying degrees of signal change in response to the secondary ion chemistry might be a clue to inform OVOCs' functionalities. Specifically, in the a-pinene ozonolysis system, the extents of ion signal reduction in the presence of additional acids in the IMR suggest that $C_9H_{14}O_4$ produced in the gas phase is a peracid, rather than the often-assumed pinic acid. Thus, we suggest that the potential application of the secondary ion chemistry to inform organic functionalities is promising, which could help better understand the molecular compositions of gas-phase OVOCs and the reaction mechanisms therein.

Chapter 3 shifts the focus of aerosol chemistry to multiphase oxidation mechanism and kinetics under atmospheric-like hydroxyl radical ($^{\bullet}OH$) conditions. We performed heterogeneous oxidation experiments of several model OA systems under varied aging timescales and gas-phase oxidant concentrations. Our results suggest that OA heterogeneous oxidation may be 2–3 orders of magnitude faster than previously reported when [$^{\bullet}OH$] is decreased to atmospheric levels. Direct laboratory mass spectrometry measurements coupled with kinetic simulations suggest that an autoxidation mechanism mediated by particle-phase $RO_2^{\bullet}$ greatly accelerates OA oxidation, with enhanced formation of organic hydroperoxides, alcohols, and fragmentation products. With autoxidation, we estimate that the OA oxidation timescale in the atmosphere may be from less than a day to several days. Thus, OA oxidative aging can have greater atmospheric impacts than previously expected. Furthermore, our findings reveal the nature of heterogeneous aerosol oxidation chemistry in the atmosphere and may reconcile the discrepancies between atmospheric observations and laboratory studies on OA aging.

Chapter 4 builds on the work from the previous chapter to explore the role of hydroperoxyl radicals ($HO_2^{\bullet}$), as important oxidant in the troposphere coupled with •OH, in heterogeneous OA oxidative aging. We carry out •OH-initiated heterogeneous oxidation of several OA model systems under different $HO_2^{\bullet}$ conditions in a flow tube reactor and characterize the molecular oxidation products using a suite of mass spectrometry instrumentation. By using hydrogen-deuterium exchange with thermal desorption iodide-adduct chemical ionization mass spectrometry, we provide direct observation of organic hydroperoxide formation from heterogeneous $HO_2^{\bullet}$ and $RO_2^{\bullet}$ reactions for the first time. The hydroperoxides may contribute substantially to the oxidation products, varied with the parent OAs chemical structure. Furthermore, by regulating $RO_2^{\bullet}$ reaction pathways, $HO_2^{\bullet}$ also greatly influence the overall composition of the oxidized OAs. Lastly, we suggest that the $RO_2^{\bullet}$ + $HO_2^{\bullet}$ reactions readily occur at the OA particle interface rather than in the particle bulk. These findings provide new mechanistic insights into the heterogeneous OA oxidation chemistry and help fill the critical knowledge gap in understanding atmospheric OA oxidative aging.

1.7 References

(1) Merikanto, J.; Spracklen, D. V.; Mann, G. W.; Pickering, S. J.; Carslaw, K. S. Impact of nucleation on global CCN. *Atmos. Chem. Phys.* **2009**, *9* (21), 8601-8616.

(2) Dockery, D. W.; Pope, C. A.; Xu, X.; Spengler, J. D.; Ware, J. H.; Fay, M. E.; Ferris, B. G.; Speizer, F. E. An Association between Air Pollution and Mortality in Six U.S. Cities. *N. Engl. J. Med.* **1993**, *329* (24), 1753-1759.

(3) Boucher, O.; Randall, D.; Artaxo, P.; Bretherton, C.; Feingold, C.; Forster, P.; Kerminen, V.-M.; Kondo, Y.; Liao, H.; Lohmann, U.; et al. *Clouds and Aerosols*; IPCC, 2013.

(4) Watson, J. G. Visibility: Science and Regulation. *J. Air Waste Manage.* **2002**, *52* (6), 628-713.

(5) Jones, A. P. Indoor air quality and health. *Atmos. Environ.* **1999**, *33* (28), 4535-4564.

(6) Claflin, M. S.; Krechmer, J. E.; Hu, W.; Jimenez, J. L.; Ziemann, P. J. Functional Group Composition of Secondary Organic Aerosol Formed from Ozonolysis of α-Pinene Under High VOC and Autoxidation Conditions. *ACS Earth Space Chem.* **2018**, *2* (11), 1196-1210.

(7) Kroll, J. H.; Seinfeld, J. H. Chemistry of secondary organic aerosol: Formation and evolution of low-volatility organics in the atmosphere. *Atmos. Environ.* **2008**, *42* (16), 3593-3624.

(8) Goldstein, A. H.; Galbally, I. E. Known and unexplored organic constituents in the Earth's atmosphere. *Geochimica et Cosmochimica Acta.* **2009**, *73*, A449.

(9) Hallquist, M.; Wenger, J. C.; Baltensperger, U.; Rudich, Y.; Simpson, D.; Claeys, M.; Dommen, J.; Donahue, N. M.; George, C.; Goldstein, A. H.; et al. The formation, properties and impact of secondary organic aerosol: current and emerging issues. *Atmos. Chem. Phys.* **2009**, *9* (14), 5155-5236.

(10) De Gouw, J.; Jimenez, J. L. Organic Aerosols in the Earth's Atmosphere. *Environ. Sci. Technol.* **2009**, *43* (20), 7614-7618.

(11) Zhang, Q.; Jimenez, J. L.; Canagaratna, M. R.; Allan, J. D.; Coe, H.; Ulbrich, I.; Alfarra, M. R.; Takami, A.; Middlebrook, A. M.; Sun, Y. L.; et al. Ubiquity and dominance of oxygenated species in organic aerosols in anthropogenically-influenced Northern Hemisphere midlatitudes. *Geophys. Res. Lett.* **2007**, *34*, L13801.

(12) Jimenez, J. L.; Canagaratna, M. R.; Donahue, N. M.; Prevot, A. S. H.; Zhang, Q.; Kroll, J. H.; DeCarlo, P. F.; Allan, J. D.; Coe, H.; Ng, N. L.; et al. Evolution of Organic Aerosols in the Atmosphere. Science. **2009**, *326* (5959), 1525-1529.

(13) Laskin, J.; Laskin, A.; Nizkorodov, S. A. Mass Spectrometry Analysis in Atmospheric Chemistry. *Anal. Chem.* **2018**, *90* (1), 166-189.

(14) Pratt, K. A.; Prather, K. A. Mass spectrometry of atmospheric aerosols—Recent developments and applications. Part I: Off-line mass spectrometry techniques. *Mass Spectrom. Rev.* **2012**, *31* (1), 1-16.

(15) Riva, M.; Rantala, P.; Krechmer, J. E.; Peräkylä, O.; Zhang, Y.; Heikkinen, L.; Garmash, O.; Yan, C.; Kulmala, M.; Worsnop, D.; et al. Evaluating the performance of five different chemical ionization techniques for detecting gaseous oxygenated organic species. *Atmos. Meas. Tech.* **2019**, *12* (4), 2403-2421.

(16) Covey, T. R.; Lee, E. D.; Henion, J. D. High-speed liquid chromatography/tandem mass spectrometry for the determination of drugs in biological samples. *Anal. Chem.* **1986**, *58* (12), 2453-2460.

(17) Larsen, B. S.; McEwen, C. N.; Kitson, F. G. Dedication. In *Gas Chromatography and Mass Spectrometry*, Kitson, F. G., Larsen, B. S., McEwen, C. N. Eds.; Academic Press, 1996; p v.

(18) Yu, J.; Flagan, R. C.; Seinfeld, J. H. Identification of Products Containing −COOH, −OH, and −CO in Atmospheric Oxidation of Hydrocarbons. *Environ. Sci. Technol.* **1998**, *32* (16), 2357-2370.

(19) Yu, J.; Cocker, D. R.; Griffin, R. J.; Flagan, R. C.; Seinfeld, J. H. Gas-Phase Ozone Oxidation of Monoterpenes: Gaseous and Particulate Products. *J. Atmos. Chem.* **1999**, *34* (2), 207-258.

(20) Kubátová, A.; Vermeylen, R.; Claeys, M.; Cafmeyer, J.; Maenhaut, W.; Roberts, G.; Artaxo, P. Carbonaceous aerosol characterization in the Amazon basin, Brazil: novel dicarboxylic acids and related compounds. *Atmos. Environ.* **2000**, *34* (29), 5037-5051.

(21) Kawamura, K.; Sempéré, R.; Imai, Y.; Fujii, Y.; Hayashi, M. Water soluble dicarboxylic acids and related compounds in Antarctic aerosols. *J. Geophys. Res. Atmos.* **1996**, *101* (D13), 18721-18728.

(22) J. Weschler, C. Identification of selected organics in the Arctic aerosol. *Atmos. Environ. (1967)* **1981**, *15* (8), 1365-1369.

(23) Yokouchi, Y.; Ambe, Y. Aerosols formed from the chemical reaction of monoterpenes and ozone. *Atmos. Environ. (1967)* **1985**, *19* (8), 1271-1276.

(24) Willoughby, R. C.; Browner, R. F. Monodisperse aerosol generation interface for combining liquid chromatography with mass spectroscopy. *Anal. Chem.* **1984**, *56* (14), 2626-2631.

(25) Winkler, P. C.; Perkins, D. D.; Williams, W. K.; Browner, R. F. Performance of an improved monodisperse aerosol generation interface for liquid chromatography/mass spectrometry. *Anal. Chem.* **1988**, *60* (5), 489-493.

(26) Murray, K. K.; Lewis, T. M.; Beeson, M. D.; Russell, D. H. Aerosol matrix-assisted laser desorption ionization for liquid chromatography/time-of-flight mass spectrometry. *Anal. Chem.* **1994**, *66* (10), 1601-1609.

(27) DeCarlo, P. F.; Kimmel, J. R.; Trimborn, A.; Northway, M. J.; Jayne, J. T.; Aiken, A. C.; Gonin, M.; Fuhrer, K.; Horvath, T.; Docherty, K. S.; et al. Field-Deployable, High-Resolution, Time-of-Flight Aerosol Mass Spectrometer. *Anal. Chem.* **2006**, *78* (24), 8281-8289.

(28) Tobias, H. J.; Kooiman, P. M.; Docherty, K. S.; Ziemann, P. J. Real-time chemical analysis of organic aerosols using a thermal desorption particle beam mass spectrometer. *Aerosol Sci. Technol.* **2000**, *33*, 170-190.

(29) Canagaratna, M. R.; Jayne, J. T.; Jimenez, J. L.; Allan, J. D.; Alfarra, M. R.; Zhang, Q.; Onasch, T. B.; Drewnick, F.; Coe, H.; Middlebrook, A.; et al. Chemical and microphysical characterization of ambient aerosols with the aerodyne aerosol mass spectrometer. *Mass Spectrom. Rev.* **2007**, *26* (2), 185-222.

(30) Pratt, K. A.; Prather, K. A. Mass spectrometry of atmospheric aerosols—Recent developments and applications. Part II: On-line mass spectrometry techniques. *Mass Spectrom. Rev.* **2012**, *31* (1), 17-48.

(31) Jayne, J. T.; Leard, D. C.; Zhang, X.; Davidovits, P.; Smith, K. A.; Kolb, C. E.; Worsnop, D. R. Development of an Aerosol Mass Spectrometer for Size and Composition Analysis of Submicron Particles. *Aerosol Sci. Technol.* **2000**, *33* (1-2), 49-70.

(32) Jimenez, J. L.; Jayne, J. T.; Shi, Q.; Kolb, C. E.; Worsnop, D. R.; Yourshaw, I.; Seinfeld, J. H.; Flagan, R. C.; Zhang, X.; Smith, K. A.; et al. Ambient aerosol sampling using the Aerodyne Aerosol Mass Spectrometer. *J. Geophys. Res. Atmos.* **2003**, *108* (D7).

(33) Kroll, J. H.; Donahue, N. M.; Jimenez, J. L.; Kessler, S. H.; Canagaratna, M. R.; Wilson, K. R.; Altieri, K. E.; Mazzoleni, L. R.; Wozniak, A. S.; Bluhm, H.; et al. Carbon oxidation state as a metric for describing the chemistry of atmospheric organic aerosol. *Nat. Chem.* **2011**, *3* (2), 133-139.

(34) Ng, N. L.; Canagaratna, M. R.; Jimenez, J. L.; Chhabra, P. S.; Seinfeld, J. H.; Worsnop, D. R. Changes in organic aerosol composition with aging inferred from aerosol mass spectra. *Atmos. Chem. Phys.* **2011**, *11* (13), 6465-6474.

(35) Chhabra, P. S.; Flagan, R. C.; Seinfeld, J. H. Elemental analysis of chamber organic aerosol using an aerodyne high-resolution aerosol mass spectrometer. *Atmos. Chem. Phys.* **2010**, *10* (9), 4111-4131.

(36) Hu, W.; Campuzano-Jost, P.; Day, D. A.; Croteau, P.; Canagaratna, M. R.; Jayne, J. T.; Worsnop, D. R.; Jimenez, J. L. Evaluation of the new capture vapourizer for aerosol mass spectrometers (AMS) through laboratory studies of inorganic species. *Atmos. Meas. Tech.* **2017**, *10* (8), 2897-2921.

(37) Sato, K.; Takami, A.; Kato, Y.; Seta, T.; Fujitani, Y.; Hikida, T.; Shimono, A.; Imamura, T. AMS and LC/MS analyses of SOA from the photooxidation of benzene and 1,3,5-trimethylbenzene in the presence of NOx: effects of chemical structure on SOA aging. *Atmos. Chem. Phys.* **2012**, *12* (10), 4667-4682.

(38) Fortenberry, C. F.; Walker, M. J.; Zhang, Y.; Mitroo, D.; Brune, W. H.; Williams, B. J. Bulk and molecular-level characterization of laboratory-aged biomass burning organic aerosol from oak leaf and heartwood fuels. *Atmos. Chem. Phys.* **2018**, *18* (3), 2199-2224.

(39) Takegawa, N.; Miyazaki, Y.; Kondo, Y.; Komazaki, Y.; Miyakawa, T.; Jimenez, J. L.; Jayne, J. T.; Worsnop, D. R.; Allan, J. D.; Weber, R. J. Characterization of an aerodyne aerosol mass spectrometer (AMS): Intercomparison with other aerosol instruments. *Aerosol Sci. Technol.* **2005**, *39* (8), 760-770.

(40) Qi, L.; Chen, M.; Stefenelli, G.; Pospisilova, V.; Tong, Y.; Bertrand, A.; Hueglin, C.; Ge, X.; Baltensperger, U.; Prévôt, A. S. H.; et al. Organic aerosol source apportionment in Zurich using an extractive electrospray ionization time-of-flight mass spectrometer (EESI-TOF-MS) – Part 2: Biomass burning influences in winter. *Atmos. Chem. Phys.* **2019**, *19* (12), 8037-8062.

(41) Ye, C.; Yuan, B.; Lin, Y.; Wang, Z.; Hu, W.; Li, T.; Chen, W.; Wu, C.; Wang, C.; Huang, S.; et al. Chemical characterization of oxygenated organic compounds in the gas phase and particle phase using iodide CIMS with FIGAERO in urban air. *Atmos. Chem. Phys.* **2021**, *21* (11), 8455-8478.

(42) Alfarra, M. R.; Coe, H.; Allan, J. D.; Bower, K. N.; Boudries, H.; Canagaratna, M. R.; Jimenez, J. L.; Jayne, J. T.; Garforth, A. A.; Li, S.-M.; et al. Characterization of urban and rural organic particulate in the Lower Fraser Valley using two Aerodyne Aerosol Mass Spectrometers. *Atmos. Environ.* **2004**, *38* (34), 5745-5758.

(43) Chen, Y.; Takeuchi, M.; Nah, T.; Xu, L.; Canagaratna, M. R.; Stark, H.; Baumann, K.; Canonaco, F.; Prévôt, A. S. H.; Huey, L. G.; et al. Chemical characterization of secondary organic aerosol at a rural site in the southeastern US: insights from simultaneous high-resolution time-of-flight aerosol mass spectrometer (HR-ToF-AMS) and FIGAERO chemical ionization mass spectrometer (CIMS) measurements. *Atmos. Chem. Phys.* **2020**, *20* (14), 8421-8440.

(44) Brüggemann, M.; Karu, E.; Stelzer, T.; Hoffmann, T. Real-time analysis of ambient organic aerosols using aerosol flowing atmospheric-pressure afterglow mass spectrometry (AeroFAPA-MS). *Environ. Sci. Technol.* **2015**, *49* (9), 5571-5578.

(45) Huey, L. G. Measurement of trace atmospheric species by chemical ionization mass spectrometry: Speciation of reactive nitrogen and future directions. *Mass Spectrom. Rev.* **2007**, *26* (2), 166-184.

(46) Viggiano, A. A. In situ mass spectrometry and ion chemistry in the stratosphere and troposphere. *Mass Spectrom. Rev.* **1993**, *12* (2), 115-137.

(47) de Gouw, J.; Warneke, C. Measurements of volatile organic compounds in the earth's atmosphere using proton-transfer-reaction mass spectrometry. *Mass Spectrom. Rev.* **2007**, *26* (2), 223-257.

(48) Hansel, A.; Jordan, A.; Warneke, C.; Holzinger, R.; Lindinger, W. Improved detection limit of the proton-transfer reaction mass spectrometer: on-line monitoring of volatile organic compounds at mixing ratios of a few pptv. *Rapid Com. Mass Spectrom.* **1998**, *12* (13), 871-875.

(49) Bertram, T. H.; Kimmel, J. R.; Crisp, T. A.; Ryder, O. S.; Yatavelli, R. L. N.; Thornton, J. A.; Cubison, M. J.; Gonin, M.; Worsnop, D. R. A field-deployable, chemical ionization time-of-flight mass spectrometer. *Atmos. Meas. Tech.* **2011**, *4* (7), 1471-1479.

(50) Ehn, M.; Kleist, E.; Junninen, H.; Petäjä, T.; Lönn, G.; Schobesberger, S.; Dal Maso, M.; Trimborn, A.; Kulmala, M.; Worsnop, D. R.; et al. Gas phase formation of extremely oxidized pinene reaction products in chamber and ambient air. *Atmos. Chem. Phys.* **2012**, *12* (11), 5113-5127.

(51) Crounse, J. D.; Paulot, F.; Kjaergaard, H. G.; Wennberg, P. O. Peroxy radical isomerization in the oxidation of isoprene. *Phys. Chem. Chem. Phys.* **2011**, *13* (30), 13607-13613, 10.1039/C1CP21330J.

(52) Lee, B. H.; Lopez-Hilfiker, F. D.; Mohr, C.; Kurtén, T.; Worsnop, D. R.; Thornton, J. A. An Iodide-Adduct High-Resolution Time-of-Flight Chemical-Ionization Mass Spectrometer: Application to Atmospheric Inorganic and Organic Compounds. *Environ. Sci. Technol.* **2014**, *48* (11), 6309-6317.

(53) Lopez-Hilfiker, F. D.; Mohr, C.; Ehn, M.; Rubach, F.; Kleist, E.; Wildt, J.; Mentel, T. F.; Lutz, A.; Hallquist, M.; Worsnop, D.; et al. A novel method for online analysis of gas and particle composition: description and evaluation of a Filter Inlet for Gases and AEROsols (FIGAERO). *Atmos. Meas. Tech.* **2014**, *7* (4), 983-1001.

(54) Yatavelli, R. L. N.; Lopez-Hilfiker, F.; Wargo, J. D.; Kimmel, J. R.; Cubison, M. J.; Bertram, T. H.; Jimenez, J. L.; Gonin, M.; Worsnop, D. R.; Thornton, J. A. A Chemical

Ionization High-Resolution Time-of-Flight Mass Spectrometer Coupled to a Micro Orifice Volatilization Impactor (MOVI-HRToF-CIMS) for Analysis of Gas and Particle-Phase Organic Species. *Aerosol Sci. Technol.* **2012**, *46* (12), 1313-1327.

(55) Eichler, P.; Müller, M.; D'Anna, B.; Wisthaler, A. A novel inlet system for online chemical analysis of semi-volatile submicron particulate matter. *Atmos. Meas. Tech.* **2015**, *8* (3), 1353-1360.

(56) Bateman, A. P.; Nizkorodov, S. A.; Laskin, J.; Laskin, A. High-Resolution Electrospray Ionization Mass Spectrometry Analysis of Water-Soluble Organic Aerosols Collected with a Particle into Liquid Sampler. *Anal. Chem.* **2010**, *82* (19), 8010-8016.

(57) De Haan, D. O.; Tolbert, M. A.; Jimenez, J. L. Atmospheric condensed-phase reactions of glyoxal with methylamine. *Geophys. Res. Lett.* **2009**, *36* (11), L11819.

(58) Hastings, W. P.; Koehler, C. A.; Bailey, E. L.; De Haan, D. O. Secondary Organic Aerosol Formation by Glyoxal Hydration and Oligomer Formation: Humidity Effects and Equilibrium Shifts during Analysis. *Environ. Sci. Technol.* **2005**, *39* (22), 8728-8735.

(59) George, I. J.; Vlasenko, A.; Slowik, J. G.; Broekhuizen, K.; Abbatt, J. P. D. Heterogeneous oxidation of saturated organic aerosols by hydroxyl radicals: uptake kinetics, condensed-phase products, and particle size change. *Atmos. Chem. Phys.* **2007**, *7* (16), 4187-4201.

(60) Lim, Y. B.; Tan, Y.; Perri, M. J.; Seitzinger, S. P.; Turpin, B. J. Aqueous chemistry and its role in secondary organic aerosol (SOA) formation. *Atmos. Chem. Phys.* **2010**, *10* (21), 10521-10539.

(61) Nguyen, T. B.; Bateman, A. P.; Bones, D. L.; Nizkorodov, S. A.; Laskin, J.; Laskin, A. High-resolution mass spectrometry analysis of secondary organic aerosol generated by ozonolysis of isoprene. *Atmos. Environ.* **2010**, *44* (8), 1032-1042.

(62) Bateman, A. P.; Laskin, J.; Laskin, A.; Nizkorodov, S. A. Applications of High-Resolution Electrospray Ionization Mass Spectrometry to Measurements of Average Oxygen to Carbon Ratios in Secondary Organic Aerosols. *Environ. Sci. Technol.* **2012**, *46* (15), 8315-8324.

(63) Warnke, J.; Bandur, R.; Hoffmann, T. Capillary-HPLC-ESI-MS/MS method for the determination of acidic products from the oxidation of monoterpenes in atmospheric aerosol samples. *Anal. Bioanal. Chem.* **2006**, *385* (1), 34-45.

(64) Claeys, M.; Iinuma, Y.; Szmigielski, R.; Surratt, J. D.; Blockhuys, F.; Van Alsenoy, C.; Böge, O.; Sierau, B.; Gómez-González, Y.; Vermeylen, R.; et al. Terpenylic Acid and Related Compounds from the Oxidation of α-Pinene: Implications for New Particle Formation and Growth above Forests. *Environ. Sci. Technol.* **2009**, *43* (18), 6976-6982.

(65) Surratt, J. D.; Kroll, J. H.; Kleindienst, T. E.; Edney, E. O.; Claeys, M.; Sorooshian, A.; Ng, N. L.; Offenberg, J. H.; Lewandowski, M.; Jaoui, M.; et al. Evidence for Organosulfates in Secondary Organic Aerosol. *Environ. Sci. Technol.* **2007**, *41* (2), 517-527.

(66) Surratt, J. D.; Murphy, S. M.; Kroll, J. H.; Ng, N. L.; Hildebrandt, L.; Sorooshian, A.; Szmigielski, R.; Vermeylen, R.; Maenhaut, W.; Claeys, M.; et al. Chemical Composition of Secondary Organic Aerosol Formed from the Photooxidation of Isoprene. *J. Phys. Chem. A* **2006**, *110* (31), 9665-9690.

(67) Müller, L.; Reinnig, M. C.; Warnke, J.; Hoffmann, T. Unambiguous identification of esters as oligomers in secondary organic aerosol formed from cyclohexene and cyclohexene/α-pinene ozonolysis. *Atmos. Chem. Phys.* **2008**, *8* (5), 1423-1433.

(68) Yasmeen, F.; Szmigielski, R.; Vermeylen, R.; Gómez-González, Y.; Surratt, J. D.; Chan, A. W. H.; Seinfeld, J. H.; Maenhaut, W.; Claeys, M. Mass spectrometric characterization of isomeric terpenoic acids from the oxidation of α-pinene, β-pinene, d-limonene, and Δ3-carene in fine forest aerosol. *J. Mass Spectrom.* **2011**, *46* (4), 425-442.

(69) Zhang, H.; Surratt, J. D.; Lin, Y. H.; Bapat, J.; Kamens, R. M. Effect of relative humidity on SOA formation from isoprene/NO photooxidation: enhancement of 2-methylglyceric acid and its corresponding oligoesters under dry conditions. *Atmos. Chem. Phys.* **2011**, *11* (13), 6411-6424.

(70) Bateman, A. P.; Walser, M. L.; Desyaterik, Y.; Laskin, J.; Laskin, A.; Nizkorodov, S. A. The Effect of Solvent on the Analysis of Secondary Organic Aerosol Using Electrospray Ionization Mass Spectrometry. *Environ. Sci. Technol.* **2008**, *42* (19), 7341-7346.

(71) Hu, K. S.; Darer, A. I.; Elrod, M. J. Thermodynamics and kinetics of the hydrolysis of atmospherically relevant organonitrates and organosulfates. *Atmos. Chem. Phys.* **2011**, *11* (16), 8307-8320.

(72) Fuller, S. J.; Wragg, F. P. H.; Nutter, J.; Kalberer, M. Comparison of on-line and off-line methods to quantify reactive oxygen species (ROS) in atmospheric aerosols. *Atmos. Environ.* **2014**, *92*, 97-103.

(73) Rindelaub, J. D.; Wiley, J. S.; Cooper, B. R.; Shepson, P. B. Chemical characterization of α-pinene secondary organic aerosol constituents using gas chromatography, liquid chromatography, and paper spray-based mass spectrometry techniques. *Rapid Com. Mass Spectrom.* **2016**, *30* (13), 1627-1638.

(74) Roach, P. J.; Laskin, J.; Laskin, A. Nanospray desorption electrospray ionization: an ambient method for liquid-extraction surface sampling in mass spectrometry. *Analyst* **2010**, *135* (9), 2233-2236.

(75) Liu, J.; Wang, H.; Manicke, N. E.; Lin, J.-M.; Cooks, R. G.; Ouyang, Z. Development, Characterization, and Application of Paper Spray Ionization. *Anal. Chem.* **2010**, *82* (6), 2463-2471.

(76) Doezema, L. A.; Longin, T.; Cody, W.; Perraud, V.; Dawson, M. L.; Ezell, M. J.; Greaves, J.; Johnson, K. R.; Finlayson-Pitts, B. J. Analysis of secondary organic aerosols in air using extractive electrospray ionization mass spectrometry (EESI-MS). *RSC Adv.* **2012**, *2* (7), 2930-2938.

(77) Gallimore, P. J.; Kalberer, M. Characterizing an Extractive Electrospray Ionization (EESI) Source for the Online Mass Spectrometry Analysis of Organic Aerosols. *Environ. Sci. Technol.* **2013**, *47* (13), 7324-7331.

(78) Horan, A. J.; Gao, Y.; Hall, W. A.; Johnston, M. V. Online Characterization of Particles and Gases with an Ambient Electrospray Ionization Source. *Anal. Chem.* **2012**, *84* (21), 9253-9258.

(79) Nah, T.; Chan, M.; Leone, S. R.; Wilson, K. R. Real Time in Situ Chemical Characterization of Submicrometer Organic Particles Using Direct Analysis in Real Time-Mass Spectrometry. *Anal Chem* **2013**, *85* (4), 2087-2095.

(80) Chan, M. N.; Nah, T.; Wilson, K. R. Real time in situ chemical characterization of sub-micron organic aerosols using Direct Analysis in Real Time mass spectrometry (DART-MS): the effect of aerosol size and volatility. *Analyst* **2013**, *138* (13), 3749-3757.

(81) Chan, M. N.; Zhang, H.; Goldstein, A. H.; Wilson, K. R. Role of Water and Phase in the Heterogeneous Oxidation of Solid and Aqueous Succinic Acid Aerosol by Hydroxyl Radicals. *J. Phys. Chem. C* **2014**, *118* (50), 28978-28992.

(82) Huey, L. G. Measurement of trace atmospheric species by chemical ionization mass spectrometry: Speciation of reactive nitrogen and future directions. *Mass Spectrom. Rev.* **2007**, *26* (2), 166-184.

(83) Blake, R. S.; Monks, P. S.; Ellis, A. M. Proton-Transfer Reaction Mass Spectrometry. *Chem. Rev.* **2009**, *109* (3), 861-896.

(84) Laskin, J.; Laskin, A.; Nizkorodov, S. A. New mass spectrometry techniques for studying physical chemistry of atmospheric heterogeneous processes. *Int. Rev. Phys. Chem.* **2013**, *32* (1), 128-170.

(85) Yuan, B.; Koss, A. R.; Warneke, C.; Coggon, M.; Sekimoto, K.; de Gouw, J. A. Proton-transfer-reaction mass spectrometry: Applications in atmospheric sciences. *Chem. Rev.* **2017**, *117* (21), 13187-13229.

(86) Laskin, J.; Laskin, A.; Nizkorodov, S. A. Mass spectrometry analysis in atmospheric chemistry. *Anal. Chem.* **2018**, *90* (1), 166-189.

(87) Zhao, R. The Recent Development and Application of Chemical Ionization Mass Spectrometry in Atmospheric Chemistry. In *Encyclopedia of Analytical Chemistry*, 2018; pp 1-33.

(88) Sekimoto, K.; Koss, A. R. Modern mass spectrometry in atmospheric sciences: Measurement of volatile organic compounds in the troposphere using proton-transfer-reaction mass spectrometry. *J. Mass Spectrom.* **2021**, *56* (3), e4619.

(89) Lindinger, W.; Jordan, A. Proton-transfer-reaction mass spectrometry (PTR–MS): on-line monitoring of volatile organic compounds at pptv levels. *Chem. Soc. Rev.* **1998**, *27* (5), 347-375.

(90) Graus, M.; Müller, M.; Hansel, A. High resolution PTR-TOF: Quantification and formula confirmation of VOC in real time. *J. Am. Soc. Mass Spectrom.* **2010**, *21* (6), 1037-1044.

(91) Kim, S.; Karl, T.; Helmig, D.; Daly, R.; Rasmussen, R.; Guenther, A. Measurement of atmospheric sesquiterpenes by proton transfer reaction-mass spectrometry (PTR-MS). *Atmos. Meas. Tech.* **2009**, *2* (1), 99-112.

(92) Cappellin, L.; Biasioli, F.; Fabris, A.; Schuhfried, E.; Soukoulis, C.; Märk, T. D.; Gasperi, F. Improved mass accuracy in PTR-TOF-MS: Another step towards better compound identification in PTR-MS. *Int. J. Mass Spectrom.* **2010**, *290* (1), 60-63.

(93) Lopez-Hilfiker, F. D.; Iyer, S.; Mohr, C.; Lee, B. H.; D'Ambro, E. L.; Kurtén, T.; Thornton, J. A. Constraining the sensitivity of iodide adduct chemical ionization mass spectrometry to multifunctional organic molecules using the collision limit and thermodynamic stability of iodide ion adducts. *Atmos. Meas. Tech.* **2016**, *9* (4), 1505-1512.

(94) Sanchez, J.; Tanner, D. J.; Chen, D.; Huey, L. G.; Ng, N. L. A new technique for the direct detection of HO2 radicals using bromide chemical ionization mass spectrometry (Br-CIMS): initial characterization. *Atmos. Meas. Tech.* **2016**, *9* (8), 3851-3861.

(95) Brophy, P.; Farmer, D. K. Clustering, methodology, and mechanistic insights into acetate chemical ionization using high-resolution time-of-flight mass spectrometry. *Atmos. Meas. Tech.* **2016**, *9* (8), 3969-3986.

(96) Nah, T.; Ji, Y.; Tanner, D. J.; Guo, H.; Sullivan, A. P.; Ng, N. L.; Weber, R. J.; Huey, L. G. Real-time measurements of gas-phase organic acids using SF6− chemical ionization mass spectrometry. *Atmos. Meas. Tech.* **2018**, *11* (9), 5087-5104.

(97) Zaytsev, A.; Breitenlechner, M.; Koss, A. R.; Lim, C. Y.; Rowe, J. C.; Kroll, J. H.; Keutsch, F. N. Using collision-induced dissociation to constrain sensitivity of ammonia chemical ionization mass spectrometry (NH4+ CIMS) to oxygenated volatile organic compounds. *Atmos. Meas. Tech.* **2019**, *12* (3), 1861-1870.

(98) Berry, J. L.; Day, D. A.; Elseberg, T.; Palm, B. B.; Hu, W.; Abdelhamid, A.; Schroder, J. C.; Karst, U.; Jimenez, J. L.; Browne, E. C. Laser Ablation-Aerosol Mass Spectrometry-Chemical Ionization Mass Spectrometry for Ambient Surface Imaging. *Anal. Chem.* **2018**, *90* (6), 4046-4053.

(99) Benson, D. R.; Markovich, A.; Al-Refai, M.; Lee, S. H. A chemical ionization mass spectrometer for ambient measurements of ammonia. *Atmos. Meas. Tech.* **2010**, *3* (4), 1075-1087.

(100) Lawler, M. J.; Sander, R.; Carpenter, L. J.; Lee, J. D.; von Glasow, R.; Sommariva, R.; Saltzman, E. S. HOCl and Cl2 observations in marine air. *Atmos. Chem. Phys.* **2011**, *11* (15), 7617-7628.

(101) Krechmer, J.; Lopez-Hilfiker, F.; Koss, A.; Hutterli, M.; Stoermer, C.; Deming, B.; Kimmel, J.; Warneke, C.; Holzinger, R.; Jayne, J.; et al. Evaluation of a New Reagent-Ion Source and Focusing Ion–Molecule Reactor for Use in Proton-Transfer-Reaction Mass Spectrometry. *Anal. Chem.* **2018**, *90* (20), 12011-12018.

(102) Krechmer, J.; Lopez-Hilfiker, F.; Koss, A.; Hutterli, M.; Stoermer, C.; Deming, B.; Kimmel, J.; Warneke, C.; Holzinger, R.; Jayne, J.; et al. Evaluation of a New Reagent-Ion Source and Focusing Ion–Molecule Reactor for Use in Proton-Transfer-Reaction Mass Spectrometry. *Anal. Chem.* **2018**, *90* (20), 12011-12018.

(103) Wang, Y.; Mehra, A.; Krechmer, J. E.; Yang, G.; Hu, X.; Lu, Y.; Lambe, A.; Canagaratna, M.; Chen, J.; Worsnop, D.; et al. Oxygenated products formed from OH-initiated reactions of trimethylbenzene: autoxidation and accretion. *Atmos. Chem. Phys.* **2020**, *20* (15), 9563-9579.

(104) Wu, R.; Vereecken, L.; Tsiligiannis, E.; Kang, S.; Albrecht, S. R.; Hantschke, L.; Zhao, D.; Novelli, A.; Fuchs, H.; Tillmann, R.; et al. Molecular composition and volatility of multi-generation products formed from isoprene oxidation by nitrate radical. *Atmos. Chem. Phys.* **2021**, *21* (13), 10799-10824.

(105) Koss, A. R.; Canagaratna, M. R.; Zaytsev, A.; Krechmer, J. E.; Breitenlechner, M.; Nihill, K. J.; Lim, C. Y.; Rowe, J. C.; Roscioli, J. R.; Keutsch, F. N.; et al. Dimensionality-reduction techniques for complex mass spectrometric datasets: application to laboratory atmospheric organic oxidation experiments. *Atmos. Chem. Phys.* **2020**, *20* (2), 1021-1041.

(106) Breitenlechner, M.; Fischer, L.; Hainer, M.; Heinritzi, M.; Curtius, J.; Hansel, A. PTR3: An Instrument for Studying the Lifecycle of Reactive Organic Carbon in the Atmosphere. *Anal. Chem.* **2017**, *89* (11), 5824-5831.

(107) Lehtipalo, K.; Yan, C.; Dada, L.; Bianchi, F.; Xiao, M.; Wagner, R.; Stolzenburg, D.; Ahonen, L. R.; Amorim, A.; Baccarini, A.; et al. Multicomponent new particle formation from sulfuric acid, ammonia, and biogenic vapors. *Sci. Adv.* **2018**, *4* (12), eaau5363.

(108) Koss, A. R.; Sekimoto, K.; Gilman, J. B.; Selimovic, V.; Coggon, M. M.; Zarzana, K. J.; Yuan, B.; Lerner, B. M.; Brown, S. S.; Jimenez, J. L.; et al. Non-methane organic gas emissions from biomass burning: identification, quantification, and emission factors from PTR-ToF during the FIREX 2016 laboratory experiment. *Atmos. Chem. Phys.* **2018**, *18* (5), 3299-3319.

(109) Pagonis, D.; Sekimoto, K.; de Gouw, J. A Library of Proton-Transfer Reactions of H3O+ Ions Used for Trace Gas Detection. *J. Am. Soc. Mass. Spectrom.* **2019**, *30* (7), 1330-1335.

(110) Piel, F.; Müller, M.; Winkler, K.; Skytte af Sätra, J.; Wisthaler, A. Introducing the extended volatility range proton-transfer-reaction mass spectrometer (EVR PTR-MS). *Atmos. Meas. Tech.* **2021**, *14* (2), 1355-1363.

(111) Holzinger, R.; Acton, W. J. F.; Bloss, W. J.; Breitenlechner, M.; Crilley, L. R.; Dusanter, S.; Gonin, M.; Gros, V.; Keutsch, F. N.; Kiendler-Scharr, A.; et al. Validity and limitations of simple reaction kinetics to calculate concentrations of organic compounds from ion counts in PTR-MS. *Atmos. Meas. Tech.* **2019**, *12* (11), 6193-6208.

(112) Palm, B. B.; Liu, X.; Jimenez, J. L.; Thornton, J. A. Performance of a new coaxial ion–molecule reaction region for low-pressure chemical ionization mass spectrometry with reduced instrument wall interactions. *Atmos. Meas. Tech.* **2019**, *12* (11), 5829-5844.

(113) Pagonis, D.; Krechmer, J. E.; de Gouw, J.; Jimenez, J. L.; Ziemann, P. J. Effects of gas–wall partitioning in Teflon tubing and instrumentation on time-resolved measurements of gas-phase organic compounds. *Atmos. Meas. Tech.* **2017**, *10* (12), 4687-4696.

(114) Deming, B. L.; Pagonis, D.; Liu, X.; Day, D. A.; Talukdar, R.; Krechmer, J. E.; de Gouw, J. A.; Jimenez, J. L.; Ziemann, P. J. Measurements of delays of gas-phase compounds in a wide variety of tubing materials due to gas–wall interactions. *Atmos. Meas. Tech.* **2019**, *12* (6), 3453-3461.

(115) Liu, X.; Deming, B.; Pagonis, D.; Day, D. A.; Palm, B. B.; Talukdar, R.; Roberts, J. M.; Veres, P. R.; Krechmer, J. E.; Thornton, J. A.; et al. Effects of gas–wall interactions on measurements of semivolatile compounds and small polar molecules. *Atmos. Meas. Tech.* **2019**, *12* (6), 3137-3149.

(116) Jokinen, T.; Sipilä, M.; Junninen, H.; Ehn, M.; Lönn, G.; Hakala, J.; Petäjä, T.; Mauldin Iii, R. L.; Kulmala, M.; Worsnop, D. R. Atmospheric sulphuric acid and neutral cluster measurements using CI-APi-TOF. *Atmos. Chem. Phys.* **2012**, *12* (9), 4117-4125.

(117) Massoli, P.; Stark, H.; Canagaratna, M. R.; Krechmer, J. E.; Xu, L.; Ng, N. L.; Mauldin, R. L., III; Yan, C.; Kimmel, J.; Misztal, P. K.; et al. Ambient measurements of highly oxidized gas-phase molecules during the southern oxidant and aerosol study (SOAS) 2013. *ACS Earth Space Chem.* **2018**, *2* (7), 653-672.

(118) Lee, B. H.; Lopez-Hilfiker, F. D.; Veres, P. R.; McDuffie, E. E.; Fibiger, D. L.; Sparks, T. L.; Ebben, C. J.; Green, J. R.; Schroder, J. C.; Campuzano-Jost, P.; et al. Flight deployment of a high-resolution time-of-flight chemical ionization mass spectrometer: Observations of reactive halogen and nitrogen oxide species. *J. Geophys. Res. Atmos.* **2018**, *123* (14), 7670-7686.

(119) Hansel, A.; Jordan, A.; Holzinger, R.; Prazeller, P.; Vogel, W.; Lindinger, W. Proton transfer reaction mass spectrometry: on-line trace gas analysis at the ppb level. *Int. J. Mass Spectrom. Ion Processes* **1995**, *149-150*, 609-619.

(120) de Gouw, J.; Warneke, C.; Karl, T.; Eerdekens, G.; van der Veen, C.; Fall, R. Sensitivity and specificity of atmospheric trace gas detection by proton-transfer-reaction mass spectrometry. *Int. J. Mass Spectrom.* **2003**, *223-224*, 365-382.

(121) Karl, T.; Hansel, A.; Cappellin, L.; Kaser, L.; Herdlinger-Blatt, I.; Jud, W. Selective measurements of isoprene and 2-methyl-3-buten-2-ol based on NO+ ionization mass spectrometry. *Atmos. Chem. Phys.* **2012**, *12* (24), 11877-11884.

(122) Koss, A. R.; Warneke, C.; Yuan, B.; Coggon, M. M.; Veres, P. R.; de Gouw, J. A. Evaluation of NO+ reagent ion chemistry for online measurements of atmospheric volatile organic compounds. *Atmos. Meas. Tech.* **2016**, *9* (7), 2909-2925.

(123) Kim, M. J.; Zoerb, M. C.; Campbell, N. R.; Zimmermann, K. J.; Blomquist, B. W.; Huebert, B. J.; Bertram, T. H. Revisiting benzene cluster cations for the chemical ionization of dimethyl sulfide and select volatile organic compounds. *Atmos. Meas. Tech.* **2016**, *9* (4), 1473-1484.

(124) Lavi, A.; Vermeuel, M. P.; Novak, G. A.; Bertram, T. H. The sensitivity of benzene cluster cation chemical ionization mass spectrometry to select biogenic terpenes. *Atmos. Meas. Tech.* **2018**, *11* (6), 3251-3262.

(125) Nowak, J. B.; Huey, L. G.; Eisele, F. L.; Tanner, D. J.; Mauldin III, R. L.; Cantrell, C.; Kosciuch, E.; Davis, D. D. Chemical ionization mass spectrometry technique for detection of dimethylsulfoxide and ammonia. *J. Geophys. Res. Atmos.* **2002**, *107* (D18), ACH-10.

(126) Yu, H.; Lee, S.-H. Chemical ionisation mass spectrometry for the measurement of atmospheric amines. *Environ. Chem.* **2012**, *9* (3), 190-201.

(127) Canaval, E.; Hyttinen, N.; Schmidbauer, B.; Fischer, L.; Hansel, A. NH4+ Association and Proton Transfer Reactions With a Series of Organic Molecules. *Front. Chem.* **2019**, *7* (191).

(128) Müller, M.; Piel, F.; Gutmann, R.; Sulzer, P.; Hartungen, E.; Wisthaler, A. A novel method for producing NH4+ reagent ions in the hollow cathode glow discharge ion source of PTR-MS instruments. *Int. J. Mass Spectrom.* **2020**, *447*, 116254.

(129) Xu, L.; Coggon, M. M.; Stockwell, C. E.; Gilman, J. B.; Robinson, M. A.; Breitenlechner, M.; Lamplugh, A.; Crounse, J. D.; Wennberg, P. O.; Neuman, J. A.; et al. Chemical ionization mass spectrometry utilizing ammonium ions (NH4+ CIMS) for measurements of organic compounds in the atmosphere. *Atmos. Meas. Tech.* **2022**, *15* (24), 7353-7373.

(130) Khare, P.; Krechmer, J. E.; Machesky, J. E.; Hass-Mitchell, T.; Cao, C.; Wang, J.; Majluf, F.; Lopez-Hilfiker, F.; Malek, S.; Wang, W.; et al. Ammonium-adduct chemical ionization to investigate anthropogenic oxygenated gas-phase organic compounds in urban air. *Atmos. Chem. Phys. Discuss.* **2022**, *2022*, 1-39.

(131) Berndt, T.; Scholz, W.; Mentler, B.; Fischer, L.; Herrmann, H.; Kulmala, M.; Hansel, A. Accretion Product Formation from Self- and Cross-Reactions of RO2 Radicals in the Atmosphere. *A Angew. Chem. Int. Ed.* **2018**, *57* (14), 3820-3824.

(132) Ji, Y.; Huey, L. G.; Tanner, D. J.; Lee, Y. R.; Veres, P. R.; Neuman, J. A.; Wang, Y.; Wang, X. A vacuum ultraviolet ion source (VUV-IS) for iodide–chemical ionization mass spectrometry: a substitute for radioactive ion sources. *Atmos. Meas. Tech.* **2020**, *13* (7), 3683-3696.

(133) Breitenlechner, M.; Novak, G. A.; Neuman, J. A.; Rollins, A. W.; Veres, P. R. A versatile vacuum ultraviolet ion source for reduced pressure bipolar chemical ionization mass spectrometry. *Atmos. Meas. Tech.* **2022**, *15* (5), 1159-1169.

(134) Rissanen, M. P.; Mikkilä, J.; Iyer, S.; Hakala, J. Multi-scheme chemical ionization inlet (MION) for fast switching of reagent ion chemistry in atmospheric pressure chemical ionization mass spectrometry (CIMS) applications. *Atmos. Meas. Tech.* **2019**, *12* (12), 6635-6646.

(135) Veres, P.; Roberts, J. M.; Warneke, C.; Welsh-Bon, D.; Zahniser, M.; Herndon, S.; Fall, R.; de Gouw, J. Development of negative-ion proton-transfer chemical-ionization mass spectrometry (NI-PT-CIMS) for the measurement of gas-phase organic acids in the atmosphere. *Int. J. Mass Spectrom.* **2008**, *274* (1), 48-55.

(136) Eisele, F. L.; Tanner, D. J. Measurement of the gas phase concentration of H2SO4 and methane sulfonic acid and estimates of H2SO4 production and loss in the atmosphere. *J. Geophys. Res. Atmos.* **1993**, *98* (D5), 9001-9010.

(137) Allen, H. M.; Crounse, J. D.; Kim, M. J.; Teng, A. P.; Ray, E. A.; McKain, K.; Sweeney, C.; Wennberg, P. O. H2O2 and CH3OOH (MHP) in the Remote Atmosphere: 1. Global Distribution and Regional Influences. *J. Geophys. Res. Atmos.* **2022**, *127* (6), e2021JD035701.

(138) Crounse, J. D.; McKinney, K. A.; Kwan, A. J.; Wennberg, P. O. Measurement of Gas-Phase Hydroperoxides by Chemical Ionization Mass Spectrometry. *Anal. Chem.* **2006**, *78* (19), 6726-6732.

(139) Bianchi, F.; Kurtén, T.; Riva, M.; Mohr, C.; Rissanen, M. P.; Roldin, P.; Berndt, T.; Crounse, J. D.; Wennberg, P. O.; Mentel, T. F.; et al. Highly Oxygenated Organic Molecules (HOM) from Gas-Phase Autoxidation Involving Peroxy Radicals: A Key Contributor to Atmospheric Aerosol. *Chem. Rev.* **2019**, *119* (6), 3472-3509.

(140) Riva, M.; Brüggemann, M.; Li, D.; Perrier, S.; George, C.; Herrmann, H.; Berndt, T. Capability of CI-Orbitrap for Gas-Phase Analysis in Atmospheric Chemistry: A Comparison with the CI-APi-TOF Technique. *Anal. Chem.* **2020**, *92* (12), 8142-8150.

(141) Breitenlechner, M.; Novak, G. A.; Neuman, J. A.; Rollins, A. W.; Veres, P. R. A versatile vacuum ultraviolet ion source for reduced pressure bipolar chemical ionization mass spectrometry. *Atmos. Meas. Tech.* **2022**, *15*, 1159-1169.

(142) Crounse, J. D.; McKinney, K. A.; Kwan, A. J.; Wennberg, P. O. Measurement of gas-phase hydroperoxides by chemical ionization mass spectrometry. *Anal. Chem.* **2006**, *78* (19), 6726-6732.

(143) Yuan, B.; Koss, A.; Warneke, C.; Gilman, J. B.; Lerner, B. M.; Stark, H.; de Gouw, J. A. A high-resolution time-of-flight chemical ionization mass spectrometer utilizing hydronium ions (H3O+ ToF-CIMS) for measurements of volatile organic compounds in the atmosphere. *Atmos. Meas. Tech.* **2016**, *9* (6), 2735-2752.

(144) Aljawhary, D.; Lee, A. K. Y.; Abbatt, J. P. D. High-resolution chemical ionization mass spectrometry (ToF-CIMS): application to study SOA composition and processing. *Atmos. Meas. Tech.* **2013**, *6* (11), 3211-3224.

(145) Nowak, J. B.; Huey, L. G.; Eisele, F. L.; Tanner, D. J.; Mauldin Iii, R. L.; Cantrell, C.; Kosciuch, E.; Davis, D. D. Chemical ionization mass spectrometry technique for detection of dimethylsulfoxide and ammonia. *J. Geophys. Res. Atmos.* **2002**, *107* (D18), ACH-10.

(146) Zhu, L.; Mikoviny, T.; Kolstad Morken, A.; Tan, W.; Wisthaler, A. A compact and easy-to-use mass spectrometer for online monitoring of amines in the flue gas of a post-combustion carbon capture plant. *Int. J. Greenh. Gas Control.* **2018**, *78*, 349-353.

(147) Xu, L.; Coggon, M. M.; Stockwell, C. E.; Gilman, J. B.; Robinson, M. A.; Breitenlechner, M.; Lamplugh, A.; Neuman, J. A.; Novak, G. A.; Veres, P. R.; et al. A chemical ionization mass spectrometry utilizing ammonium ions (NH4+ CIMS) for measurements of organic compounds in the atmosphere. *Atmos. Meas. Tech. Discuss.* **2022**, *2022*, 1-31.

(148) Hansel, A.; Scholz, W.; Mentler, B.; Fischer, L.; Berndt, T. Detection of RO2 radicals and other products from cyclohexene ozonolysis with NH4+ and acetate chemical ionization mass spectrometry. *Atmos. Environ.* **2018**, *186*, 248-255.

(149) Berndt, T.; Herrmann, H.; Kurtén, T. Direct Probing of Criegee Intermediates from Gas-Phase Ozonolysis Using Chemical Ionization Mass Spectrometry. *J. Am. Chem. Soc.* **2017**, *139* (38), 13387-13392.

(150) Berndt, T.; Mentler, B.; Scholz, W.; Fischer, L.; Herrmann, H.; Kulmala, M.; Hansel, A. Accretion Product Formation from Ozonolysis and OH Radical Reaction of α-Pinene: Mechanistic Insight and the Influence of Isoprene and Ethylene. *Environ. Sci. Technol.* **2018**, *52* (19), 11069-11077.

(151) Priestley, M.; Bannan, T. J.; Le Breton, M.; Worrall, S. D.; Kang, S.; Pullinen, I.; Schmitt, S.; Tillmann, R.; Kleist, E.; Zhao, D.; et al. Chemical characterisation of benzene oxidation products under high- and low-NOx conditions using chemical ionisation mass spectrometry. *Atmos. Chem. Phys.* **2021**, *21* (5), 3473-3490.

(152) Berndt, T.; Richters, S.; Jokinen, T.; Hyttinen, N.; Kurtén, T.; Otkjær, R. V.; Kjaergaard, H. G.; Stratmann, F.; Herrmann, H.; Sipilä, M.; et al. Hydroxyl radical-induced formation of highly oxidized organic compounds. *Nat. Comm.* **2016**, *7* (1), 13677.

(153) Ehn, M.; Thornton, J. A.; Kleist, E.; Sipilä, M.; Junninen, H.; Pullinen, I.; Springer, M.; Rubach, F.; Tillmann, R.; Lee, B.; et al. A large source of low-volatility secondary organic aerosol. *Nature* **2014**, *506* (7489), 476-479.

(154) Rissanen, M. P.; Kurtén, T.; Sipilä, M.; Thornton, J. A.; Kangasluoma, J.; Sarnela, N.; Junninen, H.; Jørgensen, S.; Schallhart, S.; Kajos, M. K.; et al. The Formation of Highly Oxidized Multifunctional Products in the Ozonolysis of Cyclohexene. *J. Am. Chem. Soc.* **2014**, *136* (44), 15596-15606.

(155) Rissanen, M. P.; Kurtén, T.; Sipilä, M.; Thornton, J. A.; Kausiala, O.; Garmash, O.; Kjaergaard, H. G.; Petäjä, T.; Worsnop, D. R.; Ehn, M.; et al. Effects of Chemical Complexity on the Autoxidation Mechanisms of Endocyclic Alkene Ozonolysis Products:

From Methylcyclohexenes toward Understanding α-Pinene. *J. Phys. Chem. A* **2015**, *119* (19), 4633-4650.

(156) Paulot, F.; Crounse, J. D.; Kjaergaard, H. G.; Kroll, J. H.; Seinfeld, J. H.; Wennberg, P. O. Isoprene photooxidation: new insights into the production of acids and organic nitrates. *Atmos. Chem. Phys.* **2009**, *9* (4), 1479-1501.

(157) Vasquez, K. A.-O.; Crounse, J. A.-O. X.; Schulze, B. A.-O.; Bates, K. A.-O.; Teng, A. P.; Xu, L. A.-O.; Allen, H. A.-O.; Wennberg, P. O. Rapid hydrolysis of tertiary isoprene nitrate efficiently removes NOx from the atmosphere. *Proc. Natl. Acad. Sci. U.S.A.* **2020**, *117* (52), 33011-33016.

(158) Huey, L. G.; Hanson, D. R.; Howard, C. J. Reactions of SF6- and I- with Atmospheric Trace Gases. *J. Phys. Chem.* **1995**, *99* (14), 5001-5008.

(159) Slusher, D. L.; Pitteri, S. J.; Haman, B. J.; Tanner, D. J.; Huey, L. G. A chemical ionization technique for measurement of pernitric acid in the upper troposphere and the polar boundary layer. *Geophys. Res. Lett.* **2001**, *28* (20), 3875-3878.

(160) Jordan, A.; Haidacher, S.; Hanel, G.; Hartungen, E.; Herbig, J.; Märk, L.; Schottkowsky, R.; Seehauser, H.; Sulzer, P.; Märk, T. D. An online ultra-high sensitivity Proton-transfer-reaction mass-spectrometer combined with switchable reagent ion capability (PTR+SRI−MS). *Int. J. Mass Spectrom.* **2009**, *286* (1), 32-38.

(161) Sulzer, P.; Agarwal, B.; Jürschik, S.; Lanza, M.; Jordan, A.; Hartungen, E.; Hanel, G.; Märk, L.; Märk, T. D.; González-Méndez, R.; et al. Applications of switching reagent ions in proton transfer reaction mass spectrometric instruments for the improved selectivity of explosive compounds. *Int. J. Mass Spectrom.* **2013**, *354-355*, 123-128.

(162) Smith, D.; Španěl, P. Selected ion flow tube mass spectrometry (SIFT-MS) for on-line trace gas analysis. *Mass Spectrom. Rev.* **2005**, *24* (5), 661-700.

(163) Brophy, P.; Farmer, D. K. A switchable reagent ion high resolution time-of-flight chemical ionization mass spectrometer for real-time measurement of gas phase oxidized species: characterization from the 2013 southern oxidant and aerosol study. *Atmos. Meas. Tech.* **2015**, *8* (7), 2945-2959.

(164) Zaytsev, A.; Koss, A. R.; Breitenlechner, M.; Krechmer, J. E.; Nihill, K. J.; Lim, C. Y.; Rowe, J. C.; Cox, J. L.; Moss, J.; Roscioli, J. R.; et al. Mechanistic study of the formation of ring-retaining and ring-opening products from the oxidation of aromatic compounds under urban atmospheric conditions. *Atmos. Chem. Phys.* **2019**, *19* (23), 15117-15129.

(165) Lopez-Hilfiker, F. D.; Mohr, C.; Ehn, M.; Rubach, F.; Kleist, E.; Wildt, J.; Mentel, T. F.; Carrasquillo, A. J.; Daumit, K. E.; Hunter, J. F.; et al. Phase partitioning and volatility

of secondary organic aerosol components formed from α-pinene ozonolysis and OH oxidation: the importance of accretion products and other low volatility compounds. *Atmos. Chem. Phys.* **2015**, *15* (14), 7765-7776.

(166) Mohr, C.; Lopez-Hilfiker, F. D.; Yli-Juuti, T.; Heitto, A.; Lutz, A.; Hallquist, M.; D'Ambro, E. L.; Rissanen, M. P.; Hao, L.; Schobesberger, S.; et al. Ambient observations of dimers from terpene oxidation in the gas phase: Implications for new particle formation and growth. *Geophys. Res. Lett.* **2017**, *44* (6), 2958-2966.

(167) Zhang, H.; Yee, L. D.; Lee, B. H.; Curtis, M. P.; Worton, D. R.; Isaacman-VanWertz, G.; Offenberg, J. H.; Lewandowski, M.; Kleindienst, T. E.; Beaver, M. R.; et al. Monoterpenes are the largest source of summertime organic aerosol in the southeastern United States. *Proc. Natl. Acad. Sci. U.S.A.* **2018**, *115* (9), 2038-2043.

(168) Zhao, Z.; Yang, X.; Lee, J.; Tolentino, R.; Mayorga, R.; Zhang, W.; Zhang, H. Diverse Reactions in Highly Functionalized Organic Aerosols during Thermal Desorption. *ACS Earth Space Chem.* **2020**, *4* (2), 283-296.

(169) Pagonis, D.; Campuzano-Jost, P.; Guo, H.; Day, D. A.; Schueneman, M. K.; Brown, W. L.; Nault, B. A.; Stark, H.; Siemens, K.; Laskin, A.; et al. Airborne extractive electrospray mass spectrometry measurements of the chemical composition of organic aerosol. *Atmos. Meas. Tech.* **2021**, *14* (2), 1545-1559.

(170) Leglise, J.; Müller, M.; Piel, F.; Otto, T.; Wisthaler, A. Bulk organic aerosol analysis by proton-transfer-reaction mass spectrometry: An improved methodology for the determination of total organic mass, O:C and H:C elemental ratios, and the average molecular formula. *Anal. Chem.* **2019**, *91* (20), 12619-12624.

(171) Häkkinen, E.; Zhao, J.; Graeffe, F.; Fauré, N.; Krechmer, J.; Worsnop, D.; Timonen, H.; Ehn, M.; Kangasluoma, J. Online measurement of highly oxygenated compounds from organic aerosol. *EGUsphere* **2022**, *2022*, 1-29.

(172) Zhao, J.; Häkkinen, E.; Graeffe, F.; Krechmer, J. E.; Canagaratna, M. R.; Worsnop, D. R.; Kangasluoma, J.; Ehn, M. A combined gas- and particle-phase analysis of highly oxygenated organic molecules (HOM) from α-pinene ozonolysis. *EGUsphere* **2022**, *2022*, 1-30.

(173) Avery, A. M.; Alton, M. W.; Canagaratna, M. R.; Krechmer, J. E.; Sueper, D. T.; Bhattacharyya, N.; Hildebrandt Ruiz, L.; Brune, W. H.; Lambe, A. T. Comparison of the yield and chemical composition of secondary organic aerosol generated from the OH and Cl oxidation of decamethylcyclopentasiloxane. *ACS Earth Space Chem.* **2023**.

(174) Zuth, C.; Vogel, A. L.; Ockenfeld, S.; Huesmann, R.; Hoffmann, T. Ultrahigh-Resolution Mass Spectrometry in Real Time: Atmospheric Pressure Chemical Ionization

Orbitrap Mass Spectrometry of Atmospheric Organic Aerosol. *Anal. Chem.* **2018**, *90* (15), 8816-8823.

(175) Riva, M.; Ehn, M.; Li, D.; Tomaz, S.; Bourgain, F.; Perrier, S.; George, C. CI-Orbitrap: An analytical instrument to study atmospheric reactive organic species. *Anal. Chem.* **2019**, *91* (15), 9419-9423.

(176) Zubarev, R. A.; Makarov, A. Orbitrap mass spectrometry. *Anal. Chem.* **2013**, *85* (11), 5288-5296.

(177) Makarov, A. Electrostatic Axially Harmonic Orbital Trapping: A High-Performance Technique of Mass Analysis. *Anal. Chem.* **2000**, *72* (6), 1156-1162.

(178) Cai, R.; Huang, W.; Meder, M.; Bourgain, F.; Aizikov, K.; Riva, M.; Bianchi, F.; Ehn, M. Improving the sensitivity of fourier transform mass spectrometer (orbitrap) for online measurements of atmospheric vapors. *Anal. Chem.* **2022**, *94* (45), 15746-15753.

(179) Feider, C. L.; Krieger, A.; DeHoog, R. J.; Eberlin, L. S. Ambient ionization mass spectrometry: Recent developments and applications. *Anal. Chem.* **2019**, *91* (7), 4266-4290.

(180) Reemtsma, T.; These, A.; Venkatachari, P.; Xia, X.; Hopke, P. K.; Springer, A.; Linscheid, M. Identification of fulvic acids and sulfated and nitrated analogues in atmospheric aerosol by electrospray ionization fourier transform ion cyclotron resonance mass spectrometry. *Anal. Chem.* **2006**, *78* (24), 8299-8304.

(181) Chen, H.; Venter A Fau - Cooks, R. G.; Cooks, R. G. Extractive electrospray ionization for direct analysis of undiluted urine, milk and other complex mixtures without sample preparation. *Chem. Commun.* **2006**, (19), 2042-2044.

(182) Lopez-Hilfiker, F. D.; Pospisilova, V.; Huang, W.; Kalberer, M.; Mohr, C.; Stefenelli, G.; Thornton, J. A.; Baltensperger, U.; Prevot, A. S. H.; Slowik, J. G. An extractive electrospray ionization time-of-flight mass spectrometer (EESI-TOF) for online measurement of atmospheric aerosol particles. *Atmos. Meas. Tech.* **2019**, *12* (9), 4867-4886.

(183) Gallimore, P. J.; Giorio, C.; Mahon, B. M.; Kalberer, M. Online molecular characterisation of organic aerosols in an atmospheric chamber using extractive electrospray ionisation mass spectrometry. *Atmos. Chem. Phys.* **2017**, *17* (23), 14485-14500.

(184) Zhao, Y.; Chan, J. K.; Lopez-Hilfiker, F. D.; McKeown, M. A.; D'Ambro, E. L.; Slowik, J. G.; Riffell, J. A.; Thornton, J. A. An electrospray chemical ionization source for real-time measurement of atmospheric organic and inorganic vapors. *Atmos. Meas. Tech.* **2017**, *10* (10), 3609-3625

(185) Pospisilova, V.; Bell, D. M.; Lamkaddam, H.; Bertrand, A.; Wang, L.; Bhattu, D.; Zhou, X.; Dommen, J.; Prevot, A. S. H.; Baltensperger, U.; et al. Photodegradation of α-pinene secondary organic aerosol dominated by moderately oxidized molecules. *Environ. Sci. Technol.* **2021**, *55* (10), 6936-6943.

(186) Kebarle, P.; Peschke, M. On the mechanisms by which the charged droplets produced by electrospray lead to gas phase ions. *Anal. Chim. Acta* **2000**, *406* (1), 11-35.

(187) Lee, C. P.; Riva, M.; Wang, D.; Tomaz, S.; Li, D.; Perrier, S.; Slowik, J. G.; Bourgain, F.; Schmale, J.; Prevot, A. S. H.; et al. Online Aerosol Chemical Characterization by Extractive Electrospray Ionization–Ultrahigh-Resolution Mass Spectrometry (EESI-Orbitrap). *Environ. Sci. Technol.* **2020**, *54* (7), 3871-3880.

(188) Pospisilova, V.; Lopez-Hilfiker, F. D.; Bell, D. M.; El Haddad, I.; Mohr, C.; Huang, W.; Heikkinen, L.; Xiao, M.; Dommen, J.; Prevot, A. S. H.; et al. On the fate of oxygenated organic molecules in atmospheric aerosol particles. *Sci. Adv. 6* (11), eaax8922.

(189) Brown, W. L.; Day, D. A.; Stark, H.; Pagonis, D.; Krechmer, J. E.; Liu, X.; Price, D. J.; Katz, E. F.; DeCarlo, P. F.; Masoud, C. G.; et al. Real-time organic aerosol chemical speciation in the indoor environment using extractive electrospray ionization mass spectrometry. *Indoor Air* **2021**, *31* (1), 141-155.

(190) Surdu, M. A.-O.; Pospisilova, V. A.-O.; Xiao, M.; Wang, M.; Mentler, B.; Simon, M.; Stolzenburg, D.; Hoyle, C. R.; Bell, D. A.-O.; Lee, C. A.-O.; et al. Molecular characterization of ultrafine particles using extractive electrospray time-of-flight mass spectrometry. *Environ. sci. Atmos.* **2021**, *1* (6), 434-448.

(191) Hems, R. F.; Schnitzler, E. G.; Liu-Kang, C.; Cappa, C. D.; Abbatt, J. P. D. Aging of atmospheric brown carbon aerosol. *ACS Earth Space Chem.* **2021**, *5* (4), 722-748.

(192) Huang, W.; Saathoff, H.; Shen, X.; Ramisetty, R.; Leisner, T.; Mohr, C. Seasonal characteristics of organic aerosol chemical composition and volatility in Stuttgart, Germany. *Atmos. Chem. Phys.* **2019**, *19* (18), 11687-11700.

(193) Brüggemann, M.; Xu, R.; Tilgner, A.; Kwong, K. C.; Mutzel, A.; Poon, H. Y.; Otto, T.; Schaefer, T.; Poulain, L.; Chan, M. N.; et al. Organosulfates in ambient aerosol: State of knowledge and future research directions on formation, abundance, fate, and importance. *Environ. Sci. Technol.* **2020**, *54* (7), 3767-3782.

(194) Zhao, Y.; Thornton, J. A.; Pye, H. O. T. Quantitative constraints on autoxidation and dimer formation from direct probing of monoterpene-derived peroxy radical chemistry. *Proc. Natl. Acad. Sci. U.S.A.* **2018**, *115* (48), 12142.

(195) Chiang, S.; Zhang, W.; Ouyang, Z. Paper spray ionization mass spectrometry: recent advances and clinical applications. *Expert Rev. Proteomics* **2018**, *15* (10), 781-789.

(196) Espy, R. D.; Muliadi, A. R.; Ouyang, Z.; Cooks, R. G. Spray mechanism in paper spray ionization. *Int. J. Mass Spectrom.* **2012**, *325-327*, 167-171.

(197) Kohli, R. K.; Davies, J. F. Measuring the chemical evolution of levitated particles: A study on the evaporation of multicomponent organic aerosol. *Anal. Chem.* **2021**, *93* (36), 12472-12479.

(198) Willis, M. D.; Rovelli, G.; Wilson, K. R. Combining mass spectrometry of picoliter samples with a multicompartment electrodynamic trap for probing the chemistry of droplet arrays. *Anal. Chem.* **2020**, *92* (17), 11943-11952.

(199) Kohli, R. K.; Davies, J. F. Paper spray mass spectrometry for the analysis of picoliter droplets. *Analyst* **2020**, *145* (7), 2639-2648, 10.1039/C9AN02534K.

(200) Zhao, Y.; Fairhurst, M. C.; Wingen, L. M.; Perraud, V.; Ezell, M. J.; Finlayson-Pitts, B. J. New insights into atmospherically relevant reaction systems using direct analysis in real-time mass spectrometry (DART-MS). *Atmos. Meas. Tech.* **2017**, *10* (4), 1373-1386.

(201) Ai, W.; Nie, H.; Song, S.; Liu, X.; Bai, Y.; Liu, H. A Versatile Integrated Ambient Ionization Source Platform. *J. Am. Soc. Mass. Spectrom.* **2018**, *29* (7), 1408-1415.

(202) Wingen, L. M.; Finlayson-Pitts, B. J. Probing surfaces of atmospherically relevant organic particles by easy ambient sonic-spray ionization mass spectrometry (EASI-MS). *Chem. Sci.* **2019**, *10* (3), 884-897.

(203) Cody, R.; Laramee, J. A.; Nilles, J. M.; Durst, H. D. Direct analysis in real time (DART) mass spectrometry. *JEOL News* **2005**, *40*, 8-12.

(204) Zhou, S.; Forbes, M. W.; Abbatt, J. P. D. Kinetics and Products from Heterogeneous Oxidation of Squalene with Ozone. *Environ. Sci. Technol.* **2016**, *50* (21), 11688-11697.

(205) Lam, H. K.; Kwong, K. C.; Poon, H. Y.; Davies, J. F.; Zhang, Z.; Gold, A.; Surratt, J. D.; Chan, M. N. Heterogeneous OH oxidation of isoprene-epoxydiol-derived organosulfates: kinetics, chemistry and formation of inorganic sulfate. *Atmos. Chem. Phys.* **2019**, *19* (4), 2433-2440.

(206) Schwartz-Narbonne, H.; Wang, C.; Zhou, S.; Abbatt, J. P. D.; Faust, J. Heterogeneous Chlorination of Squalene and Oleic Acid. *Environ. Sci. Technol.* **2019**, *53* (3), 1217-1224.

(207) Davies, J. F.; Wilson, K. R. Nanoscale interfacial gradients formed by the reactive uptake of OH radicals onto viscous aerosol surfaces. *Chem. Sci.* **2015**, *6* (12), 7020-7027.

(208) Kwong, K. C.; Chim, M. M.; Hoffmann, E. H.; Tilgner, A.; Herrmann, H.; Davies, J. F.; Wilson, K. R.; Chan, M. N. Chemical Transformation of Methanesulfonic Acid and

Sodium Methanesulfonate through Heterogeneous OH Oxidation. *ACS Earth Space Chem.* **2018**, *2* (9), 895-903.

(209) Zhou, S.; Joudan, S.; Forbes, M. W.; Zhou, Z.; Abbatt, J. P. D. Reaction of condensed-phase Criegee intermediates with carboxylic acids and perfluoroalkyl carboxylic acids. *Environ. Sci. Technol. Lett.* **2019**, *6* (4), 243-250.

(210) Zhou, Z.; Zhou, S.; Abbatt, J. P. D. Kinetics and condensed-phase products in multiphase ozonolysis of an unsaturated triglyceride. *Environ. Sci. Technol.* **2019**, *53* (21), 12467-12475.

(211) Shelley, J. T.; Wiley, J. S.; Hieftje, G. M. Ultrasensitive ambient mass spectrometric analysis with a pin-to-capillary flowing atmospheric-pressure afterglow source. *Anal. Chem.* **2011**, *83* (14), 5741-5748.

(212) Brüggemann, M.; Poulain, L.; Held, A.; Stelzer, T.; Zuth, C.; Richters, S.; Mutzel, A.; van Pinxteren, D.; Iinuma, Y.; Katkevica, S.; et al. Real-time detection of highly oxidized organosulfates and BSOA marker compounds during the F-BEACh 2014 field study. *Atmos. Chem. Phys.* **2017**, *17* (2), 1453-1469.

(213) Fandino, J.; Orejas, J.; Chauvet, L.; Blanco, D.; Guillot, P.; Pisonero, J.; Bordel, N. Evaluation of a modified halo flowing atmospheric pressure afterglow ion source for the analysis of directly injected volatile organic compounds. *J. Anal. At. Spectrom.* **2020**, *35* (9), 2002-2010.

(214) Aghaei, M.; Bogaerts, A. Flowing atmospheric pressure afterglow for ambient ionization: Reaction pathways revealed by modeling. *Anal. Chem.* **2021**, *93* (17), 6620-6628.

(215) Schilling, G. D.; Shelley, J. T.; Barnes, J. H.; Sperline, R. P.; Denton, M. B.; Barinaga, C. J.; Koppenaal, D. W.; Hieftje, G. M. Detection of positive and negative ions from a flowing atmospheric pressure afterglow using a mattauch-herzog mass spectrograph equipped with a faraday-strip array detector. *J. Am. Soc. Mass Spectrom.* **2010**, *21* (1), 97-103.

(216) Hirabayashi, A.; Sakairi, M.; Koizumi, H. Sonic Spray Ionization Method for Atmospheric Pressure Ionization Mass Spectrometry. *Anal. Chem.* **1994**, *66* (24), 4557-4559.

(217) Hirabayashi, A.; Sakairi, M.; Koizumi, H. Sonic spray mass spectrometry. *Anal. Chem.* **1995**, *67* (17), 2878-2882.

(218) Wingen, L. M.; Finlayson-Pitts, B. J. Probing surfaces of atmospherically relevant organic particles by easy ambient sonic-spray ionization mass spectrometry (EASI-MS). *Chem. Sci.* **2019**, *10* (3), 884-897.

(219) Kerecman, D. E.; Apsokardu, M. J.; Talledo, S. L.; Taylor, M. S., Jr.; Haugh, D. N.; Zhang, Y.; Johnston, M. V. Online characterization of organic aerosol by condensational growth into aqueous droplets coupled with droplet-assisted ionization. *Anal. Chem.* **2021**, *93* (5), 2793-2801.

(220) Apsokardu, M. J.; Kerecman, D. E.; Johnston, M. V. Ion formation in droplet-assisted ionization. *Rapid Commun. Mass Spectrom.* **2021**, *35* (S1), e8227.

(221) Apsokardu, M. J.; Krasnomowitz, J. M.; Jiang, S.; Johnston, M. V. Ion formation from rapidly heated aqueous droplets by droplet-assisted ionization. *J. Phys. Chem. A* **2020**, *124* (36), 7313-7321.

(222) Horan, A. J.; Apsokardu, M. J.; Johnston, M. V. Droplet Assisted Inlet Ionization for Online Analysis of Airborne Nanoparticles. *Anal. Chem.* **2017**, *89* (2), 1059-1062.

(223) Pagnotti, V. S.; Inutan, E. D.; Marshall, D. D.; McEwen, C. N.; Trimpin, S. Inlet ionization: A new highly sensitive approach for liquid chromatography/mass spectrometry of small and large molecules. *Anal. Chem.* **2011**, *83* (20), 7591-7594.

(224) Qin, Y.; Wingen, L. M.; Finlayson-Pitts, B. J. Toward a molecular understanding of the surface composition of atmospherically relevant organic particles. *Proc. Natl. Acad. Sci. U.S.A.* **2022**, *119* (35), e2209134119.

(225) Bi, C.; Krechmer, J. E.; Frazier, G. O.; Xu, W.; Lambe, A. T.; Claflin, M. S.; Lerner, B. M.; Jayne, J. T.; Worsnop, D. R.; Canagaratna, M. R.; et al. Quantification of isomer-resolved iodide chemical ionization mass spectrometry sensitivity and uncertainty using a voltage-scanning approach. *Atmos. Meas. Tech.* **2021**, *14* (10), 6835-6850.

(226) Jaoui, M.; Kleindienst, T. E.; Lewandowski, M.; Offenberg, J. H.; Edney, E. O. Identification and Quantification of Aerosol Polar Oxygenated Compounds Bearing Carboxylic or Hydroxyl Groups. 2. Organic Tracer Compounds from Monoterpenes. *Environ. Sci. Technol.* **2005**, *39* (15), 5661-5673.

(227) Jaoui, M.; Edney, E. O.; Kleindienst, T. E.; Lewandowski, M.; Offenberg, J. H.; Surratt, J. D.; Seinfeld, J. H. Formation of secondary organic aerosol from irradiated α-pinene/toluene/NOx mixtures and the effect of isoprene and sulfur dioxide. *J. Geophys. Res. Atmos.* **2008**, *113* (D9).

(228) Bates, K. H.; Crounse, J. D.; St. Clair, J. M.; Bennett, N. B.; Nguyen, T. B.; Seinfeld, J. H.; Stoltz, B. M.; Wennberg, P. O. Gas Phase Production and Loss of Isoprene Epoxydiols. *J. Phys. Chem. A* **2014**, *118* (7), 1237-1246.

(229) Teng, A. P.; Crounse, J. D.; Lee, L.; St. Clair, J. M.; Cohen, R. C.; Wennberg, P. O. Hydroxy nitrate production in the OH-initiated oxidation of alkenes. *Atmos. Chem. Phys.* **2015**, *15* (8), 4297-4316.

(230) Xu, L.; Møller, K. H.; Crounse, J. D.; Kjaergaard, H. G.; Wennberg, P. O. New Insights into the Radical Chemistry and Product Distribution in the OH-Initiated Oxidation of Benzene. *Environ. Sci. Technol.* **2020**, *54* (21), 13467-13477.

(231) Xu, L.; Møller, K. H.; Crounse, J. D.; Otkjær, R. V.; Kjaergaard, H. G.; Wennberg, P. O. Unimolecular Reactions of Peroxy Radicals Formed in the Oxidation of α-Pinene and β-Pinene by Hydroxyl Radicals. *J. Phys. Chem. A* **2019**, *123* (8), 1661-1674.

(232) Teng, A. P.; Crounse, J. D.; Wennberg, P. O. Isoprene Peroxy Radical Dynamics. *J. Am. Chem. Soc.* **2017**, *139* (15), 5367-5377.

(233) Vasquez, K. T.; Allen, H. M.; Crounse, J. D.; Praske, E.; Xu, L.; Noelscher, A. C.; Wennberg, P. O. Low-pressure gas chromatography with chemical ionization mass spectrometry for quantification of multifunctional organic compounds in the atmosphere. *Atmos. Meas. Tech.* **2018**, *11* (12), 6815-6832.

(234) Praske, E.; Otkjær, R. V.; Crounse, J. D.; Hethcox, J. C.; Stoltz, B. M.; Kjaergaard, H. G.; Wennberg, P. O. Atmospheric autoxidation is increasingly important in urban and suburban North America. *Proc. Natl. Acad. Sci. U.S.A.* **2018**, *115* (1), 64-69.

(235) Kurtén, T.; Møller, K. H.; Nguyen, T. B.; Schwantes, R. H.; Misztal, P. K.; Su, L.; Wennberg, P. O.; Fry, J. L.; Kjaergaard, H. G. Alkoxy radical bond scissions explain the anomalously low secondary organic aerosol and organonitrate yields from α-pinene + NO3. *J. Phys. Chem. Lett.* **2017**, *8* (13), 2826-2834.

(236) Bi, C.; Krechmer, J. E.; Frazier, G. O.; Xu, W.; Lambe, A. T.; Claflin, M. S.; Lerner, B. M.; Jayne, J. T.; Worsnop, D. R.; Canagaratna, M. R.; et al. Coupling a gas chromatograph simultaneously to a flame ionization detector and chemical ionization mass spectrometer for isomer-resolved measurements of particle-phase organic compounds. *Atmos. Meas. Tech.* **2021**, *14* (5), 3895-3907.

(237) Isaacman, G.; Kreisberg, N. M.; Yee, L. D.; Worton, D. R.; Chan, A. W. H.; Moss, J. A.; Hering, S. V.; Goldstein, A. H. Online derivatization for hourly measurements of gas- and particle-phase semi-volatile oxygenated organic compounds by thermal desorption aerosol gas chromatography (SV-TAG). *Atmos. Meas. Tech.* **2014**, *7* (12), 4417-4429.

(238) Williams, B. J.; Goldstein, A. H.; Kreisberg, N. M.; Hering, S. V. An In-Situ Instrument for Speciated Organic Composition of Atmospheric Aerosols: Thermal Desorption Aerosol GC/MS-FID (TAG). *Aerosol Sci. Tech.* **2006**, *40* (8), 627-638.

(239) Zhao, Y.; Kreisberg, N. M.; Worton, D. R.; Teng, A. P.; Hering, S. V.; Goldstein, A. H. Development of an In Situ Thermal Desorption Gas Chromatography Instrument for Quantifying Atmospheric Semi-Volatile Organic Compounds. *Aerosol Sci. Technol.* **2013**, *47* (3), 258-266.

(240) Isaacman-VanWertz, G.; Yee, L. D.; Kreisberg, N. M.; Wernis, R.; Moss, J. A.; Hering, S. V.; de Sá, S. S.; Martin, S. T.; Alexander, M. L.; Palm, B. B.; et al. Ambient Gas-Particle Partitioning of Tracers for Biogenic Oxidation. *Environ. Sci. Technol.* **2016**, *50* (18), 9952-9962.

(241) Szmigielski, R.; Surratt, J. D.; Gómez-González, Y.; Van der Veken, P.; Kourtchev, I.; Vermeylen, R.; Blockhuys, F.; Jaoui, M.; Kleindienst, T. E.; Lewandowski, M.; et al. 3-methyl-1,2,3-butanetricarboxylic acid: An atmospheric tracer for terpene secondary organic aerosol. *Geophys. Res. Lett.* **2007**, *34* (24).

(242) Zhang, X.; Dalleska, N. F.; Huang, D. D.; Bates, K. H.; Sorooshian, A.; Flagan, R. C.; Seinfeld, J. H. Time-resolved molecular characterization of organic aerosols by PILS + UPLC/ESI-Q-TOFMS. *Atmos. Environ.* **2016**, *130*, 180-189.

(243) Surratt, J. D.; Lewandowski, M.; Offenberg, J. H.; Jaoui, M.; Kleindienst, T. E.; Edney, E. O.; Seinfeld, J. H. Effect of acidity on secondary organic aerosol formation from isoprene. *Environ. Sci. Technol.* **2007**, *41* (15), 5363-5369.

(244) Dye, C.; Yttri, K. E. Determination of monosaccharide snhydrides in stmospheric serosols by use of high-performance liquid chromatography combined with high-resolution mass spectrometry. *Anal. Chem.* **2005**, *77* (6), 1853-1858.

(245) Souverain, S.; Rudaz, S.; Veuthey, J.-L. Matrix effect in LC-ESI-MS and LC-APCI-MS with off-line and on-line extraction procedures. *J. Chromatogr. A* **2004**, *1058* (1), 61-66.

(246) Brecht, D.; Uteschil, F.; Schmitz, O. J. Development of a fast-switching dual (ESI/APCI) ionization source for liquid chromatography/mass spectrometry. *Rapid Commun. Mass Spectrom.* **2020**, *34* (17), e8845.

(247) Docherty, K. S.; Wu, W.; Lim, Y. B.; Ziemann, P. J. Contributions of Organic Peroxides to Secondary Aerosol Formed from Reactions of Monoterpenes with O3. *Environ. Sci. Technol.* **2005**, *39* (11), 4049-4059.

(248) Mertes, P.; Pfaffenberger, L.; Dommen, J.; Kalberer, M.; Baltensperger, U. Development of a sensitive long path absorption photometer to quantify peroxides in aerosol particles (Peroxide-LOPAP). *Atmos. Meas. Tech.* **2012**, *5* (10), 2339-2348.

(249) Li, H.; Chen, Z.; Huang, L.; Huang, D. Organic peroxides' gas-particle partitioning and rapid heterogeneous decomposition on secondary organic aerosol. *Atmos. Chem. Phys.* **2016**, *16* (3), 1837-1848.

(250) Yao, M.; Zhao, Y.; Hu, M.; Huang, D.; Wang, Y.; Yu, J. Z.; Yan, N. Multiphase Reactions between Secondary Organic Aerosol and Sulfur Dioxide: Kinetics and

Contributions to Sulfate Formation and Aerosol Aging. *Environ. Sci. Technol. Lett.* **2019**, *6* (12), 768-774.

(251) Epstein, S. A.; Blair, S. L.; Nizkorodov, S. A. Direct Photolysis of α-Pinene Ozonolysis Secondary Organic Aerosol: Effect on Particle Mass and Peroxide Content. *Environ. Sci. Technol.* **2014**, *48* (19), 11251-11258.

(252) Bateman, A. P.; Nizkorodov, S. A.; Laskin, J.; Laskin, A. Photolytic processing of secondary organic aerosols dissolved in cloud droplets. *Phys. Chem. Chem. Phys.* **2011**, *13* (26), 12199-12212, 10.1039/C1CP20526A.

(253) Zhao, R.; Kenseth, C. M.; Huang, Y.; Dalleska, N. F.; Seinfeld, J. H. Iodometry-Assisted Liquid Chromatography Electrospray Ionization Mass Spectrometry for Analysis of Organic Peroxides: An Application to Atmospheric Secondary Organic Aerosol. *Environ. Sci. Technol.* **2018**, *52* (4), 2108-2117.

(254) Zhao, R.; Kenseth, C. M.; Huang, Y.; Dalleska, N. F.; Kuang, X. M.; Chen, J.; Paulson, S. E.; Seinfeld, J. H. Rapid Aqueous-Phase Hydrolysis of Ester Hydroperoxides Arising from Criegee Intermediates and Organic Acids. *J. Phys. Chem. A* **2018**, *122* (23), 5190-5201.

(255) Yao, M.; Li, Z.; Li, C.; Xiao, H.; Wang, S.; Chan, A. W. H.; Zhao, Y. Isomer-Resolved Reactivity of Organic Peroxides in Monoterpene-Derived Secondary Organic Aerosol. *Environ. Sci. Technol.* **2022**, *56* (8), 4882-4893.

(256) Wang, Y.; Zhao, Y.; Li, Z.; Li, C.; Yan, N.; Xiao, H. Importance of hydroxyl radical chemistry in isoprene suppression of particle formation from α-pinene ozonolysis. *ACS Earth Space Chem.* **2021**, *5* (3), 487-499.

(257) Zhao, Y.; Yao, M.; Wang, Y.; Li, Z.; Wang, S.; Li, C.; Xiao, H. Acylperoxy Radicals as Key Intermediates in the Formation of Dimeric Compounds in α-Pinene Secondary Organic Aerosol. *Environ. Sci. Technol.* **2022**, *56* (20), 14249-14261.

(258) Liu, Z.; Zhao, Y.; Yao, M.; Wang, S.; Li, Z.; Li, C.; Xiao, H. Persistence of monoterpene-derived organic peroxides in the atmospheric aqueous phase. *ACS Earth Space Chem.* **2022**, *6* (9), 2226-2235.

(259) Hettiyadura, A. P. S.; Stone, E. A.; Kundu, S.; Baker, Z.; Geddes, E.; Richards, K.; Humphry, T. Determination of atmospheric organosulfates using HILIC chromatography with MS detection. *Atmos. Meas. Tech.* **2015**, *8* (6), 2347-2358.

(260) Spolnik, G.; Wach, P.; Rudzinski, K. J.; Skotak, K.; Danikiewicz, W.; Szmigielski, R. Improved UHPLC-MS/MS methods for analysis of isoprene-derived organosulfates. *Anal. Chem.* **2018**, *90* (5), 3416-3423.

(261) Hettiyadura, A. P. S.; Jayarathne, T.; Baumann, K.; Goldstein, A. H.; de Gouw, J. A.; Koss, A.; Keutsch, F. N.; Skog, K.; Stone, E. A. Qualitative and quantitative analysis of atmospheric organosulfates in Centreville, Alabama. *Atmos. Chem. Phys.* **2017**, *17* (2), 1343-1359.

(262) Cui, T.; Zeng, Z.; dos Santos, E. O.; Zhang, Z.; Chen, Y.; Zhang, Y.; Rose, C. A.; Budisulistiorini, S. H.; Collins, L. B.; Bodnar, W. M.; et al. Development of a hydrophilic interaction liquid chromatography (HILIC) method for the chemical characterization of water-soluble isoprene epoxydiol (IEPOX)-derived secondary organic aerosol. *Environ. Sci.: Process. Impacts* **2018**, *20* (11), 1524-1536.

(263) Ewing, R. G.; Atkinson, D. A.; Eiceman, G. A.; Ewing, G. J. A critical review of ion mobility spectrometry for the detection of explosives and explosive related compounds. *Talanta* **2001**, *54* (3), 515-529.

(264) Kanu, A. B.; Dwivedi, P.; Tam, M.; Matz, L.; Hill Jr, H. H. Ion mobility–mass spectrometry. *J. Mass Spectrom.* **2008**, *43* (1), 1-22.

(265) Krechmer, J. E.; Groessl, M.; Zhang, X.; Junninen, H.; Massoli, P.; Lambe, A. T.; Kimmel, J. R.; Cubison, M. J.; Graf, S.; Lin, Y. H.; et al. Ion mobility spectrometry–mass spectrometry (IMS–MS) for on- and offline analysis of atmospheric gas and aerosol species. *Atmos. Meas. Tech.* **2016**, *9* (7), 3245-3262.

(266) Zhang, X.; Krechmer, J. E.; Groessl, M.; Xu, W.; Graf, S.; Cubison, M.; Jayne, J. T.; Jimenez, J. L.; Worsnop, D. R.; Canagaratna, M. R. A novel framework for molecular characterization of atmospherically relevant organic compounds based on collision cross section and mass-to-charge ratio. *Atmos. Chem. Phys.* **2016**, *16* (20), 12945-12959.

(267) Zhao, Z.; Zhang, W.; Alexander, T.; Zhang, X.; Martin, D. B. C.; Zhang, H. Isolating α-Pinene Ozonolysis Pathways Reveals New Insights into Peroxy Radical Chemistry and Secondary Organic Aerosol Formation. *Environ. Sci. Technol.* **2021**, *55* (10), 6700-6709.

(268) Zhao, Z.; Mayorga, R.; Lee, J.; Yang, X.; Tolentino, R.; Zhang, W.; Vuong, A.; Zhang, H. Site-Specific Mechanisms in OH-Initiated Organic Aerosol Heterogeneous Oxidation Revealed by Isomer-Resolved Molecular Characterization. *ACS Earth Space Chem.* **2020**, *4* (5), 783-794.

(269) Mayorga, R. J.; Zhao, Z.; Zhang, H. Formation of secondary organic aerosol from nitrate radical oxidation of phenolic VOCs: Implications for nitration mechanisms and brown carbon formation. *Atmos. Environ.* **2021**, *244*, 117910.

(270) West, C. P.; Mesa Sanchez, D.; Morales, A. C.; Hsu, Y.-J.; Ryan, J.; Darmody, A.; Slipchenko, L. V.; Laskin, J.; Laskin, A. Molecular and Structural Characterization of Isomeric Compounds in Atmospheric Organic Aerosol Using Ion Mobility-Mass Spectrometry. *J. Phys. Chem. A* **2023**, *127* (7), 1656-1674.

(271) Zhao, Z.; Tolentino, R.; Lee, J.; Vuong, A.; Yang, X.; Zhang, H. Interfacial Dimerization by Organic Radical Reactions during Heterogeneous Oxidative Aging of Oxygenated Organic Aerosols. *J. Phys. Chem. A* **2019**, *123* (50), 10782-10792.

(272) Zheng, X.; Dupuis, K. T.; Aly, N. A.; Zhou, Y.; Smith, F. B.; Tang, K.; Smith, R. D.; Baker, E. S. Utilizing ion mobility spectrometry and mass spectrometry for the analysis of polycyclic aromatic hydrocarbons, polychlorinated biphenyls, polybrominated diphenyl ethers and their metabolites. *Anal. Chim. Acta* **2018**, *1037*, 265-273.

(273) Valadbeigi, Y.; Ilbeigi, V.; Mirsharifi, M. S. Mechanism of atmospheric pressure chemical ionization of morphine, codeine, and thebaine in corona discharge–ion mobility spectrometry: Protonation, ammonium attachment, and carbocation formation. *J. Mass Spectrom.* **2020**, *55* (10), e4586.

(274) Valadbeigi, Y.; Azizmohammadi, S.; Ilbeigi, V. Small host–guest systems in the gas phase: Tartaric acid as a host for both anionic and cationic guests in the atmospheric pressure chemical ionization source of ion mobility spectrometry. *J. Phys. Chem. A* **2020**, *124* (17), 3386-3397.

(275) Valadbeigi, Y.; Ilbeigi, V.; Michalczuk, B.; Sabo, M.; Matejcik, S. Study of atmospheric pressure chemical ionization mechanism in corona discharge ion source with and without NH3 dopant by ion mobility spectrometry combined with mass spectrometry: A theoretical and experimental study. *J. Phys. Chem. A* **2019**, *123* (1), 313-322.

(276) Kaplan, K.; Graf, S.; Tanner, C.; Gonin, M.; Fuhrer, K.; Knochenmuss, R.; Dwivedi, P.; Hill, H. H. Resistive glass IM-TOFMS. *Anal. Chem.* **2010**, *82* (22), 9336-9343.

(277) Blair, S. L.; Ng, N. L.; Zambrzycki, S. C.; Li, A.; Fernández, F. M. Aerosol vacuum-assisted plasma ionization (Aero-VaPI) coupled to ion mobility-mass spectrometry. *J. Am. Soc. Mass Spectrom.* **2018**, *29* (4), 635-639.

(278) Smith, J. D.; Kroll, J. H.; Cappa, C. D.; Che, D. L.; Liu, C. L.; Ahmed, M.; Leone, S. R.; Worsnop, D. R.; Wilson, K. R. The heterogeneous reaction of hydroxyl radicals with sub-micron squalane particles: a model system for understanding the oxidative aging of ambient aerosols. *Atmos. Chem. Phys.* **2009**, *9* (9), 3209-3222.

(279) Yuan, B.; Koss, A. R.; Warneke, C.; Coggon, M.; Sekimoto, K.; de Gouw, J. A. Proton-Transfer-Reaction Mass Spectrometry: Applications in Atmospheric Sciences. *Chem. Rev.* **2017**, *117* (21), 13187-13229.

(280) Sekimoto, K.; Li, S.-M.; Yuan, B.; Koss, A.; Coggon, M.; Warneke, C.; de Gouw, J. Calculation of the sensitivity of proton-transfer-reaction mass spectrometry (PTR-MS) for organic trace gases using molecular properties. *Int. J. Mass Spectrom.* **2017**, *421*, 71-94.

(281) Sumlin, B.; Fortner, E.; Lambe, A.; Shetty, N. J.; Daube, C.; Liu, P.; Majluf, F.; Herndon, S.; Chakrabarty, R. K. Diel cycle impacts on the chemical and light absorption properties of organic carbon aerosol from wildfires in the western United States. *Atmos. Chem. Phys.* **2021**, *21* (15), 11843-11856.

(282) Li, H.; Canagaratna, M. R.; Riva, M.; Rantala, P.; Zhang, Y.; Thomas, S.; Heikkinen, L.; Flaud, P. M.; Villenave, E.; Perraudin, E.; et al. Atmospheric organic vapors in two European pine forests measured by a Vocus PTR-TOF: insights into monoterpene and sesquiterpene oxidation processes. *Atmos. Chem. Phys.* **2021**, *21* (5), 4123-4147.

(283) Li, H.; Riva, M.; Rantala, P.; Heikkinen, L.; Daellenbach, K.; Krechmer, J. E.; Flaud, P. M.; Worsnop, D.; Kulmala, M.; Villenave, E.; et al. Terpenes and their oxidation products in the French Landes forest: insights from Vocus PTR-TOF measurements. *Atmos. Chem. Phys.* **2020**, *20* (4), 1941-1959.

(284) DeVault, M. P.; Ziemann, P. J. Gas- and particle-phase products and their mechanisms of formation from the reaction of Δ-3-carene with NO3 radicals. *J. Phys. Chem. A* **2021**, *125* (47), 10207-10222.

(285) Majluf, F. Y.; Krechmer, J. E.; Daube, C.; Knighton, W. B.; Dyroff, C.; Lambe, A. T.; Fortner, E. C.; Yacovitch, T. I.; Roscioli, J. R.; Herndon, S. C.; et al. Mobile Near-Field Measurements of Biomass Burning Volatile Organic Compounds: Emission Ratios and Factor Analysis. *Environ. Sci. Technol. Lett.* **2022**, *9* (5), 383-390.

(286) Liang, Y.; Stamatis, C.; Fortner, E. C.; Wernis, R. A.; Van Rooy, P.; Majluf, F.; Yacovitch, T. I.; Daube, C.; Herndon, S. C.; Kreisberg, N. M.; et al. Emissions of organic compounds from western US wildfires and their near-fire transformations. *Atmos. Chem. Phys.* **2022**, *22* (15), 9877-9893.

(287) Jensen, A.; Liu, Z.; Tan, W.; Dix, B.; Chen, T.; Koss, A.; Zhu, L.; Li, L.; de Gouw, J. Measurements of Volatile Organic Compounds During the COVID-19 Lockdown in Changzhou, China. *Geophys. Res. Lett.* **2021**, *48* (20), e2021GL095560.

(288) Pagonis, D.; Price, D. J.; Algrim, L. B.; Day, D. A.; Handschy, A. V.; Stark, H.; Miller, S. L.; de Gouw, J.; Jimenez, J. L.; Ziemann, P. J. Time-resolved measurements of indoor chemical emissions, deposition, and reactions in a university art museum. *Environ. Sci. Technol.* **2019**, *53* (9), 4794-4802.

(289) Liu, Q.; Abbatt, J. P. D. Liquid crystal display screens as a source for indoor volatile organic compounds. *Proc. Natl. Acad. Sci. U.S.A.* **2021**, *118* (23), e2105067118.

(290) Morrison, G. C.; Eftekhari, A.; Majluf, F.; Krechmer, J. E. Yields and variability of ozone reaction products from human skin. *Environ. Sci. Technol.* **2021**, *55* (1), 179-187.

(291) Bruderer, T.; Gaisl, T.; Gaugg, M. T.; Nowak, N.; Streckenbach, B.; Müller, S.; Moeller, A.; Kohler, M.; Zenobi, R. On-line analysis of exhaled breath. *Chem. Rev.* **2019**, *119* (19), 10803-10828.

(292) Mattila, J. M.; Arata, C.; Wang, C.; Katz, E. F.; Abeleira, A.; Zhou, Y.; Zhou, S.; Goldstein, A. H.; Abbatt, J. P. D.; DeCarlo, P. F.; et al. Dark chemistry during bleach cleaning enhances oxidation of organics and secondary organic aerosol production indoors. *Environ. Sci. Technol. Lett.* **2020**, *7* (11), 795-801.

(293) Heinritzi, M.; Dada, L.; Simon, M.; Stolzenburg, D.; Wagner, A. C.; Fischer, L.; Ahonen, L. R.; Amanatidis, S.; Baalbaki, R.; Baccarini, A.; et al. Molecular understanding of the suppression of new-particle formation by isoprene. *Atmos. Chem. Phys.* **2020**, *20* (20), 11809-11821.

(294) Caudillo, L.; Rörup, B.; Heinritzi, M.; Marie, G.; Simon, M.; Wagner, A. C.; Müller, T.; Granzin, M.; Amorim, A.; Ataei, F.; et al. Chemical composition of nanoparticles from α-pinene nucleation and the influence of isoprene and relative humidity at low temperature. *Atmos. Chem. Phys.* **2021**, *21* (22), 17099-17114.

(295) Wagner, R.; Yan, C.; Lehtipalo, K.; Duplissy, J.; Nieminen, T.; Kangasluoma, J.; Ahonen, L. R.; Dada, L.; Kontkanen, J.; Manninen, H. E.; et al. The role of ions in new particle formation in the CLOUD chamber. *Atmos. Chem. Phys.* **2017**, *17* (24), 15181-15197.

(296) Pullinen, I.; Schmitt, S.; Kang, S.; Sarrafzadeh, M.; Schlag, P.; Andres, S.; Kleist, E.; Mentel, T. F.; Rohrer, F.; Springer, M.; et al. Impact of NOx on secondary organic aerosol (SOA) formation from α-pinene and β-pinene photooxidation: the role of highly oxygenated organic nitrates. *Atmos. Chem. Phys.* **2020**, *20* (17), 10125-10147.

(297) Yan, C.; Nie, W.; Vogel, A. L.; Dada, L.; Lehtipalo, K.; Stolzenburg, D.; Wagner, R.; Rissanen, M. P.; Xiao, M.; Ahonen, L.; et al. Size-dependent influence of NOx on the growth rates of organic aerosol particles. *Sci. Adv.* **2020**, *6* (22), eaay4945.

(298) Wang, M.; Kong, W.; Marten, R.; He, X.-C.; Chen, D.; Pfeifer, J.; Heitto, A.; Kontkanen, J.; Dada, L.; Kürten, A.; et al. Rapid growth of new atmospheric particles by nitric acid and ammonia condensation. *Nature* **2020**, *581* (7807), 184-189.

(299) Stolzenburg, D.; Simon, M.; Ranjithkumar, A.; Kürten, A.; Lehtipalo, K.; Gordon, H.; Ehrhart, S.; Finkenzeller, H.; Pichelstorfer, L.; Nieminen, T.; et al. Enhanced growth rate of atmospheric particles from sulfuric acid. *Atmos. Chem. Phys.* **2020**, *20* (12), 7359-7372.

(300) Krechmer, J. E.; Coggon, M. M.; Massoli, P.; Nguyen, T. B.; Crounse, J. D.; Hu, W.; Day, D. A.; Tyndall, G. S.; Henze, D. K.; Rivera-Rios, J. C.; et al. Formation of Low Volatility Organic Compounds and Secondary Organic Aerosol from Isoprene

Hydroxyhydroperoxide Low-NO Oxidation. *Environ. Sci. Technol.* **2015**, *49* (17), 10330-10339.

(301) Crounse, J. D.; Nielsen, L. B.; Jørgensen, S.; Kjaergaard, H. G.; Wennberg, P. O. Autoxidation of Organic Compounds in the Atmosphere. *J. Phys. Chem. Lett.* **2013**, *4* (20), 3513-3520.

(302) Jokinen, T.; Berndt, T.; Makkonen, R.; Kerminen, V.-M.; Junninen, H.; Paasonen, P.; Stratmann, F.; Herrmann, H.; Guenther, A. B.; Worsnop, D. R.; et al. Production of extremely low volatile organic compounds from biogenic emissions: Measured yields and atmospheric implications. *Proc. Natl. Acad. Sci. U.S.A.* **2015**, *112* (23), 7123-7128.

(303) Berndt, T.; Herrmann, H.; Sipilä, M.; Kulmala, M. Highly Oxidized Second-Generation Products from the Gas-Phase Reaction of OH Radicals with Isoprene. *J. Phys. Chem. A* **2016**, *120* (51), 10150-10159.

(304) Richters, S.; Herrmann, H.; Berndt, T. Different pathways of the formation of highly oxidized multifunctional organic compounds (HOMs) from the gas-phase ozonolysis of β-caryophyllene. *Atmos. Chem. Phys.* **2016**, *16* (15), 9831-9845.

(305) Guo, Y.; Yan, C.; Liu, Y.; Qiao, X.; Zheng, F.; Zhang, Y.; Zhou, Y.; Li, C.; Fan, X.; Lin, Z.; et al. Seasonal variation in oxygenated organic molecules in urban Beijing and their contribution to secondary organic aerosol. *Atmos. Chem. Phys.* **2022**, *22* (15), 10077-10097.

(306) Molteni, U.; Bianchi, F.; Klein, F.; El Haddad, I.; Frege, C.; Rossi, M. J.; Dommen, J.; Baltensperger, U. Formation of highly oxygenated organic molecules from aromatic compounds. *Atmos. Chem. Phys.* **2018**, *18* (3), 1909-1921.

(307) Bianchi, F.; Tröstl, J.; Junninen, H.; Frege, C.; Henne, S.; Hoyle, C. R.; Molteni, U.; Herrmann, E.; Adamov, A.; Bukowiecki, N.; et al. New particle formation in the free troposphere: A question of chemistry and timing. *Science* **2016**, *352* (6289), 1109-1112.

(308) Iyer, S.; Lopez-Hilfiker, F.; Lee, B. H.; Thornton, J. A.; Kurtén, T. Modeling the Detection of Organic and Inorganic Compounds Using Iodide-Based Chemical Ionization. *J. Phys. Chem. A* **2016**, *120* (4), 576-587.

(309) Hyttinen, N.; Kupiainen-Määttä, O.; Rissanen, M. P.; Muuronen, M.; Ehn, M.; Kurtén, T. Modeling the charging of highly oxidized cyclohexene ozonolysis products using nitrate-based chemical ionization. *J. Phys. Chem. A* **2015**, *119* (24), 6339-6345.

(310) Zhao, Y.; Thornton, J. A.; Pye, H. O. T. Quantitative constraints on autoxidation and dimer formation from direct probing of monoterpene-derived peroxy radical chemistry. *Proc. Natl. Acad. Sci. U.S.A.* **2018**, *115* (48), 12142-12147.

(311) Mutzel, A.; Poulain, L.; Berndt, T.; Iinuma, Y.; Rodigast, M.; Böge, O.; Richters, S.; Spindler, G.; Sipilä, M.; Jokinen, T.; et al. Highly Oxidized Multifunctional Organic Compounds Observed in Tropospheric Particles: A Field and Laboratory Study. *Environ. Sci. Technol.* **2015**, *49* (13), 7754-7761.

(312) Zhang, X.; McVay, R. C.; Huang, D. D.; Dalleska, N. F.; Aumont, B.; Flagan, R. C.; Seinfeld, J. H. Formation and evolution of molecular products in α-pinene secondary organic aerosol. *Proc. Natl. Acad. Sci. U.S.A.* **2015**, *112* (46), 14168-14173.

(313) Pospisilova, V.; Lopez-Hilfiker, F. D.; Bell, D. M.; El Haddad, I.; Mohr, C.; Huang, W.; Heikkinen, L.; Xiao, M.; Dommen, J.; Prevot, A. S. H.; et al. On the fate of oxygenated organic molecules in atmospheric aerosol particles. *Sci. Adv.* **2020**, *6* (11), eaax8922.

(314) Stefenelli, G.; Pospisilova, V.; Lopez-Hilfiker, F. D.; Daellenbach, K. R.; Hüglin, C.; Tong, Y.; Baltensperger, U.; Prévôt, A. S. H.; Slowik, J. G. Organic aerosol source apportionment in Zurich using an extractive electrospray ionization time-of-flight mass spectrometer (EESI-TOF-MS) – Part 1: Biogenic influences and day–night chemistry in summer. *Atmos. Chem. Phys.* **2019**, *19* (23), 14825-14848.

(315) Yan, C.; Nie, W.; Äijälä, M.; Rissanen, M. P.; Canagaratna, M. R.; Massoli, P.; Junninen, H.; Jokinen, T.; Sarnela, N.; Häme, S. A. K.; et al. Source characterization of highly oxidized multifunctional compounds in a boreal forest environment using positive matrix factorization. *Atmos. Chem. Phys.* **2016**, *16* (19), 12715-12731.

(316) Guo, Y.; Shen, H.; Pullinen, I.; Luo, H.; Kang, S.; Vereecken, L.; Fuchs, H.; Hallquist, M.; Acir, I. H.; Tillmann, R.; et al. Identification of highly oxygenated organic molecules and their role in aerosol formation in the reaction of limonene with nitrate radical. *Atmos. Chem. Phys.* **2022**, *22* (17), 11323-11346.

(317) Bell, D. M.; Wu, C.; Bertrand, A.; Graham, E.; Schoonbaert, J.; Giannoukos, S.; Baltensperger, U.; Prevot, A. S. H.; Riipinen, I.; El Haddad, I.; et al. Particle-phase processing of α-pinene NO3 secondary organic aerosol in the dark. *Atmos. Chem. Phys.* **2022**, *22* (19), 13167-13182.

(318) Zhang, X.; Lambe, A. T.; Upshur, M. A.; Brooks, W. A.; Gray Bé, A.; Thomson, R. J.; Geiger, F. M.; Surratt, J. D.; Zhang, Z.; Gold, A.; et al. Highly Oxygenated Multifunctional Compounds in α-Pinene Secondary Organic Aerosol. *Environ. Sci. Technol.* **2017**, *51* (11), 5932-5940.

(319) Mayorga, R.; Xia, Y.; Zhao, Z.; Long, B.; Zhang, H. Peroxy radical autoxidation and sequential oxidation in organic nitrate formation during limonene nighttime oxidation. *Environ. Sci. Technol.* **2022**, *56* (22), 15337-15346.

(320) Zhao, Z.; Xu, Q.; Yang, X.; Zhang, H. Heterogeneous Ozonolysis of Endocyclic Unsaturated Organic Aerosol Proxies: Implications for Criegee Intermediate Dynamics and Later-Generation Reactions. *ACS Earth Space Chem.* **2019**, *3* (3), 344-356.

(321) Thornton, J. A.; Mohr, C.; Schobesberger, S.; D'Ambro, E. L.; Lee, B. H.; Lopez-Hilfiker, F. D. Evaluating Organic Aerosol Sources and Evolution with a Combined Molecular Composition and Volatility Framework Using the Filter Inlet for Gases and Aerosols (FIGAERO). *Acc. Chem. Res.* **2020**, *53* (8), 1415-1426.

(322) Hodshire, A. L.; Akherati, A.; Alvarado, M. J.; Brown-Steiner, B.; Jathar, S. H.; Jimenez, J. L.; Kreidenweis, S. M.; Lonsdale, C. R.; Onasch, T. B.; Ortega, A. M.; et al. Aging Effects on Biomass Burning Aerosol Mass and Composition: A Critical Review of Field and Laboratory Studies. *Environ Sci Technol* **2019**, *53* (17), 10007-10022.

(323) Takhar, M.; Li, Y.; Chan, A. W. H. Characterization of secondary organic aerosol from heated-cooking-oil emissions: evolution in composition and volatility. *Atmos. Chem. Phys.* **2021**, *21* (6), 5137-5149.

(324) Heald, C. L.; Kroll, J. H. The fuel of atmospheric chemistry: Toward a complete description of reactive organic carbon. *Sci. Adv.* **2020**, *6* (6), eaay8967.

(325) Mehra, A.; Wang, Y.; Krechmer, J. E.; Lambe, A.; Majluf, F.; Morris, M. A.; Priestley, M.; Bannan, T. J.; Bryant, D. J.; Pereira, K. L.; et al. Evaluation of the chemical composition of gas- and particle-phase products of aromatic oxidation. *Atmos. Chem. Phys.* **2020**, *20* (16), 9783-9803.

(326) Qi, L.; Vogel, A. L.; Esmaeilirad, S.; Cao, L.; Zheng, J.; Jaffrezo, J. L.; Fermo, P.; Kasper-Giebl, A.; Daellenbach, K. R.; Chen, M.; et al. A 1-year characterization of organic aerosol composition and sources using an extractive electrospray ionization time-of-flight mass spectrometer (EESI-TOF). *Atmos. Chem. Phys.* **2020**, *20* (13), 7875-7893.

(327) Yazdani, A.; Dudani, N.; Takahama, S.; Bertrand, A.; Prévôt, A. S. H.; El Haddad, I.; Dillner, A. M. Characterization of primary and aged wood burning and coal combustion organic aerosols in an environmental chamber and its implications for atmospheric aerosols. *Atmos. Chem. Phys.* **2021**, *21* (13), 10273-10293.

(328) Giannoukos, S.; Lee, C. P.; Tarik, M.; Ludwig, C.; Biollaz, S.; Lamkaddam, H.; Baltensperger, U.; Henry Prevot, A. S.; Slowik, J. Real-Time Detection of Aerosol Metals Using Online Extractive Electrospray Ionization Mass Spectrometry. *Anal. Chem.* **2020**, *92* (1), 1316-1325.

(329) Liu, Q.; Liggio, J.; Wu, D.; Saini, A.; Halappanavar, S.; Wentzell, J. J. B.; Harner, T.; Li, K.; Lee, P.; Li, S.-M. Experimental study of OH-initiated heterogeneous oxidation of organophosphate flame retardants: Kinetics, mechanism, and toxicity. *Environ. Sci. Technol.* **2019**, *53* (24), 14398-14408.

(330) Liu, Q.; Liggio, J.; Wentzell, J.; Lee, P.; Li, K.; Li, S.-M. Atmospheric OH oxidation chemistry of particulate liquid crystal monomers: An emerging persistent organic pollutant in air. *Environ. Sci. Technol. Lett.* **2020**, *7* (9), 646-652.

(331) Lamkaddam, H.; Dommen, J.; Ranjithkumar, A.; Gordon, H.; Wehrle, G.; Krechmer, J.; Majluf, F.; Salionov, D.; Schmale, J.; Bjelić, S.; et al. Large contribution to secondary organic aerosol from isoprene cloud chemistry. *Sci. Adv.* **2021**, *7* (13), eabe2952.

(332) Cheng, C. T.; Chan, M. N.; Wilson, K. R. The role of alkoxy radicals in the heterogeneous reaction of two structural isomers of dimethylsuccinic acid. *Phys. Chem. Chem. Phys.* **2015**, *17* (38), 25309-25321.

(333) Cheng, C. T.; Chan, M. N.; Wilson, K. R. Importance of Unimolecular HO2 Elimination in the Heterogeneous OH Reaction of Highly Oxygenated Tartaric Acid Aerosol. *J. Phys. Chem. A* **2016**, *120* (29), 5887-5896.

(334) Chim, M. M.; Chow, C. Y.; Davies, J. F.; Chan, M. N. Effects of Relative Humidity and Particle Phase Water on the Heterogeneous OH Oxidation of 2-Methylglutaric Acid Aqueous Droplets. *J. Phys. Chem. A* **2017**, *121* (8), 1666-1674.

(335) Lam, H. K.; Shum, S. M.; Davies, J. F.; Song, M.; Zuend, A.; Chan, M. N. Effects of inorganic salts on the heterogeneous OH oxidation of organic compounds: insights from methylglutaric acid–ammonium sulfate. *Atmos. Chem. Phys.* **2019**, *19* (14), 9581-9593.

(336) Lee, L.; Wilson, K. The Reactive–Diffusive Length of OH and Ozone in Model Organic Aerosols. *J. Phys. Chem. A* **2016**, *120* (34), 6800-6812.

(337) Kwong, K. C.; Chim, M. M.; Davies, J. F.; Wilson, K. R.; Chan, M. N. Importance of sulfate radical anion formation and chemistry in heterogeneous OH oxidation of sodium methyl sulfate, the smallest organosulfate. *Atmos. Chem. Phys.* **2018**, *18* (4), 2809-2820.

(338) Xu, R.; Ge, Y.; Kwong, K. C.; Poon, H. Y.; Wilson, K. R.; Yu, J. Z.; Chan, M. N. Inorganic Sulfur Species Formed upon Heterogeneous OH Oxidation of Organosulfates: A Case Study of Methyl Sulfate. *ACS Earth Space Chem.* **2020**, *4* (11), 2041-2049.

(339) Goldstein, A. H.; Galbally, I. E. Known and unexplored organic constituents in the Earth's atmosphere. *Environ. Sci. Technol.* **2007**, *41* (5), 1514-1521.

(340) Vasquez, K. T.; Crounse, J. D.; Schulze, B. C.; Bates, K. H.; Teng, A. P.; Xu, L.; Allen, H. M.; Wennberg, P. O. Rapid hydrolysis of tertiary isoprene nitrate efficiently removes NOx from the atmosphere. *Proc. Natl. Acad. Sci. U.S.A.* **2020**, *117* (52), 33011-33016.

(341) Wang, Y.; Kim, H.; Paulson, S. E. Hydrogen peroxide generation from α- and β-pinene and toluene secondary organic aerosols. *Atmos. Environ.* **2011**, *45* (18), 3149-3156.

(342) Badali, K. M.; Zhou, S.; Aljawhary, D.; Antiñolo, M.; Chen, W. J.; Lok, A.; Mungall, E.; Wong, J. P. S.; Zhao, R.; Abbatt, J. P. D. Formation of hydroxyl radicals from photolysis of secondary organic aerosol material. *Atmos. Chem. Phys.* **2015**, *15* (14), 7831-7840.

(343) Zhao, Z.; Le, C.; Xu, Q.; Peng, W.; Jiang, H.; Lin, Y.-H.; Cocker, D. R.; Zhang, H. Compositional Evolution of Secondary Organic Aerosol as Temperature and Relative Humidity Cycle in Atmospherically Relevant Ranges. *ACS Earth Space Chem.* **2019**, *3* (11), 2549-2558.

(344) Rivera-Rios, J. C.; Nguyen, T. B.; Crounse, J. D.; Jud, W.; St. Clair, J. M.; Mikoviny, T.; Gilman, J. B.; Lerner, B. M.; Kaiser, J. B.; de Gouw, J.; et al. Conversion of hydroperoxides to carbonyls in field and laboratory instrumentation: Observational bias in diagnosing pristine versus anthropogenically controlled atmospheric chemistry. *Geophys. Res. Lett.* **2014**, *41* (23), 8645-8651.

(345) Dörich, R.; Eger, P.; Lelieveld, J.; Crowley, J. N. Iodide-CIMS and m/z 62: The detection of HNO3 as NO3− in the presence of PAN, peracetic acid and O3. *Atmos. Meas. Tech. Discuss.* **2021**, *2021*, 1-26.

(346) Zhang, W.; Zhang, H. Secondary Ion Chemistry Mediated by Ozone and Acidic Organic Molecules in Iodide-Adduct Chemical Ionization Mass Spectrometry. *Anal. Chem.* **2021**, *93* (24), 8595-8602.

(347) Bernhammer, A. K.; Fischer, L.; Mentler, B.; Heinritzi, M.; Simon, M.; Hansel, A. Production of highly oxygenated organic molecules (HOMs) from trace contaminants during isoprene oxidation. *Atmos. Meas. Tech.* **2018**, *11* (8), 4763-4773.

(348) Li, H.; Almeida, T. G.; Luo, Y.; Zhao, J.; Palm, B. B.; Daub, C. D.; Huang, W.; Mohr, C.; Krechmer, J. E.; Kurtén, T.; et al. Fragmentation inside proton-transfer-reaction-based mass spectrometers limits the detection of ROOR and ROOH peroxides. *Atmos. Meas. Tech.* **2022**, *15* (6), 1811-1827.

(349) Stark, H.; Yatavelli, R. L. N.; Thompson, S. L.; Kang, H.; Krechmer, J. E.; Kimmel, J. R.; Palm, B. B.; Hu, W.; Hayes, P. L.; Day, D. A.; et al. Impact of Thermal Decomposition on Thermal Desorption Instruments: Advantage of Thermogram Analysis for Quantifying Volatility Distributions of Organic Species. *Environ. Sci. Technol.* **2017**, *51* (15), 8491-8500.

(350) Yang, L. H.; Takeuchi, M.; Chen, Y.; Ng, N. L. Characterization of thermal decomposition of oxygenated organic compounds in FIGAERO-CIMS. *Aerosol Sci. Technol.* **2021**, *55* (12), 1321-1342.

(351) Thompson, S. L.; Yatavelli, R. L. N.; Stark, H.; Kimmel, J. R.; Krechmer, J. E.; Day, D. A.; Hu, W.; Isaacman-VanWertz, G.; Yee, L.; Goldstein, A. H.; et al. Field

intercomparison of the gas/particle partitioning of oxygenated organics during the Southern Oxidant and Aerosol Study (SOAS) in 2013. *Aerosol Sci. Technol.* **2017**, *51* (1), 30-56.

(352) Banerjee, S.; Zare, R. N. Syntheses of Isoquinoline and Substituted Quinolines in Charged Microdroplets. *Angew. Chem. Int. Ed.* **2015**, *54* (49), 14795-14799.

(353) Anglada, J. M.; Martins-Costa, M. T. C.; Francisco, J. S.; Ruiz-López, M. F. Photoinduced Oxidation Reactions at the Air–Water Interface. *J. Am. Chem. Soc.* **2020**, *142* (38), 16140-16155.

(354) Ruiz-Lopez, M. F.; Francisco, J. S.; Martins-Costa, M. T. C.; Anglada, J. M. Molecular reactions at aqueous interfaces. Nat. Rev. Chem. **2020**, *4* (9), 459-475.

(355) Jacobs, M. I.; Davis, R. D.; Rapf, R. J.; Wilson, K. R. Studying Chemistry in Micro-compartments by Separating Droplet Generation from Ionization. *J. Am. Soc. Mass Spectrom.* **2019**, *30* (2), 339-343.

(356) Colussi, J. A.; Enami, S. Detecting Intermediates and Products of Fast Heterogeneous Reactions on Liquid Surfaces via Online Mass Spectrometry. *Atmosphere* **2019**, *10* (2).

(357) Berndt, T.; Richters, S.; Jokinen, T.; Hyttinen, N.; Kurtén, T.; Otkjær, R. V.; Kjaergaard, H. G.; Stratmann, F.; Herrmann, H.; Sipilä, M.; et al. Hydroxyl radical-induced formation of highly oxidized organic compounds. *Nat. Commun.* **2016**, *7* (1), 13677. DOI: 10.1038/ncomms13677.

(358) Lin, P.; Fleming, L. T.; Nizkorodov, S. A.; Laskin, J.; Laskin, A. Comprehensive Molecular Characterization of Atmospheric Brown Carbon by High Resolution Mass Spectrometry with Electrospray and Atmospheric Pressure Photoionization. *Anal. Chem.* **2018**, *90* (21), 12493-12502.

Chapter 2 Secondary Ion Chemistry Mediated by Ozone and Acidic Organic Molecules in Iodide-adduct Chemical Ionization Mass Spectrometry

2.1 Introduction

VOCs are ubiquitous in the atmosphere with substantial emissions from numerous biogenic and anthropogenic sources.[1-3] Reactive VOCs can be oxidized by oxidants in the atmosphere, producing OVOCs which are a highly variable and complex class of organic mixtures with diverse functional groups, such as ketone, alcohol, carboxylic acid, hydroperoxide, etc.[4, 5] They play an important role as precursors to the formation of SOA which have crucial impacts on the Earth's climate, air quality, and human health.[6-9] Understanding the compositions of OVOCs is thus imperative to gain significant insights into atmospheric chemistry and climate change.

CIMS has been a popular analytical technique to measure atmospheric VOCs and OVOCs in the past decades. It is well known for the high time-resolution (< 1 Hz), high sensitivity (ppt level), and the quantitative capability.[10-13] The soft ionization approach also allows for straightforward assignment of chemical formulas. Extensive studies in recent years applied a variety of reagent ions (e.g., I^-, CH_3COO^-, CF_3O^-, CO_3^-, SF_6^-, Br^-, and NO_3^- in the negative mode; H_3O^+, NO^+, O_2^+, NH_4^+, $C_6H_6^+$, and $C_2H_5OH^+$ in the positive mode) to selectively ionize different classes of organic compounds.[14-20] I^--CIMS has been a favorite method among the various ionization schemes to detect a wide range of OVOCs due to its low selectivity.[21, 22] The detected iodide adducts are usually referred to as $[M+I]^-$, where M is considered as the molecular formula. Despite the wide usage of I^--CIMS, potential interferences caused by, for example, secondary ion chemistry other than the

iodide adducting have not been widely considered and examined.[13, 23, 24] Dörich et al. recently reported that the presence of strong oxygen donors such as O_3 and peracetic acid lead to biased detection of HNO_3 as NO_3^- using I^--CIMS by the formation of $[IO_x]^-$.[25] It is yet unclear: (1) whether such secondary ion chemistry in I^--CIMS could also affect organic compounds; (2) whether the "M" in measured iodide adducts $[M+I]^-$ can all be interpreted as molecular formulas in the samples; (3) if any secondary ion chemistry occurs, how product quantification can be affected; and (4) how the secondary ion chemistry might be utilized to help identify products. To address these questions in this work, we examined the interactions of the strong oxygen donors (i.e., O_3, peracetic acid, and hydrogen peroxide) with organic species with diverse functionalities in I^--CIMS using available OVOC chemical standards as well as produced mixtures from VOC oxidation experiments.

2.2 Experimental Section

2.2.1 I^--CIMS

The I^--CIMS used in this work is a commercial instrument (Aerodyne Research Inc.) with a time-of-flight mass spectrometer (TOFMS, $m/\Delta m \sim 5000$).[13] The I^--CIMS instrument contains differentially pumped stages with a series of optics to achieve soft ionization and transmission of target molecules in the gas phase.[13, 21, 22] Defused CH_3I as a reagent source is introduced through a ^{210}Po alpha emitter into to the IMR chamber orthogonal to the sample flow to form charged iodide adducts with analytes under 100 – 110 mbar in the IMR, where the reaction time is ~ 0.1 s.[12, 13] The IMR is followed by a collisional dissociation chamber (CDC)[10, 11, 13] containing a segmented quadrupole where

weakly bound ion-molecule clusters can dissociate into reagent ions and a neutral molecule with the changing electric strength. The CDC is followed by a second segmented quadrupole and a series of DC optics to guide, focus, and accelerate the primary beam into the TOFMS. The pressures in the two segmented quadrupoles are 4.8 (± 0.1) and 7.0 (± 0.2) × 10^{-3} mbar, respectively. The voltage difference (dV) between the two quadrupole regions can be tuned to control ion declustering.[21, 22] The operating dV is 4.8 V, determined by the tuning software (Thuner, v1.11) to optimize instrument sensitivity and resolving power. The effective ion path length of the TOFMS is approximately 0.5 m to capture the ions under vacuum (0.8 – 1.0 × 10^{-6} mbar) by the detector with different detection time corresponding to different m/Q in the mass spectra.[10, 13, 20, 22] The TOFMS was operated over an m/Q range of 0-700 Th. All data analysis was done using Tofware (v3.2.0) running with Igor Pro (WaveMetrics, OR, USA).

2.2.2 Chemicals and reagents

The following chemicals and reagents with purities and suppliers were used in the present study: formic acid (FA, 98% – 100%, LiChropur), acetic acid (AA, ≥99%, Sigma-Aldrich), propionic acid (PRA, 99%, Fisher), pyruvic acid (PYA, >97.0%, TCI), *cis*-pinonic acid (PIA, 98%, Sigma-Aldrich), peracetic acid (PAA, 32% wt.% in AA, Sigma-Aldrich), deuterated-4 acetic acid (dAA, 99.5%, CIL), acetone (99.7%, Fisher Chemical), glycerol (100%, J. T. Baker), propylene glycol (99%, Combi-Blocks), tert-butyl hydroperoxide (TBH, 70% aq. soln., Alfa Aesar), hydrogen peroxide (H_2O_2, 30% aq. soln.,

Fisher Chemical), α-pinene (98%, Acros Organics), and isoprene (99%, Alfa Aesar). None of the above reagents were further purified.

2.2.3 Secondary ion chemistry examined using chemical standards

All the above-mentioned chemical standards except α-pinene and isoprene were used to study the secondary ion chemistry in the I^--CIMS. They were introduced to the clean dry air flow (2.1 L min^{-1}, provided by a clean air generator by Aadco Inc.) into the IMR inlet by a syringe pump (Chemyx Inc.), either individually or as mixtures. In addition, O_3 was added to the sampling air flow by an O_3 generator (Ozone Solution Inc.) at 0 – 200 ppb which is a typical range for lab experiments and polluted atmosphere.[26, 27] The O_3 concentrations were measured by an O_3 analyzer (Thermo Environmental Instruments, 49C). Alternatively, H_2O_2 and PAA as oxygen donors were hypothesized to play a similar role as O_3 in the secondary ion chemistry (if any). Thus, in two separate sets of experiments, H_2O_2 or PAA was injected using a separate syringe pump into the sampling air flow at varied concentrations to interact with the other chemical standards in the IMR. The mixing time of O_3/H_2O_2/PAA with the organic standards before entering the IMR was ~ 0.2 s. Finally, we have also tested the effects of relative humidity (RH) and IMR pressure on the secondary ion chemistry using AA and O_3.

2.2.4 Gas-phase products from oxidation of α-pinene and isoprene

To examine the secondary ion chemistry with more realistic atmospherically relevant OVOCs, gas-phase oxidation experiments of two important VOCs, α-pinene and

isoprene, by O_3 were conducted in a laminar flowtube reactor (Quartz, 110 cm long, 5.5 cm id., cone-shaped ends, volume ~ 2.1 L) at room temperature (~21 ℃). The experimental setup of VOCs oxidation is shown in **Figure 2.1**. The residence times were 60 s and 70 s for the α-pinene and isoprene experiments, respectively. α-Pinene and isoprene were injected into the flowtube using a syringe pump. To minimize the influence of residual O_3 from the flowtube reactor on the secondary ion chemistry in the IMR, low initial O_3 concentrations (~ 20 ppb) and high VOC concentrations (14.7 ppm α-pinene and 68.0 ppm isoprene, respectively) were used. Under these experimental conditions, O_3 concentrations were estimated to be < 5 ppb at the exit of the flowtube reactor, based on the kinetic Master Chemical Mechanism (MCMv3.3.1) model.[28] At the exit of the flowtube, additional O_3 (~ 0.3 L min^{-1}, concentration measured by a second O_3 analyzer) was introduced to meet with the oxidation-derived OVOC mixtures (O_3 concentration after mixing ~ 0 – 200 ppb) and guided into the IMR. Because the VOC (e.g. α-pinene) ozonolysis products may contain oxygen donors themselves (i.e., peroxides and Criegee intermediates),[29-31] we added various acids (FA, AA, dAA, and PRA) into the IMR instead of H_2O_2 or PAA, with the goal to elucidate the oxygen donors in the OVOC products. Similar to the chemical standard experiments, the mixing time between the oxidation products and the additionally injected O_3 or acids was ~ 0.2 s before entering the IMR. Thus, reactions during this mixing time are expected to be negligible.

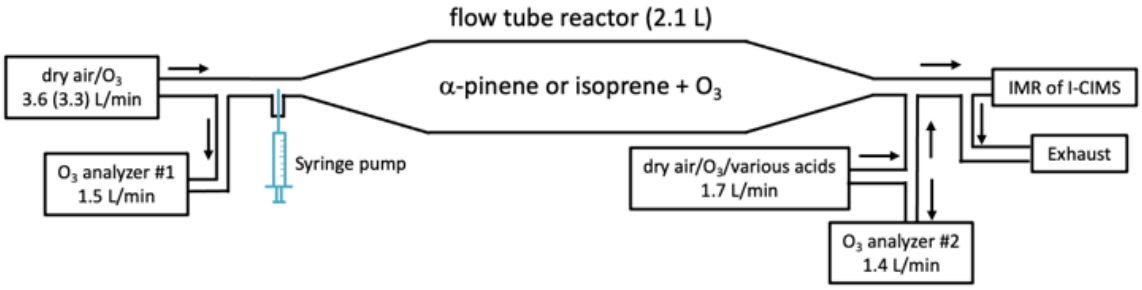

Figure 2.1 The schematic diagram of the VOC oxidation experimental setup consisting of an injection system, a self-designed flowtube reactor and the I^--CIMS. The flow rates of the various injection and sampling lines are illustrated.

2.3 Results and Discussion

2.3.1 Observation and proposed mechanism for the secondary ion chemistry

To demonstrate the secondary ion chemistry in the I^--CIMS IMR between different classes of organic compounds and oxygen donors, we performed experiments using a series of standard compounds with different functional groups. **Figure 2.2** presents the experimental results using a mixture of five carboxylic acids. The concentrations of the individual acids in the sampling air flow were in the range of 21 – 72 ppb. Upon the addition of O_3 (**Figure 2.2B**) or PAA (**Figure 2.2C**), the mass spectra clearly showed additional peaks, indicating their reactions with the acidic compounds. This is unexpected because these standard compounds do not contain C=C double bonds and should not react with O_3 or PAA on the short mixing timescale. Thus, we suggest that these new product ions were formed from secondary ion chemistry in the IMR. The detailed analysis of the I^--CIMS mass spectra allowed us to elucidate the chemical formulas of the product ions, labeled in **Figure 2.2**. Apparently, the new product ions were iodide clusters with the formulas of $[HA+IO]^-$ and $[A+B+I]^-$ (HA and HB represent generic acids). The variations

of the parent iodide clusters (i.e., $[HA+I]^-$) and the products ions with O_3 or PAA concentrations are displayed in **Figure 2.3A – B**, which clearly show the formation of $[HA+IO]^-$ monomers and $[A+B+I]^-$ dimers as a function of IMR O_3 and PAA, along with the decreased parent ion intensities. We further examined the parent and product ions under declustering dV scans where iodide adducts dissociate into I^- and neutral molecules with increasing collisional energy (**Figure 2.3C**). The parent ions signals kept decreasing with increased dV, consistent with previous work.[22] However, $[HA+IO]^-$ and $[A+B+I]^-$ exhibited different extents of delayed dissociation with increased dV. Particularly, the $[A+B+I]^-$ dimers showed an increasing trend at dV from 5 to 10 V. We suggest that the observed delayed dissociation and even enhanced ion signals with dV increase are likely caused by the secondary ion chemistry. In a test with AA by varying the RH (< 2 – 80%) and IMR pressure (65 – 100 mbar), the secondary ion chemistry products were always present, which however, became more pronounced with higher RH but exhibited a decreasing trend as the IMR pressure dropped (**Figure 2.3D**).

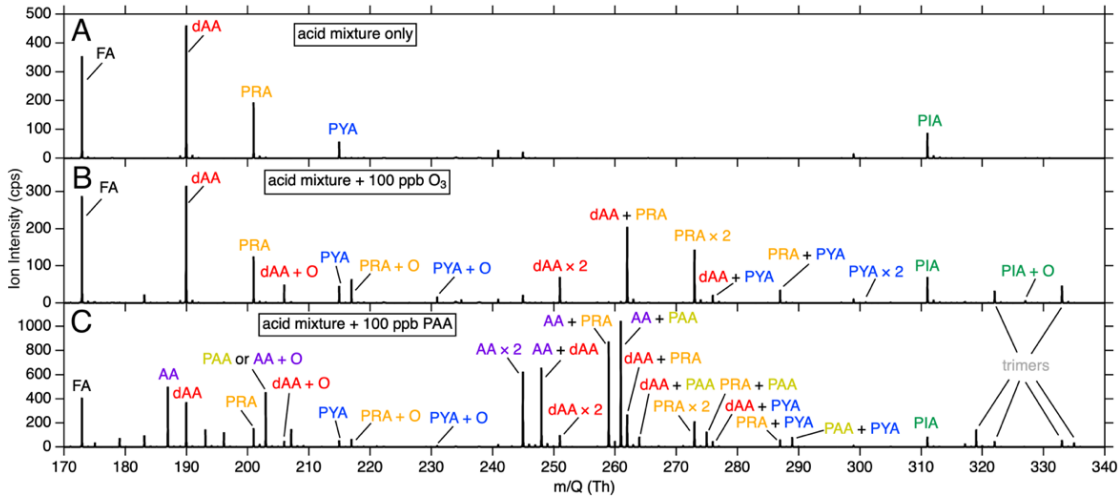

Figure 2.2 I^--CIMS mass spectra of the acid mixture experiments. (A) the acid mixture only (B) in the presence of 100 ppb O_3 in the IMR, and (C) in the presence of 100 ppb PAA in the IMR. The I^- part of the ions are omitted in the labels for clarity. Note that the signal of dAA showed up at m/Q 190 Th ($[CD_3COOH+I]^-$), resulting from a H/D exchange on the acid group. The signal of AA at m/Q 187 Th in (C) was from the impurity of PAA (32% wt.% in AA).

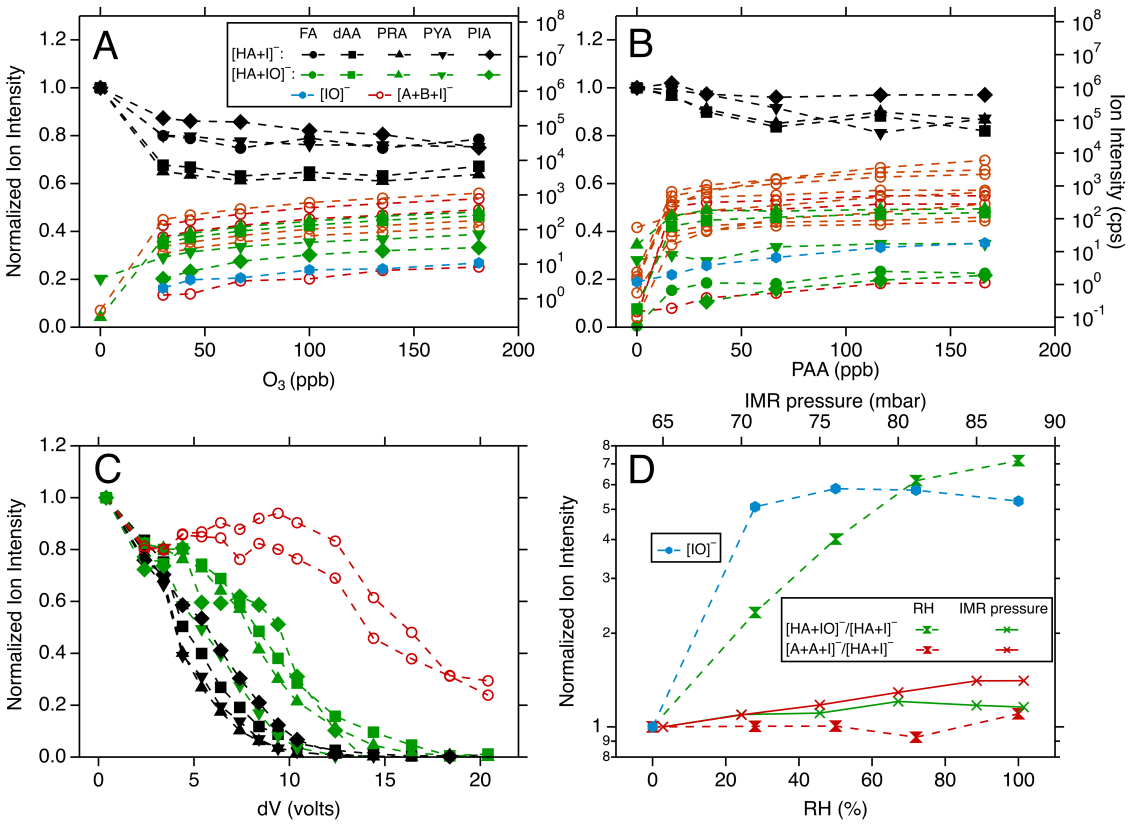

Figure 2.3 I^--CIMS ion intensities of the parent ions ($[HA+I]^-$), $[HA+IO]^-$, and $[A+B+I]^-$ as a function of (A) O_3 concentration and (B) PAA concentration in the IMR. The parent ion signals are normalized for comparison. (C) Normalized ion intensities during the dV scans. (D) Normalized intensity ratios of $[HA+IO]^-$: $[HA+I]^-$ and $[A+A+I]^-$: $[HA+I]^-$ varied with different RH conditions (bottom *x*-axis) and IMR pressures (top *x*-axis). The signals of $[IO]^-$ are also shown in (A), (B), and (D). In (A) – (C), the dimer ions $[A+B+I]^-$ can be formed from the same or different monomeric acids and hence all the dimer ions are represented by red circle symbols.

In addition to the carboxylic acids, the experiments using TBH also showed sign of the secondary ion chemistry. Although TBH itself is not detectable by the I^--CIMS, in the presence of O_3 and PAA, $[HA+IO]^-$ and $[A+B+I]^-$ were observed. In contrast, we did not observe the secondary ion chemistry in the experiments using the alcohols (propylene glycol and glycerol) or acetone. Acetone itself is not detectable by I^--CIMS similar to TBH, but the absence of products with O_3 or PAA suggests that it does not undergo the secondary ion chemistry. Interestingly, unlike O_3 and PAA, H_2O_2 does not induce the same secondary ion chemistry with the organic molecules, despite that it is also considered an oxygen donor like PAA. Moreover, when TBH was added with the organic acids, no additional products were observed, suggesting that simple hydroperoxides could not initiate the secondary ion chemistry as the oxygen donor. Based on these measurements, we propose a plausible mechanism of the observed secondary ion chemistry through the interactions of O_3 or peracids (the oxygen donors) with acidic organics (e.g., carboxylic acids and hydroperoxides) as follows:

$$I^- + O_3 \rightarrow [IO]^- + O_2 \quad \text{(R2.1)}$$

$$I^- + RC(O)OOH \rightarrow [IO]^- + RC(O)OH \quad \text{(R2.2)}$$

$$[H_2O+I]^- + O_3/RC(O)OOH \rightarrow [IO]^- + H_2O + O_2/RC(O)OH \quad \text{(R2.3)}$$

$$[IO]^- + HA \rightarrow [HA+IO]^- \quad \text{(R2.4)}$$

$$[IO]^- + HA \rightarrow A^- + HOI \quad \text{(R2.5)}$$

$$[HA+IO]^- + HB \rightarrow [A+B+I]^- + H_2O \quad \text{(R2.6)}$$

In this mechanism, O_3 and peracids (RC(O)OOH) initiate the secondary ion chemistry by reacting with I^- and produce $[IO]^-$ ((R2.1 and R2.2). The presence of water

could promote the production of $[IO]^-$ (R2.3) and hence the secondary ion chemistry (**Figure 2.3D**). This mechanism is further supported by the fact that $[IO]^-$ was observed to form in the presence of O_3 and PAA and promoted by RH (**Figure 2.3A, 2.3B, and 2.3D**). Following its formation, $[IO]^-$ can further cluster with acidic compounds (HA) to form $[HA+IO]^-$ (R2.4). In a previous study by Iyer et al., dehydroxylation of PAA in the presence of I^- and H_2O was calculated to produce AA + $[IO]^-$ and $[AA-H]^-$ + HOI, with the latter combination having lower free energy than the former. This indirectly suggests that $[IO]^-$ might be able to deprotonate organic acids (R2.5). Consistent with this reaction, the deprotonated organic acid ions are all found to be enhanced with O_3 and PAA. In addition, we propose that $[HA+IO]^-$ could cluster with another acidic molecule HB, and form the $[A+B+I]^-$ dimer clusters and water (R2.6). As the declustering dV initially increased, the enhanced neutral molecules from cluster dissociation combine with $[HA+IO]^-$ to form $[A+B+I]^-$, explaining the temporal increase of the dimer clusters shown in **Figure 2.3C**. However, how A and B are bonded with each other and with iodide in $[A+B+I]^-$ remain puzzling and warrant future computational work. Further, the influence of the secondary ion chemistry on other organic functionalities is unknown so far due to the lack of standards detectable by I^--CIMS. Small amounts of trimers were also observed (**Figure 2.2**), but their formation mechanism is not the focus of this work.

2.3.2 The effects of the secondary ion chemistry on molecular compositions of VOC oxidation products

Following the observation of the secondary ion chemistry using the chemical standards, we further performed oxidation experiments of α-pinene and isoprene in the flowtube reactor and used the I^--CIMS to measure the OVOC products (**Figure 2.1**), with the additional O_3 or acids at the IMR inlet. In the α-pinene ozonolysis experiments without additional O_3 or organic acids in the IMR (the control experiment), the gas-phase OVOC products are shown in **Figure 2.4A**, with the major peaks assigned to iodide adducts with $C_{8\text{-}10}H_{12\text{-}18}O_{3\text{-}6}$ with high-resolution peak fitting in the range of m/Q at 295 – 365 Th. These assigned formulas are consistent with prior studies of α-pinene ozonolysis gas-phase products.[4, 32, 33] In the presence of additional O_3 in the IMR, most of the α-pinene derived OVOC products are affected by the secondary ion chemistry. With 197 ppb IMR O_3, the degrees of the variations of these products measured by I^--CIMS are shown in the mass defect (δ_m) vs. m/Q plot in **Figure 2.5A**. The combination of the formation of $[HA+IO]^-$ and the decreasing signal of $[HA+I]^-$ caused by the addition of IMR O_3 likely has led to the observed relative ion intensity changes. As a result, the intensities of many ions have largely increased, and some have reduced owing to the O_3-mediated secondary ion chemistry in the IMR. The dV scanning measurements also support these results. For example, the declustering profiles of $[C_{10}H_{16}O_4I]^-$ (a major product from α-pinene ozonolysis) show delayed declustering in the presence of IMR O_3 (**Figure 2.6A**). This observation is consistent with the results using chemical standards (**Figure 2.3C**), suggesting that the observed $[C_{10}H_{16}O_4I]^-$ was partially resulted from $[C_{10}H_{16}O_3+IO]^-$

when O_3 is present in the IMR. This is likely the case for many other product ions. However, the formation of the $[A+B+I]^-$ dimer ions is unclear with additional IMR O_3, owing to the low concentrations of the individual OVOC monomers and the fact that pre-existing dimers from α-pinene ozonolysis[34] could mask the identification of the formed $[A+B+I]^-$ dimer ions.

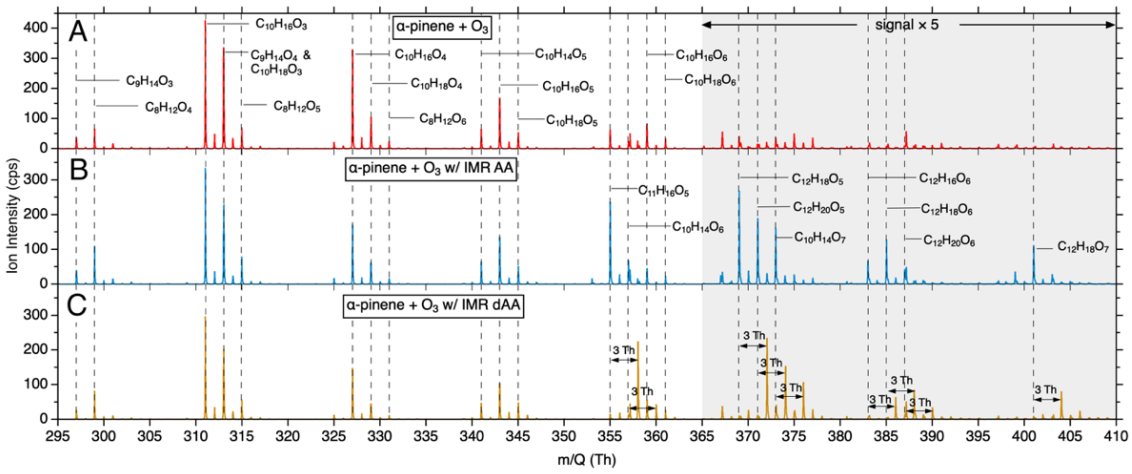

Figure 2.4 Mass spectra showing (A) the chemical composition of α-pinene ozonolysis monomer products (C_8 – C_{10}) in the absence of additional IMR O_3 or acids, (B) in the presence of IMR AA, and (C) in the presence of IMR dAA. Major products are labeled in the mass spectra, with the iodide part of the ion formulas omitted for simplification. The ion intensities are multiplied by 5 in the gray region. The vertical dashed lines are to guide the eye. The 3 Th mass shift of the same peaks between (B) and (C) was caused by the usage of dAA.

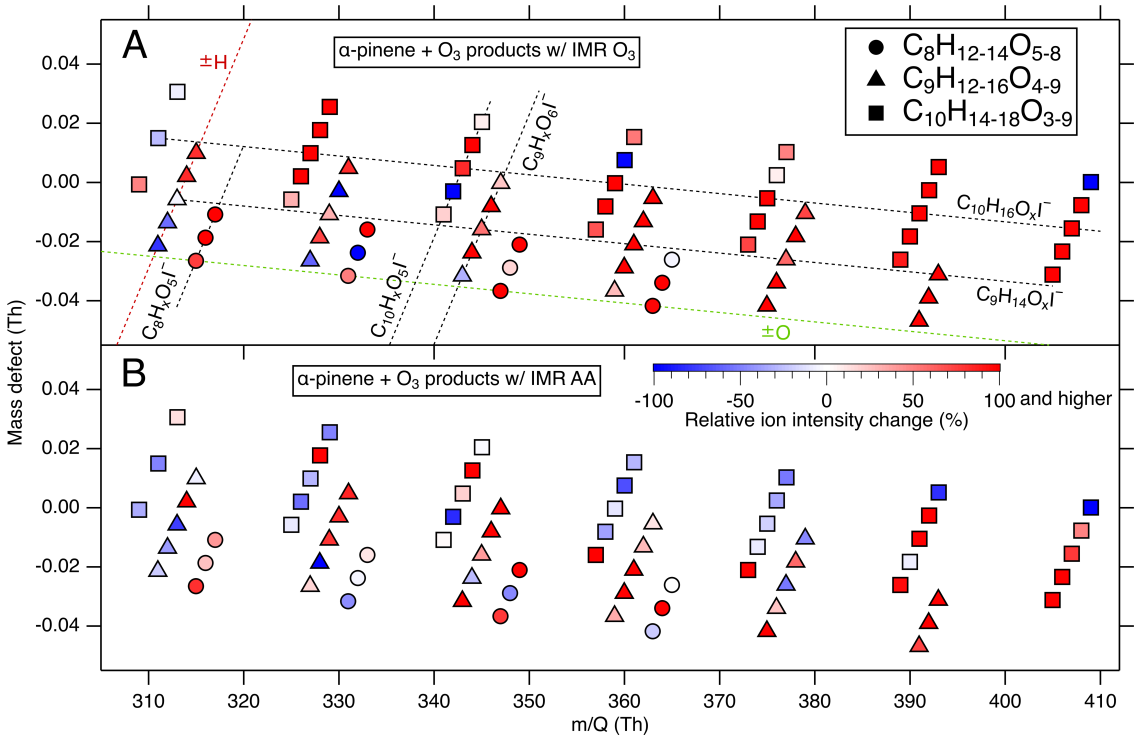

Figure 2.5 Mass defect plots of α-pinene ozonolysis C_8 – C_{10} products in the gas-phase (A) with IMR O_3 (B) and with IMR AA. The relative ion intensity change is marked by the color scheme in comparison to the products from the control experiment.

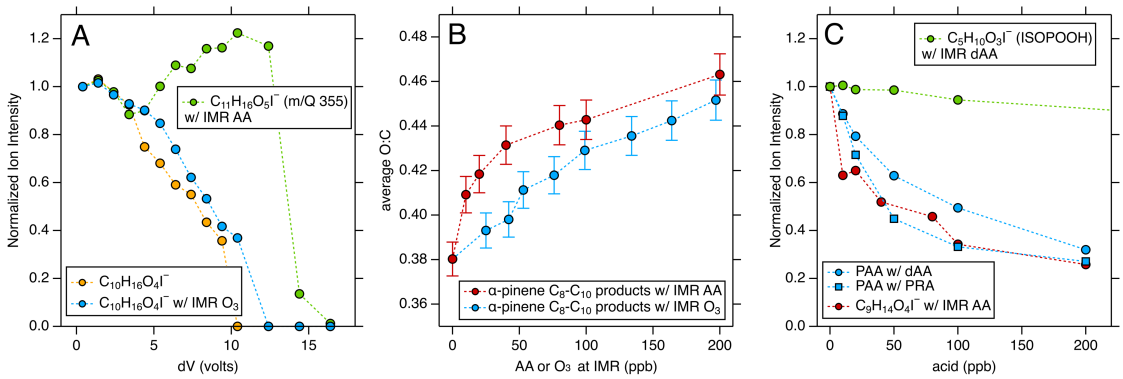

Figure 2.6 (A) Normalized ion intensities of $C_{10}H_{16}O_4I^-$ with and without IMR O_3 and $C_{11}H_{16}O_5I^-$ with IMR AA as a function of dV during the declustering scans. (B) The effect of the secondary ion chemistry on the average O/C ratio of α-pinene ozonolysis major C_8 – C_{10} products. (C) The decreasing signals of PAA, ISOPOOH and $C_9H_{14}O_4I^-$ by varying degrees as the IMR acid concentration increases.

In comparison to the results with additional IMR O_3, a number of product ions showed up more prominently in the range of m/Q at 355 – 410 Th in the presence of IMR AA, which were determined as $C_{10\text{-}12}H_{14\text{-}20}O_{5\text{-}7}$ by the high-resolution peak fitting (**Figure 2.4B**). These observations indicate that the gaseous monomers with the formulas $C_XH_YO_Z$ have largely formed the $[A+B+I]^-$ dimer adducts ions with AA resulting in the apparent chemical formulas of $C_{X+2}H_{Y+2}O_{Z+2}$ (i.e., $[C_XH_YO_Z+C_2H_4O_2\text{-}2H+I]^-$). This is further confirmed by the m/Q shift of 3 Th in the mass spectra with dAA employed instead of AA (**Figure 2.4C**). From the experiments using the various chemical standards, we suggested that the formation of such $[A+B+I]^-$ dimer clusters require an oxygen donor and acidic organics. It should be noted that in these experiments, there was very little O_3 present in the IMR. Thus, we suggest that other oxygen donors naturally present in the α-pinene ozonolysis system such as peracids could be responsible for the occurrence of the secondary ion chemistry. In fact, α-pinene ozonolysis is known to produce substantial organic acids; therefore, the secondary ion chemistry could occur even without external interference with O_3 or acids. However, the extent of such ion chemistry is unassessable only by using I^--CIMS. It is also worth studying whether other oxygen donors, such as Criegee intermediates, could play a similar role as O_3 and peracids in the studied ion chemistry since they are abundant intermediates in α-pinene ozonolysis. It is also highly likely that the OVOC products from α-pinene ozonolysis that showed the capacity of forming dimer clusters with additional IMR acids contain at least one acid, hydroperoxide or peracid functional group, as indicated by previous studies.[4] Moreover, the dimer clusters' intensities in general correspond to their monomeric precursors, except for $[C_{11}H_{16}O_5I]^-$

whose precursor, $C_9H_{14}O_3$ has a low signal. The relatively poor sensitivity of I^--CIMS to detect molecules with only two or three oxygen atoms may be partly responsible for this exception. Nonetheless, the declustering scan results shown in **Figure 2.6A** for $[C_{11}H_{16}O_5I]^-$ have clearly demonstrated that it is a dimer cluster from the secondary ion chemistry. On the other hand, more of the C_8 – C_{10} product intensities decrease with the addition of IMR AA, in contrast to the IMR O_3 experiments, as shown in **Figure 2.5B**. This is likely due to that the parent compound ($C_XH_YO_Z$) consumption by reacting with $[AA+IO]^-$ to form dimer clusters outcompetes the formation of $[C_XH_YO_{Z-1}+IO]^-$. We further examined the overall impacts of the secondary ion chemistry on the measured OVOC compositions using the elemental O/C ratios as a metric. As shown in **Figure 2.6B**, the average O/C ratios have increased by 15–20% as the concentrations of IMR O_3 or AA increased from 0 to 200 ppb. Therefore, the studied ion chemistry can lead to misinterpretation of molecular compositions by using I^--CIMS, especially when both acidic molecules and oxygen donors are naturally present in the OVOC products.

The isoprene ozonolysis experiments showed only a few major peaks in the I^--CIMS mass spectra, and thus is less focused in this work. Additionally, in comparison with the α-pinene experiments, isoprene oxidation is known to form less acidic products.[4, 33, 35-37] The only major product of interest is $[C_5H_{10}O_3I]^-$, which can be assigned to the isoprene hydroxy hydroperoxide (ISOPOOH) and the ISOPOOH-derived epoxydiol (IEPOX).[38] But based on the MCM kinetic simulations, under the short timescale in the flowtube experiments, ISOPOOH is expected to be 5 orders of magnitude more abundant than IEPOX. Thus, the observed $[C_5H_{10}O_3I]^-$ signals could be primarily contributed by

ISOPOOH. With the additions of IMR O_3, we observed enhanced $[C_5H_{10}O_3+IO]^-$, consistent with the secondary ion chemistry. With IMR dAA (dAA used instead of AA to avoid $[2AA-2H+I]^-$ confusion with $[C_5H_{10}O_3I]^-$ at m/Q 245), enhanced $[C_5H_{10}O_3+dAA-H-D+I]^-$ was also observed, but the compositional change is to a lesser degree than α-pinene ozonolysis (**Figure 2.4**), likely owing to the smaller amount of oxygen donor in isoprene ozonolysis products. These results are consistent with the TBH standard measurements, suggesting that the secondary ion chemistry occurs for hydroperoxides which are slightly acidic.

2.3.3 The potential application of the secondary ion chemistry to inform functional groups and help elucidate chemical mechanisms

In the chemical standard experiments, we found that the addition of acids into the IMR can largely consume $[PAA+I]^-$. **Figure 2.6C** shows the normalized ion intensity of $[PAA+I]^-$ as a function of the concentration of IMR acids (dAA and PRA). With 200 ppb of carboxylic acids, approximately 60% of the initial PAA adduct signals ($[C_2H_4O_3I]^-$) were reduced due to the secondary ion chemistry under study. However, because we did not have another hydroperoxide standard observable by the I^--CIMS available (TBH is not detectable by I^--CIMS), it was unclear whether the observed PAA reduction is due only to the hydroperoxide or the entire peracid functionality. This question was addressed by the measurements of ISOPOOH ($[C_5H_{10}O_3I]^-$) in the isoprene ozonolysis experiment. The intensity of ISOPOOH decreased by a much smaller degree in the presence of IMR acids than that of the PAA (**Figure 2.6C**), indicating that the peracid functionality is crucial for

the significant reduction. The dramatic difference between peracids vs. hydroperoxides also provides insights into the α-pinene ozonolysis products which decreased greatly with IMR acids (**Figure 2.5B**). In particular, the intensity of $[C_9H_{14}O_4I]^-$ in the α-pinene experiments dropped by a similar fraction to PAA, corresponding to the IMR acid (**Figure 2.6C**). The molecule $C_9H_{14}O_4$, a key product from α-pinene ozonolysis, is commonly known as pinic acid in the particle phase.[32, 33] Jenkin et al.[37] proposed a mechanism of the formation of pinic acid from the isomerization of a C_9 acyloxy radical (**Figure 2.7**). In contrast, Ma and Marston[39] showed that pinic acid was enhanced by the addition of HO_2 radicals, suggesting that pinic acid could also be formed from perpinalic acid (a peracid) through intramolecular isomerization (**Figure 2.7**). In this work, the large drop of $[C_9H_{14}O_4I]^-$ in the presence of IMR acids in I^--CIMS suggesting that the $C_9H_{14}O_4$ molecule in the gas phase is mostly likely a peracid (i.e., the perpinalic acid), in support for the Ma and Marston's work. It is possible that perpinalic acid undergoes further Baeyer-Villiger reactions[4] to further form pinic acid in the gas and/or particle phases. The investigation of the formation and structures of $C_9H_{14}O_4$ could be a focus in future experiments. Although the studied secondary ion chemistry from interactions of oxygen donors and acidic organics in I^--CIMS can affect OVOC compositional interpretations, it likely has varying degrees of impact on different classes of organic compounds. Therefore, the potential application of I^--CIMS secondary ion chemistry to inform functional groups is promising in forthcoming studies.

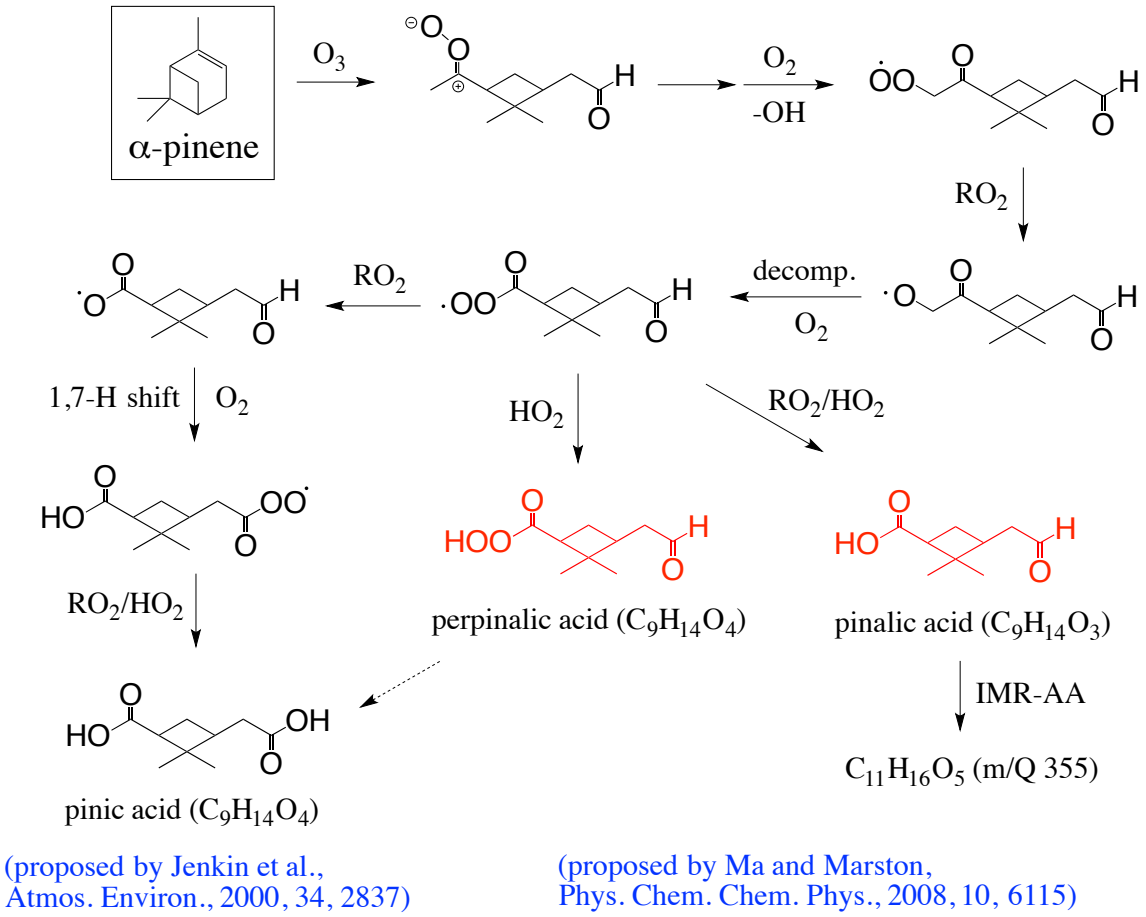

Figure 2.7 Proposed mechanism of the formation of $C_9H_{14}O_4$ in the gas phase which is identified as perpinalic acid.

2.4 Conclusions

In this work, we observed iodide clusters in the forms of $[HA+IO]^-$ and $[A+B+I]^-$ in I^--CIMS, as a result of the secondary ion chemistry other than the well-known $[HA+I]^-$ clusters. A possible mechanism of the studied ion chemistry was proposed, through which the presence of O_3 or peracid as oxygen donors mediates the secondary ion chemistry with acidic organic molecules, including carboxylic acids, hydroperoxides, and peracids. In addition, we illustrated that the secondary ion chemistry in the IMR of I^--CIMS could lead to misinterpretation of molecular compositions of oxidation products overall. The intensities of certain ions can be reduced by the formation of dimer clusters or enhanced from the secondary ion chemistry of the molecules with one fewer oxygen. As a result, the average O/C ratio of α-pinene ozonolysis products was increased by 15–20% due to the secondary ion chemistry with the addition of 200 ppb IMR O_3 or IMR acid. In the present study, we have also shown that the studied ion chemistry might be potentially applied to inform organic functionalities with the varying effect of the secondary ion chemistry. Thus, application of I^--CIMS to identify different organic classes is promising, as we demonstrated that the oxidation product $C_9H_{14}O_4$ from α-pinene ozonolysis is first formed as perpinalic acid in the gas phase.

2.5 Reference

(1) Goldstein, A. H.; Galbally, I. E., Known and unexplored organic constituents in the Earth's atmosphere. *Geochimica et Cosmochimica Acta Supplement* **2009,** *73*, A449.

(2) Hallquist, M.; Wenger, J. C.; Baltensperger, U.; Rudich, Y.; Simpson, D.; Claeys, M.; Dommen, J.; Donahue, N. M.; George, C.; Goldstein, A. H.; et al. The formation, properties and impact of secondary organic aerosol: current and emerging issues. *Atmos. Chem. Phys.* **2009,** *9* (14), 5155-5236.

(3) De Gouw, J.; Jimenez, J. L., Organic Aerosols in the Earth's Atmosphere. *Environ. Sci. Technol.* **2009,** *43* (20), 7614-7618.

(4) Claflin, M. S.; Krechmer, J. E.; Hu, W.; Jimenez, J. L.; Ziemann, P. J., Functional Group Composition of Secondary Organic Aerosol Formed from Ozonolysis of α-Pinene Under High VOC and Autoxidation Conditions. *ACS Earth Space Chem.* **2018,** *2* (11), 1196-1210.

(5) Kroll, J. H.; Seinfeld, J. H., Chemistry of secondary organic aerosol: Formation and evolution of low-volatility organics in the atmosphere. *Atmos. Environ.* **2008,** *42* (16), 3593-3624.

(6) Merikanto, J.; Spracklen, D. V.; Mann, G. W.; Pickering, S. J.; Carslaw, K. S., Impact of nucleation on global CCN. *Atmos. Chem. Phys.* **2009,** *9* (21), 8601-8616.

(7) Dockery, D. W.; Pope, C. A.; Xu, X.; Spengler, J. D.; Ware, J. H.; Fay, M. E.; Ferris, B. G.; Speizer, F. E., An Association between Air Pollution and Mortality in Six U.S. Cities. *N. Engl. J. Med.* **1993,** *329* (24), 1753-1759.

(8) Boucher, O.; Randall, D.; Artaxo, P.; Bretherton, C.; Feingold, C.; Forster, P.; Kerminen, V.-M.; Kondo, Y.; Liao, H.; Lohmann, U.; Rasch, P.; Satheesh, S. K.; Sherwood, S.; Stevens, B.; Zhang, X.-Y. *Clouds and Aerosols*; IPCC: 2013; p 657.

(9) Watson, J. G., Visibility: Science and Regulation. *J. Air Waste Manage.* **2002,** *52* (6), 628-713.

(10) Aljawhary, D.; Lee, A. K. Y.; Abbatt, J. P. D., High-resolution chemical ionization mass spectrometry (ToF-CIMS): application to study SOA composition and processing. *Atmos. Meas. Tech.* **2013,** *6* (11), 3211-3224.

(11) Huey, L. G., Measurement of trace atmospheric species by chemical ionization mass spectrometry: Speciation of reactive nitrogen and future directions. *Mass Spectrom. Rev.* **2007,** *26* (2), 166-184.

(12) Riva, M.; Brüggemann, M.; Li, D.; Perrier, S.; George, C.; Herrmann, H.; Berndt, T., Capability of CI-Orbitrap for Gas-Phase Analysis in Atmospheric Chemistry: A Comparison with the CI-APi-TOF Technique. *Anal. Chem.* **2020,** *92* (12), 8142-8150.

(13) Bertram, T. H.; Kimmel, J. R.; Crisp, T. A.; Ryder, O. S.; Yatavelli, R. L. N.; Thornton, J. A.; Cubison, M. J.; Gonin, M.; Worsnop, D. R., A field-deployable, chemical ionization time-of-flight mass spectrometer. *Atmos. Meas. Tech.* **2011,** *4* (7), 1471-1479.

(14) Breitenlechner, M.; Fischer, L.; Hainer, M.; Heinritzi, M.; Curtius, J.; Hansel, A., PTR3: An Instrument for Studying the Lifecycle of Reactive Organic Carbon in the Atmosphere. *Anal. Chem.* **2017,** *89* (11), 5824-5831.

(15) Huey, L. G.; Hanson, D. R.; Howard, C. J., Reactions of SF6- and I- with Atmospheric Trace Gases. *J. Phys. Chem.* **1995,** *99* (14), 5001-5008.

(16) Crounse, J. D.; Nielsen, L. B.; Jørgensen, S.; Kjaergaard, H. G.; Wennberg, P. O., Autoxidation of Organic Compounds in the Atmosphere. *J. Phys. Chem. Lett.* **2013,** *4* (20), 3513-3520.

(17) Hammes, J.; Lutz, A.; Mentel, T.; Faxon, C.; Hallquist, M., Carboxylic acids from limonene oxidation by ozone and hydroxyl radicals: insights into mechanisms derived using a FIGAERO-CIMS. *Atmos. Chem. Phys.* **2019,** *19* (20), 13037-13052.

(18) Laskin, J.; Laskin, A.; Nizkorodov, S. A., Mass Spectrometry Analysis in Atmospheric Chemistry. *Anal. Chem.* **2018,** *90* (1), 166-189.

(19) Sanchez, J.; Tanner, D. J.; Chen, D.; Huey, L. G.; Ng, N. L., A new technique for the direct detection of HO2 radicals using bromide chemical ionization mass spectrometry (Br-CIMS): initial characterization. *Atmos. Meas. Tech.* **2016,** *9* (8), 3851-3861.

(20) Canaval, E.; Hyttinen, N.; Schmidbauer, B.; Fischer, L.; Hansel, A., NH4+ Association and Proton Transfer Reactions With a Series of Organic Molecules. *Front. Chem.* **2019,** *7* (191).

(21) Lee, B. H.; Lopez-Hilfiker, F. D.; Mohr, C.; Kurtén, T.; Worsnop, D. R.; Thornton, J. A., An Iodide-Adduct High-Resolution Time-of-Flight Chemical-Ionization Mass Spectrometer: Application to Atmospheric Inorganic and Organic Compounds. *Environ. Sci. Technol.* **2014,** *48* (11), 6309-6317.

(22) Lopez-Hilfiker, F. D.; Iyer, S.; Mohr, C.; Lee, B. H.; D'Ambro, E. L.; Kurtén, T.; Thornton, J. A., Constraining the sensitivity of iodide adduct chemical ionization mass spectrometry to multifunctional organic molecules using the collision limit and thermodynamic stability of iodide ion adducts. *Atmos. Meas. Tech.* **2016,** *9* (4), 1505-1512.

(23) Smith, D.; McEwan, M. J.; Španěl, P., Understanding Gas Phase Ion Chemistry Is the Key to Reliable Selected Ion Flow Tube-Mass Spectrometry Analyses. *Anal. Chem.* **2020,** *92* (19), 12750-12762.

(24) Iyer, S.; He, X.; Hyttinen, N.; Kurtén, T.; Rissanen, M. P., Computational and Experimental Investigation of the Detection of HO2 Radical and the Products of Its Reaction with Cyclohexene Ozonolysis Derived RO2 Radicals by an Iodide-Based Chemical Ionization Mass Spectrometer. *J. Phys. Chem. A* **2017,** *121* (36), 6778-6789.

(25) Dörich, R.; Eger, P.; Lelieveld, J.; Crowley, J. N., Iodide-CIMS and m/z 62: The detection of HNO3 as NO3− in the presence of PAN, peracetic acid and O3. *Atmos. Meas. Tech. Discuss.* **2021,** *2021*, 1-26.

(26) von Kuhlmann, R.; Lawrence, M. G.; Crutzen, P. J.; Rasch, P. J., A model for studies of tropospheric ozone and nonmethane hydrocarbons: Model description and ozone results. *J. Geophys. Res. Atmos.* **2003,** *108* (D9).

(27) Li, Q.; Su, G.; Li, C.; Liu, P.; Zhao, X.; Zhang, C.; Sun, X.; Mu, Y.; Wu, M.; Wang, Q.; Sun, B., An investigation into the role of VOCs in SOA and ozone production in Beijing, China. *Sci. Total Environ.* **2020,** *720*, 137536.

(28) Jenkin, M. E.; Young, J. C.; Rickard, A. R., The MCM v3.3.1 degradation scheme for isoprene. *Atmos. Chem. Phys.* **2015,** *15* (20), 11433-11459.

(29) Mentel, T. F.; Springer, M.; Ehn, M.; Kleist, E.; Pullinen, I.; Kurtén, T.; Rissanen, M.; Wahner, A.; Wildt, J., Formation of highly oxidized multifunctional compounds: autoxidation of peroxy radicals formed in the ozonolysis of alkenes – deduced from structure–product relationships. *Atmos. Chem. Phys.* **2015,** *15* (12), 6745-6765.

(30) Docherty, K. S.; Wu, W.; Lim, Y. B.; Ziemann, P. J., Contributions of Organic Peroxides to Secondary Aerosol Formed from Reactions of Monoterpenes with O3. *Environ. Sci. Technol.* **2005,** *39* (11), 4049-4059.

(32) Hiberty, P. C., Mechanism of ozonolysis. Ab initio study of the primary ozonide and its cleavage to the Criegee intermediate. *J. Am. Chem. Soc.* **1976,** *98* (20), 6088-6092.

(32) Christoffersen, T. S.; Hjorth, J.; Horie, O.; Jensen, N. R.; Kotzias, D.; Molander, L. L.; Neeb, P.; Ruppert, L.; Winterhalter, R.; Virkkula, A.; Wirtz, K.; Larsen, B. R., cis-pinic acid, a possible precursor for organic aerosol formation from ozonolysis of α-pinene. *Atmos. Environ.* **1998,** *32* (10), 1657-1661.

(33) Yan, M.; Russell, A. T.; Marston, G., Mechanisms for the formation of secondary organic aerosol components from the gas-phase ozonolysis of α-pinene. *Phys. Chem. Chem. Phys.* **2008,** *10* (29), 4294-4312.

(34) Zhao, Y.; Thornton, J. A.; Pye, H. O. T., Quantitative constraints on autoxidation and dimer formation from direct probing of monoterpene-derived peroxy radical chemistry. *Proc. Natl. Acad. Sci. U.S.A.* **2018,** *115* (48), 12142.

(35) Kamens, R. M.; Gery, M. W.; Jeffries, H. E.; Jackson, M.; Cole, E. I., Ozone–isoprene reactions: Product formation and aerosol potential. *Int. J. Chem. Kinet.* **1982,** *14* (9), 955-975.

(36) Sauer, F.; Schäfer, C.; Neeb, P.; Horie, O.; Moortgat, G. K., Formation of hydrogen peroxide in the ozonolysis of isoprene and simple alkenes under humid conditions. *Atmos. Environ.* **1999,** *33* (2), 229-241.

(37) E. Jenkin, M.; Shallcross, D. E.; Harvey, J. N., Development and application of a possible mechanism for the generation of cis-pinic acid from the ozonolysis of α- and β-pinene. *Atmos. Environ.* **2000,** *34* (18), 2837-2850.

(38) Paulot, F.; Crounse, J. D.; Kjaergaard, H. G.; Kürten, A.; St. Clair, J. M.; Seinfeld, J. H.; Wennberg, P. O., Unexpected Epoxide Formation in the Gas-Phase Photooxidation of Isoprene. *Science* **2009,** *325* (5941), 730.

(39) Ma, Y.; Marston, G., Multifunctional acid formation from the gas-phase ozonolysis of β-pinene. *Phys. Chem. Chem. Phys.* **2008,** *10*, 6115.

Chapter 3 Unexpectedly Efficient Aging of Organic Aerosols Mediated by Autoxidation

3.1 Introduction

OAs are ubiquitously present in the Earth's atmosphere and greatly contribute to fine particulate matter.[1, 2] The chemical composition and properties of atmospheric OAs can significantly impact air quality, climate, and human health.[3, 4] Despite the immense ubiquity of OAs and the oxidizing nature of the atmosphere, the OA reactivity through heterogeneous oxidation by gaseous oxidants such as •OH has been considered a very slow process,[5-12] in comparison to the timescales of other important atmospheric processes and the overall aerosol lifetime.

The universal metric to quantify the heterogeneous oxidation kinetics is the effective reactive uptake coefficient of •OH (γ_{eff}), which describes the probability of •OH-particle collision leading to oxidation events:[7]

$$\gamma_{\text{eff}} = \frac{4k\rho N_A V}{\bar{c}MA} \qquad \text{(E3.1)}$$

where k is the second-order degradation rate constant of an OA surrogate, ρ is the particle density, N_A is Avogadro's number, $\bar{c}$ is the mean thermal velocity of •OH, M is the molecular weight of the OA surrogate, V is the particle volume, and A is the particle surface area. Previous studies have often reported γ_{eff} in the range of 0.01 – 1.0,[5, 8-11, 13, 14] with the smaller γ_{eff} values often observed for more viscous OAs due to that oxidation is confined at the particle surface region which the inside materials cannot efficiently diffuse to. The kinetic information expressed in γ_{eff} could also allow for estimation of the OA oxidation timescales by:[15]

$$\tau_{ox} = \frac{1}{k[\cdot OH]} = \frac{2d_p \rho N_A}{3\gamma_{\text{eff}} \bar{c} M[\cdot OH]} \quad \text{(E3.2)}$$

where d_p is the particle diameter. Thus, the γ_{eff} value of 0.01 – 1.0 translates to oxidation timescales from several days to years. These significantly longer timescales than the typical aerosol lifetime in the atmosphere (~ 10 days[16]) suggests that heterogenous oxidation of OAs in the atmosphere is unlikely a key process to significantly impact air quality and the climate. However, this long-standing view was derived from previous laboratory studies using •OH concentrations 3 – 5 orders of magnitude higher than atmospheric concentrations (i.e., [•OH] ~ 10^9 – 10^{11} molecules cm^{-3}) to offset the short oxidation time (τ ~ 1 min or less) in flow tube reactors (FTR),[6, 7, 9-11, 13, 17] such that one can interpret OA oxidation under relevant atmospheric conditions, termed as "•OH exposure" (= [•OH] × τ). But it remains unclear whether the results obtained from high-[•OH] and short-τ studies can be extended into real atmospheric conditions, where OAs are aged for many days under much lower [•OH] (~ 10^6 –10^7 molecules cm^{-3}).[18]

Here, we probe the •OH-initiated heterogeneous oxidation of a few common OA model systems in a custom-designed continuous flow stirred tank reactor (CFSTR).[19-22] Experiments were conducted under a large range of [•OH] (5 × 10^6 – 1 × 10^9 molecules cm^{-3}) to bring the OA aging conditions from typical laboratory [•OH] much closer to ambient levels. The chosen OA surrogates (adipic acid, succinic acid, citric acid, and 3-methylglutaric acid) are highly oxidized compounds (O/C ratio ~ 0.7 – 1.2) containing multiple carboxylic acid functional groups. They all have been used in prior research to represent the oxygenated and viscous nature of generic OAs in the atmosphere.[2, 10, 11, 13, 23-

[25] In these experiments, the particle diffusion coefficients (D_{org}, 10^{-8} – 10^{-13} cm^2 s^{-1}) and mixing timescales (10^{-3} – 10^{2} s) are also representative of typical aerosol phase state in the lower troposphere.[25] Their degradation upon heterogeneous •OH-oxidation was monitored in real-time using a thermal desorption iodide-adduct chemical ionization mass spectrometer (TD-CIMS) to provide accurate kinetic measurements.[26, 27] The comprehensive OA oxidation products were measured by the TD-CIMS and the IMS-MS[23, 26, 28-30] which provides additional isomer-resolved capability. Complementary FTR experiments were also performed following similar procedures as in previous studies.[26, 29] This allows for direct comparisons of the heterogeneous oxidation kinetics and products between the CFSTR and FTR experiments. In addition, a multilayer reaction-diffusion kinetic model was developed to simulate and interpret the experimental results.[26]

3.2 Materials and Methods

3.2.1 Experimental setup

All experiments were performed at 22 °C and varied water activity (a_w of 35 – 70%). A customized CFSTR (volume ~ 250 L)[30, 31] was used in this work. Here, the CFSTR was operated in the "semi-batch" mode under room temperature.[19] Before each experiment, the CFSTR was flushed overnight with clean dry air, supplied by a zero-air generator (Aadco Instrument, Inc.). At the beginning of each experiment, the CFSTR background was monitored to ensure that aerosol particles were not present. Polydisperse OAs of selected model compounds were generated into the CFSTR using a constant output aerosol atomizer (TSI, Inc.). The OA injection was stopped when targeted OA mass concentration was

reached (~ 1500 – 2000 μg m^{-3}). After OA injection, the clean air injection was adjusted to a total flow of 1.5 L min^{-1}. Two different a_w levels were studied for the OA model compounds: 0.36 ± 0.01 and 0.67 ± 0.03. For adipic acid and succinic acid, the injected OA through the dryer effloresced the particles and a_w levels does not change their phase state and D_{org}. But for citric acid that does not have an efflorescence point, different a_w levels lead to different amount of water in the OA and hence affect the phase state and D_{org}.[11, 32, 33] The 3-methylglutaric acid OA was only studied under a_w = 0.36. In all the CFSTR experiments, the mean surface-weighted particle diameters for adipic acid, succinic acid, citric acid, and 3-methylglutaric acid were 210 ± 50 nm, 420 ± 120 nm, 290 ± 15 nm, and 221 ± 17 nm, respectively. After the OA injection, a one-time injection of a VOC tracer (either acetic acid or propionic acid) was made to reach a VOC concentration of 1 – 2 ppm. After both the OA and VOC tracer have been injected, they were allowed to undergo dilution (caused by the continuous flow) and wall loss in the CFSTR. Then, either O_3 or H_2O_2 was continuously injected into the CFSTR. With the UV lamp on, this injection initiated the in-situ generation of $^{\bullet}OH$ radicals.[26, 29] By changing the injection concentration of O_3 or H_2O_2, the [$^{\bullet}OH$] was controlled. During the $^{\bullet}OH$-initiated oxidation, the total flow rate and a_w were maintained the same as the "dilution and wall loss only" period. Therefore, the changes in the decay rates of both the OA and VOC tracer were caused by oxidation. The oxidation was maintained for 1 – 2 hours. To compare results obtained from the CFSTR experiments, auxiliary FTR experiments were performed in parallel with the CFSTR studies. The setup for the FTR is the same as our previous work.[23, 26, 28, 29] The injection system and the kinetic measurements are the same as for the CFSTR experiments.

3.2.2 Instrumentation

The OA particle size distribution and number concentration were analyzed by a scanning electrical mobility spectrometer and mixing condensation particle counter (SEMS and MCPC, Brechtel Inc., 2100). A high-sensitivity proton-transfer-reaction mass spectrometer (PTR-MS, Ionicon Analytik Inc.) was used to measure the decay of the VOC tracers at 0.3 L min^{-1} in some experiments.[34] The OA composition was measured in real time by the I^--CIMS with a TD tube following a charcoal denuder to remove volatile gases.[26, 27, 30] The desorption temperature was set to 90 – 160 °C for different OA systems to vaporize most of the parent OA species. For the experiments in which the PTR-MS was unavailable, the VOC tracers were also monitored by the CIMS, where a separate gas sampling line was added bypassing the TD unit. The oxidation of 3-methylglutaric acid and adipic acid OA was used as the model system for the offline chemical composition analysis and comparison between the CFSTR and FTR results. The oxidized OA particles were collected using a sequential spot sampler (Aerosol Devices Inc., SS110) downstream of a charcoal denuder. The collected OA samples were immediately extracted by acetonitrile and infused into an electrospray ionization (ESI) IMS-MS (Aerodyne Research Inc.) in the negative ion mode. The IMS-MS measurements could provide isomer-resolved characterization by separating ionized molecules with their structure-dependent collisional cross sections.[35, 36] More details were described in our prior studies.[23, 26, 29, 31] Finally, a UV-visible spectrophotometer (Agilent Inc., 8453) was used for total hydroperoxides (ROOH) quantification.

3.2.3 Calculations of the heterogeneous oxidation kinetics and timescales

By comparing the decay rates of the parent OA compound and the VOC tracer before and after the oxidation, the [•OH] in the CFSTR and the second-order oxidation rate constants (k) of parent OA compound through heterogenous OH oxidation were determined. Specifically, the •OH oxidation rate constants of acetic acid and propionic acid ($k_{VOC+•OH}$) were known from the literature (6.6×10^{-13} cm^3 molecule^{-1} s^{-1} and 1.64×10^{-12} cm^3 molecule^{-1} s^{-1}, respectively).[37, 38] Thus, the [•OH] can be calculated by:

$$[\cdot OH] = \frac{k_{VOC,ox} - k_{VOC,DL}}{k_{VOC+\cdot OH}} \quad \text{(E3.3)}$$

where $k_{VOC,ox}$ and $k_{VOC,DL}$ are the first-order VOC decay rates during the oxidation period and the dilution-wall loss period, respectively. Then, the second-order oxidation rate constants (k) of parent OA compound through heterogenous •OH oxidation was calculated by:

$$k = \frac{k_{OA,ox} - k_{OA,DL}}{[\cdot OH]} \quad \text{(E3.4)}$$

where $k_{OA,ox}$ and $k_{OA,DL}$ are the first-order parent OA decay rates during the oxidation period and the dilution-wall loss period, respectively. The four first-order decay rates ($k_{VOC,ox}$, $k_{VOC,DL}$, $k_{OA,ox}$, and $k_{OA,DL}$) were obtained from the PTR-MS or TD-CIMS measurements. The high-frequency measurements made by the two instruments allow for high confidence decay rates, and hence reliable estimates of k. The k values were then used to calculate the effective uptake coefficient (γ_{eff}) shown in Equation (1).[7] Therefore, the relationships between the γ_{eff} and [•OH] can be obtained. The oxidation timescales are hence estimated by Equation (2).[15]

3.2.4 The reaction-diffusion multilayer kinetic model

To explain the experimental observation, a reaction-diffusion multilayer kinetic model was developed, as described in our previous work[26] and is essentially a similar representation to several other models that simulates heterogeneous OA oxidation processes.[39-41] The model constructs a multi-compartment rectangular prism to approximate the OA particle. The area of the square surface of the prism is set to be the same as the spherical OA aerosol in the experiments and the height of the rectangular prism is $d_p/6$ to maintain the same surface-to-volume ratio of the spherical aerosol and hence preserves the relevant scaling between surface and bulk processes. The thickness of each compartment is set to 0.5 nm, which was suggested to be a good representation of semisolid and solid aerosol particles.[41] Each compartment is assumed to be a well-mixed volume. The model includes (1) the adsorption, desorption, and reactions of $^{\bullet}OH$ and $HO_2^{\bullet}$ at the outermost (i.e., surface) compartment of the OA particles, (2) organic radical-centered and multi-generational reactions in each compartment, and (3) diffusions of all the species molecules between compartments and evaporation of the relatively volatile products from the surface compartment to gas phase. The FACSIMILE software was used to perform the simulations.[26]

3.3 Results and Discussion

3.3.1 Heterogeneous oxidation kinetics

As shown in **Figure 3.1**, the measured γ_{eff} exhibits striking enhancement as [$^{\bullet}OH$] decreases from ~ 1×10^9 to ~ 5×10^6 molecules cm^{-3} for all the studied OA systems. As

[•OH] approaches atmospheric levels (10^6 –10^7 molecules cm^{-3}), the γ_{eff} values are 2–3 orders of magnitude higher than those obtained from the high-[•OH] FTR experiments performed in this work and in prior studies. It is also worth noting that in the citric acid system, where varied a_w was studied, higher a_w and hence faster diffusion in the particles led to larger γ_{eff} under [•OH] > ~ 10^8 molecules cm^{-3} (**Figure 3.1C**), agreeing with prior work.[11, 13, 42] However, the difference appears to diminish as [•OH] further drops, implying that particle-phase diffusion may not be a key limitation for OA multiphase oxidative aging under ambient conditions. These kinetic results suggest that OA heterogeneous oxidation in the atmosphere may have a much shorter timescale than previously expected. For example, for a 500-nm diameter particle under [•OH] of 10^6 molecules cm^{-3}, γ_{eff} of 10 indicates an oxidation timescale of ~ 2.3 days, compared to 231 days when γ_{eff} is 0.1. Consistent with these results, a summary of the scarce kinetic measurements from prior studies presents a similar trend, but in smaller [•OH] ranges, with larger uncertainties, and to a lesser degree of γ_{eff} enhancement.[15, 18, 43] In these prior studies, the [•OH]-dependent γ_{eff} was suggested to be possibly due to (1) slower •OH reaction than the •OH adsorption at the gas-particle interface (i.e., the Langmuir-Hinshelwood mechanism),[15] (2) the diffusion limitation of organic molecules to the interface for •OH reaction,[43] or (3) O_3 (an •OH precursor) shielding the particle interface.[18]

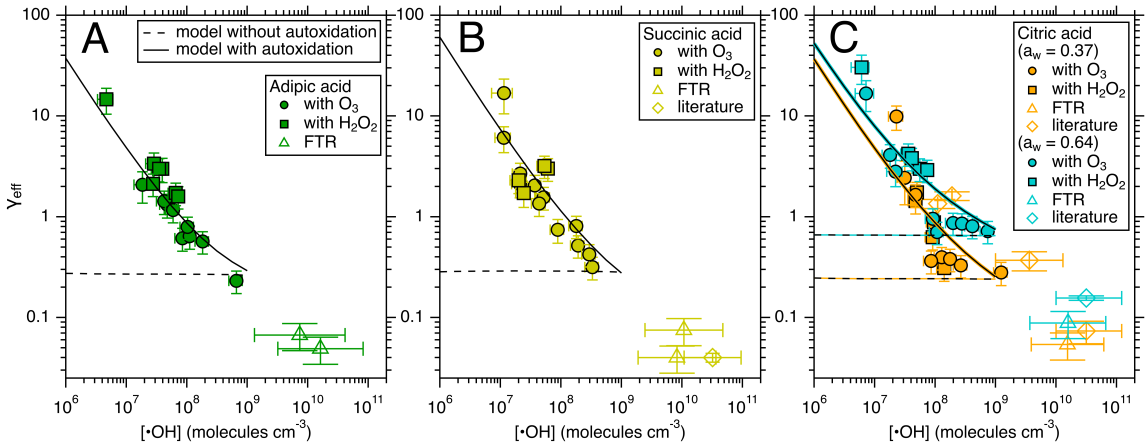

Figure 3.1 The γ_{eff} – [•OH] relationship for OA surrogate systems. (A) adipic acid, (B) succinic acid, and (C) citric acid, under various experimental conditions (see figure legend). For succinic acid (B) and citric acid (C), measurements from a few prior studies are also shown.[10, 11, 13, 43] For citric acid, experiments were performed under two different a_w conditions, resulting in different D_{org} values. Model simulations with and without the consideration of autoxidation are shown with the experimental data. Similar γ_{eff} – [•OH] trend obtained from three 3-methylglutaric acid experiments is in general consistency with the results shown here.

Hence, we used a multilayer reaction-diffusion kinetic model to investigate the cause of the [•OH]-dependent γ_{eff}. The model explicitly considers the adsorption and desorption of •OH at the gas-particle interface and the diffusion and reactions at the particle surface and in the bulk.[26, 39, 44] The main reaction mechanism in the model is shown in **Figure 3.2** (top part), where self-reaction of peroxy radical ($RO_2^•$) plays a central role: •OH oxidizes a parent OA molecule (RH) through H-abstraction and produces an alkyl radical ($R^•$); $RO_2^•$ is subsequently formed following oxygen addition; the $RO_2^•$ + $RO_2^•$ self-reaction then produce an alcohol-carbonyl pair (ROH and R=O), known as the Russell mechanism, or two alkoxy radicals ($RO^•$);[5, 45] the $RO^•$ may decompose to smaller oxidized products or undergo chain propagation reactions, forming an alcohol product and a new $RO_2^•$. The mechanism may occur at multiple generations, forming multifunctional products.[7, 23] For instance, both ROH and R=O can be further oxidized to form $R(OH)_2$ (diol), $R(=O)_2$ (dicarbonyl), and R(=O)OH (hydroxycarbonyl). This mechanism has been widely accepted to explain the major heterogeneous OA oxidation products observed in prior research. However, the kinetic model with this mechanism fails to simulate the increased γ_{eff} with reduced [•OH] (**Figure 3.1**), indicating that the traditional $RO_2^•$ + $RO_2^•$ dominant chemistry cannot explain the observations. Moreover, the results also suggest that the previously attributed Langmuir-Hinshelwood mechanism[15] and particle-phase diffusion limitation[43] do not explain the increased γ_{eff} with reduced [•OH] under the studied conditions of [•OH] and particle D_{org}, because these processes are already explicitly considered in the kinetic model. The model performance is consistent with other models developed in previous studies which also considered these processes.[14, 44] The O_3 shielding

mechanism[18] can also be ruled out as we observed similar γ_{eff} by using H_2O_2 as the •OH precursor (**Figure 3.1**); in the absence of O_3, the same γ_{eff}–[•OH] behavior was observed. Furthermore, the previously proposed RO•-driven chain propagation reactions could only slightly enhance γ_{eff},[20] and is independent of [•OH]. Therefore, the [•OH]-dependent γ_{eff} suggests that a previously unrecognized mechanism is needed to explain the unexpectedly high γ_{eff} under low [•OH].

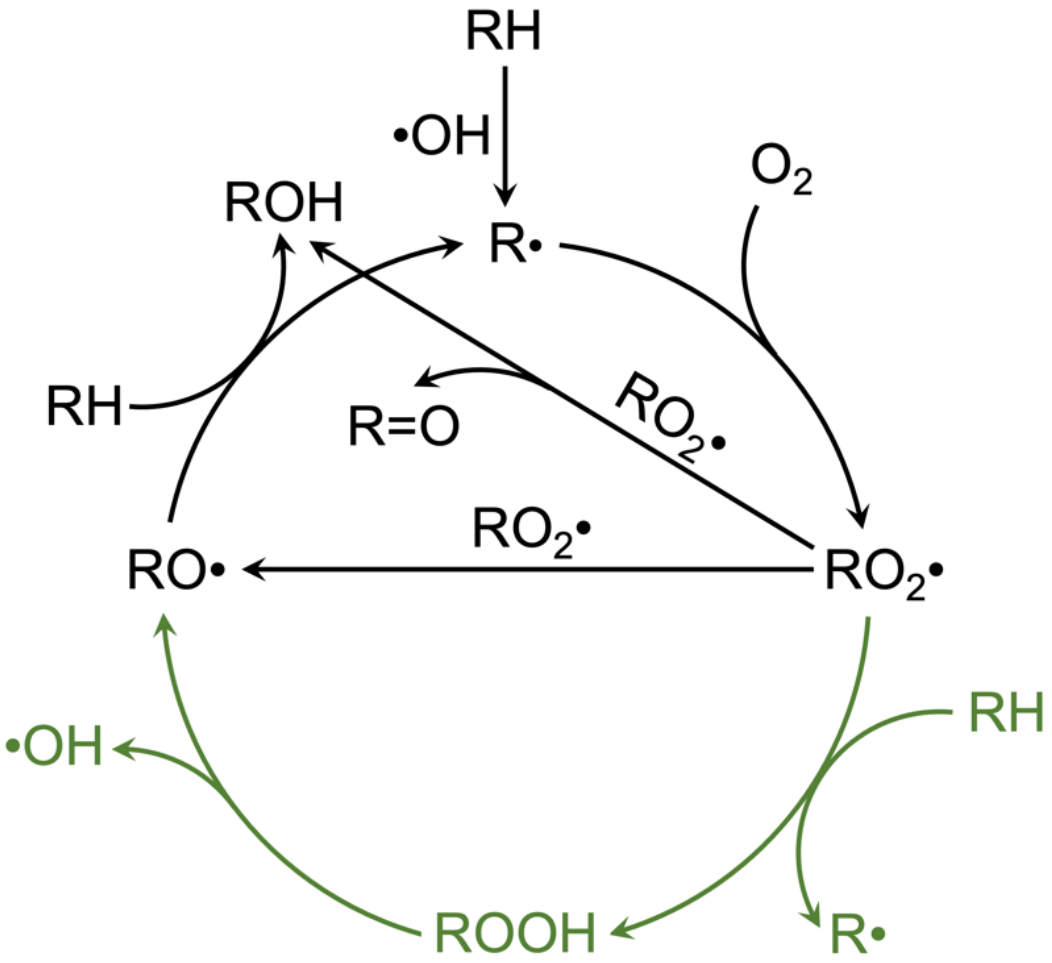

Figure 3.2 The •OH-initiated heterogeneous oxidation mechanism of organic aerosols in the atmosphere. The top part of the scheme (in black) illustrates the previous mechanistic understanding, and the bottom part (in green) shows the autoxidation mechanism proposed in this work.

3.3.2 Oxidation products highlight the formation of organic hydroperoxides

To elucidate the unrecognized mechanism, we further examined the oxidation products (**Figure 3.3**). Consistent with the above-mentioned reaction scheme, the most abundant products observed from these experiments by the TD-CIMS are R=O and ROH from the $RO_2^{\bullet}$ + $RO_2^{\bullet}$ self-reaction. Interestingly, another major product with two additional oxygens than RH ("RH+2O") was also observed in some of the studied OA systems. We determine this product to be the ROOH. Although the same chemical formula could be the second-generation products $R(OH)_2$, the absence of the other two expected concurrent second-generation products, R(=O)OH and $R(=O)_2$, ruled this out (**Figure 3.3A–B**). Additionally, the "RH+2O" signal appears almost simultaneously with the onset of $^{\bullet}$OH oxidation, while a second-generation product is usually indicated by delayed formation.[7] To further confirm its identity, the IMS-MS was used to compare the oxidation products between experiments under different [$^{\bullet}$OH] on the isomer-resolved level. In this comparison, adipic acid oxidation under very different [$^{\bullet}$OH] produced identical isomer distributions and abundances for both R=O and ROH. In contrast, "RH+2O" exhibits very different isomer distributions between the two [$^{\bullet}$OH] conditions, with a unique and dominant isomer present only under lower [$^{\bullet}$OH], providing unambiguous evidence for ROOH formation. Moreover, auxiliary total hydroperoxide analysis also supports the formation of ROOH under low [$^{\bullet}$OH] in the CFSTR. In **Figure 3.3C–D**, we present the signal-based fractions of R=O and "RH+2O" among the three major products as a function of [$^{\bullet}$OH] in the adipic acid system, where all three products were detected. The results, compared with measurements from the high-[$^{\bullet}$OH] FTR experiments, clearly show that the

formation of R=O is inhibited while "RH+2O" (mostly ROOH) is enhanced under low [$^{\bullet}$OH]. On the contrary, most of "RH+2O" detected under high [$^{\bullet}$OH] in the FTR are $R(OH)_2$. This [$^{\bullet}$OH]-dependent OA composition also explains the contradiction between this work and prior studies which reported no evidence of ROOH formation,[7, 46] as prior studies used high [$^{\bullet}$OH] to investigate OA oxidative aging. Finally, to test whether the ROOH formation is formed from the $RO_2^{\bullet}$ + $HO_2^{\bullet}$ reactions, we incorporated $HO_2^{\bullet}$ uptake and subsequent $RO_2^{\bullet}$ + $HO_2^{\bullet}$ reactions into the model using known kinetic parameters.[47, 48] However, the results suggest that this process plays a negligible role in γ_{eff} prediction and is unlikely to produce sufficient ROOH under the studied conditions. In support of this, [$^{\bullet}HO_2$] is expected to be higher with increased [$^{\bullet}$OH] and thus, ROOH formed from $RO_2^{\bullet}$ + $HO_2^{\bullet}$ should also increase with [$^{\bullet}$OH], which is opposite to the observed ROOH trend (**Figure 3.3D**). It should also be pointed out that during thermal desorption in TD-CIMS, decomposition of the products, especially ROOH, cannot be ruled out. However, thermal decomposition should not affect the ROOH trends shown in **Figure 3.3** and may indicate that the formation of ROOH through autoxidation is even more important.

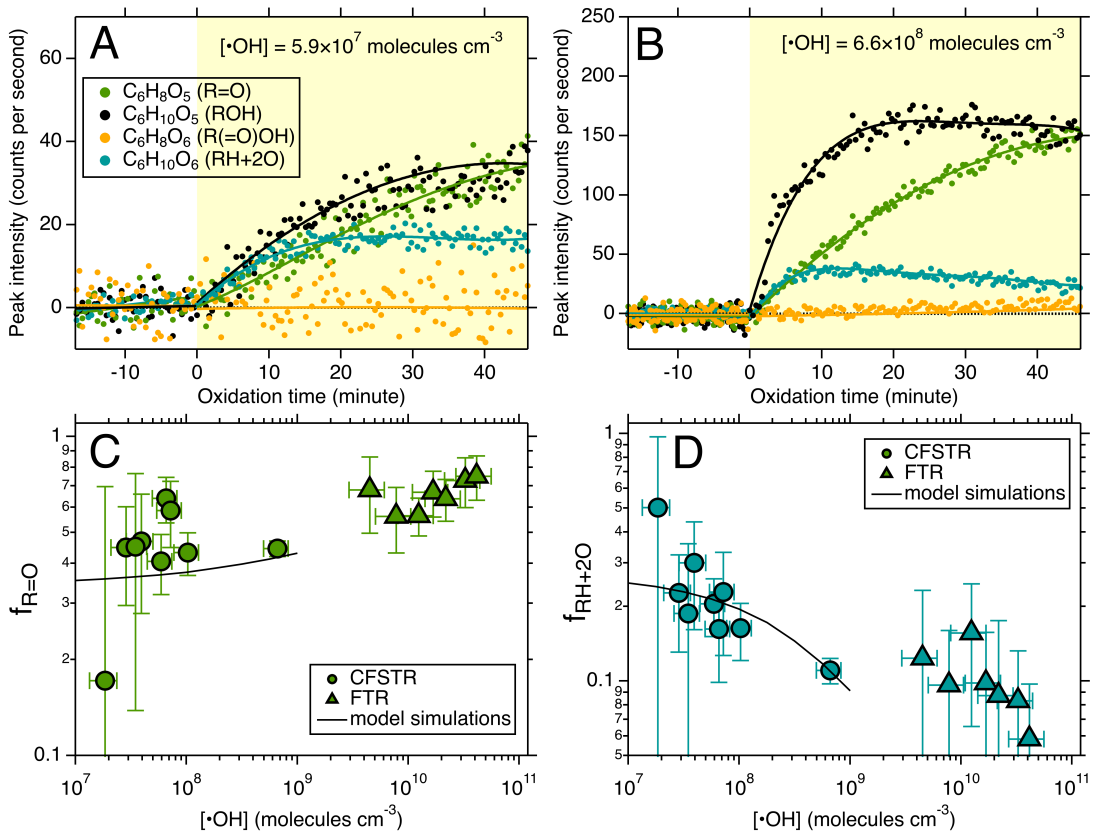

Figure 3.3 Major products from adipic acid OA oxidation. (A – B) TD-CIMS time-series of the three major first-generation products (i.e., R=O, ROH, and "RH+2O") for two adipic acids oxidation CFSTR experiments under different [•OH]. For comparison, one of the second-generation products (R(=O)OH) is shown. The other second-generation product, $R(=O)_2$, is also absent as R(=O)OH and hence is not shown. The light-yellow shades suggest the oxidation periods; the fitted curves are to guide the eye. (C – D) The fractions of R=O and "RH+2O" in the first-generation products from adipic acid oxidation experiments. The error bars represent the measurement standard deviation, and the curves are model results. The model simulations with autooxidation show consistent trends with the measurements.

3.3.3 Autoxidation as the key aging mechanism

Through relating the enhancement of both γ_{eff} and ROOH formation under low [$^{\bullet}$OH], we propose a chain reaction mechanism between $RO_2^{\bullet}$ and RH, leading to the formation of ROOH and regenerating $RO_2^{\bullet}$ in the presence of O_2 (**Figure 3.2**, bottom part). The formed ROOH may decompose into $RO^{\bullet}$ and $^{\bullet}$OH, both of which could abstract H from RH in the condensed phase. This $RO_2^{\bullet}$-mediated mechanism thus sustains the other chain reaction ($RO^{\bullet}$ + RH) and creates additional secondary pathways to consume RH, further increasing γ_{eff}. Under high [$^{\bullet}$OH], the large $^{\bullet}$OH flux at the particle surface leads to the substantial formation of $RO_2^{\bullet}$, thus favoring the $RO_2^{\bullet}$ + $RO_2^{\bullet}$ self-reaction. With lower [$^{\bullet}$OH], the interfacial and particle-phase [$RO_2^{\bullet}$] also decreases, allowing for the competing $RO_2^{\bullet}$ + RH reaction to become nonnegligible. This mechanism has been known for decades in biochemistry and polymer chemistry for lipids and rubbers (also known as "autoxidation"),[49-51] but for the first time here, this mechanism is reported in aerosol chemistry. More importantly, we demonstrate that the autoxidation mechanism exhibits a unique [$^{\bullet}$OH]-dependent behavior in aerosol chemistry, suggesting that the OA heterogeneous oxidation results obtained in the past decades may not accurately describe the processes occurring in the real atmosphere.

Following the proposal of the autoxidation mechanism, we implemented it into the kinetic model to aid the interpretation of the experimental results. The $RO_2^{\bullet}$ + RH reaction rate constant is estimated to be on the order of 10^{-6} times slower than that for $RO^{\bullet}$ + RH.[52] The ROOH decomposition rate may vary significantly, likely owing to the stability and

reactivity of the ROOH. Although some studies showed that ROOH can be stable in room temperature for as long as 24 hours,[53, 54] ROOH in atmospheric OA were more often found to be rather labile, especially for the highly functionalized molecules, with first-order decomposition rate ranging from 3×10^{-5} s^{-1} to $\sim 2 \times 10^{-3}$ s^{-1}.[55-58] Further, little in known regarding the detailed ROOH decomposition mechanism and products. Unimolecular decomposition via breaking the weak O–O bond to form $RO^{\bullet}$ and $^{\bullet}OH$ was suggested as a possible reaction at ambient temperature for peroxides with O/C ratios at 0.5 or higher.[55] In addition, bimolecular reactions were also suggested, such as the Baeyer-Villiger reaction and Korcek mechanism.[56, 59] But these bimolecular mechanisms do not directly produce free radicals, hence cannot propagate the chain reactions shown in **Figure 3.2**. The lack of detailed kinetic and mechanistic understanding leads to great challenges to explicitly incorporate the ROOH chemistry into the kinetic model. Therefore, we lumped the possible ROOH unimolecular[55] and bimolecular[56] decomposition pathways as a single pseudo first-order decomposition reaction forming $RO^{\bullet}$ + $^{\bullet}OH$ with tunable yield.

Despite the simplification, this model reasonably reflects the chain propagating nature of the autoxidation mechanism. To capture the observed γ_{eff} – [$^{\bullet}OH$] relationship over the entire studied [$^{\bullet}OH$] range, the model needs to constrain the formation rate of $RO^{\bullet}$ + $^{\bullet}OH$ from ROOH decomposition at $1 \times 10^{-5} – 1 \times 10^{-4}$ s^{-1}, while keeping the $RO_2^{\bullet}$ + RH reaction rate constant in a reasonable range (i.e., $5 – 20 \times 10^{-21}$ cm^3 $molecules^{-1}$ s^{-1}) for all the studied OA systems. Here, the formation rate of $RO^{\bullet}$ + $^{\bullet}OH$ is a combination of ROOH decomposition rate and the branching ratio of $RO^{\bullet}$ + $^{\bullet}OH$. For example, if all the ROOH decomposition forms $RO^{\bullet}$ + $^{\bullet}OH$, the decomposition rate is the same as the formation rate

of $RO^{\bullet}$ + $^{\bullet}OH$; while if only 10% of ROOH decomposes to $RO^{\bullet}$ + $^{\bullet}OH$, the overall ROOH decomposition rate needs to be approximately one order of magnitude higher, which is still within the range of previously reported ROOH decomposition rate constant mentioned above.[55-58] Model simulations of the γ_{eff} – [$^{\bullet}OH$] relationship using the autoxidation mechanism agree nicely with the measurements (**Figure 3.1**), suggesting that autoxidation in the condensed phase can indeed greatly accelerate OA aging under atmospherically relevant [$^{\bullet}OH$]. It should be noted that the good model-observation agreement does not require a certain unique set of parameters. Rather, with any formation rate of $RO^{\bullet}$ + $^{\bullet}OH$ in the above-mentioned range, a coupled $RO_2^{\bullet}$ + RH reaction rate constant can be determined to result in a similarly good agreement as shown in **Figure 3.1**. Furthermore, it is remarkable that the model results also agree with the trends of [$^{\bullet}OH$]-dependent fractions of R=O and "RH+2O" (**Figure 3.3C–D**), further supporting the autoxidation mechanism. Lastly, to test whether other radical-involved chemical processes might affect or contribute to the enhanced OA degradation, unimolecular H-shift isomerization for $RO_2^{\bullet}$ and $RO^{\bullet}$ were considered in the kinetic model. This unimolecular process has been shown to play important roles in the gas phase,[60-62] but our model simulations suggest that they are not fast enough at typical reaction rate constants to compete with the bimolecular autoxidation mechanism and play a very minor role in OA aging kinetics.

The kinetic model further suggests that autoxidation-involved reactions (i.e., RH + $RO_2^{\bullet}$, RH + $RO^{\bullet}$, and RH + $^{\bullet}OH$ from ROOH decomposition) could account for > 95% of total RH consumption under atmospheric [$^{\bullet}OH$]. This means that the collision of gas-phase

•OH with OA particles plays more of an initiator role, rather than acting as the dominant oxidant of OA under atmospheric conditions. This also implies that once the oxidation is triggered, the autoxidation may proceed even in the dark. Since most of the OA molecules are not oxidized directly by the •OH from gas-phase adsorption under low [•OH], the OA oxidation is no longer confined to the interfacial region of the particles. Consistently, model results suggest that the OA oxidation could occur throughout the entire particles under atmospherically relevant [•OH], contrary to the dominant interfacial oxidation under much higher [•OH] for all the examined OA systems. Beyond the D_{org} range for the studied OA, the simulations indicate that even for more viscous OA particle across the semi-solid and solid ranges, the OA oxidation events could still spread throughout the particles in about an hour under atmospheric [•OH]. These simulations highlight that the autoxidation mechanism leads to highly efficient OA aging by allowing the oxidation to occur in the particle bulk and bypassing diffusion limitations, hence, making the viscous particles more homogeneous during oxidation.

3.3.4 Overall aerosol composition influenced by autoxidation

Finally, we investigated how autoxidation may impact the entire OA composition. For this purpose, we focus on the 3-methylglutaric acid system which is more readily oxidized and can form diverse oxidation products.[23] The observed oxidation products ($C_{1\text{-}6}H_{2\text{-}10}O_{3\text{-}8}$) by the IMS-MS were employed to calculate the intensity-based elemental ratios, averaged carbon number (n_C), and fraction of fragmentation products in the particle phase under different oxidation conditions (**Figure 3.4**). As the Van Krevelen diagram shown in

Figure 3.4A, the FTR experiments with the highest [•OH] (> ~ 2×10^{10} molecules cm^{-3}) exhibit the steepest H/C – O/C trajectory, with a slope ~ -0.91, indicative of a mechanism that forms similar amounts of carbonyls and alcohols (consistent with the Russell mechanism). In comparison, the lower [•OH] CFSTR experiments all had shallower H/C – O/C trajectories, with slopes of -0.65 – -0.69 under [•OH] < ~ 2×10^8 molecules cm^{-3} and -0.82 under [•OH] ~ 2×10^9 molecules cm^{-3}. The slope shift as a function of [•OH] suggests that low [•OH] favors the formation of alcohols and hydroperoxides over carbonyls, consistent with the autoxidation mechanism. This mechanistic difference was also supported by comparing the major functionalization products: higher abundance of alcohols and hydroperoxides were observed in the CFSTR than the FTR and higher ratios of the "RH+2O" signals over the other two major second-generation products were found under lower [•OH]. Interestingly, the favorability of alcohol and hydroperoxide formation has been suggested as a plausible reason to explain the similarly shallow H/C – O/C relationship (slope ~ -0.6) for atmospheric OAs.[63] As expected, the low-[•OH] experiments also reached comparable carbon oxidation state with much lower •OH exposure, again owing to the highly efficient oxidation driven by autoxidation. It is also evident that under [•OH] > ~ 2×10^9 molecules cm^{-3} (in both reactors), the fraction of fragmentation products increases and n_C decreases exponentially with •OH exposure (**Figure 3.4B**), consistent with prior understanding that fragmentation is increasingly important after the functionalization products are further oxidized. However, under lower [•OH] (< ~ 2×10^8 molecules cm^{-3}), an appreciable fraction of the measured species are fragmentation products (20 – 30%,

Figure 3.4B), even with very low •OH exposure (i.e., < 10^{11} molecules cm^{-3} s). In comparison, the high-[•OH] experiments needed > 4×10^{12} molecules cm^{-3} s to reach the same fraction of fragmentation products and n_C. We suggest that this is because the enhanced autoxidation under low [•OH] promotes RO• formation through ROOH decomposition and hence increase fragmentation even with low •OH exposure. These results suggest that autoxidation could provide a new pathway to rapidly produce small, oxidized compounds which could evaporate to the gas phase and contribute to important atmospheric processes such as secondary OA formation.

Overall, the chemical composition of oxidized OAs provides observation-based support to the autoxidation mechanism and ROOH decomposition pathways. Specifically, the increased formation of alcohol and fragmentation products under lower [•OH] strongly supports the ROOH unimolecular decomposition to RO• + •OH;[55] the enhanced alcohol formation may also be partly due to the Baeyer-Villiger reactions.[59] Therefore, it is likely that both ROOH processes take place to promote autoxidation and explain the measurements.

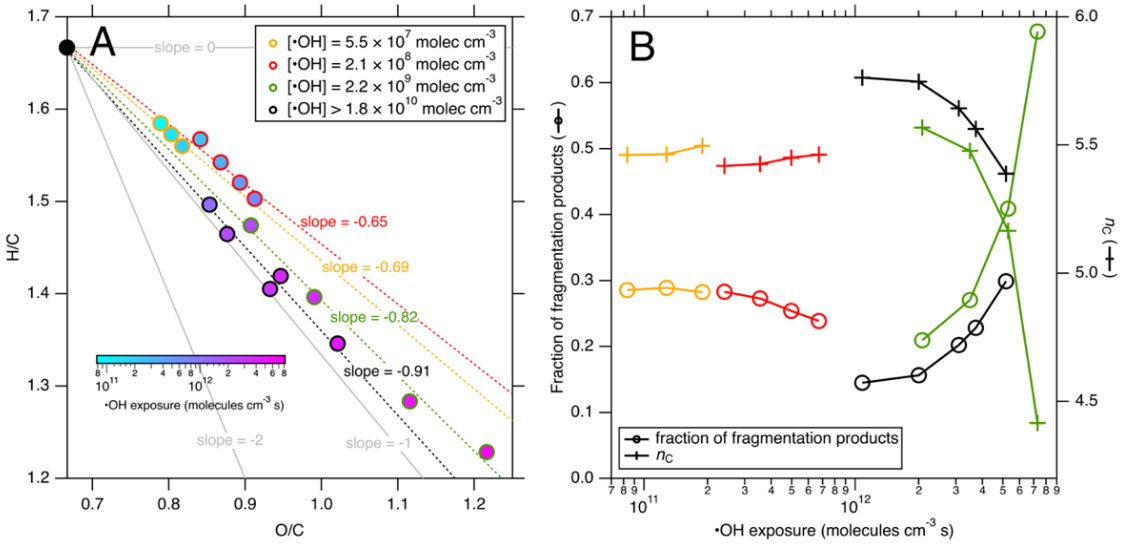

Figure 3.4 Chemical composition of oxidized 3-methylglutaric acid OAs. (A) The Van Krevelen diagram for four 3-methylglutaric acid oxidation experiments. The experiment with the highest [•OH] was performed in the FTR and the other three lower-[•OH] experiments were performed in the CFSTR. The linear fits with slopes are shown with the data; the color scale indicates the •OH exposure for each data point. (B) The fraction of fragmentation products (left axis) and n_C (right axis) as a function of •OH exposure for the same 3-methylglutaric acid oxidation experiments as in (A).

3.4 Atmospheric Implications

In this work, we report strong and direct evidence for an autoxidation mechanism in heterogeneous oxidative aging of OAs. Although only a few highly oxidized OA surrogates were examined, its nature is rather nonspecific.[50-52] We show that autoxidation may occur at much faster rates than the other particle-phase $RO_2^{\bullet}$ pathways (e.g., $RO_2^{\bullet}$ reactions with $RO_2^{\bullet}$ and $HO_2^{\bullet}$) and significantly boost OA oxidation under atmospherically relevant [$^{\bullet}$OH]. Through autoxidation, OA oxidative aging in the atmosphere may proceed on timescales from less than a day to several days, much more rapidly than prior laboratory results have suggested. This result opens up new avenues for heterogeneous OA oxidation to play key roles in various atmospheric processes. Although the laboratory studies showed clear evidence for enhanced OA aging kinetics and the formation of ROOH, ROH, and fragmentation products, the autoxidation-involved kinetic parameters have large uncertainties. This is mainly caused by: (1) the RH + $RO_2^{\bullet}$ reaction kinetics have been less studied for system relevant to atmospheric OA species;[52] and (2) the ROOH decomposition rate constant and mechanism are largely varied with chemical structures.[55-58] Therefore, the corresponding kinetic model is constrained within the wide ranges of reported values to our best knowledge. Thus, future studies are needed to help better determine the key parameters for more accurate prediction of multiphase OA aging kinetics.

In the atmosphere, many OA processes could occur simultaneous with aging (e.g., secondary aerosol formation, new particle formation and growth, aqueous-phase reactions, evaporation, etc.); thus, direct field evidence to support such rapid OA oxidation is unavailable. However, the autoxidation-mediated fast OA aging reported in this work

should be considered in the interpretation of field measurements. Another surprising outcome of our findings is that the gas-phase •OH is only an initiator of OA aging, rather than the main oxidant, implying that OA oxidative aging may efficiently take place even under dark conditions (e.g., nighttime or in indoor environments). Additionally, substantial ROOH may be present in the oxidized OA particles as reactive oxygen species, which are well known to result in health effects.[64] We also suggest that autoxidation can lead to OA oxidation throughout the entire aerosol particle even for highly viscous OA, rather than confined at the gas-particle interface, as previously understood. Lastly, we show that autoxidation may have an extending influence on the entire OA particle composition during oxidative aging. It will increase the oxygenation of OA efficiently and facilitate fragmentation chemistry. The rapid and enhanced oxygenation of aerosol particles through this mechanism may result in increased cloud formation potential than previously predicted, leading to larger indirect climate effects. Overall, the autoxidation mechanism reported here unveils the nature of heterogeneous aerosol oxidation chemistry and highlights the need to rethink aerosol aging processes in the real atmosphere.

3.5 References

(1) Zhang, Q.; Jimenez, J. L.; Canagaratna, M. R.; Allan, J. D.; Coe, H.; Ulbrich, I.; Alfarra, M. R.; Takami, A.; Middlebrook, A. M.; Sun, Y. L.; Dzepina, K.; et al. Ubiquity and dominance of oxygenated species in organic aerosols in anthropogenically-influenced Northern Hemisphere midlatitudes. *Geophys. Res. Lett.* **2007,** *34*, L13801.

(2) Jimenez, J. L.; Canagaratna, M. R.; Donahue, N. M.; Prevot, A. S. H.; Zhang, Q.; Kroll, J. H.; DeCarlo, P. F.; Allan, J. D.; Coe, H.; Ng, N. L.; et al. Evolution of Organic Aerosols in the Atmosphere. *Science* **2009**, *326* (5959), 1525-1529.

(3) Boucher, O.; Randall, D.; Artaxo, P.; Bretherton, C.; Feingold, C.; Forster, P.; Kerminen, V.-M.; Kondo, Y.; Liao, H.; Lohmann, U.; Rasch, P.; Satheesh, S. K.; Sherwood, S.; Stevens, B.; Zhang, X.-Y. *Clouds and Aerosols*; IPCC: 2013; p 657.

(4) Dockery, D. W.; Pope, C. A.; Xu, X.; Spengler, J. D.; Ware, J. H.; Fay, M. E.; Ferris, B. G.; Speizer, F. E., An Association between Air Pollution and Mortality in Six U.S. Cities. *N. Engl. J. Med.* **1993,** *329* (24), 1753-1759.

(5) George, I. J.; Abbatt, J. P. D., Heterogeneous oxidation of atmospheric aerosol particles by gas-phase radicals. *Nat. Chem.* **2010,** *2* (9), 713-722.

(6) George, I. J.; Vlasenko, A.; Slowik, J. G.; Broekhuizen, K.; Abbatt, J. P. D., Heterogeneous oxidation of saturated organic aerosols by hydroxyl radicals: uptake kinetics, condensed-phase products, and particle size change. *Atmos. Chem. Phys.* **2007,** *7* (16), 4187-4201.

(7) Smith, J. D.; Kroll, J. H.; Cappa, C. D.; Che, D. L.; Liu, C. L.; Ahmed, M.; Leone, S. R.; Worsnop, D. R.; Wilson, K. R., The heterogeneous reaction of hydroxyl radicals with sub-micron squalane particles: a model system for understanding the oxidative aging of ambient aerosols. *Atmos. Chem. Phys.* **2009,** *9* (9), 3209-3222.

(8) George, I. J.; Abbatt, J. P. D., Chemical evolution of secondary organic aerosol from OH-initiated heterogeneous oxidation. *Atmos. Chem. Phys.* **2010,** *10* (12), 5551-5563.

(9) Kroll, J. H.; Lim, C. Y.; Kessler, S. H.; Wilson, K. R., Heterogeneous Oxidation of Atmospheric Organic Aerosol: Kinetics of Changes to the Amount and Oxidation State of Particle-Phase Organic Carbon. *J. Phys. Chem. A* **2015,** *119* (44), 10767-10783.

(10) Kessler, S. H.; Nah, T.; Daumit, K. E.; Smith, J. D.; Leone, S. R.; Kolb, C. E.; Worsnop, D. R.; Wilson, K. R.; Kroll, J. H., OH-Initiated Heterogeneous Aging of Highly Oxidized Organic Aerosol. *J. Phys. Chem. A* **2012,** *116* (24), 6358-6365.

(11) Davies, J. F.; Wilson, K. R., Nanoscale interfacial gradients formed by the reactive uptake of OH radicals onto viscous aerosol surfaces. *Chem. Sci.* **2015,** *6* (12), 7020-7027.

(12) Hearn, J. D.; Renbaum, L. H.; Wang, X.; Smith, G. D., Kinetics and products from reaction of Cl radicals with dioctyl sebacate (DOS) particles in O2: a model for radical-initiated oxidation of organic aerosols. *Phys. Chem. Chem. Phys.* **2007,** *9* (34), 4803-4813.

(13) Chan, M. N.; Zhang, H.; Goldstein, A. H.; Wilson, K. R., Role of Water and Phase in the Heterogeneous Oxidation of Solid and Aqueous Succinic Acid Aerosol by Hydroxyl Radicals. *J. Phys. Chem. C* **2014,** *118* (50), 28978-28992.

(14) Arangio, A. M.; Slade, J. H.; Berkemeier, T.; Pöschl, U.; Knopf, D. A.; Shiraiwa, M., Multiphase Chemical Kinetics of OH Radical Uptake by Molecular Organic Markers of Biomass Burning Aerosols: Humidity and Temperature Dependence, Surface Reaction, and Bulk Diffusion. *J. Phys. Chem. A* **2015,** *119* (19), 4533-4544.

(15) Slade, J. H.; Knopf, D. A., Heterogeneous OH oxidation of biomass burning organic aerosol surrogate compounds: assessment of volatilisation products and the role of OH concentration on the reactive uptake kinetics. *Phys. Chem. Chem. Phys.* **2013,** *15* (16), 5898-5915.

(16) Kristiansen, N. I.; Stohl, A.; Olivié, D. J. L.; Croft, B.; Søvde, O. A.; Klein, H.; Christoudias, T.; Kunkel, D.; Leadbetter, S. J.; Lee, Y. H.; et al. Evaluation of observed and modelled aerosol lifetimes using radioactive tracers of opportunity and an ensemble of 19 global models. *Atmos. Chem. Phys.* **2016,** *16* (5), 3525-3561.

(17) Zhang, H.; Ruehl, C. R.; Chan, A. W. H.; Nah, T.; Worton, D. R.; Isaacman, G.; Goldstein, A. H.; Wilson, K. R., OH-initiated heterogeneous oxidation of cholestane: A model system for understanding the photochemical aging of cyclic alkane aerosols. *J. Phys. Chem. A* **2013,** *117* (47), 12449-12458.

(18) Renbaum, L. H.; Smith, G. D., Artifacts in measuring aerosol uptake kinetics: the roles of time, concentration and adsorption. *Atmos. Chem. Phys.* **2011,** *11* (14), 6881-6893.

(19) Che, D. L.; Smith, J. D.; Leone, S. R.; Ahmed, M.; Wilson, K. R., Quantifying the reactive uptake of OH by organic aerosols in a continuous flow stirred tank reactor. *PCCP, Phys. chem. chem. phys.* **2009,** *11* (36), 7885-7895.

(20) Richards-Henderson, N. K.; Goldstein, A. H.; Wilson, K. R., Large Enhancement in the Heterogeneous Oxidation Rate of Organic Aerosols by Hydroxyl Radicals in the Presence of Nitric Oxide. *J. Phys. Chem. Lett.* **2015,** *6* (22), 4451-4455.

(21) Richards-Henderson, N. K.; Goldstein, A. H.; Wilson, K. R., Sulfur Dioxide Accelerates the Heterogeneous Oxidation Rate of Organic Aerosol by Hydroxyl Radicals. *Environ. Sci. Technol.* **2016,** *50* (7), 3554-3561.

(22) Zeng, M.; Heine, N.; Wilson, K. R., Evidence that Criegee intermediates drive autoxidation in unsaturated lipids. *Proc. Natl. Acad. Sci. U.S.A.* **2020,** *117* (9), 4486-4490.

(23) Zhao, Z.; Yang, X.; Lee, J.; Tolentino, R.; Mayorga, R.; Zhang, W.; Zhang, H., Diverse Reactions in Highly Functionalized Organic Aerosols during Thermal Desorption. *ACS Earth Space Chem.* **2020,** *4* (2), 283-296.

(24) Virtanen, A.; Joutsensaari, J.; Koop, T.; Kannosto, J.; Yli-Pirilä, P.; Leskinen, J.; Mäkelä, J. M.; Holopainen, J. K.; Pöschl, U.; Kulmala, M.; Worsnop, D. R.; Laaksonen, A., An amorphous solid state of biogenic secondary organic aerosol particles. *Nature* **2010,** *467* (7317), 824-827.

(25) Shiraiwa, M.; Li, Y.; Tsimpidi, A. P.; Karydis, V. A.; Berkemeier, T.; Pandis, S. N.; Lelieveld, J.; Koop, T.; Pöschl, U., Global distribution of particle phase state in atmospheric secondary organic aerosols. *Nat. Commun.* **2017,** *8* (1), 15002.

(26) Zhao, Z.; Tolentino, R.; Lee, J.; Vuong, A.; Yang, X.; Zhang, H., Interfacial Dimerization by Organic Radical Reactions during Heterogeneous Oxidative Aging of Oxygenated Organic Aerosols. *J. Phys. Chem. A* **2019,** *123* (50), 10782-10792.

(27) Zhao, Z.; Xu, Q.; Yang, X.; Zhang, H., Heterogeneous Ozonolysis of Endocyclic Unsaturated Organic Aerosol Proxies: Implications for Criegee Intermediate Dynamics and Later-Generation Reactions. *ACS Earth Space Chem.* **2019,** *3* (3), 344-356.

(28) Zhao, Z.; Le, C.; Xu, Q.; Peng, W.; Jiang, H.; Lin, Y.-H.; Cocker, D. R.; Zhang, H., Compositional Evolution of Secondary Organic Aerosol as Temperature and Relative Humidity Cycle in Atmospherically Relevant Ranges. *ACS Earth Space Chem.* **2019,** *3* (11), 2549-2558.

(29) Zhao, Z.; Mayorga, R.; Lee, J.; Yang, X.; Tolentino, R.; Zhang, W.; Vuong, A.; Zhang, H., Site-Specific Mechanisms in OH-Initiated Organic Aerosol Heterogeneous Oxidation Revealed by Isomer-Resolved Molecular Characterization. *ACS Earth Space Chem.* **2020,** *4* (5), 783-794.

(30) Zhao, Z.; Zhang, W.; Alexander, T.; Zhang, X.; Martin, D. B. C.; Zhang, H., Isolating α-Pinene Ozonolysis Pathways Reveals New Insights into Peroxy Radical Chemistry and Secondary Organic Aerosol Formation. *Environ. Sci. Technol.* **2021,** *55* (10), 6700-6709.

(31) Mayorga, R. J.; Zhao, Z.; Zhang, H., Formation of secondary organic aerosol from nitrate radical oxidation of phenolic VOCs: Implications for nitration mechanisms and brown carbon formation. *Atmos. Environ.* **2021,** *244*, 117910.

(32) Price, H. C.; Murray, B. J.; Mattsson, J.; O'Sullivan, D.; Wilson, T. W.; Baustian, K. J.; Benning, L. G., Quantifying water diffusion in high-viscosity and glassy aqueous solutions using a Raman isotope tracer method. *Atmos. Chem. Phys.* **2014,** *14* (8), 3817-3830.

(33) Song, Y. C.; Haddrell, A. E.; Bzdek, B. R.; Reid, J. P.; Bannan, T.; Topping, D. O.; Percival, C.; Cai, C., Measurements and Predictions of Binary Component Aerosol Particle Viscosity. *J. Phys. Chem. A* **2016,** *120* (41), 8123-8137.

(34) Yuan, B.; Koss, A. R.; Warneke, C.; Coggon, M.; Sekimoto, K.; de Gouw, J. A., Proton-Transfer-Reaction Mass Spectrometry: Applications in Atmospheric Sciences. *Chem. Rev.* **2017,** *117* (21), 13187-13229.

(35) Zhang, X.; Krechmer, J. E.; Groessl, M.; Xu, W.; Graf, S.; Cubison, M.; Jayne, J. T.; Jimenez, J. L.; Worsnop, D. R.; Canagaratna, M. R., A novel framework for molecular characterization of atmospherically relevant organic compounds based on collision cross section and mass-to-charge ratio. *Atmos. Chem. Phys.* **2016,** *16* (20), 12945-12959.

(36) Krechmer, J. E.; Groessl, M.; Zhang, X.; Junninen, H.; Massoli, P.; Lambe, A. T.; Kimmel, J. R.; Cubison, M. J.; Graf, S.; Lin, Y. H.; et al. Ion mobility spectrometry–mass spectrometry (IMS–MS) for on- and offline analysis of atmospheric gas and aerosol species. *Atmos. Meas. Tech.* **2016,** *9* (7), 3245-3262.

(37) Butkovskaya, N. I.; Kukui, A.; Pouvesle, N.; Le Bras, G., Rate Constant and Mechanism of the Reaction of OH Radicals with Acetic Acid in the Temperature Range of 229−300 K. *J. Phys. Chem. A* **2004,** *108* (34), 7021-7026.

(38) Singleton, D. L.; Paraskevopoulos, G.; Irwin, R. S., Rates and mechanism of the reactions of hydroxyl radicals with acetic, deuterated acetic, and propionic acids in the gas phase. *J. Am. Chem. Soc.* **1989,** *111* (14), 5248-5251.

(39) Houle, F. A.; Hinsberg, W. D.; Wilson, K. R., Oxidation of a model alkane aerosol by OH radical: the emergent nature of reactive uptake. *Phys. Chem. Chem. Phys.* **2015,** *17* (6), 4412-4423.

(40) Shiraiwa, M.; Pfrang, C.; Koop, T.; Pöschl, U., Kinetic multi-layer model of gas-particle interactions in aerosols and clouds (KM-GAP): linking condensation, evaporation and chemical reactions of organics, oxidants and water. *Atmos. Chem. Phys.* **2012,** *12* (5), 2777-2794.

(41) Wiegel, A. A.; Liu, M. J.; Hinsberg, W. D.; Wilson, K. R.; Houle, F. A., Diffusive confinement of free radical intermediates in the OH radical oxidation of semisolid aerosols. *Phys. Chem. Chem. Phys.* **2017,** *19* (9), 6814-6830.

(42) Slade, J. H.; Knopf, D. A., Multiphase OH oxidation kinetics of organic aerosol: The role of particle phase state and relative humidity. *Geophys. Res. Lett.* **2014,** *41* (14), 5297-5306.

(43) Chim, M. M.; Lim, C. Y.; Kroll, J. H.; Chan, M. N., Evolution in the Reactivity of Citric Acid toward Heterogeneous Oxidation by Gas-Phase OH Radicals. *ACS Earth Space Chem.* **2018,** *2* (12), 1323-1329.

(44) Houle, F. A.; Wiegel, A. A.; Wilson, K. R., Changes in Reactivity as Chemistry Becomes Confined to an Interface. The Case of Free Radical Oxidation of C30H62 Alkane by OH. *J. Phys. Chem. Lett.* **2018,** *9* (5), 1053-1057.

(45) Russell, G. A., Deuterium-isotope Effects in the Autoxidation of Aralkyl Hydrocarbons. Mechanism of the Interaction of PEroxy Radicals1. *J. Am. Chem. Soc.* **1957,** *79* (14), 3871-3877.

(46) McNeill, V. F.; Yatavelli, R. L. N.; Thornton, J. A.; Stipe, C. B.; Landgrebe, O., Heterogeneous OH oxidation of palmitic acid in single component and internally mixed aerosol particles: vaporization and the role of particle phase. *Atmos. Chem. Phys.* **2008,** *8* (17), 5465-5476.

(47) Lakey, P. S. J.; George, I. J.; Whalley, L. K.; Baeza-Romero, M. T.; Heard, D. E., Measurements of the HO2 Uptake Coefficients onto Single Component Organic Aerosols. *Environ. Sci. Technol.* **2015,** *49* (8), 4878-4885.

(48) Liu, M. J.; Wiegel, A. A.; Wilson, K. R.; Houle, F. A., Aerosol Fragmentation Driven by Coupling of Acid–Base and Free-Radical Chemistry in the Heterogeneous Oxidation of Aqueous Citric Acid by OH Radicals. *J. Phys. Chem. A* **2017,** *121* (31), 5856-5870.

(49) Smith, L. M.; Aitken, H. M.; Coote, M. L., The Fate of the Peroxyl Radical in Autoxidation: How Does Polymer Degradation Really Occur? *Acc. Chem. Res.* **2018,** *51* (9), 2006-2013.

(50) Foret, M. K.; Lincoln, R.; Do Carmo, S.; Cuello, A. C.; Cosa, G., Connecting the "Dots": From Free Radical Lipid Autoxidation to Cell Pathology and Disease. *Chem. Rev.* **2020,** *120* (23), 12757-12787.

(51) Helberg, J.; Pratt, D. A., Autoxidation vs. antioxidants – the fight for forever. *Chem. Soc. Rev.* **2021,** *50* (13), 7343-7358.

(52) Denisov, E.; Afanas'ev, I., *Oxidation and Antioxidants in Organic Chemistry and Biology*. 2005; p 1-981.

(53) Bakker-Arkema, J. G.; Ziemann, P. J., Measurements of Kinetics and Equilibria for the Condensed Phase Reactions of Hydroperoxides with Carbonyls to Form Peroxyhemiacetals. *ACS Earth Space Chem.* **2020,** *4* (3), 467-475.

(54) Maben, H. K.; Ziemann, P. J., Kinetics of oligomer-forming reactions involving the major functional groups present in atmospheric secondary organic aerosol particles. *Environmental Science: Processes & Impacts* **2022**.

(55) Krapf, M.; El Haddad, I.; Bruns, Emily A.; Molteni, U.; Daellenbach, Kaspar R.; Prévôt, André S. H.; Baltensperger, U.; Dommen, J., Labile Peroxides in Secondary Organic Aerosol. *Chem* **2016,** *1* (4), 603-616.

(56) Pospisilova, V.; Lopez-Hilfiker, F. D.; Bell, D. M.; El Haddad, I.; Mohr, C.; Huang, W.; Heikkinen, L.; Xiao, M.; Dommen, J.; Prevot, A. S. H.; et al. On the fate of oxygenated organic molecules in atmospheric aerosol particles. *Sci. Adv.* **2020,** *6* (11), eaax8922.

(57) Mertes, P.; Pfaffenberger, L.; Dommen, J.; Kalberer, M.; Baltensperger, U., Development of a sensitive long path absorption photometer to quantify peroxides in aerosol particles (Peroxide-LOPAP). *Atmos. Meas. Tech.* **2012,** *5* (10), 2339-2348.

(58) Pagonis, D.; Ziemann, P. J., Chemistry of hydroperoxycarbonyls in secondary organic aerosol. *Aerosol Sci. Technol.* **2018,** *52* (10), 1178-1193.

(59) Claflin, M. S.; Krechmer, J. E.; Hu, W.; Jimenez, J. L.; Ziemann, P. J., Functional Group Composition of Secondary Organic Aerosol Formed from Ozonolysis of α-Pinene Under High VOC and Autoxidation Conditions. *ACS Earth Space Chem.* **2018,** *2* (11), 1196–1210.

(60) Crounse, J. D.; Nielsen, L. B.; Jørgensen, S.; Kjaergaard, H. G.; Wennberg, P. O., Autoxidation of organic compounds in the atmosphere. *J. Phys. Chem. Lett.* **2013,** *4* (20), 3513-3520.

(61) Ehn, M.; Thornton, J. A.; Kleist, E.; Sipila, M.; Junninen, H.; Pullinen, I.; Springer, M.; Rubach, F.; Tillmann, R.; Lee, B.; et al. A large source of low-volatility secondary organic aerosol. *Nature* **2014,** *506* (7489), 476-479.

(62) Atkinson, R., Atmospheric reactions of alkoxy and β-hydroxyalkoxy radicals. *Int. J. Chem. Kinet.* **1997,** *29* (2), 99-111.

(63) Chen, Q.; Heald, C. L.; Jimenez, J. L.; Canagaratna, M. R.; Zhang, Q.; He, L.-Y.; Huang, X.-F.; Campuzano-Jost, P.; Palm, B. B.; Poulain, L.; et al. Elemental composition of organic aerosol: The gap between ambient and laboratory measurements. *Geophys. Res. Lett.* **2015,** *42*, 4182-4189.

(64) Pöschl, U.; Shiraiwa, M., Multiphase Chemistry at the Atmosphere–Biosphere Interface Influencing Climate and Public Health in the Anthropocene. *Chem. Rev.* **2015,** 115 (10), 4440-4475.

Chapter 4 Role of Hydroperoxyl Radicals in Heterogeneous Oxidation of Oxygenated Organic Aerosols

4.1 Introduction

OAs account for a large fraction of fine particulate matter ($PM_{2.5}$) in the atmosphere, significantly impacting climate, visibility and human health.[1-3] Throughout their lifetime, OA particles undergo heterogeneous oxidative aging by gaseous oxidants, such as $^{\bullet}OH$, which continuously affect their reactivity, chemical composition, and properties.[4-6] $HO_2^{\bullet}$ closely coupled with $^{\bullet}OH$, are another important gas-phase reactive oxidants in the atmosphere and are primarily generated by daytime photochemical reactions.[7-9] The typical tropospheric $[HO_2^{\bullet}]/[^{\bullet}OH]$ ratios are approximately within the range of 10–100, with $[HO_2^{\bullet}]$ up to the order of 10^8 molecules cm^{-3}.[10-13]

The oxidation mechanism and related kinetics of $HO_x^{\bullet}$ ($\equiv HO_2^{\bullet} + {}^{\bullet}OH$) reactions are well-studied in the gas phase.[14-17] $^{\bullet}OH$ initiates the oxidation of a generic gas-phase organic molecule (R–H) by H abstraction to produce an alkyl radical ($R^{\bullet}$), and a subsequent peroxy radical ($RO_2^{\bullet}$) is formed after molecular oxygen addition. In the absence of nitrogen oxides, the $RO_2^{\bullet}$ primarily undergo bimolecular reactions with $HO_2^{\bullet}$ to form organic hydroperoxides (ROOH) and with another $RO_2^{\bullet}$ to produce an alcohol-carbonyl pair (i.e., ROH and R=O), wherein both pathways could also form $RO^{\bullet}$ with varied branching ratios depending on the $RO_2^{\bullet}$ structure.[18-23] The labile hydroperoxide functionality in ROOH has a significant impact on the subsequent organic degradation and evolution in both the gas and particle phases.[19, 24-26] In strong contrast to this well-known gas-phase $HO_2^{\bullet}$ chemistry,

the mechanistic understanding of the multiphase $HO_2^•$ processes is very limited despite that kinetic observations of $HO_2^•$ uptake on the interface of aerosol particles have been widely reported, especially for aqueous aerosols.[27-32] For example, Lakey et al.[29] reported $HO_2^•$ uptake onto aerosol particles with the uptake coefficient from < 0.004 (dry particles) to ~0.09 (aqueous particles) in laboratory studies; Copper et al.[27] and Zhou et al.[31] observed $HO_2^•$ uptake onto ambient aerosols with the uptake coefficient of 0.025 – 0.24. George and Abbatt[6] summarized the heterogeneous $^•OH$ oxidation mechanisms of OAs in analogy to the gas-phase oxidation and proposed that the $RO_2^• + HO_2^•$ reactions proceed in a similar manner leading to ROOH formation. But to our knowledge, no prior work has reported the direct observation of this pathway. For instance, previous studies have attempted to indirectly probe ROOH formation by including the reaction mechanism in a kinetic model[23] or estimating the number of oxygen atoms added per reacted parent OAs.[33] But conclusive evidence for ROOH formation in heterogeneous oxidation was not provided due to the challenges in directly detecting ROOH. Furthermore, it is unclear how gaseous $HO_2^•$ affects heterogeneous OA oxidation kinetics and molecular composition by regulating $RO^•$ formation and hence secondary chain propagation chemistry.[6, 23, 34] Lastly, it is also elusive whether the $RO_2^• + HO_2^•$ reactions (if any) occur at the particle interface following collisions or in the bulk by the absorption mechanism.[29]

In the study, we perform $^•OH$-initiated heterogeneous oxidation experiments of several oxygenated OA model systems under varied [$^•OH$] and [$HO_2^•$] with controlled [$HO_2^•$]/[$^•OH$] ratios. These OA model surrogates contain multiple functional groups with

a wide range of O/C ratios of 0.40 – 1.00, representing moderately to highly oxidized OAs in the atmosphere. We characterize the molecular composition of the heterogeneously oxidized OAs by a suite of mass spectrometry instrumentation.[5, 35-37] From these measurements, we report direct observation of ROOH formation and propose the $^{\bullet}$OH-initiated heterogeneous OA oxidation mechanisms under atmospherically relevant $[HO_2^{\bullet}]/[^{\bullet}OH]$ ratios.

4.2 Materials and Methods

4.2.1 Chemicals and reagents

The chemicals and reagents with their purities and suppliers used in this study are as follows: 3-methylglutaric acid (TCI, >99.0%), adipic acid (Sigma-Aldrich, ≥99.5%), glucose (TCI, >98%), tricarballylic acid (Acros Organics, 99%), 1, 2, 3, 4-butanetetracarboxylic acid (Acros Organics, >99%), camphoric acid (Sigma-Aldrich, 99%), 1, 3, 5-cyclohexanetricarboxylic acid (Sigma-Aldrich, cis 90%), suberic acid (TCI, >99%), xylitol (Acros Organics, >99%), methanol (Fisher Chemical, 99.9%), hydrogen peroxide (H_2O_2, Fisher Chemical, 30% aq. soln.), water (Fisher Chemical, HPLC Grade Submicron Filtered), deuterium oxide (thermo scientific, 99.8 atom % D), toluene (Certified ACS, 99.9%), pyridine (DriSolv., 99.8%), BSTFA W/1% TMCS (Restek Corporation), acetonitrile (Fisher Chemical, 99.95%), tartaric acid (TCI, >99.0%) and isoprene (Alfa Aesar, 99%). None of the above chemicals nor regents were used with further purification.

4.2.2 Experimental details

All experiments were carried out in a Quartz laminar FTR (~4.12 L) under room temperature (~ 295 ± 2 K).[5, 35-39] The relative humidity (RH) was adjusted by controlling the fractions of clean dry air through vs. bypassing a water bubbler to achieve the wet condition (77 ± 3%) or dry condition (32 ± 3%). The total flow rate in the FTR was 4 L min^{-1}, corresponding to a residence time of ~ 60 s. O_3 was introduced into the FTR by passing pure O_2 through an ozone generator (Jelight, Model 610). $^{\bullet}OH$ were generated by O_3 photolysis in the presence of water vapor by two mercury UV lamps (λ = 254 nm). A

total of nine OA model compounds with multiple different functional groups were studied under wet conditions, including 3-methylglutaric acid ($C_6H_{10}O_4$), adipic acid ($C_6H_{10}O_4$), glucose ($C_6H_{12}O_6$), tricarballylic acid ($C_6H_8O_6$), 1, 2, 3, 4-butanetetracarboxylic acid ($C_8H_{10}O_8$), camphoric acid ($C_{10}H_{16}O_4$), 1, 3, 5-cyclohexanetricarboxylic acid ($C_9H_{12}O_6$), suberic acid ($C_8H_{14}O_4$), and xylitol ($C_5H_{12}O_5$). A constant output aerosol atomizer (TSI Inc. Model 3076) was used to generate polydisperse OA particles from aqueous solutions (1 g L^{-1}) of these model compounds. The typical OA particle mass loading in the FTR was 2600 – 5000 μg m^{-3}; the mean surface-weighted particle diameters of the generated OA surrogates were in the range of 200 ± 20 nm – 240 ± 30 nm. The high aerosol mass loadings are necessary to ensure that minimal fractions of the OA species, which already have low volatilities, are in the gas phase such that any observed ROOH is formed in the condensed phase. For these nine model systems, two oxidation conditions were examined, i.e., $[HO_2^\bullet]/[^\bullet OH] < 1$ vs. $[HO_2^\bullet]/[^\bullet OH] \sim 40$ (see the section below). Among these OA surrogates, 3-methylglutaric acid was investigated in greater detail under more experimental conditions, including varied RH and particle sizes, more scattered $[HO_2^\bullet]/[^\bullet OH]$ scenarios, and more comprehensive product characterization. This allows for a closer examination of the $HO_2^\bullet$ heterogeneous chemistry and its impacts on the oxidation kinetics and OA molecular composition.

The OA particle size distribution and number concentration were measured by the SEMS and the MCPC, respectively. O_3 concentration was measured by an ozone analyzer after a HEPA filter that removes particles at the FTR exit. The OA particles were guided through a charcoal denuder to remove gas-phase compounds followed by a 1.6 L min^{-1}

dilution flow containing humidified air with H_2O or D_2O. With D_2O, it allows for hydrogen-deuterium exchange (HDX) on any labile H atoms (i.e., H in –O–H and –O–O–H converted to D).[40] The diluted OA particles were then sampled by the TD-CIMS Aerodyne Research with the I^- chemical ionization source for real-time molecular composition analysis, with the TD temperature set to 180 °C to vaporize most OA species.[5, 38] Under this TD temperature, only ~0.8% and ~1.6% of unoxidized and oxidized 3-methylglutaric acid particles were remained in the particle phase, respectively, indicating the high efficiencies of vaporizing the OA particles into the gas phase. In addition to real-time characterization, aerosol samples at all oxidation stages were collected by a sequential spot sampler for offline analyses using an electrospray ionization time-of-flight mass spectrometer in the negative ion mode ((–)ESI-MS, Aerodyne Research Inc.)[38] and a gas chromatography mass spectrometer (GC-MS, Agilent Inc., 7890 GC and 5975 MSD) with prior derivatization[39, 41, 42] in the 3-methylglutaric acid experiments. The (–)ESI-MS was utilized to examine the role of $HO_2^\bullet$ in the comprehensive OA molecular composition. The GC-MS analysis was conducted to study the $HO_2^\bullet$ impacts on heterogeneous OA oxidation kinetics and provide some insights into the isomer-resolved products.

4.2.3 $HO_x^\bullet$ control and estimation

For the heterogeneous oxidation experiments requiring higher $[HO_2^\bullet]/[^\bullet OH]$, methanol was continuously injected into the FTR by a syringe pump at controlled rates. The $^\bullet OH$ oxidation of methanol is known to efficiently generate $HO_2^\bullet$.[43-45] Without a detection method to directly quantify $[^\bullet OH]$ and $[HO_2^\bullet]$, their concentrations were

estimated by a photochemical box model based on MCM v3.2 including all the inorganic gas-phase reactions and methanol oxidation mechanism.[39, 46, 47] The chemical reactions to generate $^{\bullet}OH$ and $HO_2^{\bullet}$ in the box model are listed in the **Table 4.1**. The estimation of [$^{\bullet}OH$] was carried out using this approach in our prior studies.[39, 48] In these reactions, the only unknown parameters are O_3 photolysis rate constant and $^{\bullet}OH$ and $HO_2^{\bullet}$ wall loss rate constants.[48] We set these values as tuning parameters and optimized their values to reach the best measurement-simulation agreement. Specifically, the measured and simulated [O_3] were used to constrain O_3 photolysis rates; [$^{\bullet}OH$] experimentally determined by the consumption of methanol measured using a high-sensitivity proton-transfer-reaction mass spectrometer (PTR-MS, Ionicon Analytik Inc.) were used to constrain $^{\bullet}OH$ wall loss rate constant in the box model. Lastly, the production of H_2O_2 has been used to estimate [$HO_2^{\bullet}$] in prior research because $HO_2^{\bullet}$ is the principal H_2O_2 source.[49, 50] We followed the same approach and constrained the $HO_2^{\bullet}$ wall loss rate constant by comparing simulated [H_2O_2][50] with that quantified using H_2O_2 standards detected by I^--CIMS. The model performance was verified by comparing simulation outputs and measurements in characteristic experiments. The comparison results suggest that the model can simulate [$^{\bullet}OH$] and [$HO_2^{\bullet}$] within 30% accuracy under most experimental conditions. The model results suggest that in the absence of added methanol, $HO_2^{\bullet}$ can be produced by $^{\bullet}OH + O_3$, but the resultant [$HO_2^{\bullet}$]/[$^{\bullet}OH$] ratio is only < 1, much lower than atmospheric conditions. With methanol oxidized by $^{\bullet}OH$, we can achieve much higher [$HO_2^{\bullet}$]/[$^{\bullet}OH$] by regulating O_3 and methanol injection concentrations. We hence used this box model to design the initial [O_3] and

[methanol] in experiments to reach controllable [$HO_2^{\bullet}$]/[$^{\bullet}OH$] with maximum values ~ 55, which is relevant to real atmospheric conditions. The $^{\bullet}OH$ exposure ranged from 9×10^{10} to 4×10^{12} molecules cm^{-3} s in all experiments.

Table 4.1 Reactions and rate constants in the box model

Reactions	Rate constant (s^{-1} or cm^3 $molecule^{-1}$ s^{-1})
O_3 → O1D	J_1[a]
O1D → $^{\bullet}OH + {}^{\bullet}OH$	$2.14 \times 10^{-10} \times [H_2O]$
$^{\bullet}OH + O_3$ → $HO_2^{\bullet}$	$1.70 \times 10^{-12} \times \exp(-940/T)$[b]
$HO_2^{\bullet} + O_3$ → $^{\bullet}OH$	$2.03 \times 10^{-16} \times (T/300)^{4.57} \times \exp(693/T)$
$^{\bullet}OH + HO_2^{\bullet}$ →	$4.8 \times 10^{-11} \times \exp(250/T)$
$HO_2^{\bullet} + HO_2^{\bullet}$ → H_2O_2	$2.20 \times 10^{-13} \times KMT06$[c] $\times \exp(600/T) + 1.90 \times 10^{-33} \times M \times KMT06 \times \exp(980/T)$
H_2O_2 → $^{\bullet}OH + {}^{\bullet}OH$	J_2[d]
$CH_3OH + {}^{\bullet}OH$ → $HO_2^{\bullet} + HCHO$	$2.85 \times 10^{-14} \times \exp(-345/T)$
HCHO → $CO + HO_2^{\bullet} + HO_2^{\bullet}$	$J_1 \times 0.342 \times 0.2/1148/0.92$
HCHO → $H_2 + CO$	$J_1 \times 0.342 \times 0.497/1148/0.92$
$^{\bullet}OH$ + HCHO → $HO_2^{\bullet} + CO$	$5.40 \times 10^{-12} \times \exp(-135/T)$
$^{\bullet}OH$ → wall loss	50[e]
$HO_2^{\bullet}$ → wall loss	4[e]

[a] $J_1 = 0.17$ under wet conditions (RH ~ 74%−80%); $J_1 = 0.2$ under dry conditions (RH ~ 29%−34%).

[b] T: temperature (K).

[c] $KMT06 = 1 + (1.40 \times 10^{-21} \times \exp(2200/T) \times [H_2O]$

[d] $J_2 = 0.00254$ s^{-1} based on measurement.

[e] The wall loss rate constants are constrained by the box model.

4.3 Results and Discussion

4.3.1 ROOH formation during OA heterogeneous oxidation

Consistent with the well-accepted mechanism described above, the OH-initiated heterogeneous oxidation of all the studied oxygenated OA surrogates forms a series of multi-functionalized products through $RO_2^{\bullet}$ self-reaction, including the first-generation products of R=O (carbonyl), ROH (alcohol), along with the second-generation products of $R(=O)_2$ (dicarbonyl), R(=O)OH (hydroxycarbonyl), and $R(OH)_2$ (diol).[5, 6, 33, 35] Because ROOH and $R(OH)_2$ are isomers, it is impossible to differentiate them by typical mass spectrometry analysis, causing challenges for ROOH identification. But because they are formed by different oxidation generations and pathways, we attempt to demonstrate their different abundances under varied [$^{\bullet}$OH] and [$HO_2^{\bullet}$]. In the (–)ESI-MS results for 3-methylglutaric acid oxidation shown in **Figure 4.1A**, $C_6H_{10}O_6$ (sum of ROOH and $R(OH)_2$) were formed with very limited fraction among all the major functionalization products (< 1% signals) under [$HO_2^{\bullet}$]/[$^{\bullet}$OH] < 1 and low [$^{\bullet}$OH]. Its relative abundance increases with enhanced $^{\bullet}$OH exposure, indicative of the formation of the second-generation product $R(OH)_2$.[33] In contrast, under identical [$^{\bullet}$OH] and thus likely similar $R(OH)_2$, the fractions of $C_6H_{10}O_6$ are much greater (up to ~ 10%) with higher [$HO_2^{\bullet}$]/[$^{\bullet}$OH]. The gap is especially significant under lower [$^{\bullet}$OH], suggesting that ROOH formed from $RO_2^{\bullet}$ + $HO_2^{\bullet}$ is likely the dominant contributor to $C_6H_{10}O_6$ where multigenerational oxidation is limited. Likewise, results from the TD-CIMS measurements of relative $C_6H_{10}O_6$ signals from 3-methylglutaric acid oxidation (**Figure 4.1B**) under two constant conditions of $^{\bullet}$OH exposure conditions both exhibit increasing trends as a function of [$HO_2^{\bullet}$], supporting

formation of ROOH from $RO_2^\bullet + HO_2^\bullet$. Notably, the fractions of $C_6H_{10}O_6$ among the major products are always higher under lower $^\bullet$OH exposure condition, further suggesting that ROOH is a main contributor.

Figure 4.2 illustrates the TD-CIMS mass spectra for the heterogeneously oxidized 3-methylglutaric acid. Two conditions with identical $^\bullet$OH exposure but very different $[HO_2^\bullet]/[^\bullet OH]$ are focused with the ratio of < 1 (without methanol) and ~ 40 (with methanol, determined by the box model). The $C_6H_{10}O_6$ signals in **Figures 4.2A**–**2B** show the sum of ROOH and $R(OH)_2$, which are much stronger with higher $[HO_2^\bullet]/[^\bullet OH]$ under similar $[^\bullet OH]$, while the differences for the other major peaks are negligible (**Figure 4.2B** vs. **4.2A**), indicating the enhanced ROOH formation from $RO_2^\bullet + HO_2^\bullet$ and agreeing with results illustrated in **Figure 4.1**. To unambiguously determine ROOH formation and abundance, we applied the HDX method to couple with the TD-CIMS to separate ROOH from $R(OH)_2$. HDX is expected to occur on functional groups with labile H atoms (i.e., H in –O–H and –O–O–H).[51-53] In the experiments using D_2O, the I^- clusters of a detectable organic molecule (i.e., $[M+I]^-$) were observed to undergo a m/Q shift by mass units corresponding to the number of labile H atoms in the organic molecule structure. The I^- adduct ion of $C_6H_{10}O_6$ from 3-methylglutaric acid heterogeneous oxidation has a m/Q shift of 3 Th by ~85%, corresponding to the ROOH, and a m/Q shift of 4 Th by ~15%, corresponding to the $R(OH)_2$ (**Figure 4.2C**). This directly demonstrates that ROOH is the major form of $C_6H_{10}O_6$ under the studied conditions. We ruled out the possibility of incomplete HDX for $R(OH)_2$ by testing tartaric acid, a chemical with two carboxylic acid groups and two alcohol groups, which exhibits complete HDX with a m/Q shift of 4 Th. The other studied OA

model compounds with multiple alcohols or carboxylic acids also exhibit complete HDX. These results elucidate the formation of ROOH during heterogeneous $^{\bullet}$OH oxidation for the first time. As a minor note, the m/Q shifts for the other species in the mass spectra are also consistent with their expected functionalities. As shown in **Figure 4.2C**, most of the initial $C_6H_{10}O_6$ signals are contributed by ROOH under atmospherically relevant $[HO_2^{\bullet}]/[^{\bullet}OH]$, strongly supporting the importance of ROOH from $RO_2^{\bullet} + HO_2^{\bullet}$ during heterogeneous $^{\bullet}$OH oxidation.

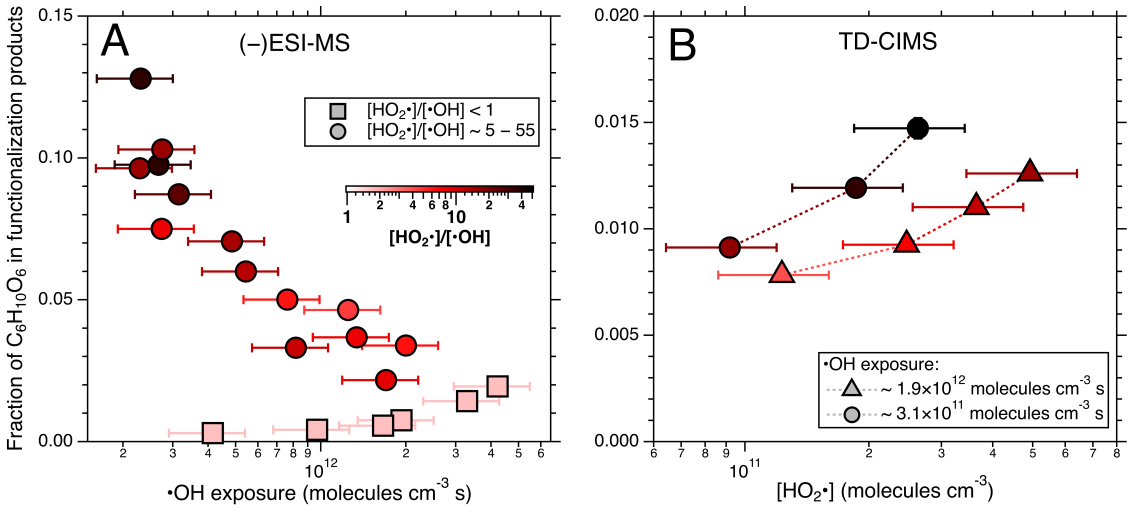

Figure 4.1 The fractions of $C_6H_{10}O_6$ in all the functionalization products, including $C_6H_8O_5$ (R=O), $C_6H_{10}O_5$ (ROH), $C_6H_6O_6$ [R(=O)$_2$], $C_6H_8O_6$ [R(=O)OH], and $C_6H_{10}O_6$ [sum of ROOH and R(OH)$_2$], from 3-methylglutaric acid oxidation in (A) (–)ESI-MS results as a function of $^{\bullet}$OH exposure; and (B) TD-CIMS results as a function of [$HO_2^{\bullet}$]. The [$HO_2^{\bullet}$]/[$^{\bullet}$OH] ratios ranged between < 1 and 55 are indicated by the color scheme shown in (A).

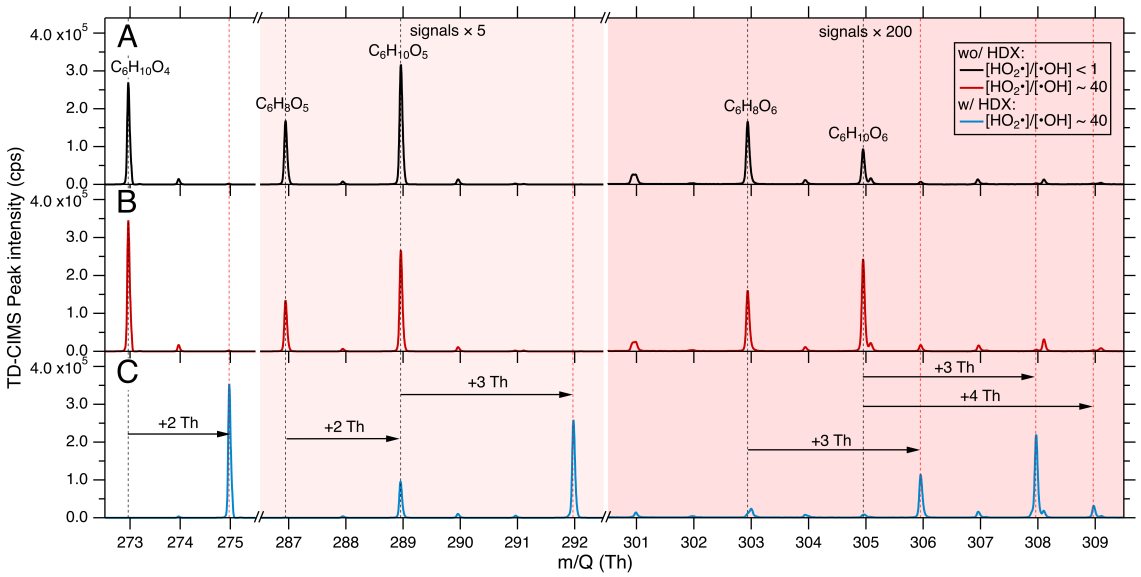

Figure 4.2 The mass spectra of •OH-initiated heterogeneous oxidation of 3-methylglutaric acid under (A) $[HO_2^{\bullet}]/[^{\bullet}OH] < 1$ in the presence of H_2O, (B) $[HO_2^{\bullet}]/[^{\bullet}OH] \sim 40$ in the presence of H_2O and (C) $[HO_2^{\bullet}]/[^{\bullet}OH] \sim 40$ in the presence of D_2O. The major products are labeled with the mass spectra peaks and the mass shifts during HDX are indicated.

The unambiguous formation of ROOH was not only observed from the 3-methylglutaric acid systems, but also from the other studied OA surrogates. We further calculated the intensity-based fractions of ROOH among the first-generation functionalization products (i.e., the sum of ROOH, R=O, and ROH) in the oxidized OA under a range of $^{\bullet}OH$ exposure (7.6×10^{11}–1.5×10^{12} molecules cm^{-3} s) for all the investigated OA surrogates (**Figure 4.3**). We found that high $[HO_2^{\bullet}]/[^{\bullet}OH]$ leads to an increase in the ROOH fractions for all the model systems except for tricarballylic acid. This suggests that the proposed ROOH formation from $RO_2^{\bullet} + HO_2^{\bullet}$ is rather a generic reaction during heterogeneous oxidation of OAs. The relative abundance of ROOH for these OA surrogates ranges from 0.37±0.02% to 10.37±1.10% under $[HO_2^{\bullet}]/[^{\bullet}OH] < 1$ but are enhanced to 1.83±0.06% − 24.95±0.53% under $[HO_2^{\bullet}]/[^{\bullet}OH] \sim 40$. It should also be emphasized that ROOH are known to be thermally labile and could undergo decomposition during thermal desorption in TD-CIMS.[54-57] To provide some quantitative constraint of the thermal decomposition, we generated a well-known gas-phase ROOH, isoprene hydroxy hydroperoxide (ISOPOOH, $C_5H_{10}O_3$)[50, 58-61] in the FTR from isoprene oxidation, which is the dominant product detected at m/Q 245 Th by I^--CIMS.[62] The isoprene oxidation products including ISOPOOH was sampled by the TD-CIMS under room temperature and 180 °C (the same operation temperature for the oxidized OA model systems). We found that the $C_5H_{10}O_3$ signal dropped by ~2/3 under 180 °C, indicating that the actual ROOH can be 3 times more substantial than the results reported in **Figure 4.3**. Taking the ROOH thermal decomposition loss into account, the ROOH relative abundance in 3-methylglutaric acid heterogeneous oxidation under $[HO_2^{\bullet}]/[^{\bullet}OH] \sim 40$ are in similar

magnitude between the TD-CIMS measurements (~6%) and the (−)ESI-MS data (~10%, **Figure 4.2**). The ROOH relative abundance among the first-generation functionalization products approximately reflects the branching ratio of $RO_2^\bullet + HO_2^\bullet$ against $RO_2^\bullet + RO_2^\bullet$. These results thus suggest that the branching ratio of $RO_2^\bullet + HO_2^\bullet$ in heterogeneous OA oxidation under atmospheric $[HO_2^\bullet]/[^\bullet OH]$ may account for up to ~50% of the $RO_2^\bullet$ bimolecular fates. We should note that this approximation assumes that all the functionalization products have similar sensitivities in I^--CIMS and similar sensitivities in (−)ESI-MS, which is not confirmed due to the lack of authentic standards. But it is likely a reasonable estimate considering the similar chemical structures of the products for each OA surrogate system. However, different ROOH may have distinct thermal decomposition behavior and treating all ROOH the same could lead to some uncertainties.

Obviously, the ROOH enhancement (by a factor of 1.3 – 5.0) is to a much lesser degree compared to that of $[HO_2^\bullet]$ (by a factor of > 40) and the reason for this is unclear. We suspect that the $HO_2^\bullet$ uptake and reaction with $RO_2^\bullet$ is more efficient under lower $[HO_2^\bullet]$. The other possible explanation is that the bimolecular autoxidation (i.e., $RO_2^\bullet$ + R−H) that we previously proposed may partly contribute to the observed ROOH.[5] This would be surprising and may suggest that the bimolecular autoxidation may be rapid enough to compete with $RO_2^\bullet + RO_2^\bullet$/ $HO_2^\bullet$ reactions even under high $[^\bullet OH]$. Future studies are warranted to elucidate the ROOH formation mechanisms under low $[HO_2^\bullet]/[^\bullet OH]$. But regardless, the enhanced ROOH formation with higher $[HO_2^\bullet]/[^\bullet OH]$ reported here clearly demonstrates the occurrence and importance of $RO_2^\bullet + HO_2^\bullet$ reactions in heterogeneous OA oxidation.

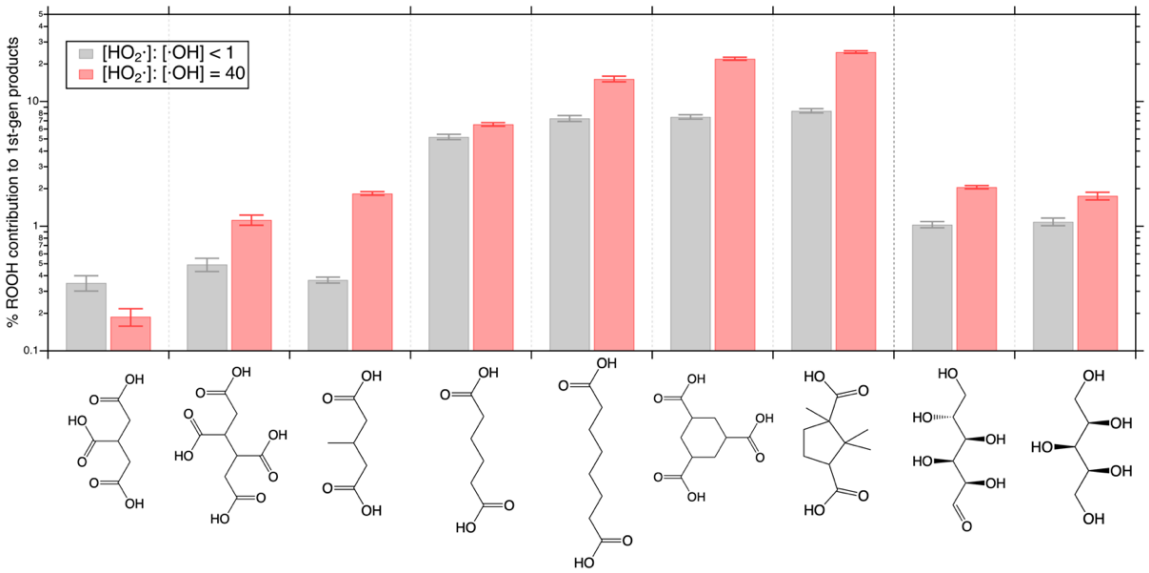

Figure 4.3 The intensity-based relative abundance (%) of ROOH among the first-generation oxidation products for different OA surrogates under $[HO_2^{\bullet}]/[^{\bullet}OH] < 1$ vs. $[HO_2^{\bullet}]/[^{\bullet}OH] \sim 40$.

4.3.2 The role of $HO_2^•$ in heterogeneous oxidation kinetics and molecular composition

With the elucidation of ROOH formation from $RO_2^•$ + $HO_2^•$ reactions, we continue to examine how $HO_2^•$ affects the OA oxidative aging kinetics. It is well known that the $RO_2^•$ + $RO_2^•$ reactions may partly form $RO^•$, which can abstract H from R–H and form $RO_2^•$ (known as chain propagation). This process effectively contributes to the R–H degradation.[6, 34] The substantial presence of $HO_2^•$ could compete with $RO_2^•$ to react with $RO_2^•$ and hence reduce the $RO^•$ formation from $RO_2^•$ + $RO_2^•$ as a smaller fraction of $RO_2^•$ undergoes self-reaction. By this mechanism, it is expected that the OA oxidation kinetics may be slower with enhanced $HO_2^•$. Here, we investigated the degradation of 3-methylglutaric acid as a function of $^•OH$ exposure and obtained the oxidation kinetics from the GC-MS measurements. The enhancement of $HO_2^•$ plays a negligible role in the decay rates of 3-methylglutaric acid within the measurement uncertainties, suggesting that the $RO_2^•$ + $HO_2^•$ reactions offset the reduced $RO^•$ formation from inhibited $RO_2^•$ + $RO_2^•$ and sustain the secondary chemistry. This can be explained by that $RO_2^•$ + $HO_2^•$ reactions also directly produce $RO^•$ (and release $^•OH$);[20-23] the ROOH may also be photolyzed into $RO^•$ and $^•OH$.[19, 23-26] Indicated by the kinetic results for the case of 3-methylglutaric acid, the $RO^•$ and $^•OH$ from $RO_2^•$ + $HO_2^•$ contributed to 3-methylglutaric acid oxidation to a similar extent as $RO^•$ from $RO_2^•$ + $RO_2^•$.

As reported by Kurtén et al.[63] for gas-phase $RO_2^•$ + $HO_2^•$, the $RO^•$ + $^•OH$ formation pathway may have a large branching ratio if the $RO_2^•$ is on a tertiary carbon.[21-23] In contrast,

the less substituted primary and secondary $RO_2^{\bullet}$ are likely the main contributors to ROOH formation. In the case of 3-methylglutaric acid, the primary oxidation site is the tertiary carbon, followed by the primary carbon, while the two secondary carbons adjacent to the carboxylic acids are less oxidized due to the mesomeric effect, as discussed in our prior work and supported by new isomer-resolved GC-MS results.[35] For example, the dominant alcohol product (> 80%) has the –OH group on the tertiary carbon; the dominant carbonyl product (> 80%) has the C=O group on the primary carbon (i.e., an aldehyde). This aldehyde tends to be further oxidized into tricarballylic acid. Based on this, a mechanism for 3-methylglutaric acid $^{\bullet}$OH oxidation is shown in **Figure 4.4**.[6, 23, 64, 65] It is expected that, by reacting with $HO_2^{\bullet}$, the dominant tertiary $RO_2^{\bullet}$ mainly produces $RO^{\bullet}$ + $^{\bullet}$OH and the less abundant primary $RO_2^{\bullet}$ mainly forms ROOH.[21-23] This agrees with that the relative abundance of ROOH during 3-methylglutaric acid oxidation is on the lower side among all the studies OA surrogates (**Figure 4.3**). In fact, as shown in **Figure 4.3**, all the studied OA model compounds with tertiary carbons as the primary oxidation sites have relatively lower ROOH abundance, while those with secondary and primary carbons as the main oxidation sites (i.e., 1, 3, 5-cyclohexanetricarboxylic acid, camphoric acid, adipic acid and suberic acid) exhibit much stronger ROOH formation. These discrepancies among different OA model systems are highly consistent with our proposed $RO_2^{\bullet}$ + $HO_2^{\bullet}$ mechanisms.

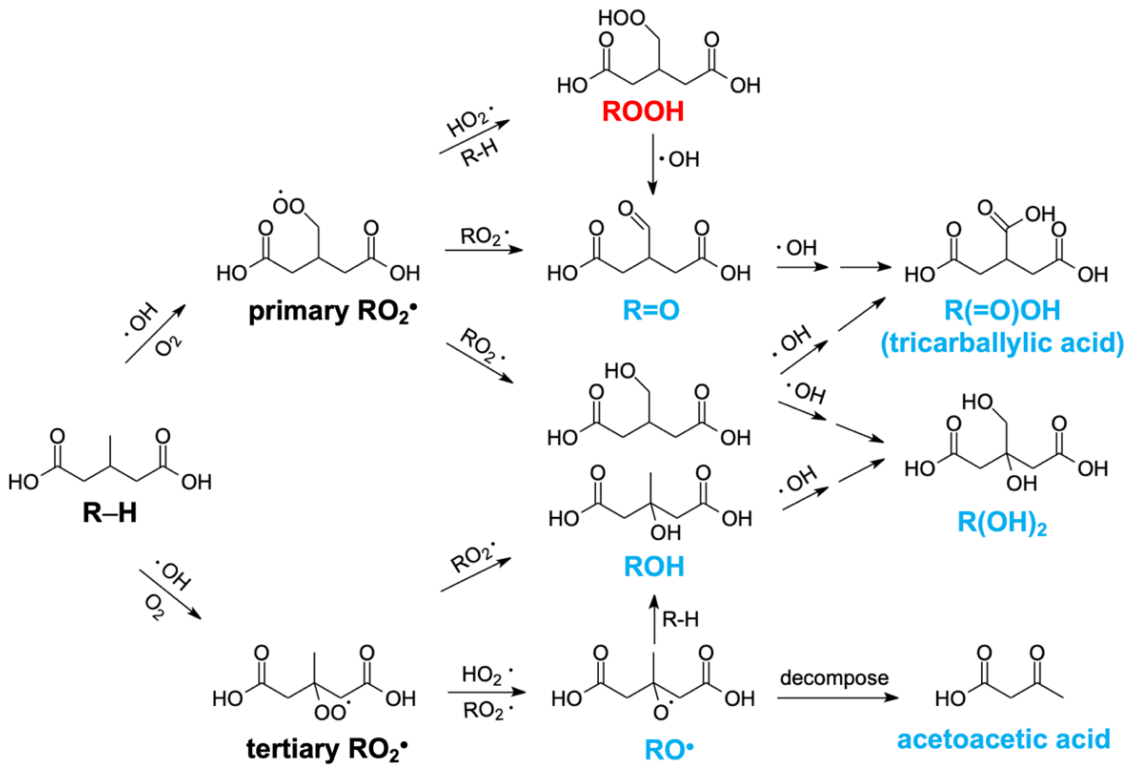

Figure 4.4 The proposed mechanism of •OH-initiated heterogeneous oxidation of 3-methylglutaric acid mediated by HO_2• reactions.

Despite the little influence on the oxidation kinetics for 3-methylglutaric acid, $HO_2^•$ have a greater impact on OA molecular composition through heterogeneous oxidation. As expected, the formation of ROH and R=O from $RO_2^•$ + $RO_2^•$ reactions is suppressed under high $[HO_2^•]/[^•OH]$ because more $RO_2^•$ react with $HO_2^•$. Due to the $RO^•$ produced from $RO_2^•$ + $HO_2^•$ sustaining the chain propagation chemistry from which ROH is a product (**Figure 4.4**),[20-23] it is also expected that suppression for ROH is to a lesser extent than R=O. However, this is not the case. In fact, the ratio of R=O/ROH slightly increases with higher $HO_2^•$, indicating an efficient pathway to form R=O with ROOH involved. We suggest that R=O can be formed from further $^•OH$ oxidation of the primary ROOH with $^•OH$ as the co-product (**Figure 4.4**). The tertiary $RO^•$ can also undergo fragmentation reactions to produce smaller molecules, mainly acetoacetic acid ($C_4H_6O_3$, **Figure 4.4**).[5, 34] The absolute intensities of acetoacetic acid measured by TD-CIMS under different $[HO_2^•]/[^•OH]$ vary insignificantly, agreeing with the discussion above that $RO_2^•$ + $HO_2^•$ reactions offset the decreased formation of $RO^•$ from $RO_2^•$ + $RO_2^•$. On the other hand, the much higher abundance of acetoacetic acid relative to ROH + R=O in the presence of additional $HO_2^•$ suggests that a great fraction of the $RO^•$ that undergoes fragmentation comes from $RO_2^•$ + $HO_2^•$, rather than $RO_2^•$ + $RO_2^•$.

Finally, we examined how $HO_2^•$ affected the overall OA composition. We present the average carbon oxidation state (OS_C) and O/C ratio from the 3-methylglutaric acid heterogeneous oxidation under different $[HO_2^•]$ and $[^•OH]$ conditions, based on the observed (–)ESI-MS intensities of all the observed oxidation products with chemical

formulas of $C_{1\text{-}6}H_{2\text{-}10}O_{3\text{-}8}$. The OS_C and O/C ratios increase by ~0.10 and ~0.05, respectively, as [$HO_2^\bullet$] increased by sevenfold under a constant lower [$^\bullet$OH] of ~ 4.4×10^9 molecules cm^{-3}, indicating that $HO_2^\bullet$ facilitates OA chemical evolution. In contrast, in similar experiments but with higher [$^\bullet$OH] of ~ 2.4×10^{10} molecules cm^{-3}, the OS_C and O/C ratios do not exhibit as prominent increasing trends with enhanced [$HO_2^\bullet$]. These results suggest that under high [$^\bullet$OH] and hence high [$RO_2^\bullet$], $RO_2^\bullet$ + $RO_2^\bullet$ reactions are already sufficient, and thus the impacts of $HO_2^\bullet$ on the overall heterogeneous oxidative aging is less pronounced.

4.3.3 The interfacial nature of $RO_2^\bullet$ + $HO_2^\bullet$

In order to further investigate where the $RO_2^\bullet$ + $HO_2^\bullet$ reactions take place in the particles, we examined ROOH formation under both wet (high-RH) and dry (low-RH) conditions. It was expected that the $HO_2^\bullet$ uptake is more effective under the wet conditions[28, 30], but surprisingly, the ROOH formation was higher under the dry condition regardless of [$HO_2^\bullet$]/[$^\bullet$OH] (**Figure 4.5A**). The higher ROOH relative abundance under the dry condition turns out to be a result of both more strongly increased ROOH signals and decreased R=O and ROH signals from the TD-CIMS data. The more prominent decrease in R=O and ROH intensities under lower RH is expected due to larger diffusion limitation and reduced parent OA reactivities.[66] But unexpectedly, the slower oxidation and hence reduced $RO_2^\bullet$ formation is somehow offset by the promoted $RO_2^\bullet$ + $HO_2^\bullet$ which leads to higher ROOH. Previous studies have reported that aerosol particles containing low water

contents tend to have negligible $HO_2^\bullet$ uptake due to the diffusion limitation.[28, 30] The key difference here is that the OA particles interacting with gaseous $HO_2^\bullet$ are oxidized and contain $RO_2^\bullet$ at the interface. We thus hypothesize that the higher ROOH fractions under the dry condition is because the $RO_2^\bullet$ + $HO_2^\bullet$ reaction takes place at the particle interface immediately after collision, rather than by the absorption mechanism. Despite the reduced total $RO_2^\bullet$ formation under the dry conditions, the formed $RO_2^\bullet$ are less mobile and more effectively accumulated at the particle surface region due to slower diffusion, allowing the colliding $HO_2^\bullet$ to react with the interfacial $RO_2^\bullet$ more readily. The (–)ESI-MS measurements are also consistent with the TD-CIMS results. In these measurements, the oxidized aerosols under two different RH conditions were collected by the spot sampler where the particles were grown into aqueous droplets under supersaturation conditions and sit in the form of droplets for minutes before the (–)ESI-MS analysis. Thus, the fact that the (–)ESI-MS results are consistent with those from TD-CIMS rules out possibility that the lower ROOH under the wet condition is due to aqueous decomposition. Rather, we suggest that the ROOH formation is indeed promoted under the dry condition. Moreover, by varying the concentration of 3-methylglutaric acid in the aerosol atomizer, the particle size distribution was also modified, resulting in varied particle surface-to-volume ratio by a factor of two. With increased surface-to-volume ratio, the ROOH relative abundance through the same heterogeneous oxidation experiments (i.e., identical [$^\bullet$OH] and [$HO_2^\bullet$]) also increased (**Figure 4.5B**), supporting the above hypothesis that the $RO_2^\bullet$ + $HO_2^\bullet$ reaction occurs at particle interface. In the atmosphere, particle surface uptake is an important loss pathway for gaseous $HO_2^\bullet$.[27, 31, 67] We suggest that the presence of $RO_2^\bullet$ at

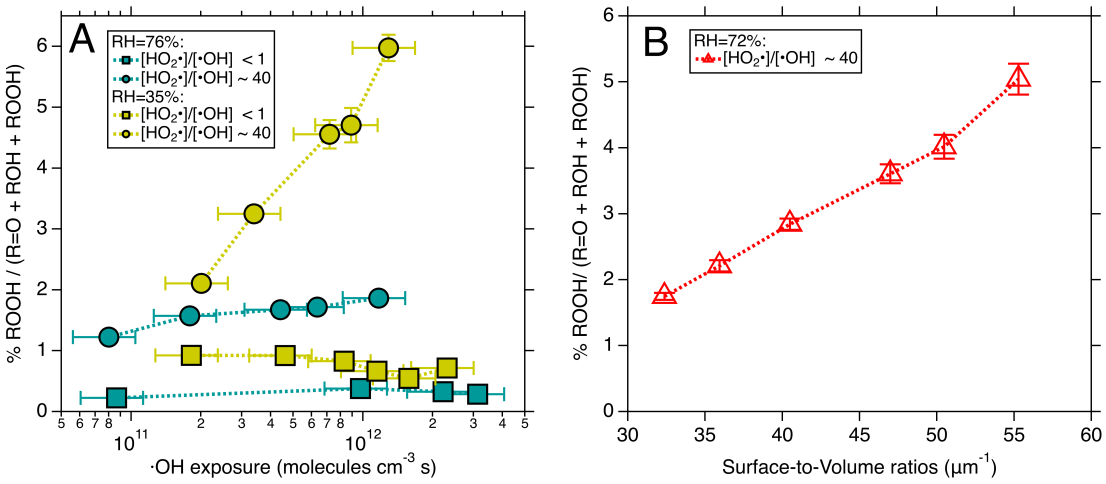

Figure 4.5 The fractions of ROOH among the first-generation functionalization products under (A) varied RH and $[HO_2^{\bullet}]/[^{\bullet}OH]$ conditions as a function of $^{\bullet}OH$ exposure, and (B) varied surface-to-volume ratios.

the interface in the particle bound could enhance the $HO_2^\bullet$ uptake and also heterogeneous ROOH formation.

4.4 Atmospheric Implications

In this work, we report heterogeneous $RO_2^\bullet + HO_2^\bullet$ reactions during $^\bullet$OH-initiated oxidative aging for several oxygenated OA model systems. Direct observations of ROOH formation from these reactions are shown for the first time by using HDX with the TD-CIMS analysis. The heterogeneously formed ROOH may contribute significantly to the total oxidized OAs. Evidence is also shown to support that the heterogeneous $RO_2^\bullet + HO_2^\bullet$ reactions may also produce $RO^\bullet + {}^\bullet OH$ for tertiary $RO_2^\bullet$, similar to that reported in the gas-phase systems.[20-23] These two $RO_2^\bullet + HO_2^\bullet$ reaction pathways together facilitate compositional change of the heterogeneously oxidized OA particles. This $HO_2^\bullet$-involved chemistry is suggested to occur at the particle interface and is promoted when the interface is enriched with $RO_2^\bullet$.

Prior field observations suggested significant loss of $HO_2^\bullet$ through aerosol uptake.[68-71] The work reported here provides new mechanistic insights into the subsequent fates of the uptaken $HO_2^\bullet$ in the particle phase. The first $RO_2^\bullet + HO_2^\bullet$ pathway leads to the formation of ROOH, which are a class of reactive oxygen species that are known to cause adverse health effects.[72] This reaction has been highly emphasized in the gas phase for decades because ROOH substantially contribute to the atmospheric SOA.[18, 61, 73] The ROOH formation via heterogeneous oxidative reactions reported here has not been

recognized despite of the general hypothesis.[6] The other $RO_2^\bullet$ + $HO_2^\bullet$ pathway forms $RO^\bullet$ + $^\bullet OH$[20-23], thus recycling radicals in the condensed phase and propagating secondary chemistry. In the explicitly studied 3-methylglutaric acid system, this pathway is likely very important, owing to the tertiary carbon as the primary oxidation site. It remains to be studied to what extent the other OA model compounds undergo this pathway and how the varied results may affect the overall oxidation kinetics. It is likely that for compounds that more dominantly undergo the first pathway and form ROOH, the overall oxidation could be slower. Nevertheless, the products from heterogeneous $RO_2^\bullet$ + $HO_2^\bullet$ reactions are crucial species and intermediates and may impact the OA composition and properties significantly.

This work, together with several of our prior studies[5, 36, 39], demonstrate that the multiphase oxidation of OA particles can have very complex mechanisms and kinetics, especially when the oxidation occurs under atmospherically relevant conditions (e.g., in the presence of inorganic species, lower [$^\bullet$OH], and higher [$HO_2^\bullet$]/[$^\bullet$OH]). These results suggest that typical laboratory experiments do not accurately mimic atmospheric multiphase oxidation processes. The key environmental factors need to be better represented in laboratory setup and their influences need to be systematically investigated in future studies to help better understand OA chemical evolution in the atmosphere.

4.5 References

(1) Boucher, O.; Randall, D.; Artaxo, P.; Bretherton, C.; Feingold, C.; Forster, P.; Kerminen, V.-M.; Kondo, Y.; Liao, H.; Lohmann, U.; et al. *Clouds and Aerosols*; IPCC: 2013; p 657.

(2) Dockery, D. W.; Pope, C. A.; Xu, X.; Spengler, J. D.; Ware, J. H.; Fay, M. E.; Ferris, B. G.; Speizer, F. E. An Association between Air Pollution and Mortality in Six U.S. Cities. *N. Engl. J. Med.* **1993**, *329* (24), 1753-1759.

(3) Ramanathan, V.; Crutzen, P. J.; Kiehl, J. T.; Rosenfeld, D. Aerosols, Climate, and the Hydrological Cycle. *Science* **2001**, *294* (5549), 2119-2124.

(4) Kristiansen, N. I.; Stohl, A.; Olivié, D. J. L.; Croft, B.; Søvde, O. A.; Klein, H.; Christoudias, T.; Kunkel, D.; Leadbetter, S. J.; Lee, Y. H.; et al. Evaluation of observed and modelled aerosol lifetimes using radioactive tracers of opportunity and an ensemble of 19 global models. *Atmos. Chem. Phys.* **2016**, *16* (5), 3525-3561.

(5) Zhang, W.; Zhao, Z.; Shen, C.; Zhang, H. Unexpectedly Efficient Aging of Organic Aerosols Mediated by Autoxidation. *Environ. Sci. Technol.* **2023**, *57* (17), 6965-6974.

(6) George, I. J.; Abbatt, J. P. D. Heterogeneous oxidation of atmospheric aerosol particles by gas-phase radicals. *Nat. Chem.* **2010**, *2* (9), 713-722.

(7) Calvert, J. G.; Pitts, J. N. *Photochemistry*; Wiley, 1966.

(8) González Palacios, L.; Corral Arroyo, P.; Aregahegn, K. Z.; Steimer, S. S.; Bartels-Rausch, T.; Nozière, B.; George, C.; Ammann, M.; Volkamer, R. Heterogeneous photochemistry of imidazole-2-carboxaldehyde: HO2 radical formation and aerosol growth. *Atmos. Chem. Phys.* **2016**, *16* (18), 11823-11836.

(9) Stone, D.; Whalley, L. K.; Heard, D. E. Tropospheric OH and HO2 radicals: field measurements and model comparisons. *Chem. Soc. Rev.* **2012**, *41* (19), 6348-6404.

(10) Fuchs, H.; Brauers, T.; Dorn, H. P.; Harder, H.; Häseler, R.; Hofzumahaus, A.; Holland, F.; Kanaya, Y.; Kajii, Y.; Kubistin, D.; et al. Technical Note: Formal blind intercomparison of HO2 measurements in the atmosphere simulation chamber SAPHIR during the HOxComp campaign. *Atmos. Chem. Phys.* **2010**, *10* (24), 12233-12250.

(11) Nussbaumer, C. M.; Fischer, H.; Lelieveld, J.; Pozzer, A. What controls ozone sensitivity in the upper tropical troposphere? *EGUsphere* **2023**, *2023*, 1-25.

(12) Levy, H. Normal Atmosphere: Large Radical and Formaldehyde Concentrations Predicted. *Science* **1971**, *173* (3992), 141-143.

(13) McConnell, J. C.; McElroy, M. B.; Wofsy, S. C. Natural Sources of Atmospheric CO. *Nature* **1971**, *233* (5316), 187-188.

(14) Atkinson, R. Kinetics and mechanisms of the gas-phase reactions of the hydroxyl radical with organic compounds under atmospheric conditions. *Chem. Rev.* **1986**, *86* (1), 69-201.

(15) Atkinson, R.; Arey, J. Atmospheric Degradation of Volatile Organic Compounds. *Chem. Rev.* **2003**, *103* (12), 4605-4638.

(16) Orlando, J. J.; Tyndall, G. S. Laboratory studies of organic peroxy radical chemistry: an overview with emphasis on recent issues of atmospheric significance. *Chem. Soc. Rev.* **2012**, *41* (19), 6294-6317.

(17) Ziemann, P. J.; Atkinson, R. Kinetics, products, and mechanisms of secondary organic aerosol formation. *Chem. Soc. Rev.* **2012**, *41* (19), 6582-6605..

(18) Kroll, J. H.; Seinfeld, J. H. Chemistry of secondary organic aerosol: Formation and evolution of low-volatility organics in the atmosphere. *Atmos. Environ.* **2008**, *42* (16), 3593-3624.

(19) Docherty, K. S.; Wu, W.; Lim, Y. B.; Ziemann, P. J. Contributions of Organic Peroxides to Secondary Aerosol Formed from Reactions of Monoterpenes with O3. *Environ. Sci. Technol.* **2005**, *39* (11), 4049-4059.

(20) D'Ambro, E. L.; Hyttinen, N.; Møller, K. H.; Iyer, S.; Otkjær, R. V.; Bell, D. M.; Liu, J.; Lopez-Hilfiker, F. D.; Schobesberger, S.; Shilling, J. E.; et al. Pathways to Highly Oxidized Products in the Δ3-Carene + OH System. *Environ. Sci. Technol.* **2022**, *56* (4), 2213-2224.

(21) Iyer, S.; Reiman, H.; Møller, K. H.; Rissanen, M. P.; Kjaergaard, H. G.; Kurtén, T. Computational Investigation of RO2 + HO2 and RO2 + RO2 Reactions of Monoterpene Derived First-Generation Peroxy Radicals Leading to Radical Recycling. *J. Phys. Chem. A* **2018**, *122* (49), 9542-9552.

(22) Hasson, A. S.; Tyndall, G. S.; Orlando, J. J.; Singh, S.; Hernandez, S. Q.; Campbell, S.; Ibarra, Y. Branching Ratios for the Reaction of Selected Carbonyl-Containing Peroxy Radicals with Hydroperoxy Radicals. *J. Phys. Chem. A* **2012**, *116* (24), 6264-6281.

(23) McNeill, V. F.; Yatavelli, R. L. N.; Thornton, J. A.; Stipe, C. B.; Landgrebe, O. Heterogeneous OH oxidation of palmitic acid in single component and internally mixed aerosol particles: vaporization and the role of particle phase. *Atmos. Chem. Phys.* **2008**, *8* (17), 5465-5476.

(24) Tong, H.; Arangio, A. M.; Lakey, P. S. J.; Berkemeier, T.; Liu, F.; Kampf, C. J.; Brune, W. H.; Pöschl, U.; Shiraiwa, M. Hydroxyl radicals from secondary organic aerosol decomposition in water. *Atmos. Chem. Phys.* **2016**, *16* (3), 1761-1771.

(25) Vereecken, L.; Müller, J. F.; Peeters, J. Low-volatility poly-oxygenates in the OH-initiated atmospheric oxidation of α-pinene: impact of non-traditional peroxyl radical chemistry. *Phys. Chem. Chem. Phys.* **2007**, *9* (38), 5241-5248.

(26) Epstein, S. A.; Blair, S. L.; Nizkorodov, S. A. Direct photolysis of α-pinene ozonolysis secondary organic aerosol: Effect on particle mass and peroxide content. *Environ. Sci. Technol.* **2014**, *48* (19), 11251-11258.

(27) Cooper, P. L.; Abbatt, J. P. D. Heterogeneous Interactions of OH and HO2 Radicals with Surfaces Characteristic of Atmospheric Particulate Matter. *J. Phys. Chem.* **1996**, *100* (6), 2249-2254.

(28) Lakey, P. S. J.; Berkemeier, T.; Krapf, M.; Dommen, J.; Steimer, S. S.; Whalley, L. K.; Ingham, T.; Baeza-Romero, M. T.; Pöschl, U.; Shiraiwa, M.; et al. The effect of viscosity and diffusion on the HO2 uptake by sucrose and secondary organic aerosol particles. *Atmos. Chem. Phys.* **2016**, *16* (20), 13035-13047.

(29) Lakey, P. S. J.; George, I. J.; Whalley, L. K.; Baeza-Romero, M. T.; Heard, D. E. Measurements of the HO2 uptake coefficients onto single component organic aerosols. *Environ. Sci. Technol.* **2015**, *49* (8), 4878-4885.

(30) Thornton, J.; Abbatt, J. P. D. Measurements of HO2 uptake to aqueous aerosol: Mass accommodation coefficients and net reactive loss. *J. Geophys. Res.: Atmos.* **2005**, *110* (D8).

(31) Zhou, J.; Murano, K.; Kohno, N.; Sakamoto, Y.; Kajii, Y. Real-time quantification of the total HO2 reactivity of ambient air and HO2 uptake kinetics onto ambient aerosols in Kyoto (Japan). *Atmos. Environ.* **2020**, *223*, 117189.

(32) Taketani, F.; Kanaya, Y.; Akimoto, H. Heterogeneous loss of HO2 by KCl, synthetic sea salt, and natural seawater aerosol particles. *Atmos. Environ.* **2009**, *43* (9), 1660-1665.

(33) Smith, J. D.; Kroll, J. H.; Cappa, C. D.; Che, D. L.; Liu, C. L.; Ahmed, M.; Leone, S. R.; Worsnop, D. R.; Wilson, K. R. The heterogeneous reaction of hydroxyl radicals with sub-micron squalane particles: a model system for understanding the oxidative aging of ambient aerosols. *Atmos. Chem. Phys.* **2009**, *9* (9), 3209-3222.

(34) Richards-Henderson, N. K.; Goldstein, A. H.; Wilson, K. R. Large enhancement in the heterogeneous oxidation rate of organic aerosols by hydroxyl radicals in the presence of nitric oxide. *J. Phys. Chem. Lett.* **2015**, *6* (22), 4451-4455.

(35) Zhao, Z.; Yang, X.; Lee, J.; Tolentino, R.; Mayorga, R.; Zhang, W.; Zhang, H. Diverse reactions in highly functionalized organic aerosols during thermal desorption. *ACS Earth Space Chem.* **2020**, *4* (2), 283-296.

(36) Zhao, Z.; Tolentino, R.; Lee, J.; Vuong, A.; Yang, X.; Zhang, H. Interfacial dimerization by organic radical reactions during heterogeneous oxidative aging of oxygenated organic aerosols. *J. Phys. Chem. A* **2019**, *123* (50), 10782-10792.

(37) Zhao, Z.; Mayorga, R.; Lee, J.; Yang, X.; Tolentino, R.; Zhang, W.; Vuong, A.; Zhang, H. Site-specific mechanisms in OH-initiated organic aerosol heterogeneous oxidation revealed by isomer-resolved molecular characterization. *ACS Earth Space Chem.* **2020**, *4* (5), 783-794.

(38) Zhao, Z.; Xu, Q.; Yang, X.; Zhang, H. Heterogeneous ozonolysis of endocyclic unsaturated organic aerosol proxies: Implications for Criegee intermediate dynamics and later-generation reactions. *ACS Earth Space Chem.* **2019**, *3* (3), 344-356.

(39) Shen, C.; Zhang, W.; Choczynski, J.; Davies, J. F.; Zhang, H. Phase State and Relative Humidity Regulate the Heterogeneous Oxidation Kinetics and Pathways of Organic-Inorganic Mixed Aerosols. *Environ. Sci. Technol.* **2022**, *56* (22), 15398-15407.

(40) Berndt, T.; Richters, S.; Jokinen, T.; Hyttinen, N.; Kurtén, T.; Otkjær, R. V.; Kjaergaard, H. G.; Stratmann, F.; Herrmann, H.; Sipilä, M.; et al. Hydroxyl radical-induced formation of highly oxidized organic compounds. *Nat. Commun.* **2016**, *7* (1), 13677.

(41) Zhao, Z.; Le, C.; Xu, Q.; Peng, W.; Jiang, H.; Lin, Y.-H.; Cocker, D. R.; Zhang, H. Compositional evolution of secondary organic aerosol as temperature and relative humidity cycle in atmospherically relevant ranges. *ACS Earth Space Chem.* **2019**, *3* (11), 2549-2558.

(42) Mayorga, R. J.; Zhao, Z.; Zhang, H. Formation of secondary organic aerosol from nitrate radical oxidation of phenolic VOCs: Implications for nitration mechanisms and brown carbon formation. *Atmos. Environ.* **2021**, *244*, 117910.

(43) Docherty, K. S.; Ziemann, P. J. Effects of Stabilized Criegee Intermediate and OH Radical Scavengers on Aerosol Formation from Reactions of β-Pinene with O3. *Aerosol Sci. Technol.* **2003**, *37* (11), 877-891.

(44) Physicochemical and Physical Treatment of Pollutants and Wastes. In *Environmental Chemistry: Fundamentals*, Ibanez, J. G., Hernandez-Esparza, M., Doria-Serrano, C., Fregoso-Infante, A., Singh, M. M. Eds.; Springer New York, 2007; pp 237-275.

(45) Atkinson, R.; Baulch, D. L.; Cox, R. A.; Crowley, J. N.; Hampson, R. F.; Hynes, R. G.; Jenkin, M. E.; Rossi, M. J.; Troe, J.; Subcommittee, I. Evaluated kinetic and photochemical data for atmospheric chemistry: Volume II – gas phase reactions of organic species. *Atmos. Chem. Phys.* **2006**, *6* (11), 3625-4055.

(46) Jenkin, M. E.; Young, J. C.; Rickard, A. R. The MCM v3.3.1 degradation scheme for isoprene. *Atmos. Chem. Phys.* **2015**, *15* (20), 11433-11459.

(47) Jenkin, M. E.; Saunders, S. M.; Wagner, V.; Pilling, M. J. Protocol for the development of the Master Chemical Mechanism, MCM v3 (Part B): tropospheric degradation of aromatic volatile organic compounds. *Atmos. Chem. Phys.* **2003**, *3* (1), 181-193.

(48) Faust, J. A.; Abbatt, J. P. D. Organic Surfactants Protect Dissolved Aerosol Components against Heterogeneous Oxidation. *J. Phys. Chem. A* **2019**, *123* (10), 2114-2124.

(49) Christensen, L. E.; Okumura, M.; Sander, S. P.; Salawitch, R. J.; Toon, G. C.; Sen, B.; Blavier, J. F.; Jucks, K. W. Kinetics of HO2 + HO2 → H2O2 + O2: Implications for Stratospheric H2O2. *Geophys. Res. Lett.* **2002**, *29* (9), 13-11-13-14.

(50) Crounse, J. D.; Paulot, F.; Kjaergaard, H. G.; Wennberg, P. O. Peroxy radical isomerization in the oxidation of isoprene. *Phys. Chem. Chem. Phys.* **2011**, *13* (30), 13607-13613, 10.1039/C1CP21330J.

(51) Russell, G. A. Deuterium-isotope effects in the autoxidation of aralkyl hydrocarbons. mechanism of the interaction of peroxy radicals1. *J. Am. Chem. Soc.* **1957**, *79* (14), 3871-3877.

(52) McCloskey, J. A. [16] Introduction of deuterium by exchange for measurement by mass spectrometry. In *Methods in Enzymology*, Vol. 193; Academic Press, 1990; pp 329-338.

(53) Custer, T. G.; Kato, S.; Fall, R.; Bierbaum, V. M. Negative ion mass spectrometry and the detection of carbonyls and HCN from clover. *Geophys. Res. Lett.* **2000**, *27* (23), 3849-3852.

(54) Krapf, M.; El Haddad, I.; Bruns, Emily A.; Molteni, U.; Daellenbach, Kaspar R.; Prévôt, André S. H.; Baltensperger, U.; Dommen, J. Labile peroxides in secondary organic aerosol. *Chem* **2016**, *1* (4), 603-616.

(55) Pospisilova, V.; Lopez-Hilfiker, F. D.; Bell, D. M.; El Haddad, I.; Mohr, C.; Huang, W.; Heikkinen, L.; Xiao, M.; Dommen, J.; Prevot, A. S. H.; et al. On the fate of oxygenated organic molecules in atmospheric aerosol particles. *Sci. Adv. 6* (11), eaax8922.

(56) Mertes, P.; Pfaffenberger, L.; Dommen, J.; Kalberer, M.; Baltensperger, U. Development of a sensitive long path absorption photometer to quantify peroxides in aerosol particles (Peroxide-LOPAP). *Atmos. Meas. Tech.* **2012**, *5* (10), 2339-2348.

(57) Pagonis, D.; Ziemann, P. J. Chemistry of hydroperoxycarbonyls in secondary organic aerosol. *Aerosol Sci. Technol.* **2018**, *52* (10), 1178-1193.

(58) Paulot, F.; Crounse, J. D.; Kjaergaard, H. G.; Kürten, A.; St. Clair, J. M.; Seinfeld, J. H.; Wennberg, P. O. Unexpected Epoxide Formation in the Gas-Phase Photooxidation of Isoprene. *Science* **2009**, *325* (5941), 730.

(59) St. Clair, J. M.; Rivera-Rios, J. C.; Crounse, J. D.; Knap, H. C.; Bates, K. H.; Teng, A. P.; Jørgensen, S.; Kjaergaard, H. G.; Keutsch, F. N.; Wennberg, P. O. Kinetics and Products of the Reaction of the First-Generation Isoprene Hydroxy Hydroperoxide (ISOPOOH) with OH. *J. Phys. Chem. A* **2016**, *120* (9), 1441-1451.

(60) Mettke, P.; Brüggemann, M.; Mutzel, A.; Gräfe, R.; Herrmann, H. Secondary Organic Aerosol (SOA) through Uptake of Isoprene Hydroxy Hydroperoxides (ISOPOOH) and its Oxidation Products. *ACS Earth Space Chem.* **2023**, *7* (5), 1025-1037.

(61) Surratt, J. D.; Chan, A. W. H.; Eddingsaas, N. C.; Chan, M.; Loza, C. L.; Kwan, A. J.; Hersey, S. P.; Flagan, R. C.; Wennberg, P. O.; Seinfeld, J. H. Reactive intermediates revealed in secondary organic aerosol formation from isoprene. *Proc. Natl. Acad. Sci. U.S.A.* **2010**, *107* (15), 6640.

(62) Zhang, W.; Zhang, H. Secondary ion chemistry mediated by ozone and acidic organic molecules in iodide-adduct chemical ionization mass spectrometry. *Anal. Chem.* **2021**, *93* (24), 8595-8602.

(63) Kurtén, T.; Møller, K. H.; Nguyen, T. B.; Schwantes, R. H.; Misztal, P. K.; Su, L.; Wennberg, P. O.; Fry, J. L.; Kjaergaard, H. G. Alkoxy radical bond scissions explain the anomalously low secondary organic aerosol and organonitrate yields from α-pinene + NO3. *J. Phys. Chem. Lett.* **2017**, *8* (13), 2826-2834.

(64) Zhang, H.; Ruehl, C. R.; Chan, A. W. H.; Nah, T.; Worton, D. R.; Isaacman, G.; Goldstein, A. H.; Wilson, K. R. OH-initiated heterogeneous oxidation of cholestane: A model system for understanding the photochemical aging of cyclic alkane aerosols. *J. Phys. Chem. A* **2013**, *117* (47), 12449-12458.

(65) Nah, T.; Zhang, H.; Worton, D. R.; Ruehl, C. R.; Kirk, B. B.; Goldstein, A. H.; Leone, S. R.; Wilson, K. R. Isomeric Product Detection in the Heterogeneous Reaction of Hydroxyl Radicals with Aerosol Composed of Branched and Linear Unsaturated Organic Molecules. *J. Phys. Chem. A* **2014**, *118* (49), 11555-11571.

(66) Chan, M. N.; Zhang, H.; Goldstein, A. H.; Wilson, K. R. Role of water and phase in the heterogeneous oxidation of solid and aqueous succinic acid aerosol by hydroxyl radicals. *J. Phys. Chem. C* **2014**, *118* (50), 28978-28992.

(67) Dyson, J. E.; Whalley, L. K.; Slater, E. J.; Woodward-Massey, R.; Ye, C.; Lee, J. D.; Squires, F.; Hopkins, J. R.; Dunmore, R. E.; Shaw, M.; et al. Impact of HO2 aerosol uptake on radical levels and O3 production during summertime in Beijing. *Atmos. Chem. Phys.* **2023**, *23* (10), 5679-5697.

(68) Brune, W. H.; Tan, D.; Faloona, I. F.; Jaeglé, L.; Jacob, D. J.; Heikes, B. G.; Snow, J.; Kondo, Y.; Shetter, R.; Sachse, G. W.; et al. OH and HO2 chemistry in the North Atlantic free troposphere. *Geophys. Res. Lett.* **1999**, *26* (20), 3077-3080.

(69) Jaeglé, L.; Jacob, D. J.; Brune, W. H.; Faloona, I.; Tan, D.; Heikes, B. G.; Kondo, Y.; Sachse, G. W.; Anderson, B.; Gregory, G. L.; et al. Photochemistry of HO x in the upper troposphere at northern midlatitudes. *J. Geophys. Res.: Atmos.* **2000**, *105* (D3), 3877-3892.

(70) Olson, J. R.; Crawford, J. H.; Chen, G.; Fried, A.; Evans, M. J.; Jordan, C. E.; Sandholm, S. T.; Davis, D. D.; Anderson, B. E.; Avery, M. A.; et al. Testing fast photochemical theory during TRACE-P based on measurements of OH, HO2, and CH2O. *J. Geophys. Res.: Atmos.* **2004**, *109* (D15).

(71) Olson, J. R.; Crawford, J. H.; Chen, G.; Brune, W. H.; Faloona, I. C.; Tan, D.; Harder, H.; Martinez, M. A reevaluation of airborne HOx observations from NASA field campaigns. *J. Geophys. Res.: Atmos.* **2006**, *111* (D10).

(72) Pöschl, U.; Shiraiwa, M. Multiphase chemistry at the atmosphere–biosphere interface influencing climate and public health in the anthropocene. *Chem. Rev.* **2015**, *115* (10), 4440-4475.

(73) Kleindienst, T. E.; Lewandowski, M.; Offenberg, J. H.; Jaoui, M.; Edney, E. O. The formation of secondary organic aerosol from the isoprene + OH reaction in the absence of NOx. *Atmos. Chem. Phys.* **2009**, *9* (17), 6541-6558.

Chapter 5 Conclusion and Future Perspectives

5.1 Summary of Dissertation Work

The work discussed in this dissertation focused on (1) the development of mass spectrometry techniques, methods, and applications in atmospheric chemistry; (2) the mechanisms and kinetics of $RO_2^{\bullet}$-centered chemistry in the gas phase and the particle phase under atmospherically relevant conditions.

In Chapter 1, we discussed advanced mass spectrometry techniques, methods, and applications in atmospheric chemistry research in the past several years while highlighting the developments of IMR, various soft ionization methods, and unique coupling with separation. The applications in laboratory studies and field measurements focused on improving the detection limits for traditional and emerging VOCs, characterizing multiphase highly oxygenated molecules, and monitoring particle bulk and surface compositions.

In Chapter 2, we reported the occurrence of interactions between O_3/H_2O_2/peracids and acidic OVOCs in the IMR region of I^--CIMS. Such interactions could lead to unexpected formation of monomer and dimer adducts, leading to misinterpretations of molecular compositions and distributions as well as an overestimation of the elemental O/C ratio overall. Nevertheless, the varying degrees of signal change in response to secondary ion chemistry might be a clue to inform OVOCs' functionalities and reaction mechanisms therein.

In Chapter 3&4 of this work we discussed new $RO_2^{\bullet}$ bimolecular oxidation reactions in heterogeneous OA aging mechanisms. Chapter 3 demonstrates an autoxidation

mechanism that $RO_2^•$ reacts with parent molecules during the heterogeneous oxidative aging of OAs. Our results suggested that OA heterogeneous oxidation might be 2–3 orders of magnitude faster than previously reported with enhanced formation of organic hydroperoxides, alcohols, and fragmentation products when [•OH] was decreased to atmospheric levels. Chapter 4 reported strong and direct evidence for the hydroperoxide formation from $RO_2^•$ + $HO_2^•$ reactions at the particle interface. Evidence was also shown that heterogeneous $RO_2^•$ + $HO_2^•$ reactions may also produce RO• + •OH for tertiary $RO_2^•$, similar to that reported in the gas-phase system. Through these projects, more mechanistic insights into OA heterogeneous would reconcile the discrepancies between atmospheric observations and laboratory studies.

5.2 Future Work

In the section, we discuss possible future developments of mass spectrometry to further advance the field of atmospheric chemistry and future work of underexplored $RO_2^•$-centered multiphase aging processes to better understand aerosol formation and evolution.

5.2.1 Quantification of complex organic mixtures

Accurate quantification using mass spectrometry remains a major challenge for atmospheric organic species, especially for the oxygenated molecules without authentic standards. The CIMS sensitivities depend on a number of factors, including the ion-molecule reaction rate, the yield of the product ion, the stability and transmission efficiency of the product ion, IMR temperature, relative humidity, electric fields, etc. As a result, it is

challenging to constrain the sensitivities using physically based models.[1] Such complex dependence could be simplified to some extent by the selection of ion chemistry and the design of IMR, allowing the sensitivities to be controlled by fewer factors.

The sensitivities of some instruments have been shown to be proportional to the ion-molecule reaction rate constants. These instruments include CF_3O^--CIMS, PTR-MS, and NO_3^--CIMS.[2-4] In CF_3O^--CIMS, the ion-molecule reaction is in the kinetic-limited regime, as the reaction time is on the order of 1 ms, enabled by the transverse IMR in the Caltech CIMS. The reaction time in PTR-MS is even shorter (i.e., ~0.1 ms) because of the drift voltage. In addition, the protonated ions produced from the proton transfer reactions are stable in the electric fields. In NO_3^--CIMS, even though the reaction time is relatively long (~200 ms), the analyte•NO_3^- cluster is extremely stable and does not break apart in the electric fields, so that it is often assumed that the analytes charges are at their collision frequency with NO_3^-.[5] The ion-molecule reaction rate constants, which are essential to constrain the sensitivities under this condition, can be calculated based on analyte dipole moment and polarizability,[4] estimated based on the analyte molecular mass, elemental composition, and functional group,[2] assumed at collision limit,[6] or considered to be the same as another analyte which can be experimentally calibrated[5, 7-12].

Instead of ion-molecule reaction rate constant, the controlling factor of sensitivities in some CIMS is the stability of product ion. This applies to the IMR design in which the ion-molecule reactions are in thermodynamic equilibrium because of the long reaction time (~100 ms in I^--CIMS,[13] $C_6H_6^+$-CIMS,[14] and $(C_2H_5OH)H^+$-CIMS[15]) or when a strong declustering electric field exists (e.g., NH_4^+-CIMS[16, 17]). To constrain the sensitivity, the

stability of product ion can be experimentally estimated using the voltage scanning tests, in which the change in the product ion signal is monitored in response of a systematic change in the voltage gradient between two ion optics.[16-18] However, the uncertainties of this approach could be substantial, as a recent study by Bi et al. showed that this method may carry uncertainties on the order of 0.5 to 1 magnitude for individual analytes in I^- CIMS.[19]

In addition to intrinsic properties of IMR, an environmental factor affecting CIMS sensitivity is the relative humidity. The sensitivities of a vast majority of analytes in most CIMS show dependence on relative humidity. The relative humidity can increase or decrease the sensitivity by affecting the distribution of reagent ion clusters and product ions, stabilizing the ion clusters with in-excess collision energy, affecting the transmission of water-soluble gases, and other mechanisms.[1, 13] Such water dependence largely complicates the quantification. It is an active research area to minimize the relative humidity dependence. For example, Vocus deliberately adds a large amount of water vapor into the IMR, such that the variation in ambient relative humidity causes minimal disturbance in the IMR and the water dependence in both H_3O^+ and $NH_4{\bullet}H_2O^+$ chemistry is negligible.[17, 20]

The quantification challenge is further compounded by the fact that atmospheric organic species are often very complex mixtures, enriched with isomers. Yet, many of the above-described mass spectrometry techniques cannot separate isomers. To explore the isomer-dependent sensitivities, Bi et al. coupled a TAG-CIMS using I^- to a quantitative flame ionization detector (FID) and reported that in I^--CIMS measurements an average

number of three to five isomers were found per chemical formula,[21] but the isomers' sensitivities could vary by a maximum of 2 orders of magnitude[19].

The quantification issues may be more challenging for particle-phase organics using ambient ionization mass spectrometry. For example, although the analyte response and sensitivity in EESI-MS is less affected by changing OA matrix compared to traditional infusion ESI systems, individual species have different sensitivities by a factor of 30 or more.[22] In contrast, in the study by Brown et al., although the measured signals using EESI-MS are correlated and comparable with those measured by FIGAERO-CIMS, the relative sensitivities to various compounds change by a factor of 100.[23] During an aircraft measurement, Pagonis et al. showed that variability of EESI-MS calibration factor is 60 % (1σ), implying further concerns of the quantitative capability of EESI-MS in field studies.[24] Moreover, the characteristic of corona discharge in DART-MS prevents the potential of precise quantitative assays due to the lack of enough desorption and ionization information.[25, 26] Very limited efforts have been made to quantify speciated OA compounds using other ambient ionization mass spectrometry techniques.[27]

5.2.2 Real-time characterization of structures or functional groups

In recent years, the focus of real-time mass spectrometry developments has been to improve mass resolution, sensitivity, and the range of detectable compounds. It remains challenging to inform chemical structures or functional groups during these measurements. Complementary analysis could fill the gap on this aspect, such as the iodometry-assisted LC-MS,[28-31] IMS-MS,[32-35] and spectrophotometric methods[36-38]. However, most of these

approaches are offline, particle-bound focused, and require sample collection, extraction, etc. It would be helpful to develop continuous sampling approaches and auxiliary platform methods to covert the "offline" mode to an "online" mode for the above techniques. The information regarding chemical structures and functional groups in real time would greatly benefit mechanistic understanding of processes in both the gas and particle phases. In Chapter 4, we use a HDX system in front of the inlet of CIMS to separate isomers though element replacements with higher atomic weight on any labile H atoms, contributing to the real-time characterization of structures or functionalities of individual OA molecules. Recently, online derivatization methods have been designed to couple with AMS for determining particle-phase peroxides based on redox reactions:[39] supersaturated gaseous triphenylphosphine is continuously added to mix with SOA samples in the front of AMS inlet, and the formed triphenylphosphine oxide is then monitored and quantified by AMS with a time resolution of 2 minutes. By combining with such online derivatization method, the real-time peroxide quantification in the SOA could be achieved. It is anticipated that other derivatization techniques could be developed for soft ionization mass spectrometry to provide functional group information.

5.2.3 New gas-phase and multiphase chemical mechanisms

OAs ubiquitously exist in substantial fractions in the atmospheric components and undergo complicated chemical processes throughout their lifetime of around a week. However, the gas-phase and multiphase chemical mechanisms in aerosol chemistry have not been sufficiently studied due to chemical composition complexity and measurement

limitation of OAs. Past studies have focused on investigations of OA formation and evolution on the molecular level, resulting in missing knowledge of OA oxidation mechanisms in the atmosphere. For instance, monoterpenes-derived HOMs are one of the largest sources of percussors leading to SOA formation, but fewer laboratories have reported its isomeric-level composition.[40] We hypothesize that isomeric constituents of monoterpene SOA are distinctive between oxidation conditions including different timescale, oxidant concentrations and reactor types. Combining with the HDX method and other advanced techniques identify the functional groups, we aim to systematically study $RO_2^{\bullet}$-centered isomer distributions to fill a critical gap of the chemical dynamics and mechanisms. Besides, nitrogen oxides enter the atmosphere primarily as nitric oxide (NO), and multifunctional alkyl nitrates ($RONO_2$) have been reported as main oxidation products in the gas phase to impact the tropospheric chemistry. As reported by Richards-Henderson et al.,[41] it is possible that $RONO_2$ is also produced in the particle phase from RO_2 + NO reactions based on prior gas-phase mechanistic understanding. We aim to study the particle-phase composition and $RO_2^{\bullet}$ behavior of various OA models both at OA particle interface and in the OA bulk in the presence of NO, highlighting a comprehensive mechanistic understanding of multiphase oxidative aging of OAs. These proposed projects will improve the understanding of OA effects to the environment and climate.

5.3 Reference

(1) Iyer, S.; Lopez-Hilfiker, F.; Lee, B. H.; Thornton, J. A.; Kurtén, T. Modeling the Detection of Organic and Inorganic Compounds Using Iodide-Based Chemical Ionization. *J. Phys. Chem. A* **2016**, *120* (4), 576-587.

(2) Sekimoto, K.; Li, S.-M.; Yuan, B.; Koss, A.; Coggon, M.; Warneke, C.; de Gouw, J. Calculation of the sensitivity of proton-transfer-reaction mass spectrometry (PTR-MS) for organic trace gases using molecular properties. *Int. J. Mass Spectrom.* **2017**, *421*, 71-94.

(3) Paulot, F.; Crounse, J. D.; Kjaergaard, H. G.; Kroll, J. H.; Seinfeld, J. H.; Wennberg, P. O. Isoprene photooxidation: new insights into the production of acids and organic nitrates. *Atmos. Chem. Phys.* **2009**, *9* (4), 1479-1501.

(4) Garden, A. L.; Paulot, F.; Crounse, J. D.; Maxwell-Cameron, I. J.; Wennberg, P. O.; Kjaergaard, H. G. Calculation of conformationally weighted dipole moments useful in ion–molecule collision rate estimates. *Chem. Phys. Lett.* **2009**, *474* (1), 45-50.

(5) Ehn, M.; Thornton, J. A.; Kleist, E.; Sipilä, M.; Junninen, H.; Pullinen, I.; Springer, M.; Rubach, F.; Tillmann, R.; Lee, B.; et al. A large source of low-volatility secondary organic aerosol. *Nature* **2014**, *506* (7489), 476-479.

(6) Hansel, A.; Scholz, W.; Mentler, B.; Fischer, L.; Berndt, T. Detection of RO2 radicals and other products from cyclohexene ozonolysis with NH4+ and acetate chemical ionization mass spectrometry. *Atmos. Environ.* **2018**, *186*, 248-255.

(7) Berndt, T.; Richters, S.; Jokinen, T.; Hyttinen, N.; Kurtén, T.; Otkjær, R. V.; Kjaergaard, H. G.; Stratmann, F.; Herrmann, H.; Sipilä, M.; et al. Hydroxyl radical-induced formation of highly oxidized organic compounds. *Nat. Comm.* **2016**, *7* (1), 13677.

(8) Jokinen, T.; Berndt, T.; Makkonen, R.; Kerminen, V.-M.; Junninen, H.; Paasonen, P.; Stratmann, F.; Herrmann, H.; Guenther, A. B.; Worsnop, D. R.; et al. Production of extremely low volatile organic compounds from biogenic emissions: Measured yields and atmospheric implications. *Proc. Natl. Acad. Sci. U.S.A.* **2015**, *112* (23), 7123-7128.

(9) Rissanen, M. P.; Mikkilä, J.; Iyer, S.; Hakala, J. Multi-scheme chemical ionization inlet (MION) for fast switching of reagent ion chemistry in atmospheric pressure chemical ionization mass spectrometry (CIMS) applications. *Atmos. Meas. Tech.* **2019**, *12* (12), 6635-6646.

(10) Molteni, U.; Bianchi, F.; Klein, F.; El Haddad, I.; Frege, C.; Rossi, M. J.; Dommen, J.; Baltensperger, U. Formation of highly oxygenated organic molecules from aromatic compounds. *Atmos. Chem. Phys.* **2018**, *18* (3), 1909-1921.

(11) Guo, Y.; Yan, C.; Liu, Y.; Qiao, X.; Zheng, F.; Zhang, Y.; Zhou, Y.; Li, C.; Fan, X.; Lin, Z.; et al. Seasonal variation in oxygenated organic molecules in urban Beijing and their contribution to secondary organic aerosol. *Atmos. Chem. Phys.* **2022**, *22* (15), 10077-10097.

(12) Bianchi, F.; Kurtén, T.; Riva, M.; Mohr, C.; Rissanen, M. P.; Roldin, P.; Berndt, T.; Crounse, J. D.; Wennberg, P. O.; Mentel, T. F.; et al. Highly Oxygenated Organic Molecules (HOM) from Gas-Phase Autoxidation Involving Peroxy Radicals: A Key Contributor to Atmospheric Aerosol. *Chem Rev* **2019**, *119* (6), 3472-3509.

(13) Lee, B. H.; Lopez-Hilfiker, F. D.; Mohr, C.; Kurtén, T.; Worsnop, D. R.; Thornton, J. A. An Iodide-Adduct High-Resolution Time-of-Flight Chemical-Ionization Mass Spectrometer: Application to Atmospheric Inorganic and Organic Compounds. *Environ. Sci. Technol.* **2014**, *48* (11), 6309-6317.

(14) Kim, M. J.; Zoerb, M. C.; Campbell, N. R.; Zimmermann, K. J.; Blomquist, B. W.; Huebert, B. J.; Bertram, T. H. Revisiting benzene cluster cations for the chemical ionization of dimethyl sulfide and select volatile organic compounds. *Atmos. Meas. Tech.* **2016**, *9* (4), 1473-1484.

(15) Yu, H.; Lee, S. H. Chemical ionisation mass spectrometry for the measurement of atmospheric amines. Environ. Chem. **2012**, *9* (3), 190-201.

(16) Zaytsev, A.; Breitenlechner, M.; Koss, A. R.; Lim, C. Y.; Rowe, J. C.; Kroll, J. H.; Keutsch, F. N. Using collision-induced dissociation to constrain sensitivity of ammonia chemical ionization mass spectrometry (NH4+ CIMS) to oxygenated volatile organic compounds. *Atmos. Meas. Tech.* **2019**, *12* (3), 1861-1870.

(17) Xu, L.; Coggon, M. M.; Stockwell, C. E.; Gilman, J. B.; Robinson, M. A.; Breitenlechner, M.; Lamplugh, A.; Crounse, J. D.; Wennberg, P. O.; Neuman, J. A.; et al. Chemical ionization mass spectrometry utilizing ammonium ions (NH4+ CIMS) for measurements of organic compounds in the atmosphere. *Atmos. Meas. Tech.* **2022**, *15* (24), 7353-7373.

(18) Lopez-Hilfiker, F. D.; Iyer, S.; Mohr, C.; Lee, B. H.; D'Ambro, E. L.; Kurtén, T.; Thornton, J. A. Constraining the sensitivity of iodide adduct chemical ionization mass spectrometry to multifunctional organic molecules using the collision limit and thermodynamic stability of iodide ion adducts. *Atmos. Meas. Tech.* **2016**, *9* (4), 1505-1512.

(19) Bi, C.; Krechmer, J. E.; Frazier, G. O.; Xu, W.; Lambe, A. T.; Claflin, M. S.; Lerner, B. M.; Jayne, J. T.; Worsnop, D. R.; Canagaratna, M. R.; et al. Quantification of isomer-resolved iodide chemical ionization mass spectrometry sensitivity and uncertainty using a voltage-scanning approach. *Atmos. Meas. Tech.* **2021**, *14* (10), 6835-6850.

(20) Krechmer, J.; Lopez-Hilfiker, F.; Koss, A.; Hutterli, M.; Stoermer, C.; Deming, B.; Kimmel, J.; Warneke, C.; Holzinger, R.; Jayne, J.; et al. Evaluation of a New Reagent-Ion Source and Focusing Ion–Molecule Reactor for Use in Proton-Transfer-Reaction Mass Spectrometry. *Anal. Chem.* **2018**, *90* (20), 12011-12018.

(21) Bi, C.; Krechmer, J. E.; Frazier, G. O.; Xu, W.; Lambe, A. T.; Claflin, M. S.; Lerner, B. M.; Jayne, J. T.; Worsnop, D. R.; Canagaratna, M. R.; et al. Coupling a gas chromatograph simultaneously to a flame ionization detector and chemical ionization mass spectrometer for isomer-resolved measurements of particle-phase organic compounds. *Atmos. Meas. Tech.* **2021**, *14* (5), 3895-3907.

(22) Lopez-Hilfiker, F. D.; Pospisilova, V.; Huang, W.; Kalberer, M.; Mohr, C.; Stefenelli, G.; Thornton, J. A.; Baltensperger, U.; Prevot, A. S. H.; Slowik, J. G. An extractive electrospray ionization time-of-flight mass spectrometer (EESI-TOF) for online measurement of atmospheric aerosol particles. *Atmos. Meas. Tech.* **2019**, *12* (9), 4867-4886.

(23) Brown, W. L.; Day, D. A.; Stark, H.; Pagonis, D.; Krechmer, J. E.; Liu, X.; Price, D. J.; Katz, E. F.; DeCarlo, P. F.; Masoud, C. G.; et al. Real-time organic aerosol chemical speciation in the indoor environment using extractive electrospray ionization mass spectrometry. *Indoor Air* **2021**, *31* (1), 141-155.

(24) Pagonis, D.; Campuzano-Jost, P.; Guo, H.; Day, D. A.; Schueneman, M. K.; Brown, W. L.; Nault, B. A.; Stark, H.; Siemens, K.; Laskin, A.; et al. Airborne extractive electrospray mass spectrometry measurements of the chemical composition of organic aerosol. *Atmos. Meas. Tech.* **2021**, *14* (2), 1545-1559.

(25) Feider, C. L.; Krieger, A.; DeHoog, R. J.; Eberlin, L. S. Ambient ionization mass spectrometry: Recent developments and applications. *Anal. Chem.* **2019**, *91* (7), 4266-4290.

(26) Brüggemann, M.; Karu, E.; Stelzer, T.; Hoffmann, T. Real-time analysis of ambient organic aerosols using aerosol flowing atmospheric-pressure afterglow mass spectrometry (AeroFAPA-MS). *Environ. Sci. Technol.* **2015**, *49* (9), 5571-5578.

(27) Kenseth, C. M.; Hafeman, N. J.; Huang, Y.; Dalleska, N. F.; Stoltz, B. M.; Seinfeld, J. H. Synthesis of Carboxylic Acid and Dimer Ester Surrogates to Constrain the Abundance and Distribution of Molecular Products in α-Pinene and β-Pinene Secondary Organic Aerosol. *Environ. Sci. Technol.* **2020**, *54* (20), 12829-12839.

(28) Zhao, R.; Kenseth, C. M.; Huang, Y.; Dalleska, N. F.; Kuang, X. M.; Chen, J.; Paulson, S. E.; Seinfeld, J. H. Rapid Aqueous-Phase Hydrolysis of Ester Hydroperoxides Arising from Criegee Intermediates and Organic Acids. *J. Phys. Chem. A* **2018**, *122* (23), 5190-5201.

(29) Zhao, R.; Kenseth, C. M.; Huang, Y.; Dalleska, N. F.; Seinfeld, J. H. Iodometry-Assisted Liquid Chromatography Electrospray Ionization Mass Spectrometry for Analysis of Organic Peroxides: An Application to Atmospheric Secondary Organic Aerosol. *Environ. Sci. Technol.* **2018**, *52* (4), 2108-2117.

(30) Yao, M.; Li, Z.; Li, C.; Xiao, H.; Wang, S.; Chan, A. W. H.; Zhao, Y. Isomer-Resolved Reactivity of Organic Peroxides in Monoterpene-Derived Secondary Organic Aerosol. *Environ. Sci. Technol.* **2022**, *56* (8), 4882-4893.

(31) Zhao, Y.; Yao, M.; Wang, Y.; Li, Z.; Wang, S.; Li, C.; Xiao, H. Acylperoxy Radicals as Key Intermediates in the Formation of Dimeric Compounds in α-Pinene Secondary Organic Aerosol. *Environ. Sci. Technol.* **2022**, *56* (20), 14249-14261.

(32) Krechmer, J. E.; Groessl, M.; Zhang, X.; Junninen, H.; Massoli, P.; Lambe, A. T.; Kimmel, J. R.; Cubison, M. J.; Graf, S.; Lin, Y. H.; et al. Ion mobility spectrometry–mass spectrometry (IMS–MS) for on- and offline analysis of atmospheric gas and aerosol species. *Atmos. Meas. Tech.* **2016**, *9* (7), 3245-3262.

(33) Zhang, X.; Zhang, H.; Xu, W.; Wu, X.; Tyndall, G. S.; Orlando, J. J.; Jayne, J. T.; Worsnop, D. R.; Canagaratna, M. R. Molecular characterization of alkyl nitrates in atmospheric aerosols by ion mobility mass spectrometry. *Atmos. Meas. Tech.* **2019**, *12* (10), 5535-5545.

(34) Zhao, Z.; Tolentino, R.; Lee, J.; Vuong, A.; Yang, X.; Zhang, H. Interfacial Dimerization by Organic Radical Reactions during Heterogeneous Oxidative Aging of Oxygenated Organic Aerosols. *J. Phys. Chem. A* **2019**, *123* (50), 10782-10792.

(35) Zhao, Z.; Yang, X.; Lee, J.; Tolentino, R.; Mayorga, R.; Zhang, W.; Zhang, H. Diverse Reactions in Highly Functionalized Organic Aerosols during Thermal Desorption. *ACS Earth Space Chem.* **2020**, *4* (2), 283-296.

(36) Aimanant, S.; Ziemann, P. J. Development of Spectrophotometric Methods for the Analysis of Functional Groups in Oxidized Organic Aerosol. *Aerosol Sci Tech* **2013**, *47* (6), 581-591.

(37) Ranney, A. P.; Ziemann, P. J. Microscale spectrophotometric methods for quantification of functional groups in oxidized organic aerosol. *Aerosol Sci Tech* **2016**, *50* (9), 881-892.

(38) Ranney, A. P.; Ziemann, P. J. Identification and quantification of oxidized organic aerosol compounds using derivatization, liquid chromatography, and chemical ionization mass spectrometry. *Aerosol Sci. Technol.* **2017**, *51* (3), 342-353.

(39) Weloe, M.; Hoffmann, T. Application of time-of-flight aerosol mass spectrometry for the real-time measurement of particle-phase organic peroxides: an online redox

derivatization–aerosol mass spectrometer (ORD-AMS). *Atmos. Meas. Tech.* **2020**, *13* (10), 5725-5738.

(40) Jaoui, M.; Kleindienst, T. E.; Lewandowski, M.; Offenberg, J. H.; Edney, E. O. Identification and Quantification of Aerosol Polar Oxygenated Compounds Bearing Carboxylic or Hydroxyl Groups. 2. Organic Tracer Compounds from Monoterpenes. *Environmental Science & Technology* **2005**, *39* (15), 5661-5673.

(41) Richards-Henderson, N. K.; Goldstein, A. H.; Wilson, K. R. Large enhancement in the heterogeneous oxidation rate of organic aerosols by hydroxyl radicals in the presence of nitric oxide. *J. Phys. Chem. Lett.* **2015**, *6* (22), 4451-4455.